

Design and modelling of an efficient assistive robotic exoskeleton

With optimum active and passive degrees of freedom

By

Arman Fazeli

Submitted in accordance with the requirements for the degree of
Doctor of Philosophy

The University of Leeds
School of Mechanical Engineering
Institute of Design, Robotics and Optimisation

Sep,2017

The candidate confirms that the work submitted is his own and that appropriate credit has been given where reference has been made to the work of others.

This copy has been supplied on the understanding that it is copyright material and that no quotation from the thesis may be published without proper acknowledgement.

The candidate confirms that the work submitted is his/her own, except where work which has formed part of jointly-authored publications has been included. The contribution of the candidate and the other authors to this work has been explicitly indicated below. The candidate confirms that appropriate credit has been given within the thesis where reference has been made to the work of others. Further details of the jointly-authored publications and the contributions of the candidate and the other authors to the work should be included below this statement.

This copy has been supplied on the understanding that it is copyright material and that no quotation from the thesis may be published without proper acknowledgement.

Assertion of moral rights (optional):

The right of Arman Fazeli to be identified as Author of this work has been asserted by <him/her> in accordance with the Copyright, Designs and Patents Act 1988.

© 2017The University of Leeds and Arman Fazeli

Abstract

Strength, power and functional ability of human lower limb muscles can be affected by numerous muscular, neuro, skeletal diseases and illnesses.

Aging is associated with the loss of muscle strength and difficulties in functional activities, with the ageing population growing fast due to advancement of medical technologies and treatments, rises the vast demand of new technologies which can assist users with lower limb difficulties.

Robotic exoskeletons aims to enhance the ability of their user's by providing structural support along with external forces to carry their user.

Research on robotic exoskeletons could be divided into three main groups in the field of robotics, namely Assistive, Adaptive and Rehabilitative Technologies (AART). The assistive technologies are the main focus of this research. Such devices could help the growing aging population and certain patients to regain their independent living. It is essential for the assistive devices to follow, support and carry the human body.

The main aim of this research is to systematically design an assistive exoskeleton that provide 100% assistant to the limbs of its user while reducing the metabolic effort of the user.

Lack of physiological consideration in the previous assistive exoskeleton designs lead to in metabolic inefficiency. This research addressed this issue by using human biomechanics along with physiological parameters as direct inputs to the design of the exoskeleton.

Another factor affecting the efficiency of previous designs found to be using inaccurate mechanical design parameters, this is because previous designers used healthy human anatomical forces and positions directly in their robot's designs.

During this research all the design parameters and specifications have been adopted from the physical prototype of the robot, all the calculations and simulations have also been done on the experimentally measured physical model of the robot.

Another aim of this research was to make the robot mechanically efficient. This has been achieved by finding an efficient (lower mechanical power) healthy gait and adopting its motions to the robot to follow.

The heavy active actuation system has to be able to carry a heavy user along the entire weight of the robot itself, so the user not to have the need to spend lower energy. This research focused on lowering the power requirements, weight and size of the active actuation system by using energy storage and release system where possible (passive actuation).

Combination of a light, anthropomorphic, durable and powerful exoskeleton would be able to provide up to 100% assistant to its user while reduce its user's metabolic energy cost.

Acknowledgment

I would like to take this opportunity to thank everyone who helped and supported me throughout my PhD study.

I offer my sincerest gratitude to my supervisor professor Abbas Dehghani for his tireless support, encouragement and guidance throughout the entire PhD study, his belief in me has given me the motivation to tackle all the challenges and obstacles on the way.

I am grateful to my PhD fellow Sina Firouzy, Thomas McGill, Pouyan Mehryar and all the participants who truly contributed to this work and their effort and kindness will always be with me, I have learnt a great deal from all these amazing people and I wish all success in their professional and personal life.

I must thank my parents who have been a constant source of inspiration for me. They have provided me with values that rank high in morals and character. I am especially grateful to my number one role model in life my true inspiration, my brother Dr Amir Fazeli who has supported me in every way possible during life, without my family support this would not have been possible.

Contents

Abstract	iii
Acknowledgment	v
LIST OF FIGURES	xii
LIST OF TABLES	xviii
List of Abbreviations	xix
List of Publications	xx
Chapter 1 Introduction	1
1.1 Background	1
1.2 Motivation	5
1.3 Research Aims and Objectives	7
1.3.1 Aim 7	
1.3.2 Objectives	7
1.4 Contribution of this research	8
1.5 Organization of the Report	9
Chapter 2 Literature Review	12
2.1 Introduction.....	12
2.2 Biomechanics of human gait cycle	13
2.2.1 Power distribution at the joints during gait.....	14
2.2.2 Biomechanical specifications of human and gait.....	16
2.2.3 Joint Power & Moment of the Gait Cycle	17
2.2.4 Range of Motion of human during the gait cycle	19
2.3 Biomechanical and physiological design considerations	20
2.3.1 The Ankle	21
2.3.2 The HIP joint.....	21
2.3.3 The knee joint.....	22
2.3.4 The human elbow	22
2.3.5 The shoulder joint.....	22
2.4 Metabolic effect of forces applied to the human	23
2.5 Biomechanics as a design tool in existing design.....	24

2.6 Physiological knowledge relating to exoskeleton design	25
2.6.1 The relationship between the mechanical and metabolic power consumptions.....	25
2.6.2 Relation between joint work and muscle work.....	25
2.6.3 Relating mechanical energy to metabolic energy.....	26
2.6.4 Physiological considerations in leg swing motion to reduce the metabolic expenditure	27
2.6.5 Physiological considerations during stance phase to reduce the metabolic expenditure	27
2.6.6 Physiological consideration as a design tool	28
2.7 State of the art projects	29
2.7.1 Hybrid Assistive Limb	32
2.7.2 BLEEX.....	35
2.7.3 Re Walk.....	36
2.7.4 eLEGS.....	38
2.7.5 Vanderbilt Exoskeleton.....	39
2.7.6 Lower Extremity Powered Exoskeleton	40
2.8 Existing passive exoskeletons.....	41
2.8.1 Passive ankle exoskeleton	41
2.8.2 XPED2	42
2.8.3 MIT Exoskeleton	44
2.9 Design approaches on active actuation system selection	46
2.9.1 Joint Torques	46
2.9.2 Motion Velocity and Bandwidth Considerations	47
2.10 Mechanical Design Challenges	48
2.10.1 Actuation design challenges.....	49
2.10.2 Mechanical design	49
2.10.3 Power supply.....	50
2.10.4 Energy expenditure	50
2.11 Summary.....	51
Chapter 3 Analysis of human locomotion and exoskeleton frame requirements	53
3.1 Introduction	53
3.2 CGA's kinematic as inputs of the exoskeleton dynamic simulation ..	54
3.3 Visual 3D human model and inverse dynamic method	56
3.3.1 Assumption and key concepts.....	56
3.4 Inverse kinematic global optimization used in visual 3D.....	58

3.5 Motion capture experiments	59
3.5.1 Purpose of the Study	60
3.5.2 Participants	60
3.5.3 Materials.....	61
3.5.4 Methods	61
3.6 Human model experimental and simulation methods.....	63
3.6.1 Subjects marker and sensing placement and experimental measurement.....	63
3.6.2 Qualisys marker recognition (position data capture)	64
3.6.3 Visual3D static model.....	65
3.6.4 Visual 3D numerical human model.....	65
3.6.5 Visual3D inverse dynamic Gait.....	67
3.6.6 The Filter	68
3.7 Results of healthy human experiment for clinical gait analysis.....	68
3.7.1 Ankle Joint.....	70
3.7.2 Knee joint	73
3.7.3 Hip joint	75
3.8 Summary	81
Chapter 4 Selected human degrees of freedom focusing on their physiological efficiencies during human gait	82
4.1 Introduction:.....	82
4.2 Methods	83
4.2.1 Subjects	83
4.2.2 Sampling Reliability	84
4.2.3 Procedure.....	84
4.2.4 Data Collection and extraction	86
4.3 Mechanical Restrictions on Joints	88
4.5 Effect of the weight of the braces on metabolic cost of the users.....	91
4.6 Results	91
4.6.1 Statistical Analysis.....	94
4.7 DSummary	95
4.8 Summary.....	98
Chapter 5 Clinical gait analysis comparison in finding the most efficient gait.....	99
5.1 Introduction.....	99
5.2 Method	100

5.3 Results	101
5.3.1 Ankle joint mechanical power consumption.....	101
5.3.2 Knee joint	106
5.3.3 Hip joint	109
5.4 Reaction forces measured during various walking speeds.....	115
5.5 Discussion.....	117
5.6 Summary.....	120
Chapter 6 Exoskeleton model building	121
6.1 Introduction	121
6.2 Simulation setup and assumptions.....	122
6.2.1 Rigid body	122
6.2.2 Fixed part	122
6.2.3 Moving parts & joints.....	122
6.2.4 Motion motors in dynamic simulation	123
6.2.5 Gravity and external forces	124
6.3 Theory ADAMS solver.....	124
6.4 Simulation of inverse kinematics of the exoskeleton carrying human.....	126
6.4.1 Exoskeleton experiment for the purpose of 3D model building.....	126
6.4.2 Experimental procedure	127
6.5 Linear velocity motion motors for solving the inverse kinematics of the exoskeleton model.....	130
6.6 Rotary velocity motors for solving the inverse dynamics of the exoskeleton model.....	133
6.7 Summary.....	136
Chapter 7 Exoskeleton active actuation parametric design	137
7.1 Introduction	137
7.2 Most efficient exoskeleton mechanical power consumption	138
7.3 Comparison of exoskeleton and healthy human kinematics.....	140
7.3.1 Ankle angular displacement-human vs robot	141
7.3.2 Knee angular displacement human vs robot	143
7.3.3 Hip angular displacement-human vs robot	144
7.4 Velocity results	147
7.5 Robot's joint power requirements.....	149
7.5.1 Ankle joint power	149
7.5.2 Knee joint power	150

7.5.3 Hip joint power.....	151
7.6 Comparison of healthy human and exo joints power consumption	156
7.6.1 Ankle Joint.....	156
7.6.2 Knee Joint	158
7.6.3 Hip Joint	159
7.7 Parametric design of the active actuation and gear system	161
7.8 Summary	166
Chapter 8 Exoskeleton passive system parametric design (energy storage and release)	168
8.1 Introduction.....	168
8.2 Torsional spring design	169
8.2.1 Joint stiffness.....	170
8.3 Joint damping.....	171
8.3.1 Translational damper.....	171
8.4 Optimization method used for parallel elastic actuator	172
8.5 Passive (spring and dampers) and active (motors) system simulation model.....	173
8.6 Results	175
8.6.1 Ankle flexion/extension.....	175
8.7 Hip rotation.....	180
8.7.1 Hip Abduction/adduction	184
8.8 Spring parametric design	186
8.8.1 Results with active system and spring weight included.....	187
8.8.2 Ankle	188
8.8.3 Hip rotation.....	188
8.8.4 Hip abduction/adduction.....	189
8.9 Discussion.....	190
8.9.1 Ankle flexion/extension.....	190
8.9.2 Hip Joint	191
8.9.3 Passive system energy saving contribution.....	195
8.10 Summary.....	197
Chapter 9 Summary, conclusions and future work.....	198
9.1 Summary and assessment of the research objectives	198
9.2 Conclusions.....	201
9.3 Future work	206

List of References	207
APPENDICES.....	215
A. Visula3D Solver and methodology	215
B. ADAMS solver and methodology	215
C. Active actuation system design and specification	215
Appendix A	216
A.1 Visual 3D solver	216
A.1.1 Inverse dynamics used in visual 3D.....	217
A.1.2 König theorem kinetics.....	218
A.1.3 Measurement of external work.....	220
A.1.4 Computation of internal work	221
A.1.5 Solving nonlinear equations. (The Newton Raphson Method).....	223
A.1.5.1 Newton like method	223
Appendix B	225
B.1 Generalised coordinates used in ADAMS.....	225
B.2 Joints in ADAMS	226
B.2.1 Motions in ADMAS.....	228
B.2.2 Initial condition analysis	228
B.3 Kinematic analysis position, velocity and acceleration.....	231
B.3.1 Dynamic analysis using motion solver	232
B.3.2 Equations of motions	233
Appendix C	235
C.1 Electric motor system design and specification.	235
C.2 Planetary gear system design and specification.....	238

LIST OF FIGURES

Figure 2.1 Detailed classification of human gait cycle (Perry J 2010)..	13
Figure 2.2 Power generation at the joints during the human gait cycle(Walsh et al., 2006b).....	16
Figure 2.3 The six fundamental models of synovial joints (a) condyloid joint (b) ball and socket joint (c) pivot joint (d) hinge joint (e) planar joint (f) saddle joint (Moeslund et al.,).	20
Figure 2.4 Metabolic Cost Behaviour against the Speed(.....	23
Figure 2.5 Examples of HAL 5 and HAL3 as manufactured products (CYBERDYNE, 2017). a) HAL5 full body exoskeleton b) HAL3 lower body exoskeleton.....	33
Figure 2.6 HAL therapy (CYBERDYNE, 2017) a) subject using HAL therapy b) wall mounted , railing assisted HAL during operation c) subject capable of keeping a seated posture d) subject capable of standing by aid of a walker e) subject capable of walking by aid of a walker	34
Figure 2.7 HAL fit therapy (CYBERDYNE, 2017) a) gait training in combination with a walker b) gait training in combination with a lifter	34
Figure 2.8 BLEEX Exoskeleton(Zoss et al., 2006) a)BLEEX close to finish product with cover, carrying backpack load b) BLEEX prototype mechanical design with engine and payload at the back c) BLEEX joint and hydraulic actuation system	35
Figure 2.9 BLEEX Combustion Engine (Raade et al., 2005).....	36
Figure 2.10 Brake Down of ReWalk Exoskeleton (walking, 2013)	38
Figure 2.11 eLEGS Exoskeleton (bionics, 2017).....	39
Figure 2.12 Vanderbilt Exoskeleton (Farris et al., 2012).	40
Figure 2.13 LOPES Exoskeleton (Veneman et al., 2007).....	41
Figure 2.14 Passive ankle exoskeleton mechanism (Ishikawa et al., 2005).....	42
Figure 2.15 XPED2 artificial tendon exoskeleton design (Wang et al., 2011).....	43
Figure 2.16 MIT Quassi passive exoskeleton (Walsh et al., 2007).....	44
Figure 2.17 MIT Quassi passive exo suit leg model (Walsh et al., 2007).....	45
Figure 3.1 Segment arrangement in visual3D (.....	57
Figure 3.2 Force arrangement	57
Figure 3.3 motion capture experiment a) Front view marker and sEMG placement b) Back view marker and sEMG placement.....	63
Figure 3.4 Qualisys motion capture recognition	64

Figure 3.5 Visual 3D static human model marker recognition	65
Figure 3.6 Visual 3D human model static position.....	66
Figure 3.7 Visual 3D human model during walking simulation on the force platforms over one gait cycle.....	67
Figure 3.8 Block diagram representation of the inputs to parametric design of the robot.....	69
Figure 3.9 Ankle flexion/extension angular displacement for one complete gait	71
Figure 3.10 Captured and simulated CGA data of ankle flexion/extension angular displacement for one gait.....	71
Figure 3.11 Ankle inversion/eversion angular displacement	72
Figure 3.12 Ankle inversion/eversion collected and simulated CGA data for one gait	73
Figure 3.13 Knee flexion/extension angular displacement	74
Figure 3.14 Knee flexion/extension angular displacement, captured and simulated CGA data.....	74
Figure 3.15 Hip flexion/extension angular displacement data.	76
Figure 3.16 Hip flexion/extension angular displacement, captured and simulated CGA data.....	76
Figure 3.17 Hip abduction/adduction angular displacement data	78
Figure 3.18 Hip abduction/adduction CGA, captured and simulated data.....	78
Figure 3.19 Hip internal/external rotation angular displacement over one gait	80
Figure 3.20 Hip internal/external rotation angular displacement capture and simulated CGA data.....	80
Figure 4.1 metabolic power consumption during unlocked mode and restricted modes through all subjects during the following modes: unlocked (UL), shoulder abduction/adduction (SAA), shoulder flexion/extension (SFE), hip abduction/adduction (HAA), hip rotation (HR), elbow flexion/extension (EFE), ankle inversion/eversion (AIE)	93
Figure 5.1 Ankle flexion/extension power consumption for one gait from literature (Margareta nordin 2001)	102
Figure 5.2 Ankle flexion/extension power consumption from captured and measured CGA data	103
Figure 5.3 Ankle flexion/extension joint torques from captured and simulated CGA data	104
Figure 5.4 Ankle inversion/eversion power consumption from captured and simulated CGA data.....	106

Figure 5.5 Knee joint flexion/extension power consumption from the literature data (Margareta nordin 2001).....	107
Figure 5.6 Knee joint flexion/extension power consumption captured and simulated from CGA data.....	108
Figure 5.7 Knee joint flexion/extension torque captured and simulated from CGA data	108
Figure 5.8 Hip joint flexion, extension power consumption from the literature (Margareta nordin 2001)	110
Figure 5.9 Hip joint flexion/extension power consumption from captured and simulated CGA data.....	110
Figure 5.10 Hip joint flexion extension torque from captured and simulated CGA data	111
Figure 5.11 Hip joint abduction/adduction power consumption from captured and simulated CGA data.....	113
Figure 5.12 Hip joint internal/external rotation power consumption from captured and simulated CGA data.....	114
Figure 5.13 Force platform collected data (N) against the time(s) over 5 trials at 3 different speeds during the stance and swing phases.....	116
Figure 5.14 Metabolic power consumption vs speed.....	119
Figure 6.1 ADAMS motor solver iteration method.....	125
Figure 6.2 Exoskeleton shoe, ankle and knee motion capture experimental setup front view.....	127
Figure 6.3 Exo shoe and ankle motion capture experimental setup side view Red arrow: position of the inversion/eversion ankle marker Purple arrow : position of the flexion/extension ankle marker	128
Figure 6.4 Exoskeleton knee and hip motion capture experiment back view Red arrow : position of the inversion/eversion hip marker green arrow : position of the internal/external rotation hip marker Orange arrow : position of the flexion/extension hip marker Purple arrow : position of the flexion/extension knee marker	129
Figure 6.5 Linear position motion motors, inputted from captured experimental positions in all planes for solving inverse kinematic simulation of the exoskeleton gait a) Isometric view of the inverse kinematic simulation b) Side view of the inverse kinematic simulation.....	132
Figure 6.6 Rotary angular velocity motion motors to solve inverse dynamics input from forward kinematic results a) Back view inverse dynamic motion motors b) Side view inverse dynamic motion motors	135

Figure 7.1 The power consumption simulated for the exoskeleton according to the subjects angular velocities at the sagittal plane joints of ankle, knee, and hip.	139
Figure 7.2 Ankle flexion/extension angular displacement from exo and human CGA data	141
Figure 7.3 Ankle inversion eversion angular displacement from exo and human CGA data	142
Figure 7.4 Knee flexion extension angular displacement from exo and human CGA data	143
Figure 7.5 Hip flexion/extension angular displacement from exo and human CGA data	144
Figure 7.6 Hip abduction/adduction angular displacement from exo and human CGA	145
Figure 7.7 Hip rotation angular displacement from exo and human CGA	146
Figure 7.8 Exoskeleton stance ankle flexion/extension power consumption	149
Figure 7.9 Exoskeleton swing ankle flexion/extension power consumption	150
Figure 7.10 Exoskeleton stance knee flexion/extension power consumption	150
Figure 7.11 Exoskeleton swing knee flexion/extension power consumption	151
Figure 7.12 Exoskeleton stance hip flexion/extension power consumption	152
Figure 7.13 Exoskeleton swing hip flexion/extension power consumption	153
Figure 7.14 Exoskeleton stance hip abduction/adduction power consumption	153
Figure 7.15 Exoskeleton swing hip abduction/adduction power consumption	154
Figure 7.16 Exoskeleton stance hip rotation power consumption	155
Figure 7.17 Exoskeleton swing hip rotation power consumption	155
Figure 7.18 Ankle flexion/extension power consumption comparison healthy human vs robot during one gait cycle	157
Figure 7.19 Knee flexion/extension power consumption comparison healthy human vs robot during one gait cycle	158
Figure 7.20 Hip flexion extension power consumption comparison healthy human vs robot during one gait cycle	159
Figure 7.21 Hip abduction/adduction power consumption comparison healthy human vs robot during one gait cycle	160

Figure 7.22 Hip rotation power consumption comparison healthy human vs robot during one gait cycle.....	160
Figure 7.23 Performance curve of the selected servo motor SMH60 series (Kinavo.....	163
Figure 7.24 Maxon-GPX45 Performance Curve	164
Figure 7.25 Specified and motor performance (torque vs speed) curves.....	165
Figure 8.1 Passive system inverse dynamic simulation to find new actuation system requirements a) Initial swing inverse dynamics with spring and actuation system b) Mid swing inverse dynamics with spring and actuation system c) Terminal stance inverse dynamic with spring and actuation system	174
Figure 8.2 Exoskeleton ankle flexion/extension stance phase displacement springs, Exo ankle flexion/extension stance phase power consumption with and without passive system, Exo ankle flexion/extension stance phase Torque vs angular displacement (joint stiffness).....	176
Figure 8.3 Exoskeleton ankle flexion/extension stance swing phase displacement springs, Exo ankle flexion/extension stance swing phase Torque vs time without passive system, Exo ankle flexion/extension stance swing phase Torque vs angular displacement (joint stiffness).....	178
Figure 8.4 Exoskeleton hip rotation swing phase displacement springs, Exo hip rotation swing phase power consumption with and without passive system, Exo hip rotation swing phase Torque vs angular displacement (joint stiffness).....	181
Figure 8.5 Exoskeleton hip rotation motor torque vs time, stance+swing with and without springs, exo hip rotation angular displacement vs time, stance+swing phase	183
Figure 8.6 Exoskeleton hip abduction/adduction angular displacement vs time ,stance swing phase (m/s) spring, exo hip abduction/adduction stance+ swing phase power torque vs time with and without passive system, exo hip abduction/adduction stance+ swing phase torque vs angular displacement.	185
Figure 8.7 Spring drawing of the torsional springs provided by JB Springs Ltd.	186
Figure 8.8 Ankle power consumption with weight of the springs included	188
Figure 8.9 Hip rotation power consumption with weight of the springs included	189
Figure 8.10 Hip aa (abduction/adduction) power consumption with weight of the springs included	189
Figure 8.11 Exoskeleton stance ankle power consumption vs time with and without passive system	191

Figure 8.12 Exoskeleton stance hip abduction/adduction power consumption vs time with and without passive system.....	192
Figure 8.13 Exoskeleton swing hip abduction/adduction power consumption vs time with and without passive system.....	193
Figure 8.14 Exoskeleton stance hip rotation power consumption vs time with and without passive system	193
Figure 8.15 Exoskeleton swing hip rotation power consumption vs time with and without passive system	194
Figure 0.1 local coordinate system Defines location of centre of mass b) proximal forces and torques due to inertia and joints c) External forces and couples	218

LIST OF TABLES

Table 2.1 maximum joint powers (Margareta nordin 2001).....	17
Table 2.2 Produced Moments at the Lower Limb Joints	18
Table 2.3 Angular Movement for biological Hip, Knee and Ankle (.....	19
Table 2.4 Design specification of existing state of the art exoskeletons	30
Table 2.5 (Cont.)	31
Table 3.1 Visual 3D numerical inputs for human model	66
Table 4.1 The mechanical restrictions used for lower extremity	89
Table 4.2 The mechanical restrictions used for upper extremity.....	90
Table 4.3. Average power consumption (J/kg) values collected for all 5 participants during the 3 repeats.....	92
Table 4.4 Percentile increase/decrease of metabolic expenditure restricted compared to unrestricted.....	94
Table 5.1 Ankle joint flexion/extension absolute power consumption, absolute torque consumption, average velocity from captured and simulated CGA data.....	105
Table 5.2 Knee joint flexion/extension absolute power consumption, absolute torque and, average velocity from Captured and simulated CGA data	109
Table 5.3 Subjects absolute power consumption, peak torque, and average velocity	112
Table 5.4 Positive mechanical power consumption, positive work efficiency, metabolic cost rate of various subjects at different speeds.....	118
Table 5.5 Absolute power consumption at lower limb joints from captured and measured CGA data	120
Table 6.1 Percentage weight of human body segments (Leva, 1996).	134
Table 7.1 Human Vs Exo angular velocities in the sagittal plane	148
Table 7.2 Active system design requirements output at the joints of the exoskeleton	161
Table 7.3 Active system design requirements-motor	162
Table 7.4 Active system design specifications-gear.....	163
Table 8.1 Detailed design specifications of the torsional springs for all selected passive joints	187
Table 8.2 Efficiency of the passive system from kinetic data simulated	196

List of Abbreviations

AART	Assistive Adaptive Rehabilitative Technologies
ADL	Activities of Daily living
ALS	Amyotrophic Lateral Sclerosis
CAD	Computer Aided Design
CGA	Clinical Gait Analysis
DOF	Degree of Freedom
EMG	Electromyography
HAL	Hybrid Assistive Limb
QTM	Qualisys track manager
RPE	Rating of Perceived Exertion
SCS	Segment Coordinates System

List of Publications

A poster presentation:

A.Fazeli, A.Deighani, R.Richardson, C.Ferguson "A novel Assistive Exoskeleton Design Approach on Selecting the Optimum Number of degrees of Freedom to Minimize the Metabolic Cost Rate of the User", MEIBioeng/MPEC 2015, IPEM (institute of physics and Engineering in Medicine) conference.

Due to confidentiality agreement with this projects industrial partner (Mecha Tech Ltd) following journal papers are under preparation and need to be approved before submission:

" A novel Design Approach on Selecting the Optimum degrees of Freedom for an Assistive Exoskeleton, to minimize the Metabolic Cost Rate of the User by measuring the effect on the cost rate of the human walking at moderate speed while restricting the ranges of movement of the selected joints"

"A Novel Approach on Active Actuation Parametric Design of an Assistive Exoskeleton to Lower The Metabolic Efficiency of the User"

"An Energetic Efficient Passive Actuation Design for an Active Assistive Exoskeleton by Modelling and Experimental Techniques"

Chapter 1

Introduction

1.1 Background

This research is aiming to design an exoskeleton that could benefit patients with lower limb difficulties and lower limb muscular and neural diseases along with ageing population to regain independence in accomplishing the most important activities of daily living (ADL). During the ADL, the human body constantly becomes subject to external and internal forces and stresses, the magnitude of which vary depending on the nature of the ADL. The wear build up caused by these forces in time causes the ageing population to struggle in performing activities of daily living. Other factors such as diseases and genetic imperfections, also cause patients lower limb difficulties and disabilities.

Other causes of limitations of human physical performance include specific diseases and illnesses that attack the human limbs and nervous systems. One of the most popular types of such diseases is called ALS (Amyotrophic Lateral Sclerosis). Research has revealed that this disease is common in 2 out of 100,000 people. The disease is not limited to the race or location and can affect any person from any race or background. ALS affects the brain cells and the nervous systems of the human body at the first stage, and eventually attacks the spinal cord, and will leave the patients with no physical ability to move their limbs (Walling, 1999)

Another similar common disease is called motor neuron disease. The effect of this disease is similar to the ALS and the percentage of the population that is affected by it is also similar to that of the ALS. A study shows that about 2 in every 100,000 are affected, and that there are around 5000 patients who suffer from motor neuro disease just in the UK. The ALS disease affects the nervous system of the brain and the spinal cord, which causes the patients to lose their limbs motor function (Boillee et al., 2006). Furthermore, stroke can cause loss of motor functions. A recent study in the United States has

discovered that around 4.7 million patients are suffering from such disabilities (Dollar and Herr, 2008).

Other surveys show diseases such as post-polio, sclerosis and cerebral palsy affect around 800,000 just in the United States (Nerri, 2010).

The research on the exoskeletons could be divided into three main groups in the field of robotics, namely Assistive, Adaptive and Rehabilitative Technologies.. patients with no lower limb ability are the users of rehabilitative systems, while the enhanceive technology user's do not suffer from any disabilities and the robot is aiming to enhance their natural abilities further. The assistive robot would provide some level of assistance up to 100% to their users, thus the user might have some level of ability but below the natural required amount to accomplish their ADL tasks without need of any external assistants. The assistive technologies are the main focus of this research. Some of the exoskeleton projects mentioned in the literature review section of this report are enhanceive and rehabilitative devices, but are still mentioned in this report due to the similarities in the mechanical design between the above-mentioned AART technologies. Chapter 2 of this report reviews the various robotic exoskeleton designs in the existing and successful projects.

It is essential for the assistive devices to follow and support the human body, and for the design to be anthropomorphic, as the main application if the device is to carry the supported limbs of the human. The actuation system in the assistive devices needs to generate enough power to carry the weight of the exoskeleton as well as that of the user, as the users of such devices do not have the ability to carry their own limbs. Thus, it is important to optimize the design to achieve a low-weight device, so that power is conserved. The heaviest sections of an assistive exoskeleton are the joints (degrees of freedom) of the device, especially in cases of direct drive motors.

The history of exoskeleton goes back to 1960 when General Electric's invested in making a prototype of an enhanceive exoskeleton that was capable of lifting up to 680kg. The name of the prototype was Hardiman. The project, which was the first of its kind in the field of the exoskeletons, the Hardiman project faced many serious obstacles such as the issues caused by the large weight and size, as well as the control and applications of the exoskeleton. But it

revealed the need for research on many aspects of the involved technologies in this field (Dollar and Herr, 2008).

There are many research projects being conducted in the field of the exoskeletons as mentioned in State of the art projects of the literature review in this report, but there are not many exoskeletons in the mass production stages, due to various design fails such as functionality and cost. One of the main available assistive exoskeleton devices in the market is HAL, this device was built by CYBERDYNE, a Japanese company that has introduced two variations of this exoskeleton. The first variation is called HAL3 which is a lower limb assistive exoskeleton, and the second device is called HAL5 which is a full body exoskeleton. The HAL exoskeletons are available for rent in the Europe, Canada and the United States(CYBERDYNE).

Some research in the field of exoskeletons was carried by Professor Kazerooni in the University of Berkeley of United States; the most prominent Berkley project is called BLEEX. The BLEEX has two variations of the device, one is enhance and the other is rehabilitative with use of pre gate control algorithm. (Kazerooni, 2006)

The research reported in this thesis is based on identifying a gap in design of the exoskeleton frame and design requirements used for the active and passive system in the field. As pointed by (Yan et al., 2015) in one of the most recent exoskeleton published reviews, the existing designs have not taken into consideration factors such as, their exoskeleton's metabolic effect on the user caused by external forces from the robot. The existing designs use assumptions and underestimated human collected gait analysis kinetic and kinematic data as specifications in design of their actuation systems, joint and chassis and other hardware.

The mentioned assumptions are not valid due to differences in mechanical properties between the human and the exoskeleton (geometry, moment of inertias, and etc..), along with other factors such as miss alignment between the human joint and the exoskeleton joint, and lack of design in non-sagittal plane degrees of freedom, which have caused many of the existing designs to be inefficient once the prototypes have been tested.

This research has aimed to provide a quantitative method to select the exoskeleton's degrees of freedom by means of biomechanical and metabolic methods, as well as an accurate model of the exoskeleton's dynamics while following the kinematics of the healthy human by means of experimental and simulation methods. The research then investigates into making the actuation design more efficient and feasible by using energy storage and release mechanisms looking at 14 degrees of freedom.

1.2 Motivation

This study has been initiated by an industrial sponsor with the purpose of developing a modular exoskeleton as a marketable product. Several factors contribute to the desirability of a modular exoskeleton, which are explained in the following paragraphs.

The purpose of an assistive exoskeleton is to carry the limbs of the user, and therefore, lower the metabolic cost of ADLs as compared to the case when the user is not wearing the exoskeleton. Assistive and rehab devices share this purpose, but their difference is that the users of assistive devices have some muscle functions which allow them to be the pilot of the device, whereas in case of rehab devices, the controller of the device works based on a pre-defined gait (Walling, 1999). This work is focusing on providing 100% assistance to the user inside, as this would consider the worst case to match with the ability of a healthy human gait.

The assistive exoskeleton which will be developed in this project should be designed in a way that allows the user to do ADLs without causing any discomfort or putting the user at any risks. The other goal is to have a good user interface and an untethered device that could be used in home environment and potentially outdoors. One of the most important factors in the mechanical design and performance of the exoskeleton is the number of degrees of freedom used in the system. Assistive devices need to have control of all their degrees of freedom as this cannot be done by the users with low muscle abilities. The control of degrees of freedom can be done by active actuations such as DC motors, hydraulic or pneumatic systems. The other method to control the designed degrees of freedom is by using passive elements such as springs and dampers. Depending on the generated torque needed the control method will be decided.

Actuation systems are typically the heaviest hardware in the exoskeleton joint, thus the actuation design has a significant effect on the efficiency, functionality and safety of the robot. It is important to efficiently choose the active and passive degrees of freedom of the robot, without sacrificing the comfort and safety of the user. Less critical degrees of freedom are preferred to be

excluded from the design in order to minimise the weight of the exoskeleton. To find out the optimum number of degrees of freedom for the assistive device, it is essential to investigate the human degrees of freedom efficiency in terms of mechanical and metabolic power produced. For this purpose full kinematic and kinetic investigations have been done on the human and the exoskeleton models. The healthy human kinematics was chosen to be the map for the exoskeleton's joints motion to follow.

It is also important to study the power consumption of the body as one entity, and investigate the efficiency of individual degrees of freedom as well as a quantitative method in setting efficiency standard for selecting an efficient healthy human gait, to be used for the exoskeleton dynamic analysis, and passive and active actuation selections.

1.3 Research Aims and Objectives

In this section the overall aims and objectives of the project are explained.

1.3.1 Aim

The aim of this project is to design an energetic (metabolic) efficient assistive robotic exoskeleton, while improving the mechanical performance of the robot.

1.3.2 Objectives

To achieve the aim of the project, the following objectives need to be accomplished:

- Analysis of human locomotion and exoskeleton frame requirements;
- Investigation on metabolic efficiency of individual degrees of freedom as a design approach for selecting the exoskeleton's degrees of freedom;
- Systematic selection of efficient human kinematic parameters for the robotic exoskeleton to follow;
- Building a full model of the exoskeleton with chosen degrees of freedom in all planes for the purpose of performing exoskeleton parameters calculations;
- A dynamic analysis on exoskeleton's kinematics and kinetics to design the active actuation system required for the robot;
- A dynamic analysis to design the passive system (energy storage), to reduce the active system requirements;

1.4 Contribution of this research

The novel contribution of this research can be summarised as:

- Developing a quantitative biomechanical and physiological design method for selecting exoskeleton's most efficient degrees of freedom.
- Using analysis of healthy human locomotion with focus on determining the efficient locomotion to be duplicated to the kinematics of the exoskeleton gait cycle.
- Building a precise full degree of freedom dynamic model of the exoskeleton with 14 degrees of freedom in all planes by a combination of experimental and simulation methods.
- Full design specifications and dynamic analysis of the actuation systems by using a precise model of the exoskeleton while carrying the user inside, which is controlled by inputting any desirable healthy human gait data at the joints axes.
- Full design specifications and dynamic analysis of passive actuation system (springs and dampers) with focus on increasing the efficiency of the active actuation system and lowering the motor sizes and active power requirements.

1.5 Organization of the Report

This thesis is divided into nine chapters.

Chapter 2 includes a review of the literature and of the existing projects, the aim of this chapter is to provide information about the existing designs as much as possible which found to be not vastly available. The chapter also presents the required background information on the biomechanics of the human body and the biomechanics use as a design tool. The biomechanics investigation continues into human and robot interface and physiological methods such as VO₂ measurements as a precise method of determining the exoskeletons efficiencies and performance. Other parts are aiming to identify the gap in the design procedure of the existing exoskeletons and how this research can contribute to this field mentioned in the discussion section.

Chapter 3 starts the design procedure by analysing the human locomotion using experimental measurements, and inputting the captured kinematics into a virtual human model to perform the inverse dynamic simulation. The study aimed to have full kinematic and kinetic parameters of the human walking. The results of the work, reported in chapter 3, have been verified by the existing literature data.

Chapter 4 presents a novel methodology in determining the human degrees of freedom efficiency in preliminary design stage, by using experiments measuring the gas expenditure of users while mechanical restrictions have been applied to individual degrees of freedom of the joints and comparing every subject to when they walked free of any restrictions. The gas measurements were found to be one of the most accurate methods of determining the human overall power consumption. The results did have a clear outcome and justification on selection of the exoskeleton's degrees of freedom.

Chapter 5 focuses on analysing the kinematic data collected with the aim of determining the most efficient gait as reported in chapter 3, of the healthy human within the study. This chapter provides the detail kinetic analysis of 5 subjects by using the developed human model. The kinetics results show the power consumption at each joint and the overall mechanical power

consumption of the activity for all 5 subjects. This chapter also investigates the metabolic effect of gait with various speeds, this is done by using metabolic measurement techniques experimentally. The aim of this chapter is to identify the subject with an efficient gait as a typical example. The kinetic data from this subject would be the input for the simulation work in chapter 7.

The focus of chapter 6 is on the set up of the exoskeleton simulation. To achieve the most precise design specifications of the exoskeleton active and passive actuation system, the first prototype of an assistive exoskeleton was built at the University of Leeds with 14 degrees of freedom. The prototype then was worn by a healthy subject in an experiment in the motion capture laboratory at the University of Leeds to capture the true initial positions and be able to use the experimentally measured position data to perform the forward kinematic and inverse dynamic calculations. The simulations carried out and reported in this chapter provide a dynamic model of the exoskeleton which can then be adapted to any size of the users and can also be driven by any kinematic human inputs from any users at the joints of the exoskeleton.

In chapter 7, the kinematic data from all human participants have been inputted into the exoskeleton simulation and it was verified that the most efficient gait found in chapter 5 from analysis of the human model was also the most efficient gait on the exoskeleton model. Full design specifications can be provided for the active system requirements by inputting the most efficient kinematics found in chapter 5 into the exoskeleton simulation. Chapter 7 also investigates and compares the kinematics of the exoskeleton with the kinematics of the human to verify the performance of the exoskeleton.

Chapter 8 provides an investigation into the stiffness and damping efficiency of the exoskeleton joints looking at all 14 degrees of freedom lower body main joints by using simulation and experimental techniques, the joints for which the spring and damping system are feasible to be used were found, and optimized for torsional springs, the design specification of torsional springs are presented. The simulation of the active and passive systems working together, to lower the power consumption and peak torques of the active system are also covered in this chapter.

Chapter 9 presents a summary of achievements of this research work along with conclusions and suggestions for future work.

Chapter 2

Literature Review

2.1 Introduction

This chapter starts by reviewing the characteristics of state of the art projects in the field of assistive, adaptive and rehabilitation (AART) exoskeletons. The projects which are very promising and have novel designs and approaches are mentioned in the second section of this chapter under the exoskeletons in making. The third section is also dedicated to the existing mechanical design, found from the literature. The final parts of this chapter are discussing the available materials for similar mechanical structures in the material selection section followed by the design approach section that explains methods available to evaluate the approach to a valuable design.

2.2 Biomechanics of human gait cycle

The human gait cycle can be divided into two main phases: stance and swing. The stance phase takes up to 60% of the gait cycle, while the remaining 40% occurs during the swing phase (Swift, 2008).

The gait speed determines the contribution of each body segment, during the normal walking speed, the majority of the work is done by the lower limb joints and pelvis, while the upper body and trunk provides stability and balance for the entire body (Shultz 2005).

A gait cycle consists of repetitive actions of steps and strides. A step time is defined from the moment the foot of the human hits the ground until the time of the other foot's contact with the ground, also a stride is completion of one gait cycle, which consists of two continuous steps (Swift, 2008). A more detailed classification of the gait cycle is shown in

Figure 2.1.

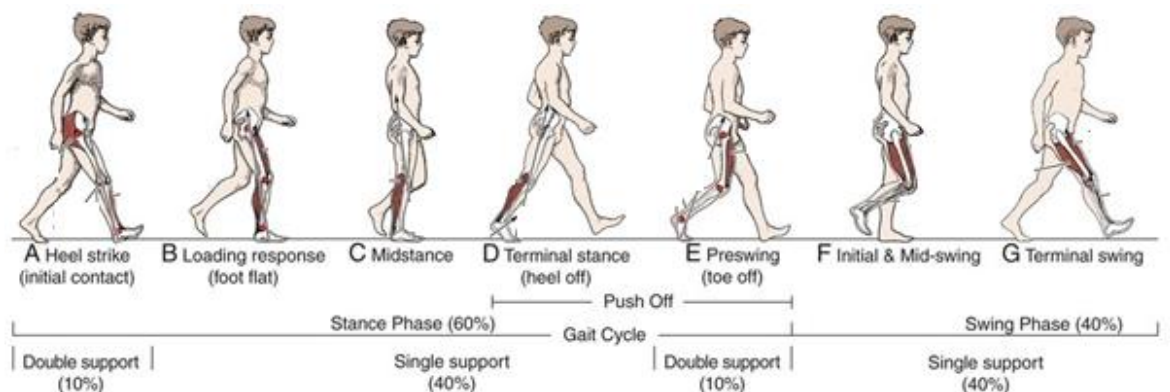


Figure 2.1 Detailed classification of human gait cycle (Perry J 2010).

The stance phase begins at the heel strike, during the initial contact phase. During the heel strike the hip undergoes a flexion of 30° while the knee extends, and the ankle undergoes a plantar flexion of 5° from a neutral position (Shultz 2005). The knee follows into a small flexion of 5° , as the heel the plantar flexion increases (Swift, 2008).

The foot flat stage occurs after the initial contact phase, otherwise known as loading response as shown in

Figure 2.1. At the loading response the hip moves into an extension, while the knee faces a further flexion of up to 15° to 20° (Shultz 2005). At this stage the ankle continues to plantar flexion of around 10° to 15° (Swift, 2008).

The next phase as shown in

Figure 2.1 is mid stance, where the body changes from absorbing the impact from ground reaction forces to force propulsion, causing the body to move forward. At this stage the body is supporting itself only on one leg on the ground. This is done while the knee is reaching its maximum flexion and the ankle is going under a dorsiflexion of 5° (Swift, 2008).

The heel off begins when the heel leave of the ground , while the hip goes under hyper extension between 10° to 13° , the knee flexes up to 5° , and the ankle plantar flexes. During the final stage of the stance phase, the toe off occurs by a knee flexion of 35° to 40° , while the ankle continues plantar flexion up to 20° (Swift, 2008).

In the early swing stage of the swing phase the ankle comes to a neutral position by under taking a dorsiflexion, while the hip and knee respectively flexing to 20° and 40° to 60° . During the mid-swing phase the hip and knee respectively flexes to 30° and 60° , and the ankle carry's on to be dorsiflexed. The swing phase finishes by placing the ankle joint at a neutral position , while the knee is at a locked extension , and the hip goes under final flexion between 25° to 30° ("Swift, 2008", "Shultz 2005").

2.2.1 Power distribution at the joints during gait

During the gait cycle the nature of the power can be negative or positive, negative power is generated during the absorption to resist the gravity force. Positive power is generated in phases were the force is generated to create

the moment to activate the joint and limbs and accelerate. The biggest positive power is generated at the following joints: hip and ankle, during the gait cycle, as shown in Figure 2.2 by (Walsh et al., 2006b)

Figure 2.2 maps the joint by its first capital letter also the radius of the circle is a direct indication of the amount of power generated or absorbed. The generated (positive) power is shown by the red circle, as the absorbed (negative) power is shown by the blue circle.

Figure 2.2 shows the highest power occur terminal stance phase at the ankle pushing the body forward as shown by A2. The biggest negative power consumption is at the hip joint during the same phase of terminal stance, as shown by H2.

The hip joint is mainly responsible for generating the positive power required for the swing phase, as shown in both H1 and H3.

Below H1, H3 and A2 are the largest causes of the positive power during the whole gait cycle. The knee joint is mostly absorbs the negative. The other phases where smaller amount of negative power is generated are the A1 and H2, this is because during these two phases the body of the user tilts forward in the sagittal plane and the gravity is the main cause of this negative power.

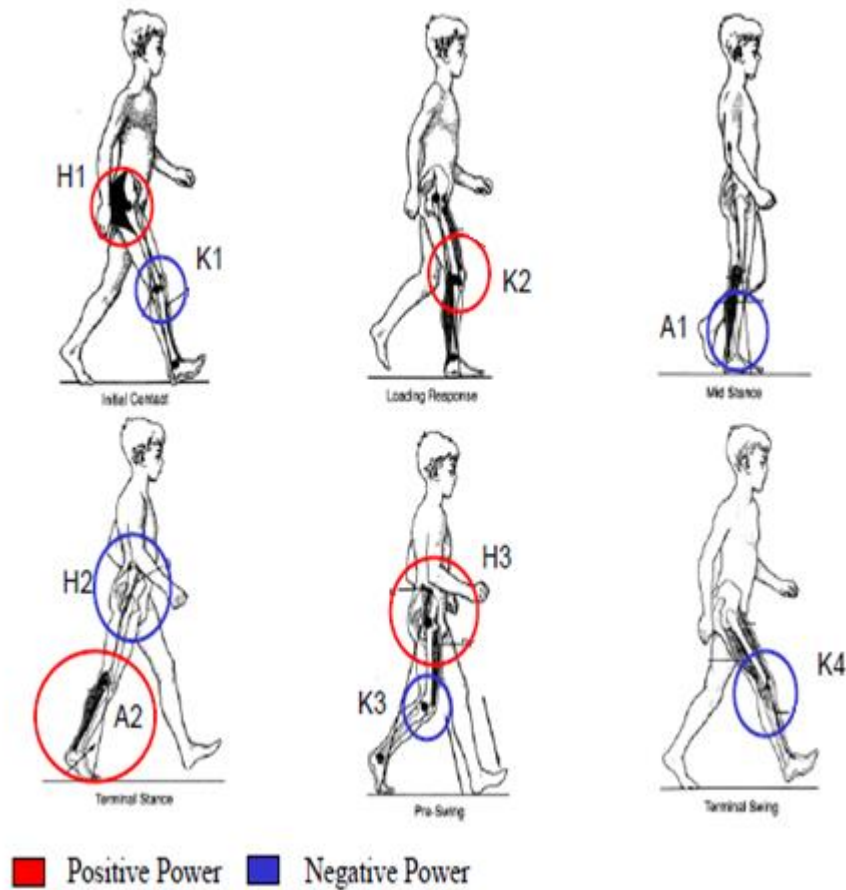


Figure 2.2 Power generation at the joints during the human gait cycle(Walsh et al., 2006b).

2.2.2 Biomechanical specifications of human and gait

2.2.2.1 Segment Densities

The density of a body segment is the combination of the muscle, bone and fat densities, the ratio of these three would vary in different body segments thus the density of the segment would not be uniform. The segment with the higher ratio of bones such as the proximal segments has a higher density in comparison to the distal segments with lower amount of bones. The (de Leva, 1996).provides the segment density data of the human body.

2.2.3 Joint Power & Moment of the Gait Cycle

2.2.3.1 Internal Moments

The resultant of all the forces acting on a joint is called the internal joint moment; the forces could be generated from the muscle as well as other factors such as joint's friction and ligaments. For the calculation of the joint moment the created moments around the joint centre are calculated. This value could be normalised to the user's body mass by adding the body mass and the unit is Nm/Kg.

2.2.3.2 External moments

In case of assistive exoskeleton the biggest and most regular external moment is caused by the ground reaction force. The reaction force is the force exerted from one body to another, the amount of reaction force would be the same as the initial force; the force just has the opposite direction. In case of the assistive exoskeletons during the human gait cycle, the reaction force is consisted of forces caused by the interaction with the user and the exoskeleton foot with the ground.

Table 2.1 maximum joint powers (Margareta nordin 2001).

Maximum Joint Power(Watts)			
Joint	Muscle Group	Walking	Running
Hip	Extensors	0-175	160-660
Knee	Extensors	10-235	210-1050
Knee	Flexors	10-50	-
Ankle	plantar flexors	180-790	550-1580

During walking activity most of the power is generated by the Hip (Extensor, Knee (extensor), Ankle (Plantar, flexor), and possibly on the Hip (Flexor), during running activity most of the power is generated on the Knee (extensor), and Ankle (planter, flexor) this can be seen in Table 2.1 (Margareta nordin 2001).

During walking activity most of the moment is acting on the Hip (Extensor), Knee (extensor), Ankle (Plantar, flexor), and possibly on the Hip (Flexor). During running activity most of the moment is acting on the Knee (extensor), and Ankle (plantar, flexor) , the Maximum moment values supporting this statement is presented in Table 2.2 (Margareta nordin 2001).

Table 2.2 Produced Moments at the Lower Limb Joints (Margareta nordin 2001).

Variable	Plane	Action	Hip	Knee	Ankle
Moment (Nm/Kg)	Sagittal	Extensor	1.15	0.46	1.73
Moment (Nm/Kg)	Sagittal	Flexor	1.1	0.43	0.2
Moment (Nm/Kg)	Frontal	Abductor	1.2	1.1	0.13
Moment (Nm/Kg)	Frontal	Adductor	0.1	-	0.04
Moment (Nm/Kg)	Transverse	Inversion	0.2	0.11	-
Moment (Nm/Kg)	Transverse	Eversion	0.2	0.09	0.1
Power(W/Kg)	Sagittal	Generation	1.8	0.6	4.4
Power(W/Kg)	Sagittal	Absorption	1	1.5	0.5
Power(W/Kg)	Frontal	Generation	0.55	0.18	0.07
Power(W/Kg)	Frontal	Absorption	0.9	0.18	0.12
Power(W/Kg)	Transverse	Generation	0.02	0.04	0.01
Power(W/Kg)	Transverse	Absorption	0.17	0.15	0.02

2.2.4 Range of Motion of human during the gait cycle

The biggest Ranges of movements is at the Knee joint which is a range of 120 degrees , the second biggest range is at the Hip flexion of 110 degrees as shown in Table 2.3.

Table 2.3 Angular Movement for biological Hip, Knee and Ankle (Margareta nordin 2001).

Movement Angle for biological Hip ,Knee and Ankle	
Description	Angle(Degrees)
Hip sagittal plane	95 to -11
Hip coronal plane	5 to -50
Hip transverse plane	20 to -20
Knee sagittal plane	0 to -120
Ankle sagittal plane	30 to -30

As mentioned previously an assistive exoskeleton is in direct interaction with the user at the connection points. An ideal exoskeleton needs to follow the human degrees of freedom as close as possible. In this section of the literature review the degrees of freedom for the lower and upper body limbs are shown in Table 2.3.

2.3 Biomechanical and physiological design considerations

The purpose of an assistive exoskeleton structure is to assist the user to perform desired tasks to the level of a healthy human. Thus it is an exoskeleton design requirement to be anthropomorphic and ergonomic in shape and function.

The positions of the exoskeleton joints have to be as close as possible to the positions of the main human joints. These main joints are the synovial joints. The synovial joints in the human body can be differentiated by number of their degree of freedom. The 6 different types of synovial joints (Tortora, 2006) , are planar, hinge, ball and socket, saddle, pivot, and condyloid joints ,as shown in the Figure 2.3.

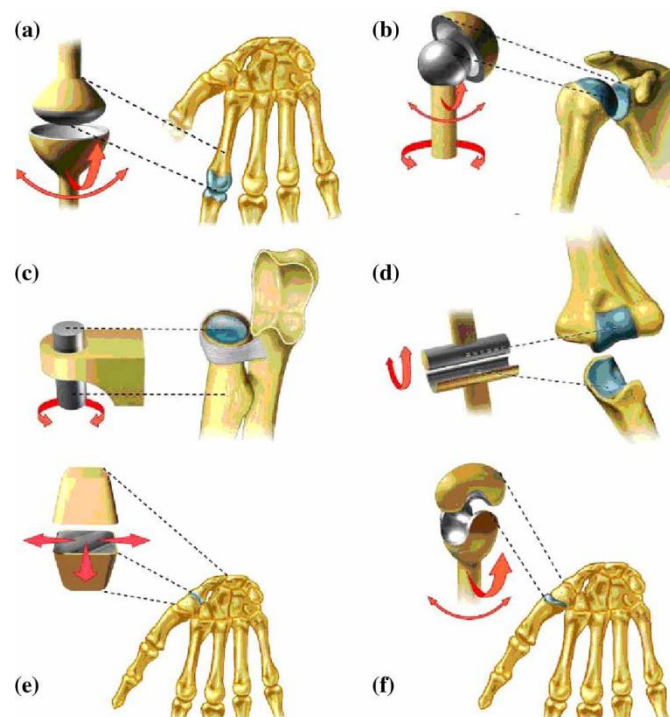


Figure 2.3 The six fundamental models of synovial joints (a) condyloid joint (b) ball and socket joint (c) pivot joint (d) hinge joint (e) planar joint (f) saddle joint (Moeslund et al., 2005).

A healthy human body works as a generator and power house. The human body uses the energy to power the human muscles and ligaments. The muscles then transfer the generated power to the joints and limbs of the human in order to achieve the desired locomotion(Sawicki and Ferris, 2009).

For the exoskeleton to be assisting the lower ability users to match the 100% ability of the healthy human subject it is necessary to have the mentioned energy supply, power generation, structure and degree of freedom as part of the design requirement.

It is also a safety and design requirement for the exoskeleton to provide enough flexibility to its user to move, swing, bend, and moving in sideways, as well as being adaptable to users with different sizes (Cenciarini and Dollar, 2011).

2.3.1 The Ankle

The natural healthy human ankle consists of 3 degrees of freedom; the sagittal plane's movements are the flexion and extension. The transverse plane is where the abduction and adduction occur. The third plane is the coronal plane where the inversion and eversion movements occur. Depending on the task and the purpose of the robot, the designer has to decide which degrees of freedom are necessary to activate (Hong and Chok, 2013).

In the exoskeleton design the foot of the exoskeleton is constructed in a manner to provide the flexibility at the ankle as it can provide ankle inversion eversion as implemented for example in the MIT and BLEEX cases (Zoss et al., 2006, Walsh et al., 2006a).

2.3.2 The HIP joint

The human's healthy natural hip joint can be duplicated by a mechanical ball and socket joint the hip has movements in all three planes including rotational, flexion /extension and abduction/adduction movements.

In the design of the previous exoskeleton(MIT, BLEEX) system's with a hip, the main designed active degree of freedom is flexion/extension (Kazerooni and Steger, 2006).The duplication of this degree of freedom has proven to be simple due to easy alignment of the structure in the sagittal plane to the human user. The design challenge in the exoskeleton hip arises due to adjustability of the human abduction adduction and rotation during the walking and challenging to follow the same kinematic in a rigid structure which will have misalignments and offsets. The designers in MIT (Walsh et al., 2006a) have proposed a CAM mechanism as a solution (Walsh et al., 2006a), and the

designers of the BLEEX (Kazerooni, 2006) have positioned the rotation as part of the flexion extension by having two centres of the flexion extension and rotation joints to move accordingly. Other researchers have LOPES (Veneman et al., 2007) and ALEX (Banala et al., 2007) implemented the BLEEX solution to the hip abduction adduction rotation but no justification has been published on these solutions so far (Low et al., 2005).

2.3.3 The knee joint

The knee joint is active in all three planes but the transitional motion is much greater than the other two rotational degrees of freedom (Margareta nordin 2001).

Majority of the designed exoskeletons only cater for the knee flexion extension, apart from the LOPES exoskeleton (Veneman et al., 2007), where the designers mentioned that the knee rotation has been left unconstrained to cater for the flexibility of the user knee inside.

2.3.4 The human elbow

The human elbow consists of humeroulnar joint, humeroradial and proximal radioulnar joint. The elbow's flexion and extension is caused by the humeroulnar and humeroradial joints in the sagittal plane and can be duplicated by a hinge joint. (Margareta nordin 2001)

2.3.5 The shoulder joint

The shoulder joint has 3 degrees of freedom and can be duplicated mechanically by a ball and socket joint which is moving actively in all 3 planes very similar to the hip joint (Margareta nordin 2001).

2.4 Metabolic effect of forces applied to the human

The metabolic cost rate measures the amount of the power consumption of the user while performing a set task (Griffin et al., 2003). The purpose of the assistive exoskeleton is to decrease the metabolic cost of a certain task by providing assistance to the user.

In 1976 Pandolf concluded from their experiment that a user whom was carrying a load equivalent of 40% of their body weight their metabolic cost rate respectively increased by 40% (Pandolf et al., 1976). In 2003 experiments by Griffin concluded that a user who was carrying a load of 30% of their body weight has shown metabolic rate was increased between 30 to 64% (Griffin et al., 2003).

The other factor that is directly affecting the metabolic cost rate is the speed of the user during the gait cycle as shown in Figure 2.4.

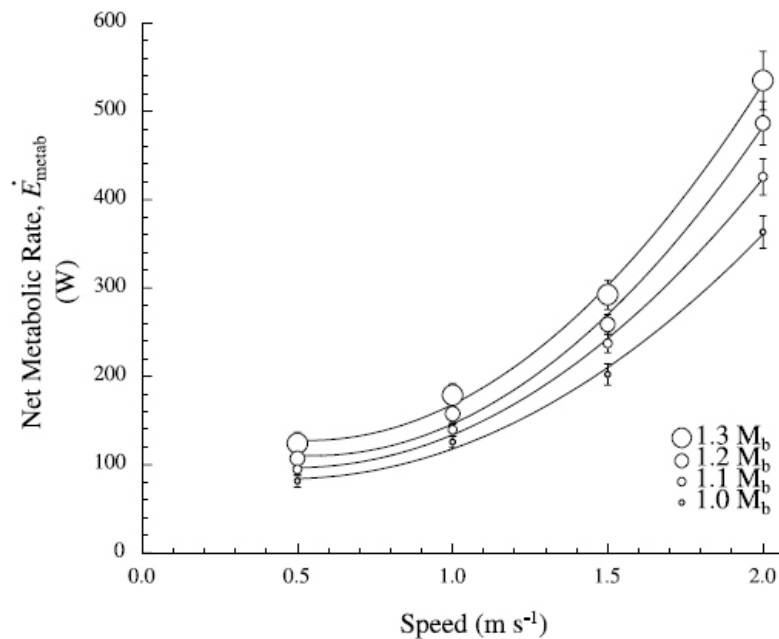


Figure 2.4 Metabolic Cost Behaviour against the Speed(Griffin et al., 2003).

2.5 Biomechanics as a design tool in existing design

The benefits of using an assistive exoskeleton is to aid the user's limbs and increase their load carrying capability. The main difference between the assistive and enhancement exoskeletons is that the assistive exoskeleton carry the weight of the user and the frame, but an enhancement exoskeleton will be carrying extra load as well as the weight of the user and the frame so the two device are very similar in terms of mechanical principles. In order to measure the performance of an assistive exoskeleton the following criteria's should be considered: the load carrying capacity, the speed that the task is performed, and the endurance of the device, improving the efficiency and reducing the perceived level of difficulty (Herr et al, 2006).

Biomechanics is an important topic in this project as the device under consideration would be connected to the human body and the user is the main pilot of this device. In order for the device to copy most of the degrees of freedom of the human body, it is essential to learn about the kinematic and kinetic behaviour of the human and how that compares to the exoskeleton's similar mechanical characteristics.

The human muscle fibres generate the required power by human muscle contractions. Other sources of power generation found by Ferris are the ligaments and tendons of the human which have elastic characteristics and can save and release energy in time (Ferris et al., 2007). Once the power reaches the joints of a human the body will start performing the desired task's motions. The exoskeleton will shadow the same mechanism, and generate power by the use of active actuation systems (electrical, hydraulic, pneumatic motors), and passive actuation systems (springs and dampers). The degrees of freedom are placed by mechanical joints (revolute, hinge, ball and socket, saddle joints).

The generated power will be transferred through the frame of the exoskeleton until it reaches the joints of the device, and by use of the connections (straps, shoes, waist belt) with the human user it carries the limbs of the user while following the natural motions of the user for achieving the safest possible motions along with aiming to lowering the metabolic power consumption of the user.

2.6 Physiological knowledge relating to exoskeleton design

This section provides an insight to the physiological research done considering the relationship between the mechanical power and metabolic power consumption.

2.6.1 The relationship between the mechanical and metabolic power consumptions

The metabolic energy provides the fuel required for the muscle tendon complex .in order to generate force by means of lengthening, isometric, and shortening contraction of the muscles. The positive work is usually associated with shortening contractions of the muscles , and the negative work is caused by muscle's lengthening contractions, and in case of isometric contractions due to no change of displacement the work is negligible but the muscles are still producing force (Rall, 1985).

Studies used the ratio of mechanical energy input and metabolic energy output as a factor known to be as muscular efficiency to relate the mechanical energy to metabolic expenditure. Researchers studied the mechanical power consumption at the joints of the human to find if there is any relationship between the metabolic energy consumption and mechanical power output. The results found the muscular efficiency to be around 25% for positive work, and -120%of muscular efficiency during negative work. (Biglandritchie and Woods, 1976).

The research carried by Alexander and Bennet Clark has found that for a metabolic efficient human gait, the body needs to take advantage of its passive dynamics from close inverted pendulum behaviour to save and store energy. The efficiency of the gait increases significantly while the tendon's elastic energy is used to carry the motion of the gait when possible, so the body is not constantly expending metabolic energy to cover for positive and negative mechanical work (Alexander and Bennetclark, 1977).

2.6.2 Relation between joint work and muscle work

Exoskeletons typically use parallel actuation systems with power transfer to the joints of the exoskeleton, aiming to compensate for the full or partial

workload of the human muscles that is needed to perform a particular task. The designers up to now, have based their actuation and system requirements under the assumption that joint torques of a healthy human have direct relationship with the muscular work about the particular joint (Robertson and Winter, 1980). This assumption can be contradictory when taking apart the biauriculate muscles which cross more than one joint and also when the work is done by contraction of the ligaments and tendons rather than muscles.

Thus the best reliable output from the human joints would be the kinematics rather than relying on the kinetics (torques, power, work) at the joints (Ferris et al., 2007).

2.6.3 Relating mechanical energy to metabolic energy

Some research has been done to find a more specific relation between the body mechanics and metabolic energy consumption. As mentioned above, due to anatomical complexities such as biarticular muscles and elasticity of tendons and ligaments in providing energy to the human body, it is not feasible to assume that the joint work represents the muscular work about the joint. Thus the researchers have divided the human walking into three phases for investigation on relations between the mechanical and metabolic work. The three phases are the leg swing, body weight support and forward propulsion.

The work on the leg swing was done by Doke suggests a 10 – 33% of metabolic energy expenditure is spent on the leg swing and the remaining 67 – 90% is for the remaining phases (Doke et al., 2005).

In a method by Gottschall and Kram, by exerting external horizontal force to mimic the cost of horizontal propulsive force during normal walking there was a 53% reduction in metabolic rate. An increase in the mean EMG of the medial gastrocnemius by 59% was also observed (Gottschall and Kram, 2003).

The research on the metabolic expenditure for supporting body weight and accelerating the centre of mass was carried out by Grabowski. Their research method used a climbing harness that applied constant upward force near the body centre of mass, aiming to reduce the gravity on the centre of mass. identified the 28% of the total metabolic energy expended on the support of the body weight (Grabowski et al., 2005).

2.6.4 Physiological considerations in leg swing motion to reduce the metabolic expenditure

This section provides an overview of some research carried out on the specific swing phase of the human walking and the effects of it on the power consumption of walking.

The motion of the swing phase in human walking has been found by Mochon and McMahon to be a pendula driven motion which is oscillating close to its natural frequency of the lower limb and the centre of the mass of the human body (Mochon and McMahon, 1980).

The research on the mechanics and energetics of the leg swing by Doke found that the metabolic expenditure in leg swing is greatly related to the frequency of the event (Doke et al., 2007). In another research by Soule and Goldman it is reported the metabolic expenditure has a direct relationship with the rise of the swing amplitude (speed of the swing) , and limb mass distribution of the person (Soule and Goldman, 1969).

The research carried out by Ferris found the human walking is most efficient when it is operated at its natural frequency of its limbs so the energy is provided to the body is cyclical , and can be recycled by storing and releasing the energy by the tendon muscle complex . The cyclic motion has been observed during the lower speed gaits, while the tendons generate the required energy to the joints by stretching and releasing against the muscles. At the higher speed the gait becomes more muscular driven motion by lengthening and shortening contractions of the muscles which result in a more expensive metabolic manoeuvre (Ferris et al., 2007). The work of Doke has showed that the human leg swing contributes up to one third of the whole metabolic cost of the walking in humans(Doke et al., 2005).

2.6.5 Physiological considerations during stance phase to reduce the metabolic expenditure

The work of Cavagana and Margaria found the human body has very close characteristics to the inverted pendulum mechanism and further the work of Cavagana, analysed the human motion by means of measuring the energy expenditure i.e. the created kinetic energy from the limbs being converted to

potential energy and then back to kinetic energy in a cyclic manner (Cavagna and Margaria, 1966).

The inverted pendulum motion during the swing phase occurs at the single support phase of the leg during stance. During this phase the mechanical work is minimized and gets close to zero. The force generated is from isometric contraction of the muscles which consist of substantial amount of energy (Neptune et al., 2004).

Most of the physiological work expended during the double support phase and during the collision (contact) between the human foot and the ground, as well as raising the entire centre of mass of the body for the next stage of single support, can take up to 70% of the total metabolic consumption (Donelan et al., 2002).

2.6.6 Physiological consideration as a design tool

The research mentioned in this section concentrates on the passive dynamics of the human motion and how it can affect the efficiency of the human locomotion by lowering the mechanical work thus lowering the metabolic power consumption of the human gait. For exoskeleton design this means that smaller actuation system would be required as the power requirements to move the joints of the exoskeleton while carrying the human is lower.

The exoskeleton needs to follow close kinematics to the human natural frequencies and amplitude to be sure of a metabolic efficient performance of the device. A work has confirmed increasing the step length and step width of the human walking will directly be proportional to the increase in metabolic efficiency (Ferris et al., 2007) .

To be able to achieve a close dynamics to the human's, it is important for the designers to consider the geometry and mass distribution of the exoskeleton in a way to provide the human with natural kinematics , so it will not cause any increase in step length and width for the human user to accomplish the task of walking (Ferris et al., 2007).

2.7 State of the art projects

The robotic exoskeletons mentioned in this section are the most advanced and available exoskeletons in research and the market. The detailed as available in the literature, specifications of the exoskeletons are shown in Table 2.4 (Cenciarini and Dollar, 2011).

The assistive exoskeletons shown in Table 2.4 fail to provide 100% assistance to their user's this is concluded from their active degrees of freedom. The ALEX (Mind Walker) and LOPES are providing more assistance to the user in compare to the other mentioned exo skeletons in Table 2.4. ALEX and LOPES both provides active actuation at the hip abduction adduction, hip flexion extension, and knee flexion extension. ALEX and LOPES does not provide any active actuation at the ankle of the user, the robots are tethered and are restricted to indoor use only.

2.7.1 Hybrid Assistive Limb

The HAL exoskeleton is manufactured by the Japanese company called CYBERDYNE in collaboration with Tsukuba University in Japan. The development of HAL was for rehabilitation and assistive purposes. The HAL5 which is the latest version of this device is a full body exoskeleton and the HAL 3 version is a lower limb exoskeleton (Kawamoto et al., 2003). The CYBERDYNE has made the devices available to rent to the hospitals and medical facilities in Japan. HAL is the first exoskeleton to gain a global safety certificate in 2013. Both HAL5 and HAL3 use battery power (DC) to operate. The battery used in HAL can operate up to 2 and half hours. The weight of the HAL5 is 23 kg. Its height is 1.6 meters and has a maximum lifting capacity of 70 kg (including the weight of the device). The weight of the HAL3 is 15 kg. The powered actuators are placed at the Hip and the Knee joints (DC motor and harmonic drive gears) and the ankle joint is passive in this device (Guizzo and Goldstein, 2005). The control system of these devices is using the EMG (Electromyography), the EMG signals are used to feed the controller and actuation system of the robot. In order to record the human movements the surface electrodes (surface EMG sensors) are attached to the skin of the user (Kawamoto et al., 2003). The downside of the HAL control system is that it is not immediately user adoptable, thus for every new user it can take up to few months to read all the EMG signal and predict the individual gait pattern before the user can start using the device without supervision (Guizzo and Goldstein, 2005). The control unit is portable and is carried by the user in a backpack attached to the back of the exoskeleton. The operational and communication system of the control unit is Linux and the monitoring is done by a remote computer using wireless local area network (Lee and Sankai, 2005). There is

not a lot of information available regarding the detailed design of these two devices, but by investigating the available pictures and videos as shown in Figure 2.5, HAL is designed to be attached closely to the user's limbs by use of straps and the joints are placed directly on the axis of the user's natural joints. The chosen joints are acting in 1 degree of freedom which can cause discomfort and movements restrictions. The HAL is also using a light weight alloy of aluminium which is called Duralumin. This alloy is used in the aircraft industry due to its light weight and high impact characteristics (Thurston, 1919).

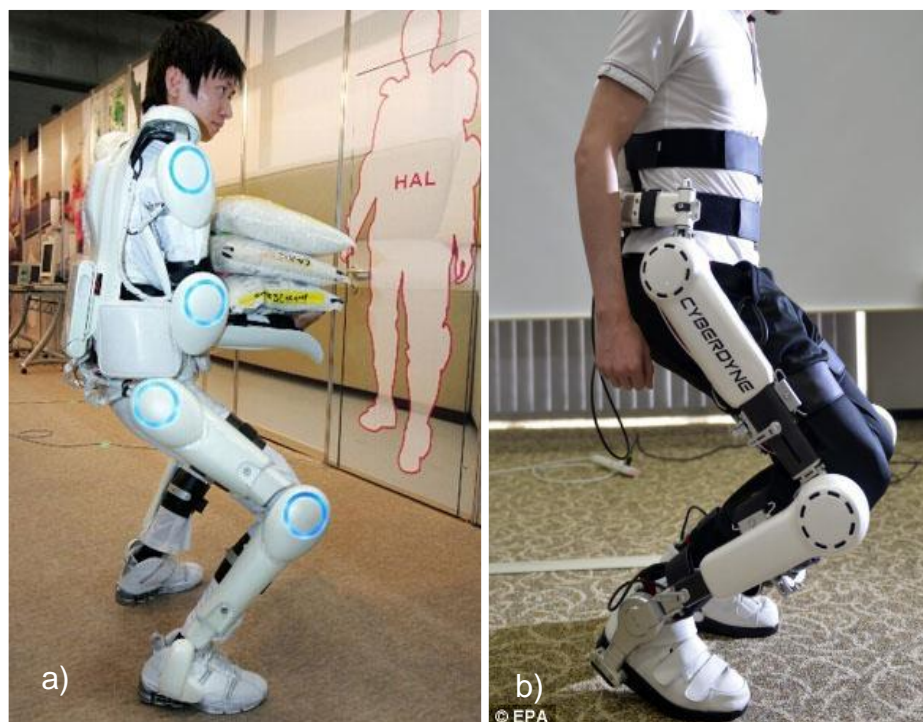


Figure 2.5 Examples of HAL 5 and HAL3 as manufactured products (CYBERDYNE, 2017). a) HAL5 full body exoskeleton b) HAL3 lower body exoskeleton

Cyberdyne offers two different type of services for HAL, so called HAL therapy and HAL fit.

The HAL therapy as shown in



Figure 2.6 uses a treadmill, railing, and a roof mounted harness as well as the robot to support and walk the patient. The main aim of the therapy is for functional improvement of the disordered lower limbs.



Figure 2.6 HAL therapy (CYBERDYNE, 2017) a) subject using HAL therapy b) wall mounted , railing assisted HAL during operation c) subject capable of keeping a seated posture d) subject capable of standing by aid of a walker e) subject capable of walking by aid of a walker

HAL fit offers gait training with a walker, gait training in combination with a lifter , and fitness training as mentioned by (CYBERDYNE, 2017) and shown in Figure 2.7. The condition for the participants as given by Cyberdyne is a person who can keep a standing posture by support of a caregiver, and the patient can hold a sitting posture with no assistants, with no severe joint disorder. The HAL can only support users up to 80 Kg, and has no height between 145 cm to 185cm (CYBERDYNE, 2017).

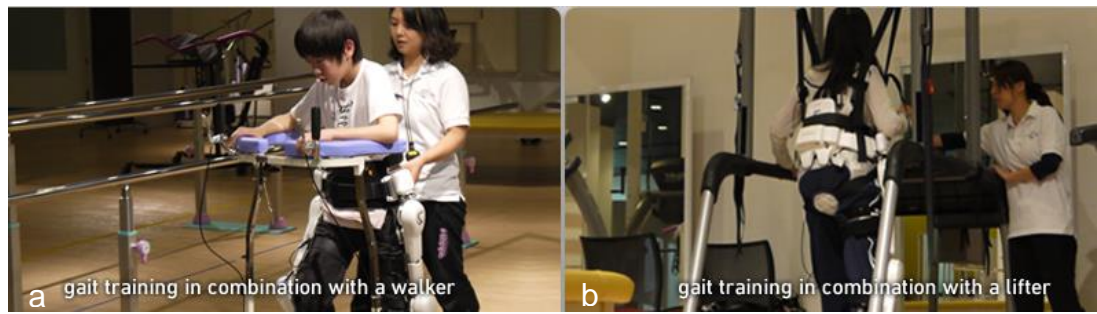


Figure 2.7 HAL fit therapy (CYBERDYNE, 2017) a) gait training in combination with a walker b) gait training in combination with a lifter

2.7.2 BLEEX

The main purpose of the BLEEX project was to allow the user to carry significant load on their back and keep the metabolic cost rate of the user to as minimum as possible. The BLEEX system is designed in a way to be able to operate over unstructured outdoor paths.

This exoskeleton has 14 degrees of freedom in total, which have been distributed evenly in each leg, not all the DOFs are powered; only 4 in each leg are powered. The powered joints in BLEEX design are placed on the hip, ankle and knee joints of the exoskeleton. The exoskeleton uses linear hydraulic actuation system to power the exoskeleton (Kazerooni et al., 2005). The exoskeleton is untethered which means the exoskeleton carries its own combustion engine at the back of the user. This engine also provides the electrical power as well as the mechanical power required to power the whole system. Figure 2.8 shows this exoskeleton.



Figure 2.8 BLEEX Exoskeleton(Zoss et al., 2006) a)BLEEX close to finish product with cover, carrying backpack load b) BLEEX prototype mechanical design with engine and payload at the back c) BLEEX joint and hydraulic actuation system

The exoskeleton is anthropomorphic, the selected ranges of motions allow the user to perform the following manoeuvres; squat, bend, swing from side to side , twist , walking on ascending/descending slopes, step over and under

obstacles. The device is foldable and the entire device will fold into the backpack, the user could carry the device by wearing it as a backpack has a load carrying capacity of 34 kg without the weight of the exoskeleton (Kazerooni et al., 2005). The BLEEX engineers have developed a Hybrid Hydraulic Electric Power (HEPU) engine; this engine provides the whole power to activate actuators, sensors, and the computer of the exoskeleton. This combustion engine weighs about 1.4 Kg on an empty tank and it consist of two stroke twin cylinder combustion engine as shown in Figure 2.9 (Raade et al., 2005).

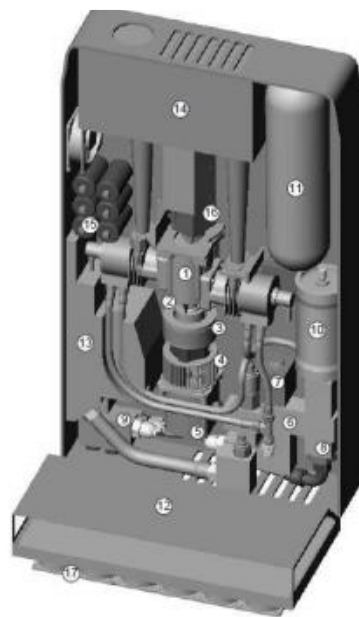


Figure 2.9 BLEEX Combustion Engine (Raade et al., 2005).

The BLEEX's engine mainly is responsible for generating power to move the hydraulic actuators but this engine as mentioned above is a multipurpose engine and does generate electric power by using a shaft that connects to an alternator. A gear pump is also placed to generate the pressure difference so the fluid starts moving in the hydraulic system (Zoss et al., 2006).

The BLEEX system is connected at the torso and the feet of the user, it is not connected at the knee joint, the reason for that is for the exoskeleton to be adjustable for different users (Zoss et al., 2006).

2.7.3 Re Walk

The Argo medical technologies Inc. have introduced the Re Walk exoskeleton to the market. The use of this device is mainly for therapeutic purposes

(Goffer, 2006). This exoskeleton has active actuator on the Hip and the knee joint. The directions of the forces are in the sagittal plane. The suit consists of a backpack which is supported around the user's shoulders by braces, the rechargeable batteries and the computer control system along with the sensors are placed in the backpack which is carried by the user. The actuators are DC powered direct feed at the joints (Dollar and Herr, 2008). The device's battery is completely rechargeable and is designed to cover the all-day activity of the user. Re Walk is size adaptable for each individual patient.

One of the main issues with using Re Walk is the lack of balance control, because this device is designed for patients with lower limb disabilities, crutches are used to help the user maintain their balance while they are performing tasks. By calculating the changes in the centre of the gravity of the user, the device can perform the gait cycle, a remote control is also placed at the user's wrist to be able to control certain manoeuvres such as sit to stand and climbing the stairs.

The Argo medical has intended two different designs of the Re Walk in the market, the first design is to fulfil the assistive aids which is called Re Walk personal, and the second device is called Re Walk rehabilitation. The Re Walk personal has been in the European market since 2012 and could be purchased and used for the assistive purposes by the user after they have accomplished their training by Argo. The Re Walk rehabilitation is also available at the rehabilitation centres across Europe, Israel, and United States (Esquenazi et al., 2012). Figure 2.10 shows this system.

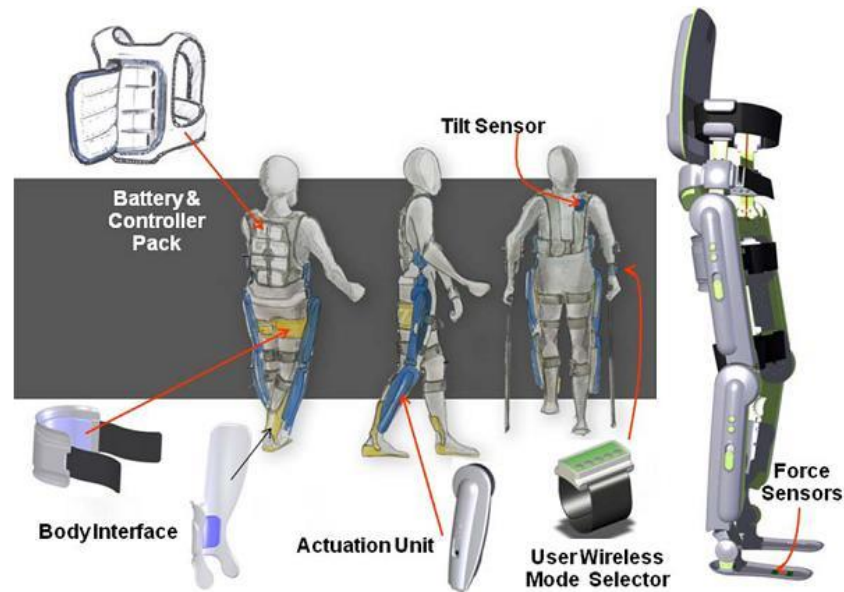


Figure 2.10 Brake Down of ReWalk Exoskeleton (walking, 2013)

2.7.4 eLEGS

The American company of Exo bionics is known for developing military used exoskeletons, it was in 2012 when they released their rehabilitation device called e LEGS. The device has a back pack where the computer control system and the main battery power source are based at.

eLEGS Figure 2.10 weight is around 20 kg and can perform tasks at the maximum speed of 3.2 Km/h. The battery life is aimed to operate the device for approximately 6 hours, and it is fully rechargeable. Due to the nature of the device being a rehabilitation device it is only designed to cover the pre-programmed tasks which are erecting from a sited position and vice versa as well as the gait cycle in the sagittal plane on even surfaces as shown in Figure 2.11.



Figure 2.11 eLEGS Exoskeleton (bionics, 2017)

2.7.5 Vanderbilt Exoskeleton

This exoskeleton was built in the University of Vanderbilt. This device is a lower limb exoskeleton which helps to restore gait rehabilitation in paraplegic patients. The device weighs 12 Kg. The power is generated using a 29.6 V, 3.9 A.hr lithium polymer battery which runs the device for up to an hour with the speed of 0.8 Km/hr. The device does not provide any support for the ankle of the patients and it uses off the shelf ankle arthrodeses. The knee and the hip joint are actuated (Farris et al., 2012).

The actuation uses DC motors with gear box of 24:1 ratio, the maximum generated torque by these actuators are around 12 Nm. The safety features of this exoskeleton is developed by designing locks at the knee joint, the locking system uses a electromechanical brake, which acts when there is a power failure in the system (Farris et al., 2012). The Vanderbilt exoskeleton (Figure 2.12) is a modular device which can be broken down into three pieces, thus the user can mount the device while they are in a seated position. This exoskeleton could support the weight of the users up to 91 kg.



Figure 2.12 Vanderbilt Exoskeleton (Farris et al., 2012).

2.7.6 Lower Extremity Powered Exoskeleton

This exoskeleton has gait rehabilitation purposes and is designed to be used in the physical therapy clinics by being mounted from the ceiling using a harness and using a treadmill as a platform, under the supervision of the therapist (Veneman et al., 2007). The LOPES control is programmed in a way that the robot is doing all the work and gets no influence from the patient, but because the user is connected to the robot, the robot carries the user while doing the manoeuvres. The actuation of the LOPES is done by series of elastic actuators and Bowden cables for power transmission (Veneman et al., 2007).

The LOPES system (Figure 2.13) has two rotation joints at the hip for purposes of hip abduction/adduction and flexion/extension. It also caters for the knee joint's flexion/extension. The active actuator used in the LOPES is a 567 Watts servo motor with maximum speed of 8000 rpm and has a continuous torque of 0.87Nm, with peak torque of 2.73 Nm. The planetary gear head uses a ratio of 64:1 to reduce the speed while increasing the torque output (Veneman et al., 2007).

The passive system for flexion extension at the knee and the hip both have a stiffness of 35.1 kN/m, while the abduction/adduction hip joint's spring has a stiffness of 57.2 kN/m (Veneman et al., 2007).

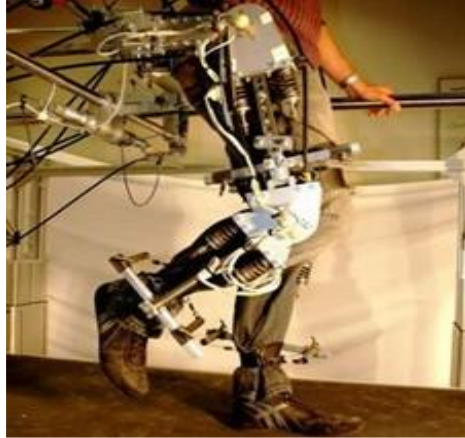


Figure 2.13 LOPES Exoskeleton (Veneman et al., 2007).

2.8 Existing passive exoskeletons

The purpose of passive assistive exoskeletons is to improve the energy exchange between the kinetic energy and potential energy by use of passive elements such as springs and dampers. In previous designs the passive spring engages and disengages by using clutch systems, Cam mechanisms and time pins (Farris et al., 2013, Wang et al., 2011, van Dijk et al., 2011, Collins et al., 2015).

Some designs use the passive systems in parallel or in series with their active actuation systems in order to reduce the peak torques and power requirements of their active actuation system such as the work done by (van Dijk et al., 2011, Wang et al., 2011).

The passive systems bio mechanically mimic the work done by the tendons and ligaments in the body. The work carried out by (Ferris et al., 2007) indicates the importance of using passive systems on the overall metabolic performance of the exoskeleton systems. In this section some developed exoskeletons which use passive systems in their designs are mentioned.

2.8.1 Passive ankle exoskeleton

This single joint passive exoskeleton device developed by (Collins et al., 2015) uses carbon fibre frame, a clutch system and tension spring connected to the gear system (clutch) by a cable as shown in Figure 2.14.

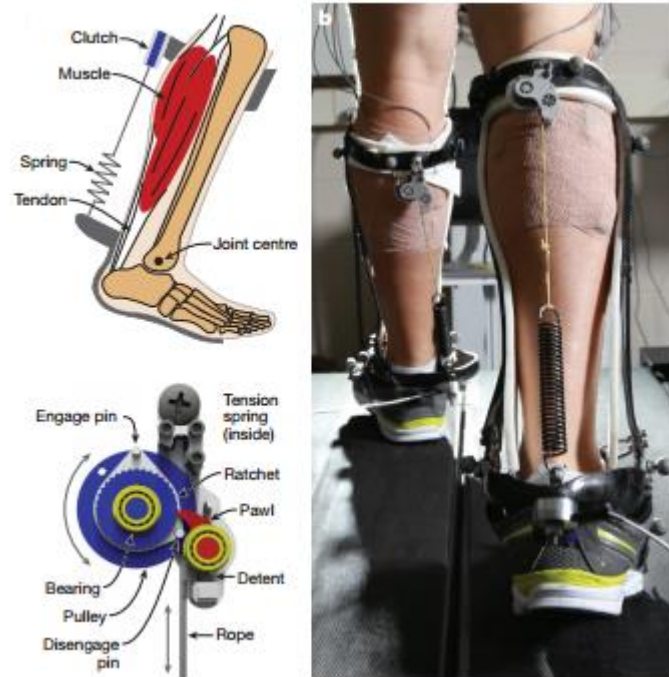


Figure 2.14 Passive ankle exoskeleton mechanism (Ishikawa et al., 2005)

The system is placed in parallel with the Achilles tendon and calf muscle (Ishikawa et al., 2005).

The system is engaged when the wearer is under the heel strike phase and disengages during the terminal stance phase and let the user swing freely. The designed spring rate was chosen to be at 180Nm/rad, and has been measured to reduce the metabolic cost of the user's walking by $7.26 \pm 2.6\%$. The device was designed in two foot sizes of US8 and US13 with a weight of 408 and 503 grams respectively.

The purpose of the device is to increase the metabolic efficiency of the healthy users, and is not practical for users with lower and no muscle and motor abilities.

2.8.2 XPED2

The XPED2 is built by (van Dijk et al., 2011)) at Delft university. The exo suits uses long elastic cable passing through hip, knee, ankle and the foot of the user. The cable uses the hip flexion/extension degree of freedom as a lever and knee as the pulley connecting to the leaf springs placed at the foot. The

leaf spring would provide elasticity to the foot thus the user can mimic the real human foot motion as shown in Figure 2.15.

According to simulation work (van Dijk et al., 2011), it is predicted that there is 46% reduction in joint torques. The results from the treadmill experimental walking comparing the gait with and without XPED2 shows 12% reduction in the absolute joint torques.

The metabolic measurements of the user with and without the exoskeleton in the study show a 27% reduction in the metabolic expenditure from using the XPEND2.



Figure 2.15 XPED2 artificial tendon exoskeleton design (Wang et al., 2011)

The weight of the whole device is 6.91 Kg, and the cable stretches and stores the energy during the midstance phases at the ankle plantar flexion and hip flexion, while it releases the stored energy during the terminal stance phase at the ankle and hip extension. The provided degrees of freedom are hip abduction/adduction, flexion/extension at the knee and hip, along with ankle dorsi/plantarflexion.

2.8.3 MIT Exoskeleton

The MIT exoskeleton is a quasi-passive system (Walsh et al., 2007) which is designed for enhancing healthy users on augmenting their load carrying capacities as shown in Figure 2.16.



Figure 2.16 MIT Quassi passive exoskeleton (Walsh et al., 2007)

The lower limb exo suit provides degrees of freedom in the sagittal plane at the hip, knee, and ankle joints along with coronal plane degrees of freedom at the hip and the ankle. The tension springs used were placed at the hip and ankle sagittal joints along with the hip frontal plane joint. The springs are designed to engage and store energy during the midstance and release during the terminal stance phase.

Variable dampers placed at the knee joint, six monoarticular series elastic clutches and three biarticular series elastic clutches as shown in Figure 2.17.

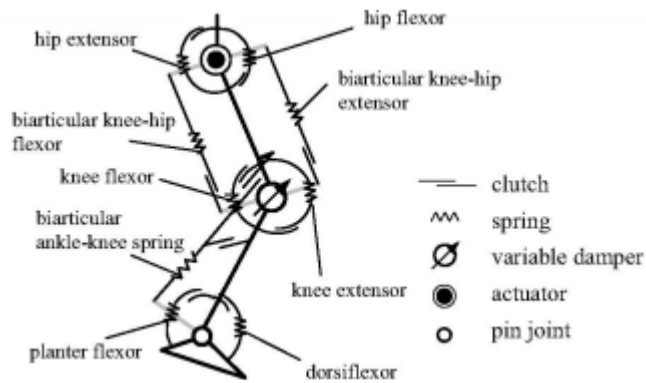


Figure 2.17 MIT Quassi passive exo suit leg model (Walsh et al., 2007)

The only joint actuated is the hip flexion/extension, the variable damper at the knee is aiming to dissipate the mechanical energy. The biarticular clutches and springs are used to transfer the energy across the joints of the device while aiming to store the energy and release in a time and direction to assist the user's motion.

The spring stiffness found in the ankle joint during the dorsi flexor and plantar flexor are found to be 25.7 and 360.5 Nm/rad. Along with the stiffness at the hip flexor and extensor found to be 103.1 and 53.5 Nm/rad. The knee extensor and flexor stiffness found to be 206.3 and 190.2 Nm/rad (Walsh et al., 2007).

The testing of the prototype, consisting of healthy users wearing a 36Kg bag pack while walking, found a 10% increase in the metabolic power consumption while using the device, compared to the subjects carrying the load without the device according to (Walsh et al., 2007).

2.9 Design approaches on active actuation system selection

The exoskeletons are devices that influence the human limbs and joint directly so it is essential for the designers to be familiar with how such a device can affect the human limbs and joints and what the restrictions are. This section covers the movements of the human's lower limb during the most important activity which is walking; it also mentions which muscles and joints are mostly active during this task.

The upper body movement has also been investigated, as well as specifications of the joints such as ranges of motions, density of the segments and joints moments.

2.9.1 Joint Torques

The energy assistance to the user during the operation of an assistive exoskeleton is provided by the designed active (Zoss et al., 2006) and passive systems (Dollar and Herr, 2008, Walsh et al., 2007). The generated torques need to be transferred to the exoskeleton joints at the right time, in the right direction with the appropriate intensity. The majority of the designed exoskeletons use the sagittal plane joints as the main source of assistance (Beyl et al., 2008, Dollar and Herr, 2008, Zoss et al., 2006), but in (Zoss et al., 2006) it is found that the hip abduction/adduction has a larger power demand compared to the hip flexion/extension. MIT, LOPES and BLEXX, have provided some assistance at the non -sagittal joints especially hip abduction/adduction and ankle inversion/eversion, in some cases by means of passive actuations (springs).

The existing exoskeleton designs have mostly used the CGA data as the initial design and specifications for selecting their active and passive actuation system's (Zoss et al., 2006), however Beyl has made a remark about the large variability and inaccuracies that this method has and that basing the design of the robot on the CGA data is not reliable (Beyl et al., 2008). Some designers use optimization and scaling methods from the CGA data for design of the actuation systems (Walsh et al., 2007).

2.9.2 Motion Velocity and Bandwidth Considerations

The designers have evaluated the static characteristics of exoskeletons by examining the position of the joints (DOF and ROM) and joint torques. The biggest dynamic variables affecting the exoskeleton design is the velocity and the bandwidth of the system, the following dynamic characterizations have been investigated in previous works (Colombo et al., 2000, Dollar and Herr, 2008, Beyl et al., 2008). The dynamic properties affect the actuation design and actuation efficiency, depending on the angular acceleration of the joint and the payload mass, the amount of torque needed to be generated by the actuation system varies directly. The power consumption of the motors needs to support the torque and angular displacement required at each active joint of the exoskeleton to complete the gait.

2.9.2.1 Considerations on Other Design Factors

Other design considerations are the weight and inertia properties of the exoskeleton and how it will be connected with the human, and the method and timing of the actuation system so it will not provide any restrictions for the human user. Depending on the requirements and purposes of the exoskeleton the choices of the actuation system and power supply varies, the existing designs consist of purely active or passive and quasi active or passive systems with series or parallel springs. Depending on the arrangement of the actuation system the amount of power supply and energy expenditure of the system varies. The main purpose in the design of the assistive robots is to guide the frame along with the user inside (exoskeleton carrying the user and itself) to natural human movements such as Lokomat, LOPES, and KNEXO (Veneman et al., 2007, Colombo et al., 2000).

It is necessary to have active actuation system, as the users may not have the capability to perform the desired task on their own.

The connection points between the exoskeleton and the human users are another consideration due to high level of stress and force interaction between the user, the robot, and the world (ground).

2.10 Mechanical Design Challenges

The following are the expected mechanical design challenges in design of exoskeletons:

- Size adjustability features for the frame so it could benefit a broader range of consumers as well as obeying the anthropomorphic design of the exoskeleton so the joint of the user.
- The exoskeleton joints will be placed on the same axis as the human joints.
- Assistive device should be able to carry the user's joint without causing any discomfort.
- The exoskeleton should be structural integrity sound against the forces and moments by using optimized materials with characteristic of high impact and light weight. A lighter exoskeleton would require smaller actuators to power.
- Function of modularity makes this device more efficient in terms of mass production, maintenance, and assembly by the user from various positions.
- The material selection is a vital step of the design as it can affect the weight, hardness and cost of the exoskeleton.
- The exoskeleton must use minimum power and minimises the metabolic rate of the user.
- The exoskeleton should be designed in a way so it will transfer all the loads to the ground and not the user's body.
- The exoskeleton should be able to carry the user without causing any discomfort to the user's limbs , not limiting any necessary degrees of freedom and ranges of motions

A number of assumptions were made in the application of the human biomechanical data to the design of the exoskeleton. The first was that the exoskeleton carried its own weight, power supply and payload. The second assumption was that joint torques and joint powers scaled linearly with mass. This second assumptions seemed reasonable given that increases in vertical ground reaction force have been found to be proportional to increases in the

load being carried (Llyod, 2000). The third assumption was that the exoskeleton would not greatly affect the gait of the wearer.

2.10.1 Actuation design challenges

The actuation design raised many challenges to the exoskeleton design. The ideal exoskeleton suit is aiming to activate as many necessary degrees of freedom as possible to provide the full flexibility and manoeuvrability for the user inside. Activating high number of degrees of freedom increases the weight of the exoskeleton suits which directly affects the efficiency of the exoskeleton application. The example of this issue was first seen in the design of the Hardiman exoskeleton suit made in the 1960's by the general electric and Cornell University, the Hardiman had 30 hydraulic active degrees of freedom which caused the suit to weight 680 kg. Other researchers aimed to solve this issue by choosing other efficient types of actuation systems such as pneumatic, hydraulic, electrical, and hybrid actuation systems as a solution. More recent research is aiming to use passive actuation systems (springs) to store the kinetic energy during the walking stages depending on the stiffness characteristics of various joints. Using passive systems has been found to decrease the high torque requirement of the active actuation systems (Yeo Wei Hong and Chok, 2013).

2.10.2 Mechanical design

the Selcuk university (Onen et al., 2014) have outlined the following as mechanical design challenges

- ergonomic between the user and the exoskeleton device
- high manoeuvrability of the exoskeleton
- structure durability with light weight characteristics
- size and user adoptability
- safety

The ergonomic of the user has been investigated by measuring the metabolic efficiency i.e. comparing the metabolic expenditure of the user with and without the exoskeleton. An example of this was seen in BLEEX as Vo₂ measurements method was used to evaluate the ergonomic and efficiency of their device.

The designed exoskeleton ranges of movements and degrees of freedom specify the amount of manoeuvrability, these data from similar exoskeleton projects have been provided in section 2.2.3 .

The exoskeleton should provide the frame strength to cater for the actuation system and power supply and other payloads. Light weight and high strength materials such as duralumin, titanium and carbon fibre have been used to achieve these characteristics for example in the design of exoskeletons such as HAL and BLEEX. According to (Yan et al., 2015) review paper on the safety of the exoskeleton designs, there are no safety standards available on the human exoskeleton interaction as yet .

2.10.3 Power supply

Another challenge in the exoskeleton design is the feasibility of untethered power supply system, as a large power demand can restrict the application of the exoskeleton to be only tethered supplying powers indoor. Thus the number of active degrees of freedom on the suit has a direct effect on the feasibility of having untethered power supply. A great example of the on board power supply is the HAL exo suit as they claim the upper and lower body suit's battery system can supply up to 2 hours and 40 minutes of functioning with use of lithium and bickelmetal hydride origin (Dollar and Herr, 2008).

2.10.4 Energy expenditure

The energy expenditure of exoskeleton systems is the most accurate way of measuring the efficiency of the device by means of its effect on the human user. The method is vastly used to measure the metabolic efficiency of the designed exoskeletons by comparing the metabolic efficiency of the healthy human subject with and without the use of the exoskeleton. These are based on oxygen and carbon dioxide expenditure measurements as well as EMG measurements to determine the muscle contribution while performing the specified tasks, and also include heart rate monitoring. Example of these measurements are done by (Gams et al., 2013) on the knee exoskeleton which has shown that the metabolic cost rate has been reduced by using the exoskeleton. Many other research studies specially in a task such as walking, using exoskeleton have shown an increase in the metabolic cost rate of the user (Kim et al., 2010). Another assistive exoskeleton project at the university

of Delaware (Lenzi et al., 2012) is ALEX2 which showed a reduction in muscle effort by conducting an experiment on two healthy subjects using a treadmill based exoskeleton suit (36.5% efficiency).

2.11 Summary

The exoskeleton research has been actively progressing for the past four decades starting with the HARDIMAN project by the General Electric. Exoskeletons have proved to augment the human ability in various ways depending on their application.

The reviewed designs vary by their chosen degrees of freedom and which degrees of freedom are activated by an actuator. Other issues include kinematic inaccuracy between the exoskeleton robot and the human and the effect of that on inaccurate estimation of the designed active and passive system used in the robot design. Based on the literature the accuracy of the existing systems on state of the art projects such as; the BLEEX and MIT exoskeletons is dependent on clinical gait analysis of the human walking which was used for establishing specifications and requirements of their actuation system and frame design prior to building the device. It is also found that the previous designers have based their design on the assumption that the exoskeleton will have the same kinematics as the user inside. The same assumption was also made in designing the passive systems (springs and dampers) in the existing exoskeleton systems. The clinical gait analysis (CGA) data of the human joints kinetics (torque at the joints) and kinematics (angular displacement and angular velocity at the joints) are not a good kinematic or kinetic indication for designing the passive system of the robot which has caused inefficiency in the system and also inefficiency in metabolic consumption of the user inside as reported in the work of BLEEX and MIT. This work recommends the designers not to use the clinical gait analysis data as specifications for design of their active and passive actuation systems and other design specifications (frame and joints).

The review on the physiological performance of these devices shows there is a big lack of biomechanical and physiological consideration in the existing designs, and points to the lack of information on the biomechanical and

physiological insight as a measure of the efficiency and performance of these exoskeletons. Most of the previous designs does not show their devices effectiveness in lowering the effort of the user while performing the desired tasks using the exoskeleton.

In conclusion, it is found that there is a necessity for using experimental and simulation tools to identify the interaction between the human and the exoskeleton physiologically and biomechanically, along with using the robot kinematic and kinetics to establish the design specifications of the robot instead of just using human clinical gait analysis (CGA) data.

Chapter 3

Analysis of human locomotion and exoskeleton frame requirements

3.1 Introduction

It is a requirement for the exoskeleton design to be following the acceptable healthy human ranges of movements, as well as other kinematic parameters such as velocities and accelerations (Yeo Wei Hong and Chok, 2013).

The aim of the assistive robot is to provide some degree of assistance to the user inside by generating power at the joints of the exoskeleton. The assistive exoskeleton is anthropomorphic to the user inside, this means the user joints and the exoskeleton joints would be very closely aligned and ideally sharing the same axis of rotation, or as close as possible. Thus it is essential for the exoskeleton to follow healthy human kinematics to minimise any unwanted interactions between the user and the exoskeleton. This could result the achievement of the most natural gait, without causing any metabolic inefficiencies for the user inside the robotic exoskeleton.

This has been done by measuring and simulating the kinematics and kinetics of a healthy human and implying those kinematics as end effector's maps for the exoskeleton's joints axis of rotations to follow.

This chapter includes the results of angular joint displacement of healthy human gait over five subjects. The gait differs in speed and angular displacements, while the weight and duration of the trail have been standardised. The exoskeleton joints angular displacement have to be within an acceptable range as the healthy human and ideally follow the healthy human joint displacement results as close as possible.

The results from this section will be used as inputs to the simulation models in chapters 7 and 8, so the exoskeleton's active and passive actuation parametric designs are based on healthy human motions.

3.2 CGA's kinematic as inputs of the exoskeleton dynamic simulation

Other researchers (Onen et al., 2014, Zoss et al., 2006) have used the clinical gait analysis (CGA) kinetic data (e.g. Torques and powers) at the joints of the human segments for the design of their power system of their assistive and rehabilitative robots. Some have used such techniques as scaling and other normalization techniques to estimate a more accurate specifications for their design. According to (Zoss et al., 2006) this has not offered a similarly scaled or normalised compared to true exoskeleton specifications.

The human joints and body do not behave exactly similar to exoskeleton's joints and frame, the differences are; rigidity, misalignment, different moments of inertia, geometry, and other mechanical properties such as weight and density. This leads to kinematic differences between the exoskeleton and the human's kinematics and kinetics and specifications.

To overcome modelling issues and to avoid extrapolation of inaccurate actuation specification some assumptions and considerations were made in building both the exoskeleton and the human models. It is a necessity for the exoskeleton to be following the joint kinematics of a healthy human joints during the gait of the robot as mentioned before.

The CGA data were collected at the University of Leeds in the Faculty of biological sciences by using motion capture systems (reflective markers, infrared cameras). The experiments consisted of measurement of positions of the segments and the joints of the healthy human users (using reflective markers and infrared cameras) with the set laboratory coordinate system along with kinetic measurements of reaction forces of the human gait cycle (2 sets of force platforms), as well as measurements of muscle activities (EMG muscle sensing).

The captured position data were then collected in the Qualisys track manager (QTM) format, the QTM also recognizes the data collected from 13 active infrared cameras and other measurement hardware such as the EMG sensors, reflective markers and Force platforms.

QTM initially collects the 2D (x, y) positions data, and calculates the remaining position (z) by implementing marker occlusion and merging detection of the reflective markers into a tracking algorithm.

Captured and calculated six degrees of freedom reflective markers positions data from the human walking and statics from Qualisys track manager 2.11 was inputted into the built subject's specific human model and ready to perform the full inverse dynamics in visual3D software.

3.3 Visual 3D human model and inverse dynamic method

Human body is actuated by using muscles and tendons. Biomechanically the muscles can act as active actuation systems that use contractions to create forces to generate the required power for the motion. Ligaments can act as passive actuation systems such as springs to store the already existing energy in the system and release in time to assist in the direction of the motion (Farris et al., 2013). The motion capture technique is used to get an accurate analysis of all the forces and moments internally and externally exerted at the joints of the human as well as the position, velocity and acceleration of the human joints to each other and to the world.

The visual 3D human model is adaptable to change with height and mass of individual users.

3.3.1 Assumption and key concepts

To create the human model in Visual 3D software, static calibration is used to recognise the reflective marker's positions which then define the segments. The tracking reflective markers are used to create the model and as points to compute the kinematics and kinetics. The other types of marker are the calibration markers which define the segments geometrical characteristics (cylinder, cone, sphere and ellipsoid). The segments are visual modelling representation of the bones and skeletal structure of the human body.

The created segments will have mass properties (based on the textbook averages in the library of the visual3D). Length (measured from end points), and defined distal and proximal end points (distal furthest away from the centre of mass).The link recognizes the two segments in proximity, as shown in Figure 3.1.

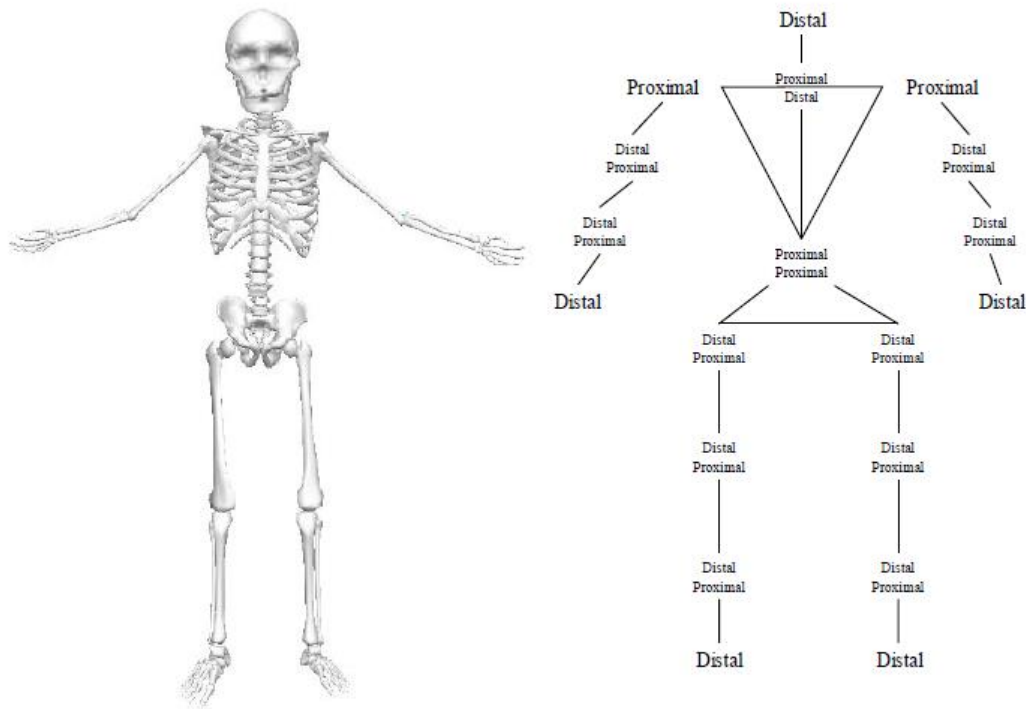


Figure 3.1 Segment arrangement in visual3D (biomechanics, 2016)

To define the joint of the human model in the visual 3D simulation the following assumption has been considered, that the joint is consisted of the two distal and proximal segments which share the same axis of rotation as shown in Figure 3.2.

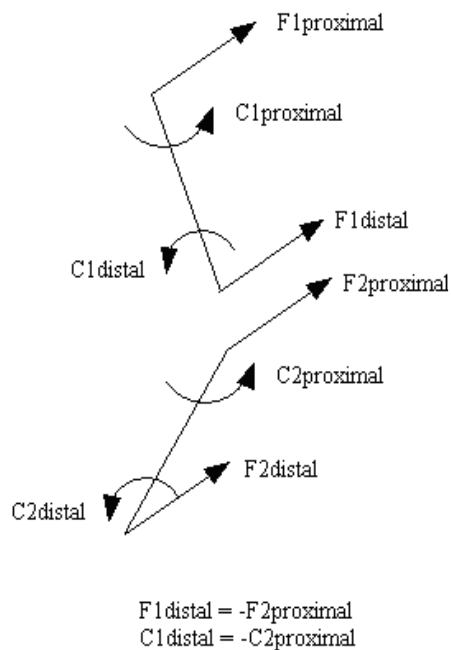


Figure 3.2 Force arrangement (biomechanics, 2016)

It is assumed that the proximal force at the distal segment F_1 is equal in magnitude but opposite in direction to the distal force at the proximal segment F_2 . The other assumption is that the moments created at the joint C_1 (distal moment acting on the proximal segment) and C_2 (proximal moment created at the distal joint) are also equal and opposite as shown in Figure 3.2.

The moments externally acting on the segment is assumed to be equal in magnitude but reverse in direction of the net internal moment at that joint which caused by the human muscles and ligaments in visual 3D solver.

Visual3D model does not create any physical joints between the segments, instead it assumes two segments are in proximity. The proximity assumption works by considering the distal end of distal segment and proximal end of the proximal segment to be within the radius of segment ends. The segments are then assumed to be two linkages with a reference joint connecting the linkages. This also counts into the previous assumption of the joint reaction forces acting on the endpoints are same in magnitude but reversed in direction (biomechanics, 2016).

3.4 Inverse kinematic global optimization used in visual 3D

The motion of the joint in visual 3D is collected at six degrees of freedom assuming the joint has no constraint on any degrees of freedom. In order to have a photogrammetric measurement of the position of the human joints and measure of its motion in space the joint of the human is recognised by three non-collinear reflective markers for each section of the body. These section markers will specify the orthogonal segment coordinates of the human (SCSs) the details of inverse kinematic global optimisation used in visual 3D is explained in appendix A.

3.5 Motion capture experiments

The biomechanical design approach of this work, is based on using the healthy human subjects kinematics at its most efficient state to be inputs of the parameters for the motors of the 14 degree of freedom exoskeleton while carrying the human user inside.

The degrees of the freedom of the robot is selected from the conclusion of the work in chapter 4, which is aiming to provide active and passive degrees of freedom to the exoskeleton and the user inside for purpose of user safety and flexibility while keeping the robot's weight down by not activating any unnecessary degrees of freedoms.

The robots inverse dynamic simulation uses the angular velocity at the joints of the healthy human at its most efficient as inputs to the joints of the robot model. The results of the simulation shown in chapter 7 and 8 provides full specification and parameters for the appropriate active and passive actuation systems. The benefit of this approach is the robot is following the closest kinematics to the healthy human which minimise any unwanted interactions and creation of external forces between the robot and the user inside.

The gait analysis data of the healthy human walking was collected independently at the University of Leeds for the purpose of this project.

3.5.1 Purpose of the Study

The purpose of this experiment was to collect all the subjects kinematic data, i.e. healthy human joint positions in all six degrees of freedom during the activity of gait cycle, along with collected static position for each subject. This was done by capturing the positions of the placed reflective markers on each subject's skin surfaces, with the set coordinate system in the motion capture laboratory at the University of Leeds, to be able to build the dynamic model as explained in the method.

Electro myography signals (EMGs) have also been collected for purposes of estimating the most significant parameters in user intent and to relate basic mechanical sensory data to output of Mo-Cap analysis (e.g. power, metabolic energy consumption).

External forces during the walking activity was measured by collecting the reaction forces while the user was stepping on the force platforms. The collected reaction forces were used to simulate the kinetics of each subject.

Due to lack of kinetic data on healthy human degrees of freedoms in the literature and for purposes of verifications of the model and results of the work in chapter 7 and 8, the experimental and the simulation work on the healthy human walking have been carried out in this chapter.

3.5.2 Participants

The participant included five healthy male subjects with body mass of 81.33 ± 9.31 kg; height ranges from 176.78 ± 8.95 cm, with no previous gait abnormality. All the participants signed consent forms, with full information about the experiments prior to the study.

3.5.3 Materials

In order to measure the 3D kinematics, kinetics and EMG for subjects, the following instruments were used:

- 13 camera 3D motion analysis system (Qualisys).
- 2 force plates integrated into the ground floor
- Reflective markers
- EMG Electrodes
- Visual3D software for inverse dynamics and data analysis.
- 5 Control group (5 healthy subjects)

3.5.4 Methods

Testing took place in the biomechanics laboratory, Faculty of Biological Sciences. Subjects were asked to attend the laboratory for a period of approximately four hours. During this time they were asked to wear shorts and t-shirts and no footwear. Small retro-reflective markers were placed on the subject to facilitate tracking by a thirteen-camera three-dimensional motion analysis system (Qualisys).

In order to capture the motion of the subjects, reflective markers had to be placed at certain designated anatomical landmarks of the participant to obtain meaningful information about the kinematics changes of different limbs. These markers can be categorised into two types; individual or cluster. Individual markers are used to place at the anatomical joints of the human, i.e. hip, knee, and ankle, in order to define the geometry of thigh and shank. Cluster markers are marker groups that are used to place at the human body segments to track its position and orientation. The full marker placement is illustrated in Figure 3.3. The patterns of muscle activation will be measured and data will be collected using surface EMG electrodes. EMG is a technique for evaluating and recording the electrical activity signals produced by skeletal muscles during various ambulation activities. Noraxon sEMG electrodes (Telemyo, Noraxon, and Scottsdale, AZ) were used to collect electrical signals from subjects muscles. This system consists of a 2400R receiver which has 12 electrodes and channels connected to a computer with a visual feedback program i.e., Qualisys Track Manager (QTM). For placement of sEMG electrodes on the lower limbs, skin preparation was required. This might

include the removal of the hair, and rubbing/abrasion of the skin may also be necessary with soft sand paper, and alcohol/ether until skin is prepared for placement of the sEMG electrodes. For sEMG placement the SENIAM standard was followed. The muscles that were studied are as follows: rectus femoris, vastus lateralis, vastus medialis, biceps femoris long head, semitendinosus, gluteus medius, tensor fascia latae, gracilis, tibialis anterior, gastrocnemius lateralis, gastrocnemius medialis, and soleus. Array of force sensors will be embedded on the insole to capture the kinetic data.

3.6 Human model experimental and simulation methods

3.6.1 Subjects marker and sensing placement and experimental measurement

During the experimental work with the procedure and method explained in detail in the Visual 3D human model and inverse dynamic method, reflective markers have been placed on five subjects all in the same manner as shown in Figure 3.3. In the motion capture experiments the muscle palpation method was also used to place the markers and EMG sensors. Full lower limb marker placement was done to identify user's thigh, shank and foot in both sides along with pelvis, acromion and neck by placing markers laterally, medially, inferior and in frontal positions.

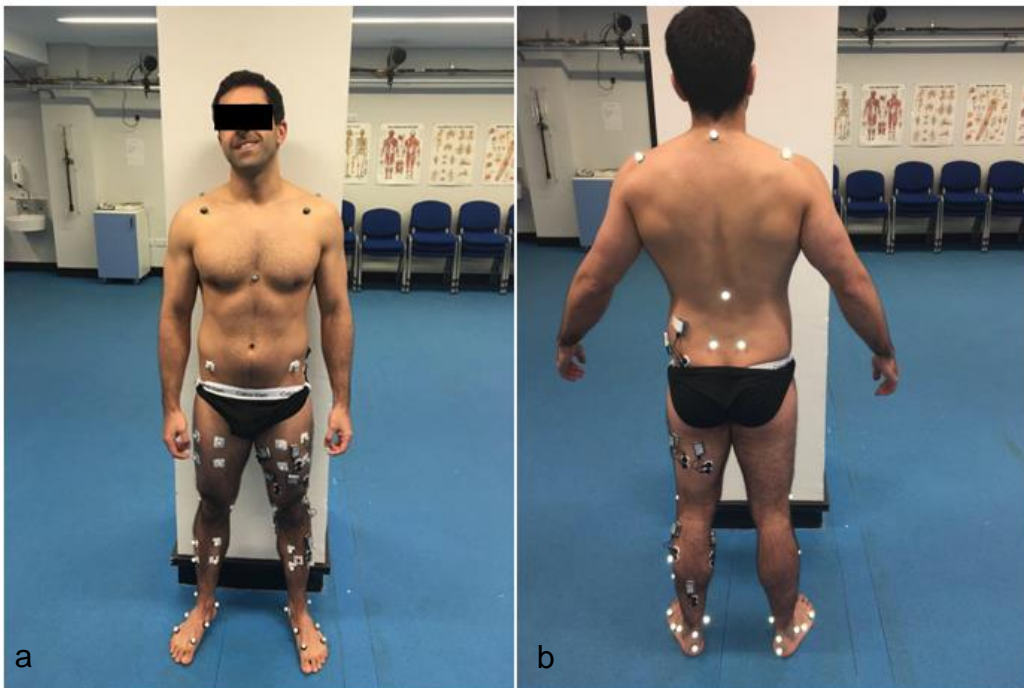


Figure 3.3 motion capture experiment a) Front view marker and sEMG placement b) Back view marker and sEMG placement

By using 13 infrared cameras all the positions were successfully captured.

3.6.2 Qualisys marker recognition (position data capture)

The infrared cameras captured positions of the reflective markers placed on the subjects, the captured positions were recognised computationally by using the Qualisys track manager 2.11 software as shown in Figure 3.4.

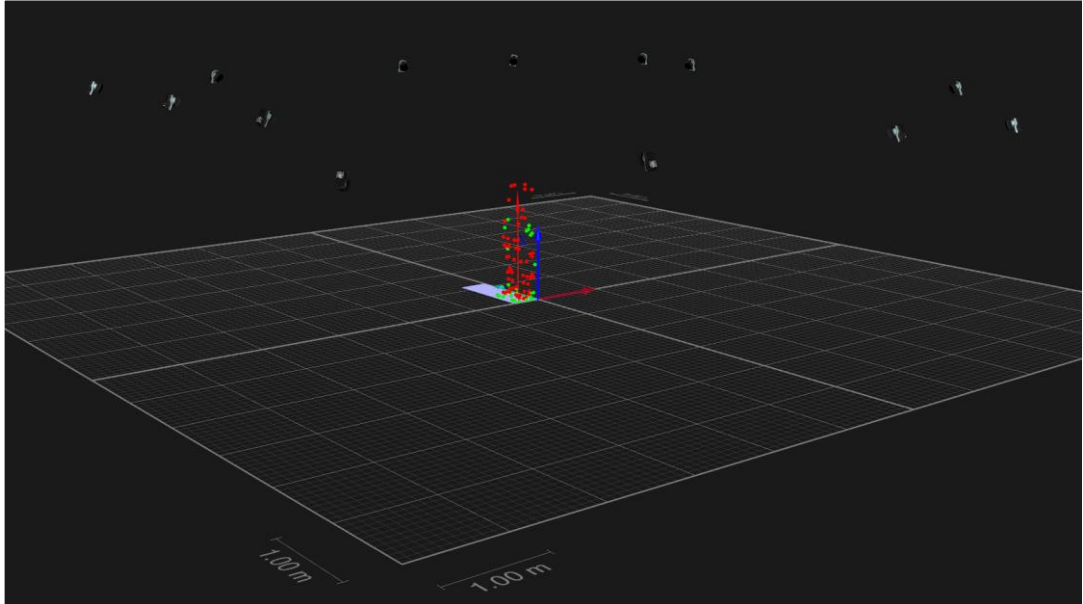


Figure 3.4 Qualisys motion capture recognition

The data were demonstrated by using the defined Cartesian reference coordinate system in the laboratory environment. During the static trials all the markers were identified and named respectively.

3.6.3 Visual3D static model

The static model built in the Visual3D inverse dynamic software used the imported marker positions captured by the Qualysis track manager 2.11. Other kinetic data were captured and recognised by the Visual3D package such as the EMG signals. The readings from the two force platforms for the static measurement are also shown in Figure 3.5.

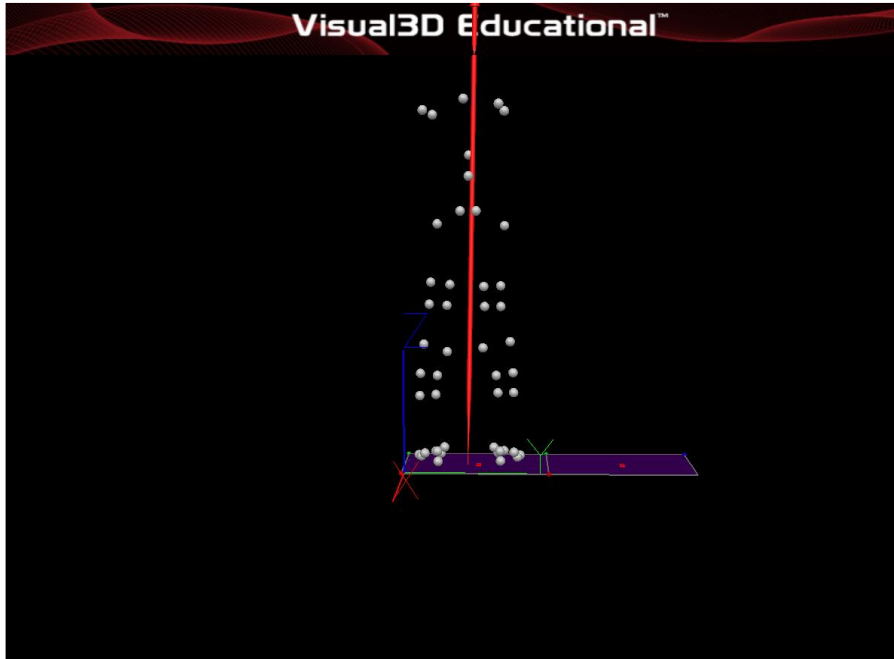


Figure 3.5 Visual 3D static human model marker recognition

3.6.4 Visual 3D numerical human model

The human model in the visual3D used the segments and joints reflective markers to numerically identify the geometry of the measured subjects limbs computationally. The static captured marker's position data were manually inputted from the visual3D library, all values are in SI units, as shown in Table 3.1.

Table 3.1 Visual 3D numerical inputs for human model

Name	Editable	Value	Name	Editable	Value
Mass	YES	94	LFT_Seg_Length	NO	0.107937
Height	YES	1.78	RFT_Distal_Radius	NO	0.0479034
Gravity	YES	9.81	RFT_Proximal_Radius	NO	0.0462051
Segment_to_COFP_Distance	YES	20	RFT_Seg_Length	NO	0.0978075
LTH_Proximal_Radius	YES	0.08	leftfootflat_Distal_Radius	NO	0.0484213
RTH_Proximal_Radius	YES	0.08	leftfootflat_Proximal_Radius	NO	0.0206384
ASIS_Distance	YES	0.277601	leftfootflat_Seg_Length	NO	0.157309
Target_Radius_ASIS	YES	0.017	rightfootflat_Distal_Radius	NO	0.038784
RTA_Segment_Depth	YES	0.05	rightfootflat_Proximal_Radius	NO	0.0196819
RPV_Segment_Depth	YES	0.0988674	rightfootflat_Seg_Length	NO	0.182873
ASIS_Distance_Calculated	NO	0.277601	RPV_Depth	NO	0.197735
LTH_Distal_Radius	NO	0.050964	RPV_ML_Direction	NO	1
LTH_Seg_Length	NO	0.449051	RPV_AP_Direction	NO	1
RTH_Distal_Radius	NO	0.0578314	RPV_Axial_Direction	NO	1
RTH_Seg_Length	NO	0.428558	RPV_Seg_Length	NO	0.0882257
LSK_Distal_Radius	NO	0.0445862	vpelvis_Distal_Radius	NO	0.0999364
LSK_Proximal_Radius	NO	0.050964	vpelvis_Proximal_Radius	NO	0.0853182
LSK_Seg_Length	NO	0.419625	vpelvis_Seg_Length	NO	0.0882258
RSK_Distal_Radius	NO	0.0462051	RTA_Distal_Radius	NO	0.0853182
RSK_Proximal_Radius	NO	0.0578314	RTA_Proximal_Radius	NO	0.150281
RSK_Seg_Length	NO	0.433834	RTA_Seg_Length	NO	0.431984
LFT_Distal_Radius	NO	0.0484213	Joint_Radius_Ratio	YES	1.1
LFT_Proximal_Radius	NO	0.0445862			

The built model is a visual representative of the human skeletal system according to the positions of the markers as shown in Figure 3.6. Each participant would have its own model according to their height and mass characteristics which was saved as a HDM file and applied specifically in simulation for their trials.

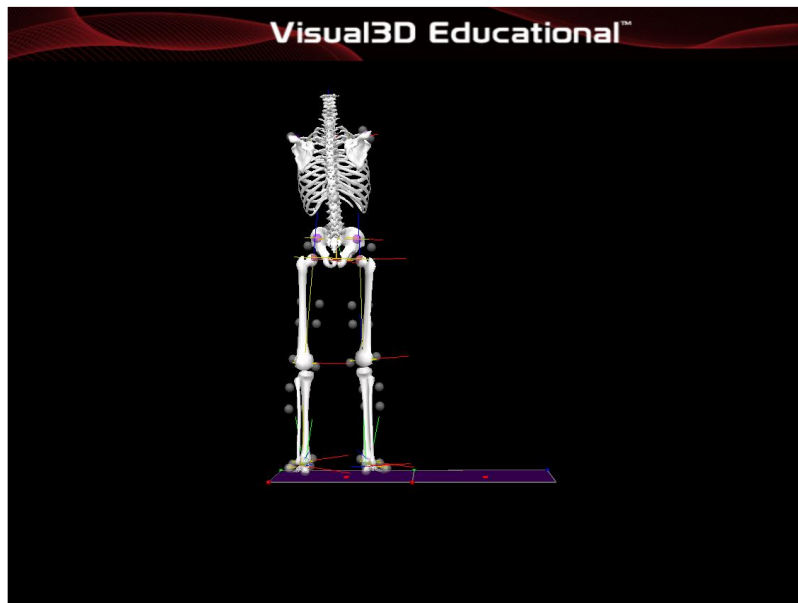


Figure 3.6 Visual 3D human model static position

3.6.5 Visual3D inverse dynamic Gait

The subjects recorded gait over the two force platforms were dynamically simulated by the use of visual 3D human model and help of reflective markers. The inverse dynamics solver in visual3D, as explained in section 3.3 of this chapter was used to extract the Kinetic and kinematic values at the joint of the subject. As shown in Figure 3.7 the one gait step over two force platforms were collected and simulated for all subjects.

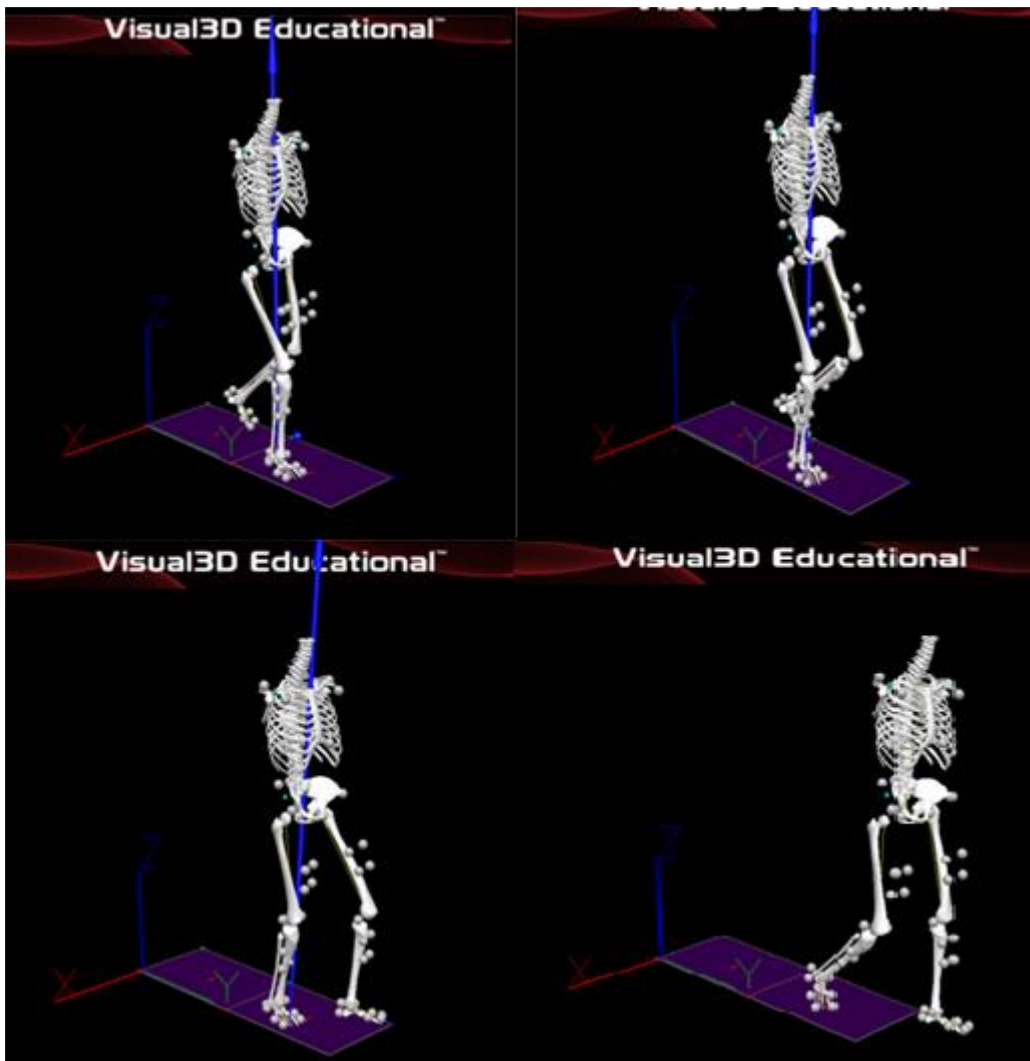


Figure 3.7 Visual 3D human model during walking simulation on the force platforms over one gait cycle

The results of this inverse dynamic simulation for all subjects are presented in the next section.

3.6.6 The Filter

As recommended by (winter, 2009) a Butterworth type Low pass filter with cut off frequency of 6HZ was used in the inverse dynamic simulation of the human gait, the chosen value is based on recommendation from winter handbook due to it being closest value to the human walking natural frequency, the type of filter is also based on recommendation by the Visual3D package for analysing the human models.

3.7 Results of healthy human experiment for clinical gait analysis

It is a kinematic assistive exoskeleton design requirement to minimise any unacceptable human joint's range of movements, which may cause the user serious injuries. Following the acceptable ranges of movements also allows extra forces to be minimised in order to increase the metabolic efficiency of the user inside. It also means less effort from the user regardless of any control system, by allowing the frame to follow human natural ranges of movements.

The captured positions of the markers were used to build the dynamic 3D visual model. The model has then been used to have full kinematic and kinetic data for all the subjects. An average of each subject's data from six trials was also collected. The main joint's activity in the sagittal plane has been compared, and for the purposes of model verification they have been also compared with the CGA data from the literature review as shown in the Results of healthy human experiment for clinical gait analysis .

The simulated kinematic outputs are used as one of the inputs to the dynamic simulation of the exoskeleton model to find the active actuation system requirements of the exoskeleton frame while carrying the human user inside as explained in CGA's kinematic as inputs of the exoskeleton dynamic simulation in chapter 6.

The outputs also were used as inputs into dynamic simulation of the exoskeleton to find the passive actuation system requirements as explained

in details in chapter 7, Rotary velocity motors for solving the inverse dynamics of the exoskeleton model .

A block diagram shown in Figure 3.8 is a visual demonstration of the explained methodology.

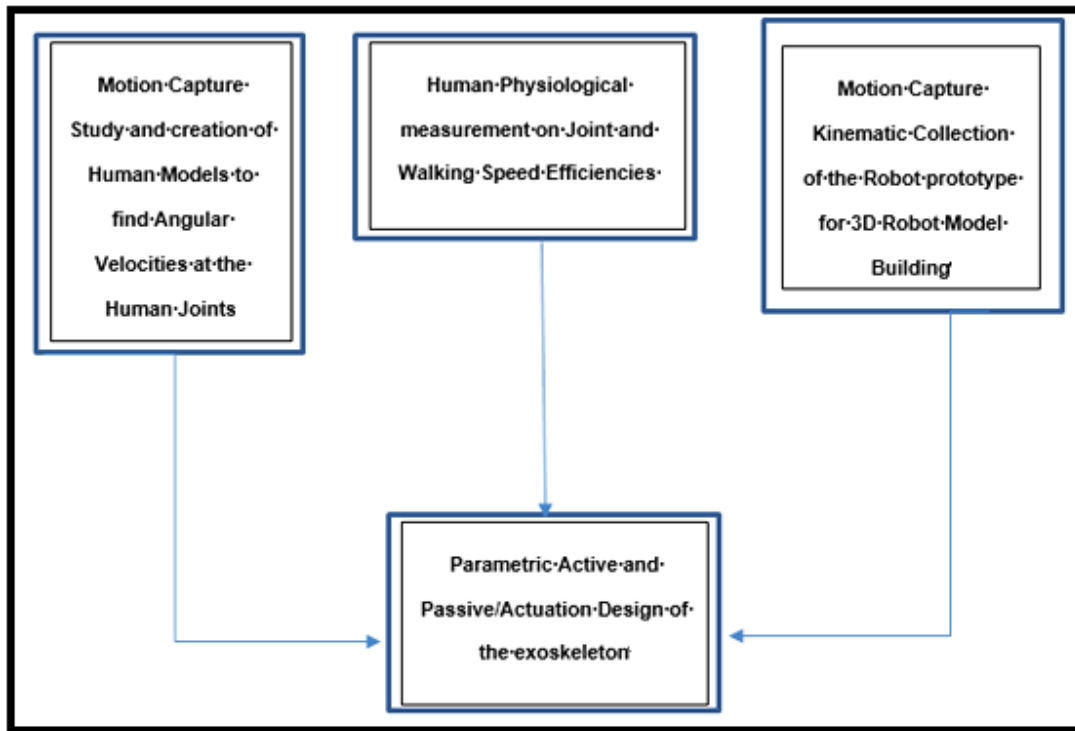


Figure 3.8 Block diagram representation of the inputs to parametric design of the robot

The angular displacement results presented in the following result section were from (Margareta Nordin 2001) for the purpose of verification of the visual 3D collected and simulated results carried out at the University of Leeds. Heel strike happens at 0 seconds, and the toe off happens at approximately 0.6 seconds in all CGA angular displacement figures simulated for one leg.

3.7.1 Ankle Joint

3.7.1.1 Ankle dorsi flexion/extension angular displacement

The ankle flexion/extension is one of the most metabolic efficient degrees of freedom during the human gait which resulted from the research work mentioned in the work of (Farris et al., 2013). The results of ankle flexion/extension range from the literature is given in Figure 3.9. Figure 3.10 shows the result of the collected CGA data, where the maximum flexion of the ankle joint recorded is $\approx +15 \text{ deg}$, and the maximum extension of the ankle joint is $\approx 25 \text{ deg}$. Both the collected and existing data from literature share the same peak values.

Figure 3.9 and Figure 3.10 are compared for the verification purposes of visual3D model and motion capture experimental work, it can clearly be observed that they have similar values and patterns, with same variations.

Figure 3.10 shows the average positions from each subject based on six trials at comfortable slow speed. The 0% of the gait cycle is the heel strike for all subjects and around 60 to 70% is when toe off happens in one leg for simulating a full gait cycle. Therefore results of the collected data can be compared with CGA data from literature (Margareta Nordin 2001).

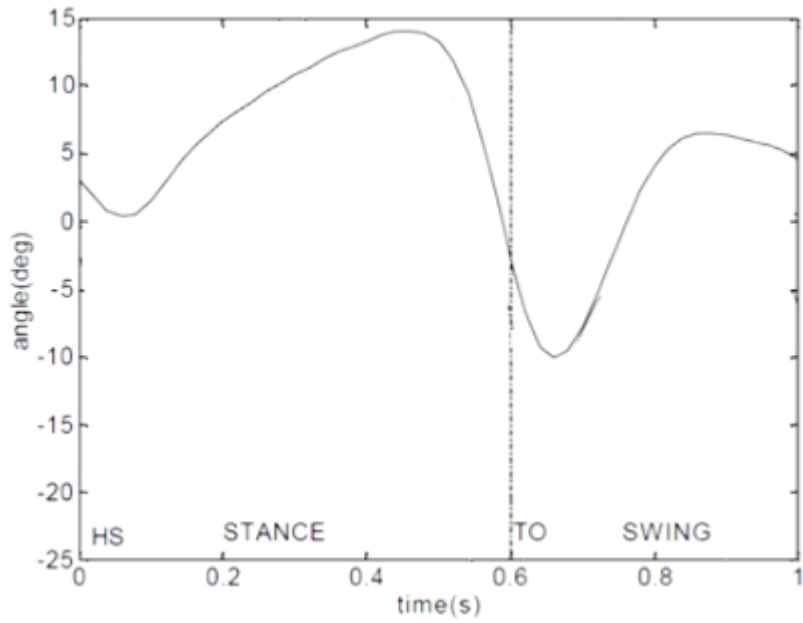


Figure 3.9 Ankle flexion/extension angular displacement for one complete gait (Margareta Nordin 2001).

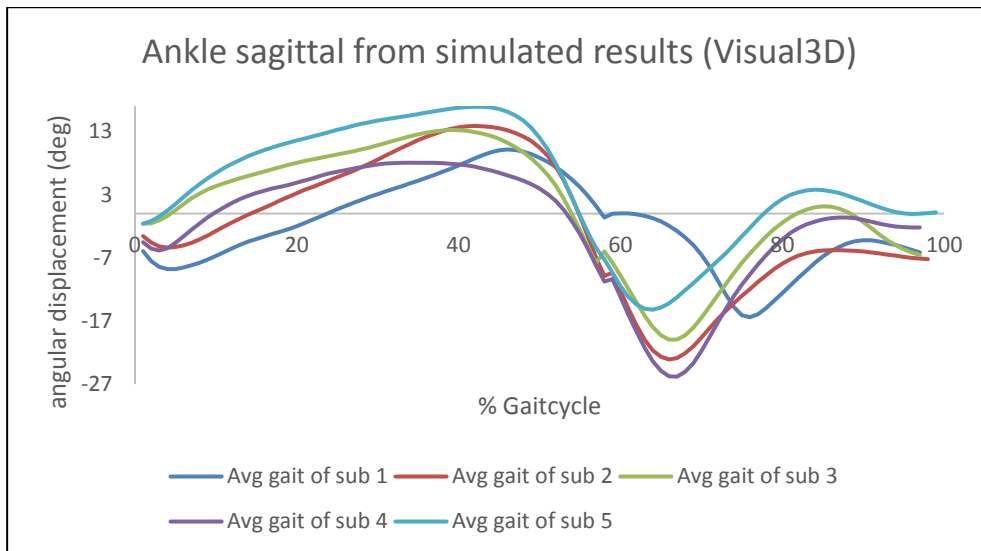


Figure 3.10 Captured and simulated CGA data of ankle flexion/extension angular displacement for one gait

3.7.1.2 Ankle inversion/eversion angular displacement

The ankle joint was measured in two degrees of freedom flexion/extension and inversion/eversion for purposes of finding the kinematic and kinetic characteristic of these as driving positions of the active exoskeleton joints.

The ankle inversion/eversion angular displacement from the literature review is shown in Figure 3.11. The maximum positive angular displacement is $\approx +17^\circ$ and it happens from inversion of the ankle at about the beginning of swing time around 60% of the gait cycle. The maximum eversion angular displacement happens at the stance phase about 20% of the gait cycle with a value of $\approx -4^\circ$ as shown in Figure 3.11.

The inversion eversion motion kinematics collected follow the same peaks as the literature data. The measured subjects have maximum positive angular displacement value at $\approx +20^\circ$ during inversion of the ankle at the swing phase right after toe off at about 60% of the gait cycle. The maximum negative angular displacement happens during the stance phase of the gait cycle and can go as low as -10° , at around 20% – 30% of the gait cycle as shown in Figure 3.12.

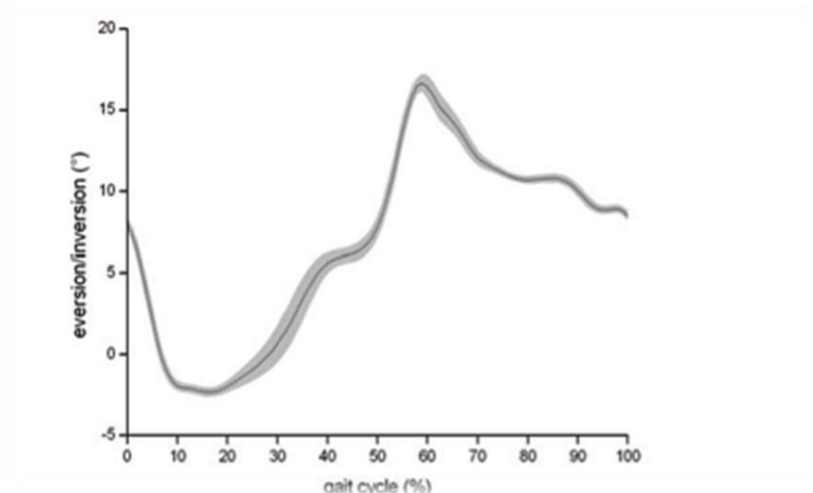


Figure 3.11 Ankle inversion/eversion angular displacement (Margareta Nordin 2001).

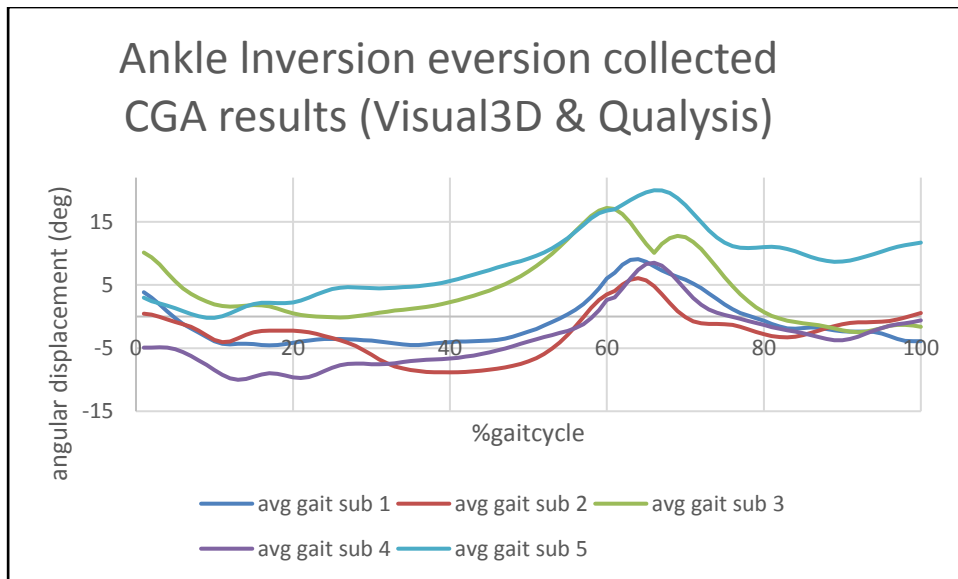


Figure 3.12 Ankle inversion/eversion collected and simulated CGA data for one gait

3.7.2 Knee joint

3.7.2.1 Knee flexion/extension

The knee joint is active at the sagittal plane. Figure 3.13 shows the literature CGA data which represent the maximum flexion of the knee occurring between the mid stance and mid swing with the maximum value of $\approx -75^\circ$. The maximum extension of the knee joint occurs initially at the mid stance, while the maximum extension occurs during the late swing phase with maximum positive value of $\approx 5^\circ$.

The collected CGA data has similar peak values and patterns to those of the literature as can be seen in Figure 3.14. The maximum flexion occurs after the mid swing after $\approx 60\%$ of the gait cycle, with the peak value of $\approx -70^\circ$ the other flexion occurs in lower values of $\approx -20^\circ$. The maximum extension occurs from mid swing to late swing with the peak positive values reaching $\approx +20^\circ$, the other extension occurs at the mid stance with the positive peak value reaching $\approx +10^\circ$.

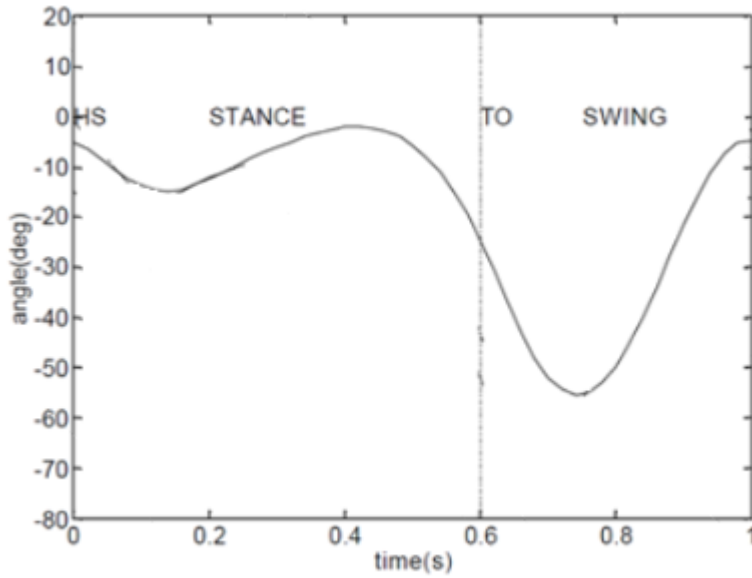


Figure 3.13 Knee flexion/extension angular displacement (Margareta Nordin 2001).

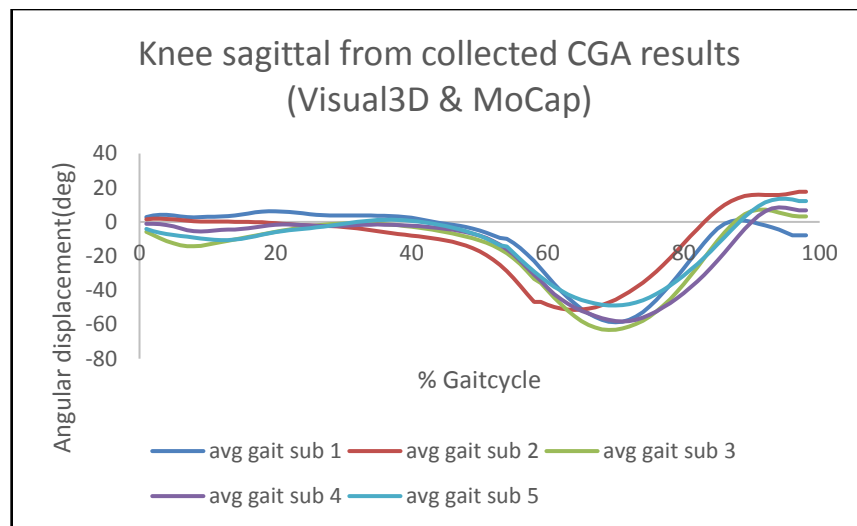


Figure 3.14 Knee flexion/extension angular displacement, captured and simulated CGA data

3.7.3 Hip joint

3.7.3.1 Hip flexion/extension

The hip maximum extension occurs from mid stance to mid swing (30% to 70%) of the gait cycle, with its peak value of $\approx -25^\circ$. The maximum flexion occurs after the toe off $\approx 60\%$ of the gait cycle, with peak positive value around $\approx +35^\circ$, as shown in Figure 3.15.

The collected CGA data shown in Figure 3.16 can be verified by comparing the trend and peak values with Figure 3.16. The maximum extension again occurs from mid stance to mid swing phase covering 30% to 70% of the gait cycle, with peak value of $\approx -25^\circ$. The measured maximum flexion similar to the literature data occurs just after the toe off at $\approx 60\%$ of the gait cycle, at peak values $\approx +30^\circ$.

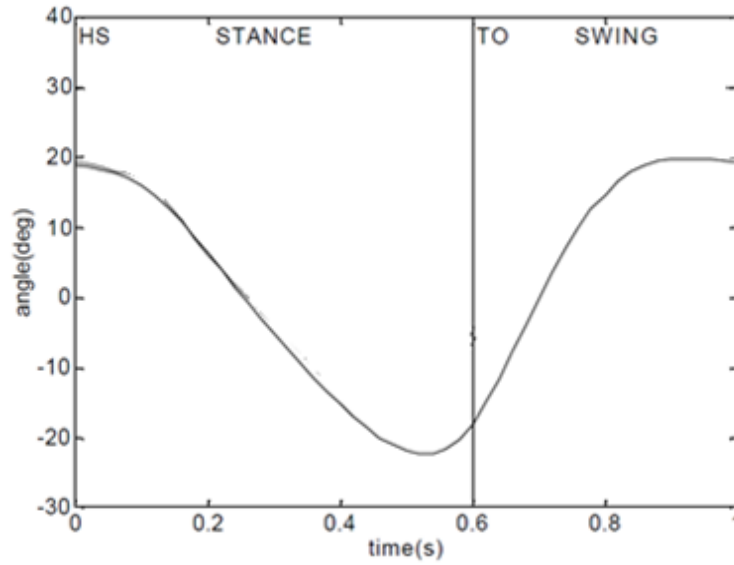


Figure 3.15 Hip flexion/extension angular displacement data(Margareta Nordin 2001).

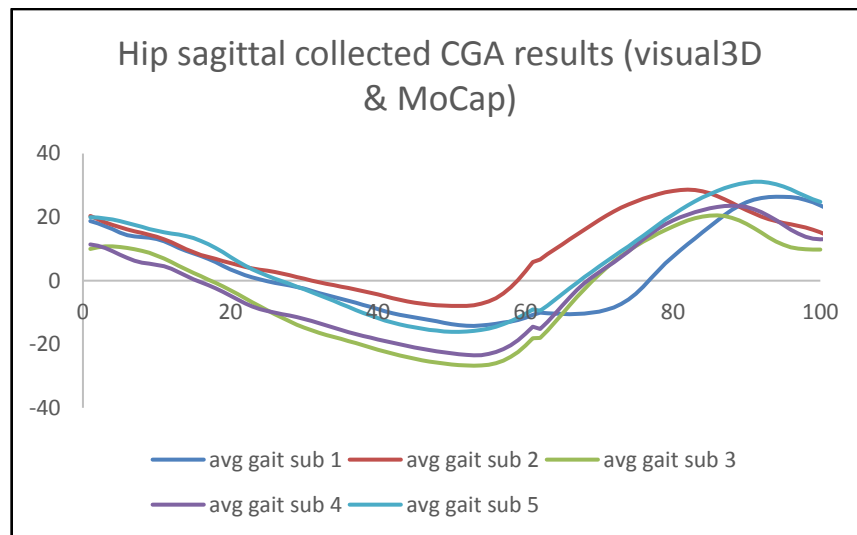


Figure 3.16 Hip flexion/extension angular displacement, captured and simulated CGA data

3.7.3.2 Hip abduction/adduction

The data presented in Figure 3.17, plots show the literature graphs of the lateral motion in the hip joint. Figure 3.18 shows the collected CGA data. In both figures the maximum adduction of the hip occurs from the heel strike at the initial stance phase and carries on to mid stance by reaching peak values $\approx +10^\circ$. The maximum abduction occurs at the swing phase specifically about the toe off, from the mid stance to mid swing reaching peak values $\approx -15^\circ$ in both figures.

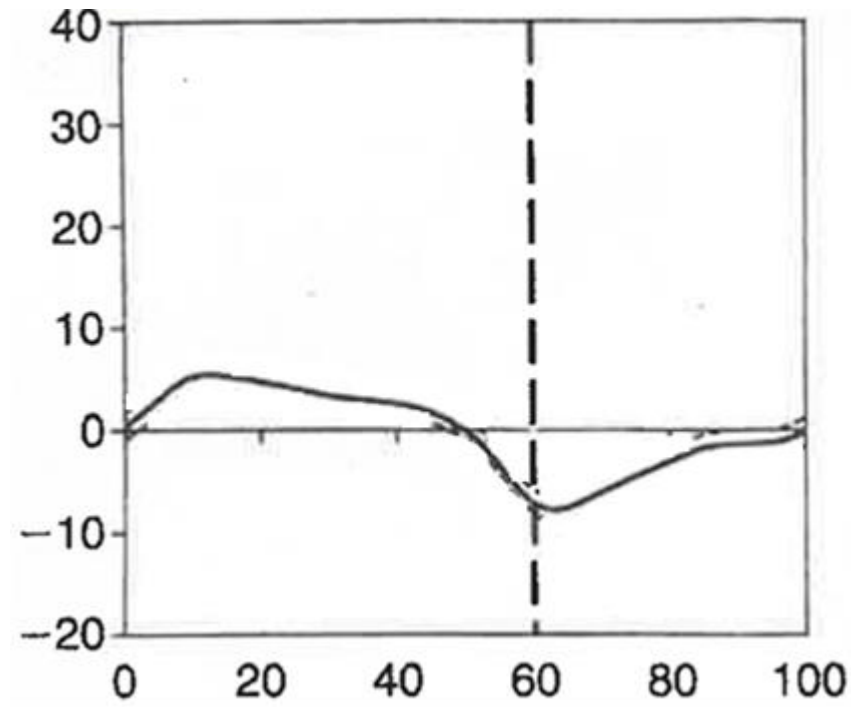


Figure 3.17 Hip abduction/adduction angular displacement data (Margareta Nordin 2001).

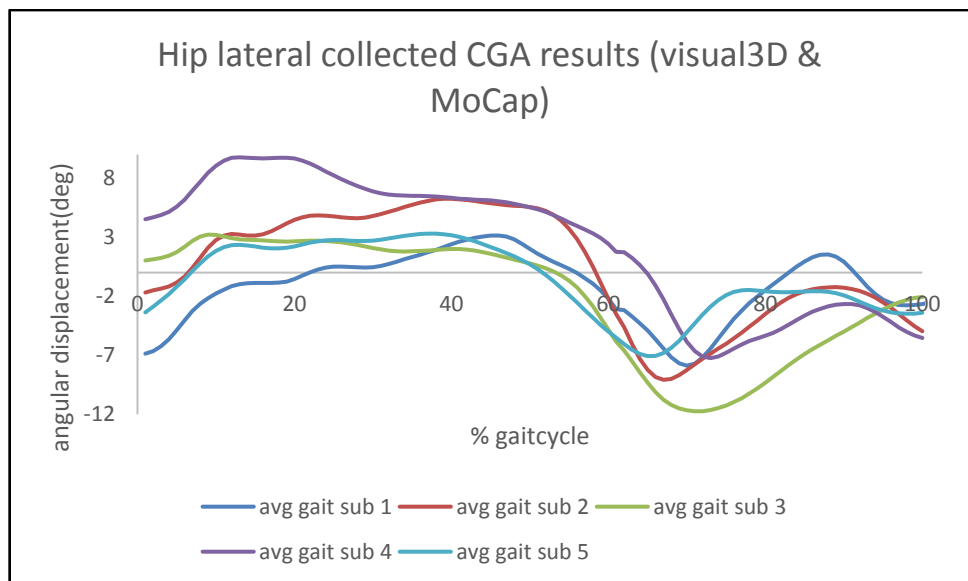


Figure 3.18 Hip abduction/adduction CGA, captured and simulated data

3.7.3.3 Hip internal external rotation

The hip rotation was measured at its highest value of $\approx +10^\circ$ after the toe off as majority of the rotational movement are in negative direction reach $\approx -30^\circ$ depending on the initial position of the hip. Figure 3.20 shows the collected average angular displacement data in the coronal plane.

Some subjects have shown differences to the literature data, this is due to the challenges of accurately palpating an axes of rotation for this joint in the motion capture experiment.

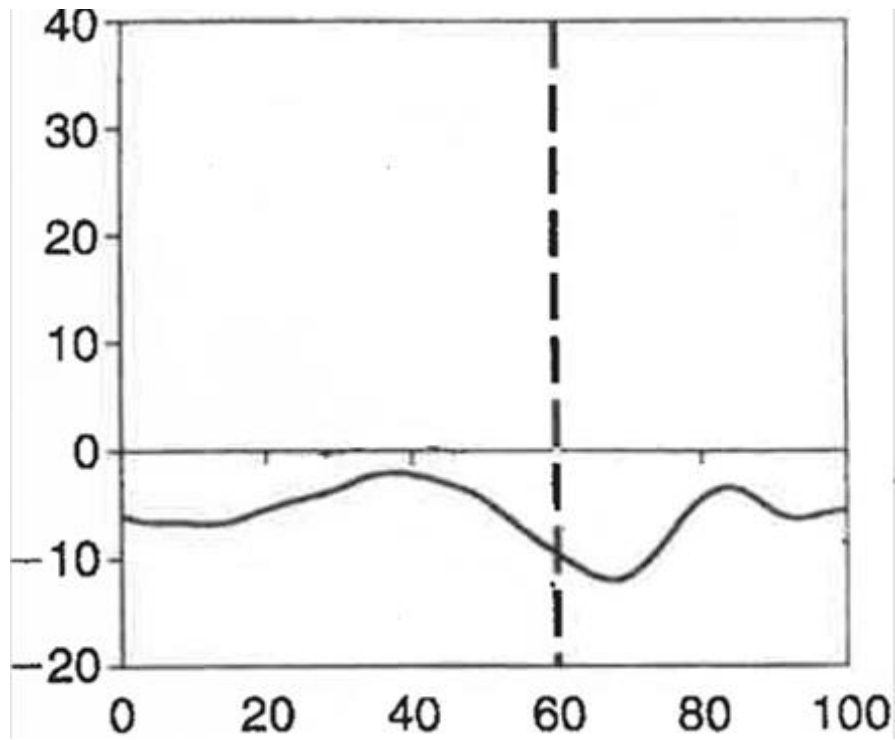


Figure 3.19 Hip internal/external rotation angular displacement over one gait (Margareta Nordin 2001).

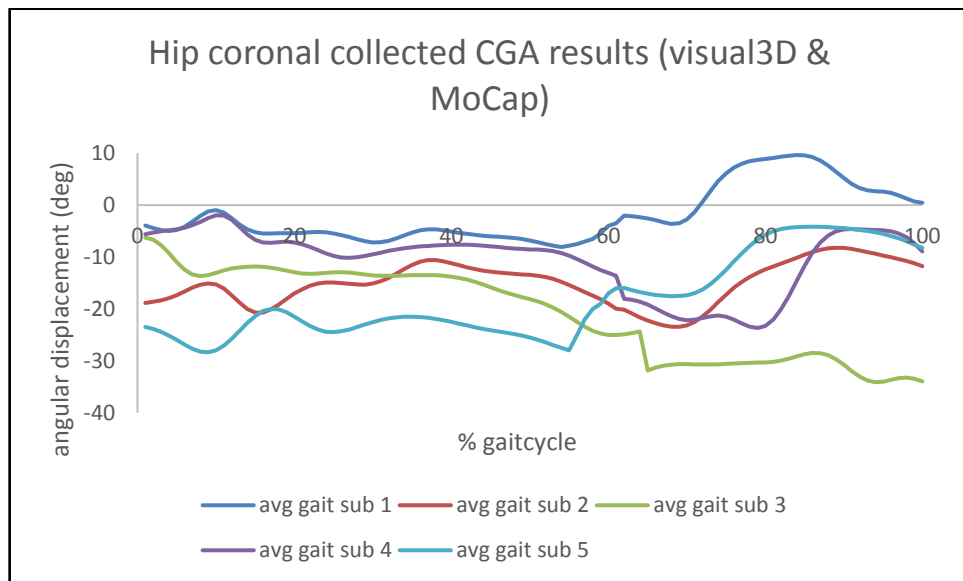


Figure 3.20 Hip internal/external rotation angular displacement capture and simulated CGA data

3.8 Summary

The 3D computational dynamic models of human gait cycle were developed based on motion capture data collected from five healthy participants at the University of Leeds, for the purposes of exoskeleton design inputs. In this chapter all degrees of freedom of the relevant joints have been verified by clinical gait analysis data from the literature for purposes of model verifications. The mechanical power consumption of the human during the activity of walking is one good indication to evaluate the effort and efficiency used to perform the task, the aim is to find healthy human walking that consumes less effort during the collected clinical gait analysis data and use the found kinematic and kinetics to come up with the parametric design and specification of the robot. Two factors effecting the significant of the mechanical power consumption in the inverse dynamic computation are the created torques at the joints of the human/exoskeleton, and the angular displacements at the joints of the human/exoskeleton, this chapter focuses on investigating the collected CGA data kinematics to find the form of walking which has the lowest average of angular displacements at the joints within all collected subjects.

The joint angular displacement will be the provided exoskeleton design maxim allowed ranges of movements for their exo joints which sets the kinematic requirements of the exoskeleton joints as shown in chapter 7.

The angular displacement results found in this chapter are used to solve the inverse kinematic dynamic of the exoskeleton computer model.

It was necessary to collect the CGA data independently, as this project is aiming to provide a detail dynamic analysis of the exoskeleton in all planes, and lack of verified data in the literature in other planes apart from the sagittal plane lead to this work.

Chapter 4

Selected human degrees of freedom focusing on their physiological efficiencies during human gait

4.1 Introduction:

The biomechanics research is used vastly in the design of robotic exoskeletons; it is used to determine part of the kinematics and kinetics specifications of the design as well as investigating the influence of the design on the metabolic cost of the user.

A design requirement of the assistive exoskeletons is to follow the as close as possible kinematic map as the human user (Correa et al., 2010). Due to exoskeleton design restrictions such as weight and cost, it is not the most efficient approach to activate the same number of joints in the exoskeleton as those in the human body. This research aims to identify the most essential joints in a healthy human during the level ground walking activity. To help toward the design of the active joints of the exoskeleton.

In this work the energy consumption of the human has been measured during the activity of the level ground walking. During various trials different mechanical restrictions have been applied to the human subjects while continuing the activity of gait cycle.

The anthropomorphic design brings two types of challenges to the application of the device; the first challenge is considered to be the safety of the user from the interference between the exoskeleton and the user without obstructing and resisting any of the user's necessary movements (Bohannon, 1997, Pandy and Andriacchi, 2010, Perkins et al., 1989). The second challenge is the increased power consumption of the user after restriction is applied (Dollar and Herr, 2008).

The metabolic measurement was done by using the Douglas bag method; while the mechanical restrictions were applied at the specified degree of freedom. The mechanical restrictions were aimed to duplicate similar to the

same mechanical restriction that may be acted exerted by the exoskeleton on the joints of the human.

The results from the experiments were analysed by using a one way ANOVA and TUCKEY test statistical methods to ensure the validity of the results and the procedure of the experiment, as well as discovering which joints have the highest contribution compared to the base line of the subject walking without any restrictions.

4.2 Methods

One of the challenges in design of an assistive exoskeleton device is to select the efficient number of joints of the exoskeleton. This directly affects the efficiency of the device due to the large concentration of the mass and applied forces at the active joints caused by the actuation system. The level ground walking at a slow speed is largely a sagittal plane lower limb activity, thus the lower limb joints in the sagittal plane such as hip (flexion/extension), knee (flexion/extension), and ankle (flexion/extension) need to be catered for in the design of the assistive exoskeleton as found in the results section of Chapter 7. This study concentrates on evaluating the efficiency of the non-sagittal joints in the lower limb (hip rotation, hip abduction/adduction, ankle inversion/eversion) and sagittal and rotational joints for the upper body (shoulder flexion/extension, shoulder abduction/adduction, and elbow flexion/extension). The mechanical restrictions are aimed to mimic the same restrictions as an exoskeleton would have on the user. The aim is to restrict each degree of freedom at a time to be able to validate the contribution of that restriction and compare the metabolic energy expenditure of the same subject with and without restriction during the walking trial.

4.2.1 Subjects

The main purpose of this experiment is to evaluate the effects of the change in healthy subject's energy expenditure from the restrictions applied on the selected joints once at a time, compared to the subject doing the same manoeuvre without any restrictions.

To reduce the factors of errors during the experiment each subject had three trials performing each restrictions , the test protocol and selection on number of trials were based on the literature work done by (Hopker et al., 2012). Subjects included 6 healthy males ages of 24 ± 6 and height of 176.5 ± 4.5 cm and weight of 83 ± 13 kg. The subjects performed the experiments during a set time for all their three repeats of each trial. The subjects were advised to be food fasting on the day of the experiment as well as avoiding any heavy physical activities, consuming nicotine, caffeine, alcohol or heavy meals as they affect the metabolic cost rate of the user. A copy of the experimental protocol and a consent form was given to the subjects prior to the experiment, which included some questions to gain information about the subjects health status as well as explaining the experimental procedure along with identifying the risks and hazards of the experiment.

4.2.2 Sampling Reliability

The experiments included from each moderate level walking on a treadmill at seven different modes. Locked ankle inversion/eversion, locked hip rotation, locked hip abduction/adduction, locked elbow flexion/extension, locked shoulder flexion/extension, locked shoulder abduction/adduction, and subject without any restrictions. The subjects expired gas was collected via a Hans Rudolph breathing valve (2700; Hans Rudolph, Inc., Kansas City, MO) into a plastic Douglas bag for gas analysis. The concentration of O_2 and CO_2 were repeatedly determined from three trials to find out the variability in sampling. During repeated sampling, the gas analysers were running continuously and were recalibrated by the laboratory technicians prior to each experiment. The concentration of the O_2 and CO_2 of the ambient air was also collected prior to each experiment by using the Servomex gas analyser to determine there is no change in the condition of the experiments (Zoss et al., 2006). The subjects wore the polar heart rate monitor in direct contact with their skin which collects the subjects heart rate during the rest time, and during the experiment.

4.2.3 Procedure

Prior and after each test, the subject is rested in a sitting position without any mechanical restrictions and strains on the subject's body for twenty minutes. This is followed by wearing the required apparatus just before switching on

the treadmill, the required apparatus are; mechanical braces, Douglas bags and accessories, Polar heart rate monitor, Servomex gas analysers, Rating of perceived exertion (RPE) card, Stop watch/timer, Stadiometer, Seca weighing scales, Pressure meter and Dry gas meter. The Hans Rudolph breathing valve connects to the Douglas bag rigs through a plastic pipe. A nose clip is worn by the subject during the experiment to ensure all the gases that the subject is inhaling and exhaling is captured through the Hans Rudolph breathing valve and collected into the bags. At -30 seconds before the gas collection starts the heart rate monitor begins to record the data; this procedure allows the polar heart rate monitor to calibrate to the correct measurement. At 0 seconds of each experiment the valve of the first bag was opened, the first bag is collecting the gases exhaled by the subject for 120 seconds which measures the subject metabolic cost rate at rest, at the 120 second mark the first valve is closed. From 120 second to 180 second the assistant adjusts the speed of the treadmill from 0 km/hr to 2.0 km/hr (0.6 m/s) which is established to be the average level ground walking speeds of older adults, stroke hemiplegia, Incomplete SCI outdoor walkers, and frail elderly (van Hedel and Group, 2009). The subject is walking until steady state speed is reached, by the 360 seconds the subject has reached the steady state and the valve on the second bag opens up to capture the expired gases for another 120 seconds. This is repeated for two more bags and at the 795 seconds the heart rate recording and the treadmill stops. The subject is then back to the seated rest position for a further 20 minutes before beginning the next experiment.

4.2.4 Data Collection and extraction

The Douglas bag method is a metabolic measurement method which aims to find the metabolic energy expenditure of the user to perform a set task. Therefore during each experiment each subject's expired gas will be collected in the Douglas bags and then analysed for their fractional concentration of O₂ and CO₂ and total volume. The oxygen consumption is determined by using indirect calorimetry method (Bohannon, 1997) where the equations used in this section extracted from.

The following equation is used to determine the volume of oxygen consumed during the walking trials.

(4-1)

$$\dot{V}O_2 = \dot{V}_I(F_I O_2) - \dot{V}_E(F_E O_2)$$

where:

$\dot{V}O_2$ is Volume of oxygen consumption (litres/minute)

\dot{V}_I is flow of inspired gas (litres/minute)

$F_I O_2$ is fraction of the oxygen in the inspired gas

\dot{V}_E is volume of gas collected in one minute (litres/minute)

$F_E O_2$ is fraction of the oxygen in the expired gas

This method uses a law of thermodynamics which entails the consumption of oxygen with the production of carbon dioxide, nitrogenous waste, and water. The consumption of VO₂ is determined by using equation (4-1).

Equation (4-2), calculates volume of the gas collected in one minute from the raw data to normalise the collected data to its duration.

(4-2)

$$\dot{V}_E = V_E * \left(\frac{60}{duration} \right)$$

where:

\dot{V}_E is volume of gas collected in one minute (litres/minute)

The second unknown is the amount of carbon dioxide output in each bag for each experiment. The carbon dioxide output is calculated using equation (4-3), which gives the difference between the amounts of carbon dioxide inhaled and exhaled per unit time (l/min):

(4-3)

$$V\dot{C}O_2 = (V_L * F_I CO_2) - (V_E * F_E CO_2)$$

where:

\dot{V}_I is flow of inspired gas (litres/minute)

$F_{L}O_2$ is fraction of the oxygen in the inspired gas

$F_{L}CO_2$ is fraction of the carbon dioxide in the inspired gas

$F_{E}O_2$ is fraction of the oxygen in the expired gas

$F_{E}CO_2$ is fraction of the carbon dioxide in the expired gas

To analyse the gas collected in the Douglas bags, all the variables are collected by using the Servomex gas analysers; the device provides the following variables; Fraction of the oxygen in the inspired gas $F_I O_2$, Fraction of the carbon dioxide in the inspired gas $F_I CO_2$, fraction of the oxygen $F_E O_2$, and fraction of the carbon dioxide $F_E CO_2$. To achieve the Volume of the exhaled gas $\dot{V}E$, the Douglas bags are connected to the dry gas meter where the gases are vacuumed and analysed. The variables are then used in a spread sheet calculator which will determine the VO_2 consumption of the user through all collected bags in litres per minute or joules per minute. The results of the calculations are presented in the Results section of this chapter.

4.3 Mechanical Restrictions on Joints

The applied mechanical restrictions were designed to mimic such restrictions as an actual exoskeleton would have on the human user. Thus by comparing the collected metabolic measurements with and without restriction for each selected degree of freedom it would be possible to rate the efficiency of each degrees of freedom during the human walking by the change in the metabolic power consumption of the user. The selected degree of freedom and the braces used for restricting these following degrees of freedom are shown in Table 4.1 for lower extremities followed by the upper extremities mechanical restrictions shown in Table 4.2.

Table 4.1 The mechanical restrictions used for lower extremity







Joint	Type of Motion	Designed Mechanical Restriction
Ankle	Inversion/eversion	 A white and blue ankle brace with multiple straps, designed to restrict inversion and eversion of the ankle.
Hip	Medial Rotation	 A beige hip brace with a central metal rod and a dial, designed to restrict medial rotation of the hip.
Hip	Abduction/Adduction	 A beige hip brace with a central metal rod and a dial, designed to restrict abduction and adduction of the hip.

Table 4.2 The mechanical restrictions used for upper extremity

Joint	Type of Motion	Designed Mechanical Restriction
Elbow	Flexion/Extension	
Shoulder	Adduction/Abduction	
Shoulder	Flexion/Extension	

4.5 Effect of the weight of the braces on metabolic cost of the users

On a separate experiment prior to the main experimental work, the effect of the weight of the mechanical braces restriction was investigated (no restriction, just the effect of the external weight, with three repeats of each mode on two healthy male subjects), by comparing the metabolic costs of a subject with and without external weight of the mechanical braces. Due to the light weight of the braces the results showed no noticeable change between the variation 1 (with the external weight of the braces on) and variation 2 (without any external weight of the braces), Thus during the main experiments each brace was worn one at a time. The statistical analysis was also performed on this case study, the p value was taken as 0.05 and the post hoc Tuckey test has shown the p value of 0.012 which means no significant difference between the energy cost expenditure in the subject while carrying the extra weight of the brace compared to no external weight modes.

4.6 Results

The effects of various joints restriction on the total power consumption of the subject have been studied. The experiments consisted seven variations, of mechanical restrictions as shown in Table 4.1 and 4.2 (locked ankle inversion/eversion, locked hip rotation, locked hip abduction/adduction, locked shoulder flexion/extension, locked shoulder abduction/adduction, locked elbow flexion/extension), along with the base line as the subject had no restriction during level ground walking. Each variation was repeated three times during three experiments.

During the analysis of the results from the main experimental work the collected gas from each subject was stored in four available Douglass bags, each bag was collecting gasses for 120 seconds.

The results have shown in Table 4.3 the restriction can have diverse effect on the metabolic cost expenditure of the subjects compared to the base line with no mechanical restrictions.

Table 4.3. Average power consumption (J/kg) values collected for all 5 participants during the 3 repeats

	No restriction(Base line)	Shoulder Abduction Adduction	Shoulder flexion extension	Hip abduction adduction	Hip rotation	Ankle inver/ever	Elbow flexion extension
Average Value	3.49	3.64	3.47	3.86	4.20	3.48	4.42

The results shown in Table 4.3 are the energy expenditure captured and calculated from each bag deducted from the base line initial resting value collected in the first bag in each trial. The metabolic energy expenditure results were initially calculated in mLitres/minute and then normalized to the weight of the user and duration of the experiment to J/kg. Each variation of the experiment has statistically been investigated to see if there is a significant difference within each group of the result. The statistical analysis showed no significant difference within group and within each variation of the experiment, thus the average value were taken from all participants for each experimental mode.

The bar graphs in Figure 4.1 represent the results give in Table 4.3.

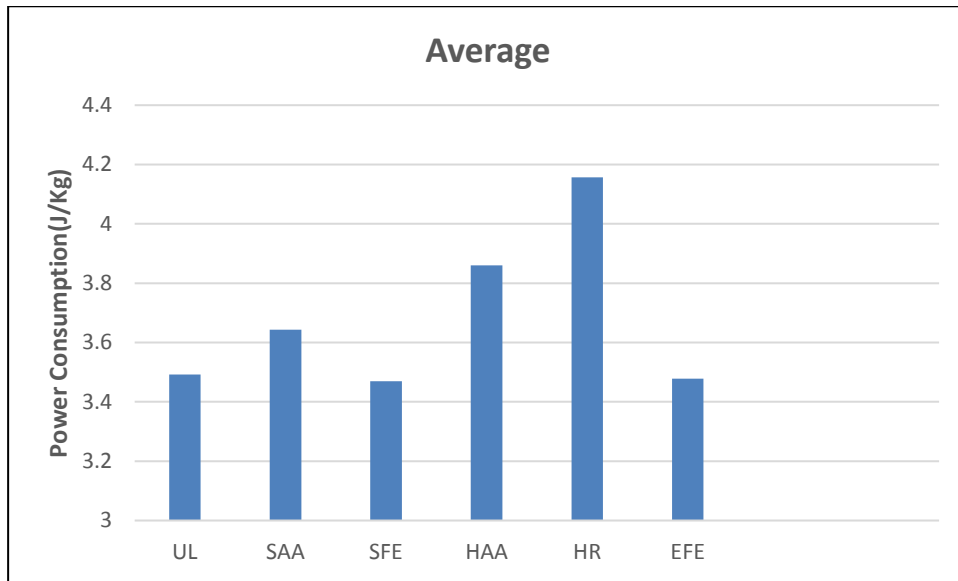


Figure 4.1 metabolic power consumption during unlocked mode and restricted modes through all subjects during the following modes: unlocked (UL), shoulder abduction/adduction (SAA), shoulder flexion/extension (SFE), hip abduction/adduction (HAA), hip rotation (HR), elbow flexion/extension (EFE), ankle inversion/eversion (AIE)

From the results shown in Figure 4.1 the most efficient degrees of freedom determined by increase in the collected metabolic consumption compared to the base line of unlocked mode. The ankle inversion/eversion and hip rotation have the highest impact on the increase of the metabolic cost rate, followed by hip abduction/adduction and slight increase in shoulder abduction/adduction. In case of elbow flexion/extension and shoulder flexion/extension the results shows a small decrease in the metabolic cost of the user. Table 4.4 represents the percentile changes after applying the mechanical restrictions, compared to the unrestricted free walking of the healthy subjects.

Table 4.4 Percentile increase/decrease of metabolic expenditure restricted compared to unrestricted

Shoulder abduction/adduction	Shoulder flexion/extension	Hip abduction/adduction	Hip rotation	Elbow flexion/extension	Ankle inversion/eversion
+4.33%	-0.61%	+10.63%	+17.23%	-0.33%	+26.84%

4.6.1 Statistical Analysis

As explained in section 4.2.3 , the experiments had seven variations and each variation was repeated three times.

Analysis of variance was the chosen method to test the differences between the means of the results. The means are relevant to the different degrees of freedom which were locked at specified joints. The ANOVA results will determine if there is any real difference between the specified means. The chosen p value was set at 0.05, the p value from the ANOVA calculation was 2.4×10^{-13} , which means there were differences within groups were seen, so the data could be averaged in each group to gain an easier understanding of the results. The Tuckey post hoc analysis was also used to verify if there was any significant differences between the groups, the chosen p value was set at 0.05, and the analysis compared the results from individual modes of the study to the base line mode (subject with no restrictions). A difference was seen between the hip rotation, hip abduction/adduction, ankle inversion/eversion when restricted cases were compared to the base line of no restriction.

4.7 Summary

Lack of information on physiological in design and performance of the existing exoskeletons designs have been found on the review work done by (Valiente, 2005).

The gap in the field of exoskeletons as mentioned by (Dollar and Herr, 2008), is the need of research into the human robot physiological interactions, and taking human physiology and biomechanics into consideration at the design stage. The ankle has the highest percentage of total positive power compared to the hip and knee joints during human walking at four various speeds from 0.75 m/s to 2m/s (Valiente, 2005).

The current research investigates how a major joint such as ankle that transfers a high amount of work power during the locomotion of level ground walking, would behave under total restrictions at flexion/extension degree of freedom. The 100% restriction (0 degree movement) condition was chosen to be used for all the joints during the lock modes so the effect of each chosen joint on the total power consumption of the user could be measured by a standard physiological gas measurement technique under the same condition (Douglas bag method). One of the major challenges in designing the assistive exoskeletons is the limitation on activating as many joint as possible; this issue is related to the high concentration of the mass and external forces at each mechanical joint due to the active and passive actuation systems. This method can be used as a guidance in design of the assistive exoskeletons to identify the most effective joints on the entire power consumption of the users during any set activity.

Human body can be looked at as a mechanical system, having bones as the frame and the joints as the degrees of freedom which transfer the forces to other limbs. In this system the muscles work as the active actuators and ligaments work as the springs and dampers. The human level ground walking is the major lower body activity. Variables affecting the metabolic energy consumption in human walking include the speed at which the human is walking at. The purpose of this study was to use the information from the metabolic measurements as a systematic method for choosing the active/passive/restricted the joints of the exoskeleton. The walking speed for

population with lower muscle abilities can vary from 0.2 m/s to 0.80 m/s (van Hedel and Group, 2009) the average recommended walking speed for patients with the following conditions : Stroke/Hemiplegia , Incomplete SCI, Frqail Elderly is chosen at 0.6m/s (van Hedel and Group, 2009) this was used as the chosen speed for this study.

The walking speed is a crucial factor affecting the intensity of walking and energy expenditure of the activity (Waters and Mulroy, 1999). The study of the Clinical gait analysis comparison in finding the most efficient gait present results on how the various speeds change the metabolic work efficiency of the human walking.

The main activity of the upper body during the human walking on a treadmill is the swing in the arm, shoulder and torso: the intensity of the swing is directly related to the speed that the human is walking at. There are two hypothesis on the upper body swing mechanism (Bramble and Lieberman, 2004). The first hypothesis, indicates that the main limbs responsible for the force generation in the swing is caused by the movements in the legs and pelvis then the transferred force will result in movements in the shoulder and elbow joint. the second hypothesis (Elftman, 1939), is indicating that the main force causing this swing is generated at the shoulder joint. These hypotheses have been studied in the literature by (Pontzer et al., 2009).

The results of this study support the first hypothesis mentioned above and suggest that the arm swing does not have a great effect on the metabolic cost of the subject during walking at slow speed (0.6 m/s). It is visible that restriction on some of the upper body joints (shoulder flexion/extension, elbow flexion/extension) as shown in Figure 4.1 has a diverse effect on the efficiency of walking, thus by providing mechanical restriction the metabolic effort has decreased compared to base line with no restriction.

The results shown the lower limbs indicate significant effect on the non-sagittal plane joints. It is obvious that the human walking is mainly a sagittal plane activity thus it is not possible to restrict any sagittal plane lower limb joints, but restricting the tested non-sagittal lower limb joints in this study (ankle inversion/eversion , hip rotation , and hip abduction/adduction) do still have a

significant effect on lowering the metabolic cost efficiency during the human walking.

These results can lead to a whole new concept in the design and use of exoskeleton devices by designing more activated joints for the lower limbs consisting two DOFs at the ankle joint, one DOF at the knee, and three DOF at the hip joint of each leg. A passive supportive structure for the upper body joints can be designed as activating the upper body joints does not have a direct effect on lowering the metabolic cost rate in walking, but it can reduce the vertical excursion of the centre of mass (Umberger, 2008), and other effects such as increasing the mechanical stability (Ortega et al., 2008), and reduction in vertical ground reaction forces (Li et al., 2001).

The design of an anthropomorphic exoskeleton frame for this project will provide fourteen degrees of freedom, supporting the hip, knee, and the ankle joint.

4.8 Summary

The physiological measurement of human VO₂ consumption was used to verify various non-sagittal joints efficiencies as a design approach in selecting the exoskeleton necessary degrees of freedom as.

This is done by applying similar mechanical restriction as an exoskeleton will have on the selected joints, and comparing the outcomes with to the base line of the healthy human with no restrictions.

The results indicate the ankle inversion eversion followed by the hip rotation and hip abduction and adduction are the most contributing non sagittal degree of freedoms during the activity of gait. While upper body joints were among the least metabolic energy contributors during this activity.

Chapter 5

Clinical gait analysis comparison in finding the most efficient gait

5.1 Introduction

As explained in Chapter 3, clinical gait analysis (CGA) data were recorded from five participants doing the activity of level ground walking at a comfortable to low speed. The dynamic models of the human trials have been built and inverse dynamic simulations carried out; the kinematic and kinetic results have been verified and compared with the literature data (Margareta Nordin 2001). The aim is to use the angular velocities at the human joints, as inputs of the motion simulation model for the exoskeleton gait, thus the exoskeleton would be following the human kinematics and the exoskeleton motion will be as close as possible to the human motion. This chapter is aiming to examine the efficiency of the collected CGA trials, by evaluating kinetic factors such as mechanical power, reaction forces and metabolic expenditure. This method will ensure the exoskeleton motion and design specification is based on an efficient and natural way of human walking.

The active actuated joints of the exoskeleton are chosen from the results and conclusion work from chapter 4.

To identify the most efficient angular joint velocity inputs for the exoskeleton model, an analysis into human kinetics was carried out by using the inverse dynamic computational human model in Visual3D package.

The inverse dynamics at the joints and segments of the human, provides the mechanical power consumed during one complete gait over the two force platforms, measured at the motion capture laboratory in the University of Leeds.

The lowest mechanical power consumption (from the human model simulation) along with the lowest reaction forces (collected) are used as direct indications for the selected motions as the exoskeleton dynamic model and inverse dynamic simulation inputs.

5.2 Method

The mechanical power at the joints of the human are calculated from the computed inverse dynamic simulation in visual 3D models, from the experimentally captured reflective marker positions (to the set laboratory reference) and collected reaction forces across all five participants. All the power results are normalized to the weight of the participants, and the duration of the gait has been normalised from one heel strike to the next heel strike of the same leg (as 100%) for one complete gait cycle.

To calculate the total power consumption of each human model, the power at the following segments mentioned in equation (5-1) are summed.

The direction of the force at each joint relative to the direction that the body mass is moving to determines the sign of the power (negative or positive).

(5-1)

$$P_{total} = |P_{ankle}| + |P_{knee}| + |P_{hip}| + |P_{torso}|$$

The instantaneous joint power at the segments was derived from the computed torques at the joints times by the changing rate of change of the joint angles during the gait cycle as shown in equation (5-2).

(5-2)

$$P_{joint} = T_{joint} \times \frac{d}{dt}(\theta_{joint})$$

Where:

T_{joint} is the torque at the joint

$\frac{d}{dt}(\theta_{joint})$ is the angular velocity at the joint

The instantaneous joint power at each segment can consist of positive and negative values; the sign indicates the rotational direction of which the power is acting around the joint. The positive power indicates the power needs to be generated by the body in order to move the body forward in space; this power is generated by the muscles and ligaments of the healthy human. The

negative power is the power absorbed by the body. The power generated and absorbed should be achieved by design of the appropriate active and passive actuators (motors, gears, springs and dampers) of the exoskeleton as will be discussed in chapters 7 and chapter 8.

5.3 Results

5.3.1 Ankle joint mechanical power consumption

5.3.1.1 Ankle sagittal plane (flexion/extension)

The ankle joint's power graphs from the literature (Kirtley, winter, Linskill.CGA data) are shown in Figure 5.1. The graph indicates that most of the power absorption starts from the initial stance phase and finishes before the flatfoot phase. The ankle joint goes through a high amount of power generation during the flatfoot and toe off stage to be able to swing the foot forward. The power consumption is at its lowest near zero during the swing phase of the ankle.

Due to nature of this research it is necessary to investigate the joint kinetics at specific chosen speeds, thus comparing to the literature data (mean speed) can some level of differences be seen in comparison.

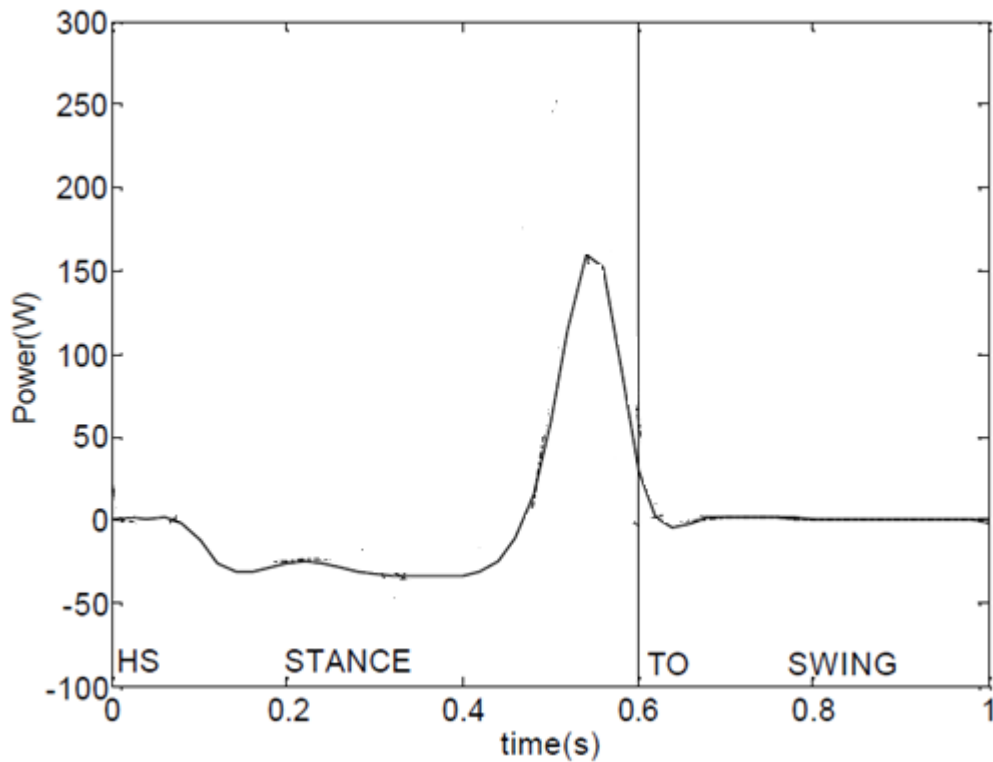


Figure 5.1 Ankle flexion/extension power consumption for one gait from literature (Margareta nordin 2001)

The computed power results using the inverse dynamic method (Visual 3D simulations) shown in Figure 5.2 has the same pattern and peak values as the literature data shown in Figure 5.1 for verification purposes.

The collected ankle power graph is covering a much bigger area during the positive power generation especially during the foot flat and at the initial swing phases. This is a good indication for design of the ankle joint of the exoskeleton to be activated by motors with high peak but small RMS power outputs.

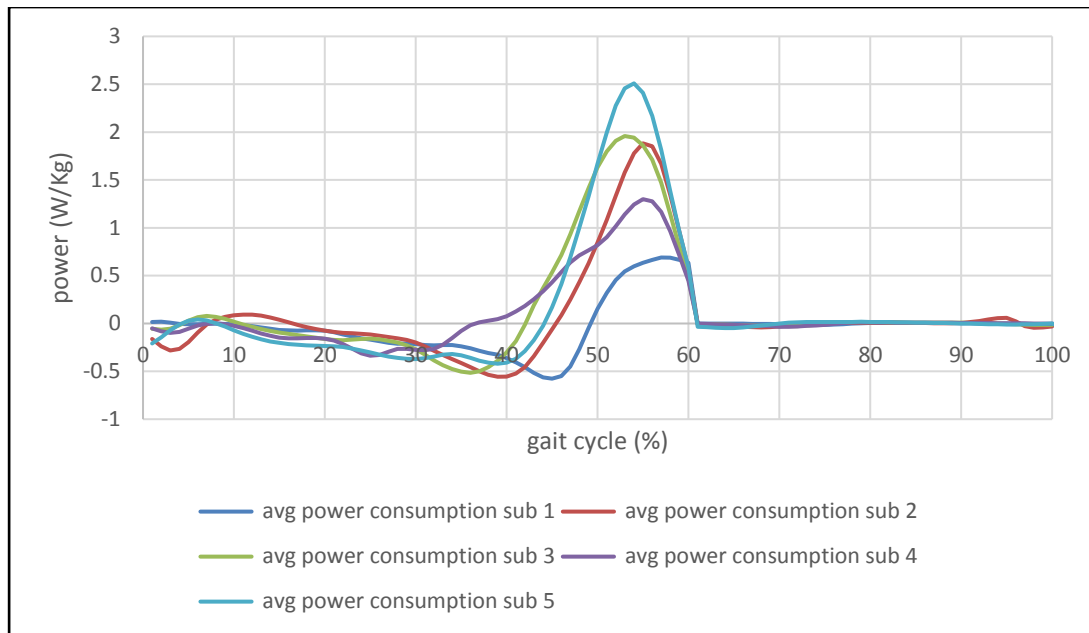


Figure 5.2 Ankle flexion/extension power consumption from captured and measured CGA data

The speed and other physiological contributors such as height, stride length and gait pattern could be driven factors for various peaks in the figure above.

The ankle joint during the stance phase has some of the highest captured and simulated torques compared to the other joints; this can be seen in Figure 5.2. These high torque results in the high power consumption are shown in Figure 5.3. The torques during the swing phase are near to zero which follow the same pattern as the power consumption of the ankle during this phase.

The direction of the joint rotation relative to the direction which the body is moving towards define the positive and negative values of the torques.

For the purpose of finding the most efficient gait within this study the energy generated along with the force acting on the ankle joint during various walking speeds have been compared in

Table 5.1.

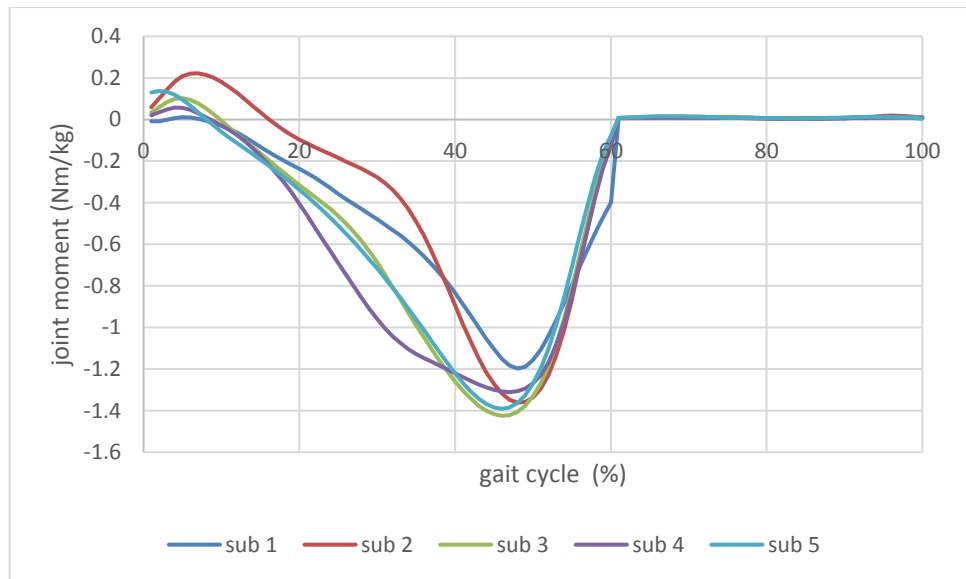


Figure 5.3 Ankle flexion/extension joint torques from captured and simulated CGA data

Table 5.1 shows the most efficient gait at the ankle joint has torque values lower but in the same range of some other subjects at value of about 30 Nm/kg but due to its low speed the power consumption found to be lower by 58% compared to the subject with faster speed of 0.9m/s.

As seen in the figure 5.2 and 5.3 the most efficient pattern covers the least area under both graphs to be the subject with the lowest speed.

Table 5.1 Ankle joint flexion/extension absolute power consumption, absolute torque consumption, average velocity from captured and simulated CGA data

DOF Ankle flexion/extension	Absolute Power consumption (Watts/kg)	Absolute Torque (Nm/kg)	Average Velocity(m/s)
Subject1	15.10	30.38	0.6
Subject2	26.22	30.19	0.9
Subject3	30.33	38.72	0.95
Subject4	21.02	41.21	0.8
Subject5	34.65	38.27	1.2

5.3.1.2 Ankle inversion/eversion mechanical power consumption

Figure 5.4 shows the graph of mechanical power consumption of the healthy subject's ankle inversion/eversion joint in the coronal plane, which indicates an overall low negative power average which means the power is being absorbed. The maximum peaks occur around the same phase as the ankle flexion/extension (foot flat to toe off) but in the reverse direction. There has been no clear reported results on the power output of the ankle Inversion/eversion in the literature.

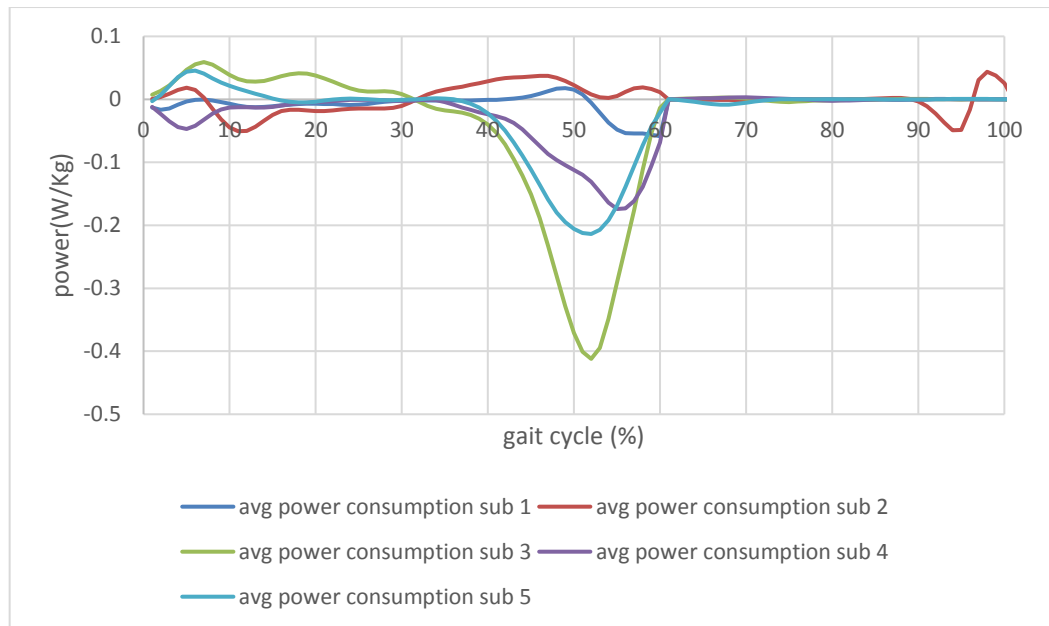


Figure 5.4 Ankle inversion/eversion power consumption from captured and simulated CGA data

5.3.2 Knee joint

5.3.2.1 Knee joint flexion/extension mechanical power consumption

The literature data in figure 5.5 shows the knee joint is mainly absorbing the power as the graph indicates mostly negative average values, with smaller positive peaks. The largest negative peak occurs at the toe off.

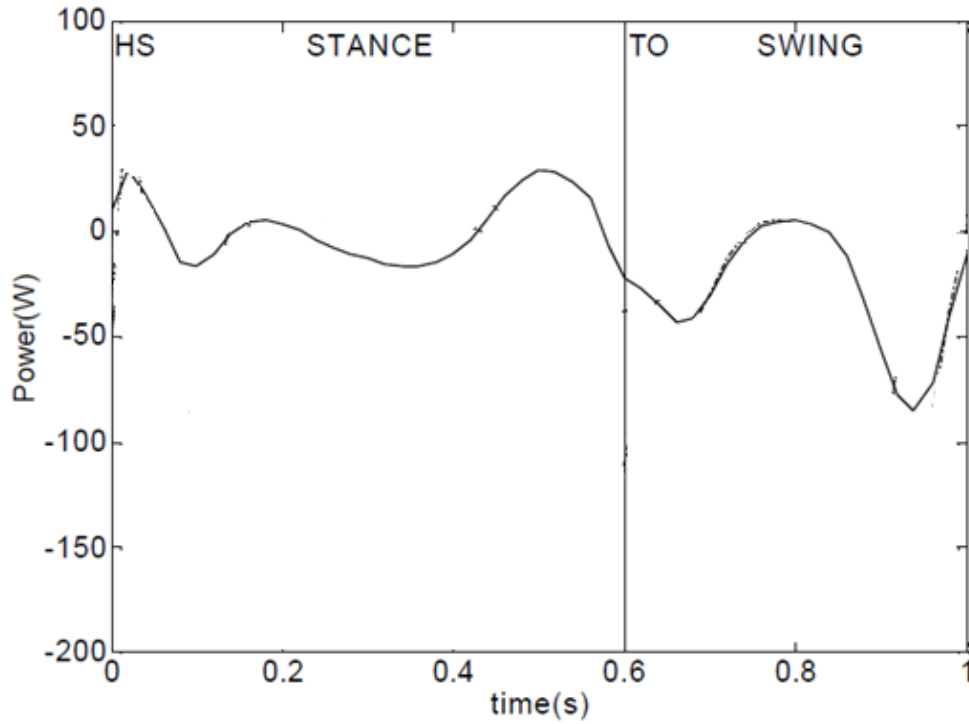


Figure 5.5 Knee joint flexion/extension power consumption from the literature data (Margareta nordin 2001)

The collected knee mechanical power consumptions follow the same pattern with the literature data as shown in Figure 5.6. The absorbing maximum powers occur mainly during the initial stance, foot flat to toe off and also at the end of the swing phase.

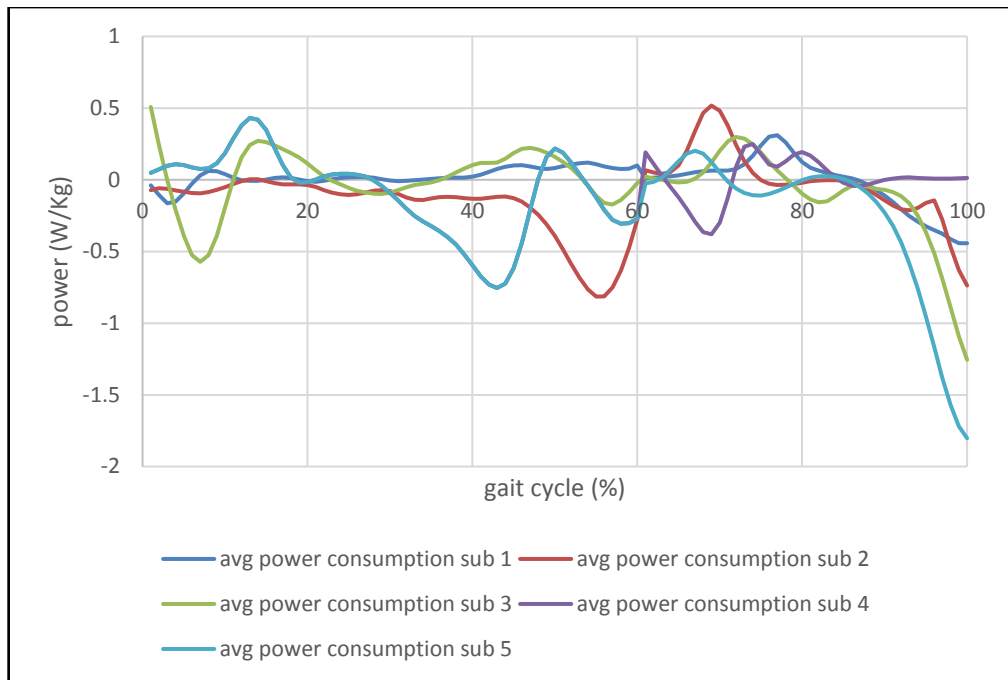


Figure 5.6 Knee joint flexion/extension power consumption captured and simulated from CGA data

The knee joint goes through its largest torque output during the heel strike and the loading strike as it is going through its largest extension which follows a flexion during the mid-stance phase, before it finishes with a final extension at the terminal stance as shown in Figure 5.7. During the swing phase the torques are at minimal and very close to zero.

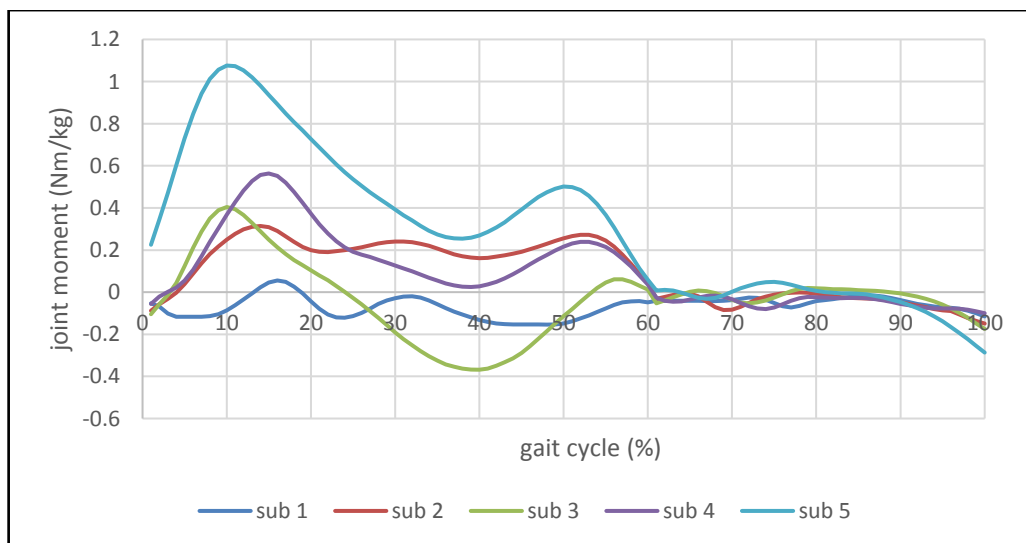


Figure 5.7 Knee joint flexion/extension torque captured and simulated from CGA data

The relationship between the speed, torque and power consumption can be seen in Table 5.2. where the most efficient recorded gait has the lowest torque along with the lowest speed and the lowest mechanical power consumption at the knee joint by 49% compared to the next most efficient gait. Some of this efficiency is due to the even power distribution between this subject's joint which is mentioned in the Discussion section of this chapter.

Table 5.2 Knee joint flexion/extension absolute power consumption, absolute torque and, average velocity from Captured and simulated CGA data

DOF Knee flexion/extension	Absolute Power consumption (Watts/Kg)	Absolute Torque (Nm/Kg)	Average Velocity(m/s)
Subject1	8.82	7.07	0.6
Subject2	18.13	13.8	0.9
Subject3	17.60	12.74	0.95
Subject4	18.13	13.74	0.8
Subject5	26.86	33.95	1.2

5.3.3 Hip joint

5.3.3.1 Hip joint flexion/extension mechanical power consumption

The hip flexion/extension literature data Figure 5.8 shows and verifies the pattern and magnitudes of the collected data shown in Figure 5.89. A larger positive average power output was recorded throughout the gait cycle as shown in both literature and simulated data. This indicates active actuation system is required for the exoskeleton hip, which is discussed in more details in Discussion section of this chapter.

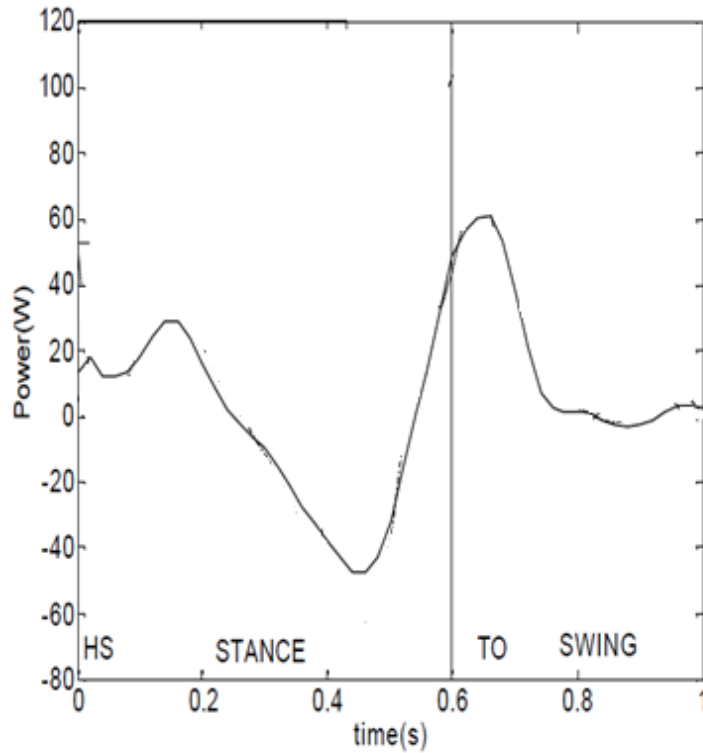


Figure 5.8 Hip joint flexion, extension power consumption from the literature (Margareta nordin 2001)

Most of the power absorption occurs during the initial to mid stance phases. The biggest power generation peaks occur at around the toe off at $\approx 60\%$ of the gait cycle.

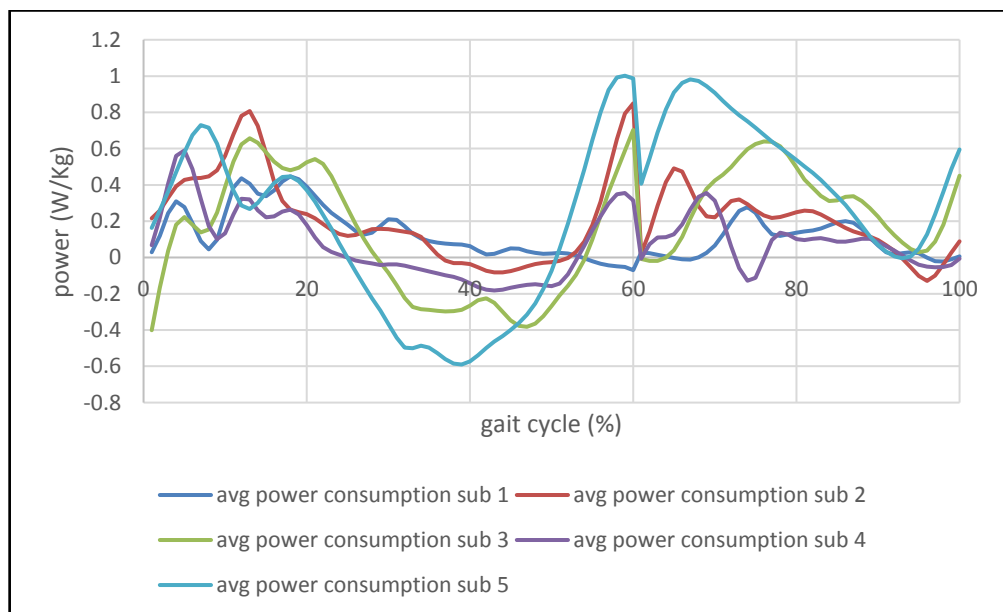


Figure 5.9 Hip joint flexion/extension power consumption from captured and simulated CGA data

The hip flexion/extension starts with a small flexion at heel strike after an immediate extension where it reaches its peak torques just before the swing phase begins. During the swing phase the hip joint is mainly going through a flexion with its peak values occurring at the pre-swing phase, as shown in Figure 5.10.

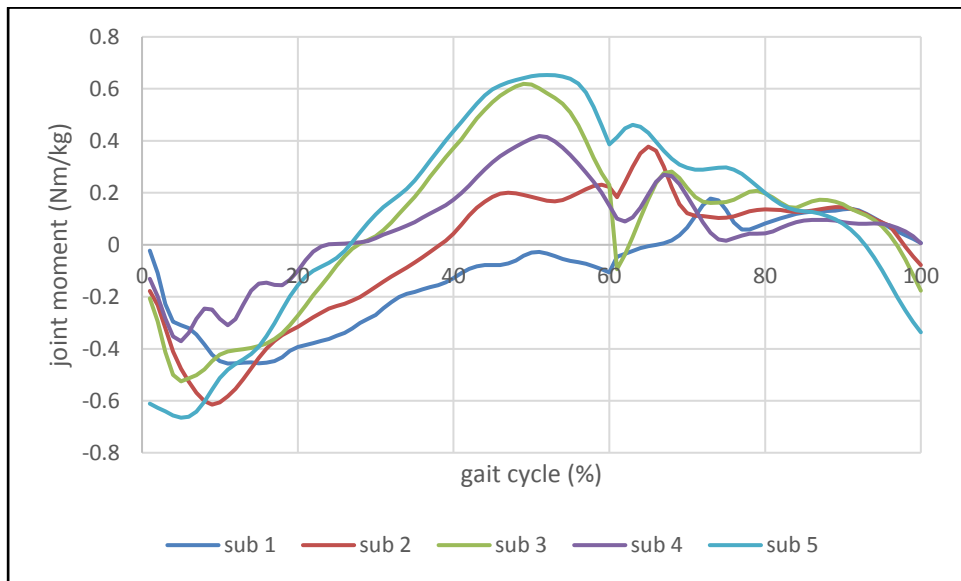


Figure 5.10 Hip joint flexion extension torque from captured and simulated CGA data

Table 5.3 shows the effect of the speed on efficiency of power consumption. As can be seen from this table subject 1 has higher torque value compared to the subject 4, but because he is functioning at a lower speed of 0.6m/s compared to the 0.8m/s speed of subject 4, he consumes less mechanical power to perform the gait.

Table 5.3 Subjects absolute power consumption, peak torque, and average velocity

DOF Hip flexion/extension	Absolute Power consumption (Watts/Kg)	peak Torque (Nm/Kg)	Average Velocity(m/s)
Subject1	13.10	17.13	0.6
Subject2	23.27	21.38	0.9
Subject3	30.87	26.97	0.95
Subject4	14.68	15.85	0.8
Subject5	45.83	34.15	1.2

The Table 5.2 shows an increase in absolute power consumption as the speed increases.

5.3.3.2 Hip joint abduction/adduction mechanical power consumption

The frontal plane motions of the hip joint was collected as shown in Figure 5.11. The abduction/adduction curve is similar to a sine curve behaviour specifically during the stance phase; this occurs to compensate for the nonlinearities and alignment of the hip joint with the rest of the body in order to keep the body and balancing of the user as mentioned for the ankle's non-sagittal degree of freedom (inversion/eversion). There is no available data in the literature on the power consumption of the human in the non-sagittal planes at the hip joint.

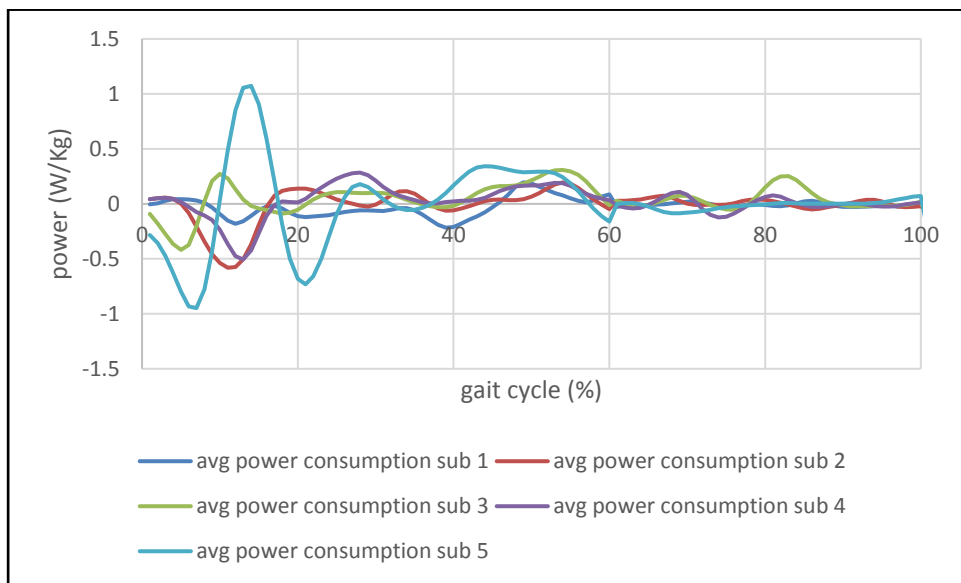


Figure 5.11 Hip joint abduction/adduction power consumption from captured and simulated CGA data

5.3.3.3 Hip joint internal/external rotation mechanical power consumption

The non-sagittal joints are mainly responsible to compensate for nonlinearity and balance of the body while keeping the motion of the user predominantly in the sagittal plane. The non-sagittal plane degree of freedom of the internal/external rotation of the hip also follow a sine curve behaviour during the stance phase as shown in Figure 5.12. The power output values are significant and it is a good indication that these cannot be ignored in the design of the exoskeleton systems.

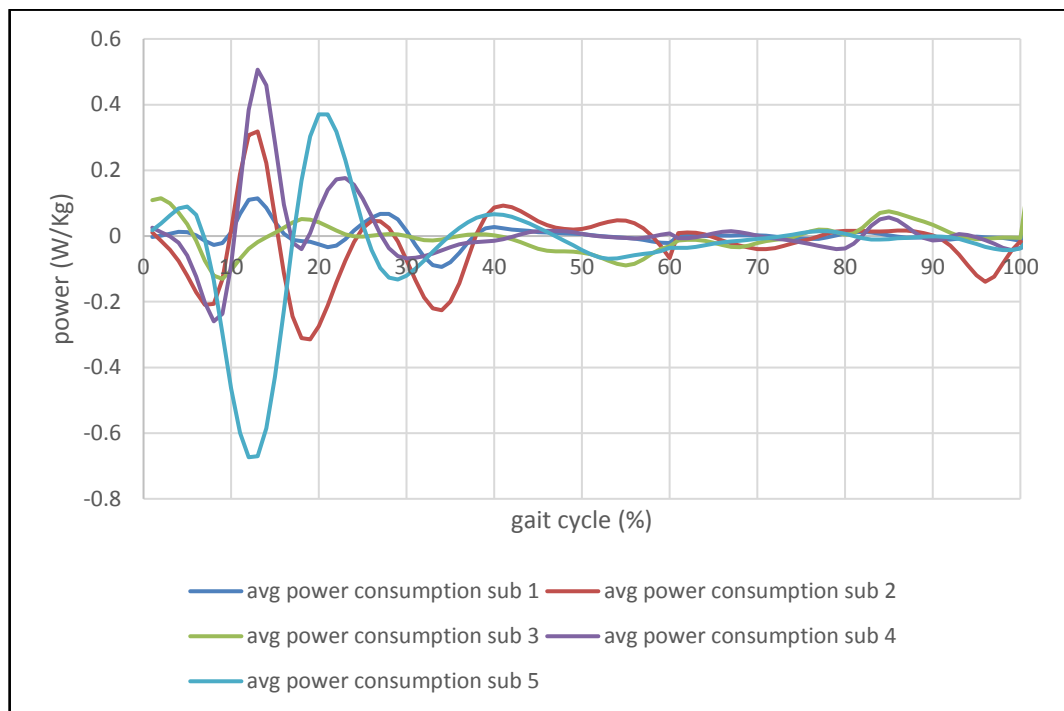


Figure 5.12 Hip joint internal/external rotation power consumption from captured and simulated CGA data

5.4 Reaction forces measured during various walking speeds

During the clinical gait analysis of the healthy human subjects, the reaction force data were collected using the force plates. The subjects walked over two force platforms, while the same leg goes through a swing phase on the first platform and a stance phase on the second platform.

The CGA with the lowest mechanical power consumption found in section 5.3 was based on walking trials in three different speeds, with five repeats at each speed. The first set of trials occurred at slow comfortable speed with overall average of 0.6 m/s (computed from visual 3D); the second set of trials occurred with normal walking speed with overall average of 0.9 m/s, and the last set of trials was fast walking at average speed of 1.1 m/s .

The ground reaction forces were measured using two force platforms explained in section 3.5.1 Efficiency is measured by comparing kinetic measurements such as external forces applied to the human.

The subjects were found to have the lowest recorded reaction forces during the slow speed gait, in comparison with normal and faster speed trials.

The recorded experimental force platform data are shown in Figure 5.13

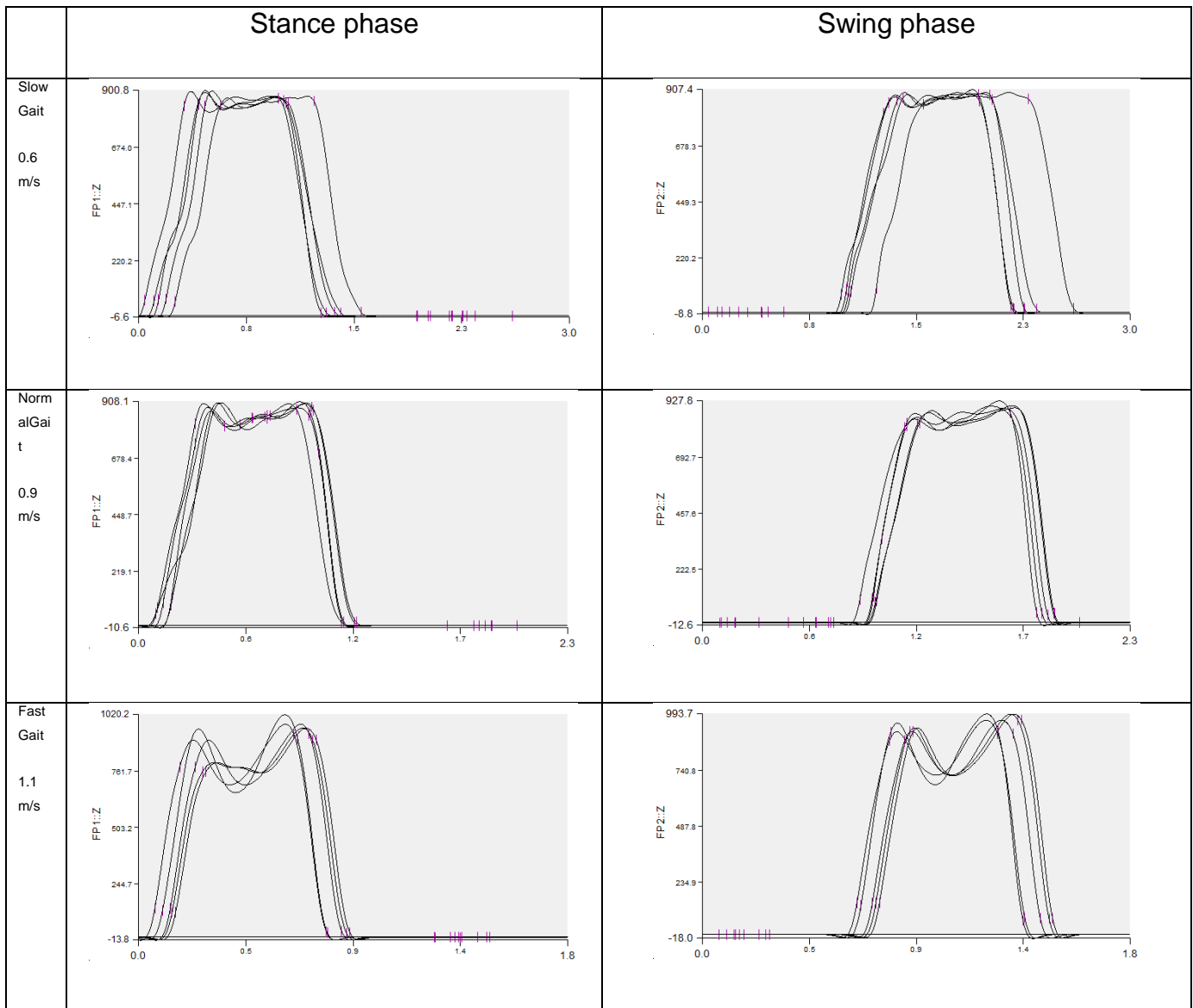


Figure 5.13 Force platform collected data (N) against the time(s) over 5 trials at 3 different speeds during the stance and swing phases

5.5 Discussion

The direction in which the forces are acting defines whether the power is being absorbed, stored and generated by the body. Positive power indicates the power that the muscles and ligaments generate in order for the body to follow the desired motions, i.e. human gait cycle. The negative mechanical power indicates the rate of work (power) absorbed by the system; this can be defined as external forces acting on the body.

To find the efficiency of the positive work, the total average rate of the positive work (P^+) is divided by the total average rate of the metabolic cost rate for the level ground walking of the participant ($P_{metabolic}$). Both power units have been converted to $Wkg^{-1}s^{-1}$ for one stride. The metabolic cost rate ($P_{metabolic}$) is a net value, which means the metabolic cost is purely the cost of the stride.

The negative mechanical work was excluded in estimating the work efficiency of each participant due to the suggestions from (Shamaei et al., 2013) which point out that the muscles tendency for negative work is five times more efficient compared to the positive work. Thus the metabolic measurement is vastly measuring the metabolic consumption expended for the positive work. Therefore negative efficiency would be very small and negligible.

The work of (Shamaei et al., 2013) mentions the fact that the negative power inserted on the body during the level ground walking is mainly stored and returned as positive works by use of human elastic elements such as ligaments and tendons, and some will be absorbed by the muscles and ligaments as damping effects. But there has been no direct measurement and ratios available in the literature; thus the assumption of positive mechanical power alone has been used to find the efficiency of the work.

Equation (5-3) was used for calculating the efficiency shown in Table 5.4.

(5-3)

$$\eta^+_{work} = P^+_{total} / P_{metabolic}$$

Where:

η^+_{work} is the positive work efficiency constant.

P^+_{total} is the positive total mechanical power consumption.

$P_{metabolic}$ is the metabolic power consumption.

Table 5.4 Positive mechanical power consumption, positive work efficiency, metabolic cost rate of various subjects at different speeds

speed ($\frac{m}{s}$)	$P^+_{mechanical}$ (Wkg^{-1})	η^+_{work}	$P_{metabolic}$ (Wkg^{-1})	subject ID
0.6	0.35	0.126	2.775	1
0.9	0.783	0.226	3.47	2
0.95	1.036	0.291	3.57	3
0.8	2.037	0.623	3.27	4
1.2	3.487	0.94	3.72	5

The most efficient walk is that of the participant with the closest positive work efficiency value to zero. In this case the subjects ID order and the order of their efficiencies are directly relevant, with subject ID 1 having the most efficient gait, and subject ID 5 having the lowest efficiency by consuming the largest work.

The average metabolic cost for the specific measured average speed of the participants during the motion capture trials have been extracted from the literature data (Bastien et al., 2005) as shown in Table 5.4. The average metabolic cost for the speed at $0.6 m_s$ is derived from the data of the previous metabolic measurement experiments desired in Chapter 4, which was also

verified by the literature data. The metabolic values have been converted to standard condition, and all data are as average standard deviation value of how much joules is expending in each second in Watts.

As shown in Figure 5.14 the metabolic power has a direct proportional relationship with the speed and has the best fit second order polynomial trend line with the least root squared (R) value closest to gradient of 1, $R^2 = 0.9982$ (closest to one) throughout all participants.

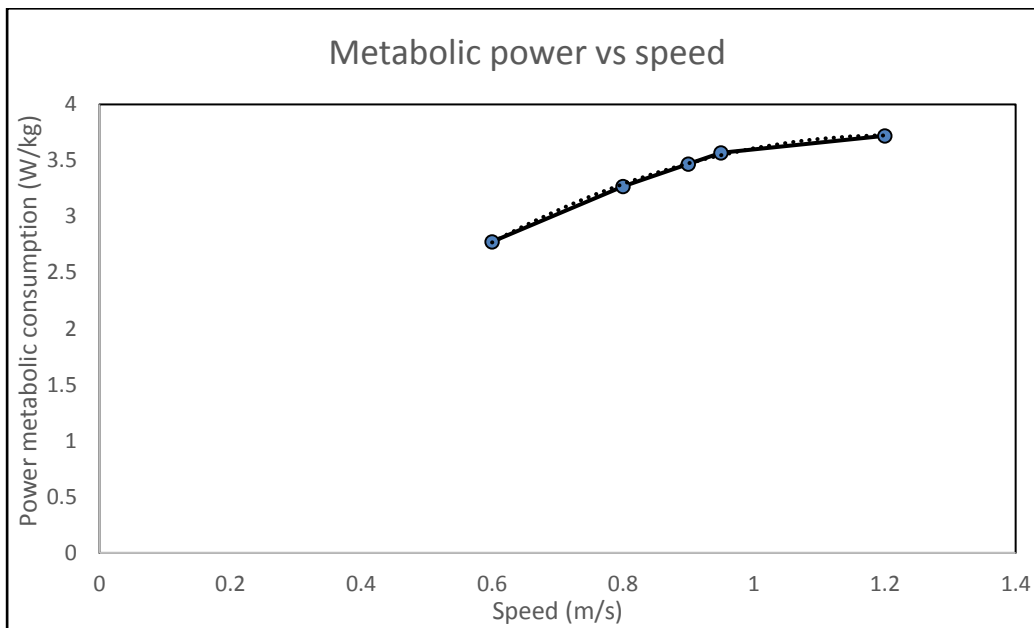


Figure 5.14 Metabolic power consumption vs speed

As found in section 5.4 the collected reaction force data support that the gait is at its most efficient at lower speeds.

The work in section 5.3 presented the results of the inverse dynamic simulation of the human walking from the measured kinematics and external forces. The gait with the lowest speed, and lowest angular displacements at the joints were found to have the lowest mechanical power consumption compared to other trials.

From Table 5.5 the main joints which consumed the biggest powers are the ankle flexion/extension and hip flexion/extension, with knee as the 3rd highest power consumer. The ankle inversion/eversion was found to be the smallest power consumer compared to all other joints, following with hip internal/external rotation. Table 5.5 also supports that subject 1 has the lowest

overall absolute mechanical power consumption compared with other subjects in these trials.

Table 5.5 Absolute power consumption at lower limb joints from captured and measured CGA data

Sub ID	Total absolute mechanical power consumption (w/kg)
1	45.56
2	84.98
3	97.99
4	71.08
5	171.18

5.6 Summary

This chapter compares the collected results and concluded the most efficient gait to be the subject with the lowest mechanical power consumption. This comparison used values across five participants. To verify these claims the kinematics of the human (angular velocity at the joints) used as the input of the exoskeleton dynamic simulation, averages from the five participant were inputted to their specific exoskeleton simulations. The results are covered in section 7.2 . Thus the most efficient gait and input to the design of the exoskeleton was chosen to be the subject found to have the lowest power consumption in this chapter.

Chapter 6

Exoskeleton model building

6.1 Introduction

The exoskeleton robot can be defined as a rigid mechanism consistent of a number of constraints fix point and set degrees of freedom, which transfer motions and forces from a source (active or passive actuations) to an output (output shaft at the exoskeleton joints).

An anthropomorphic prototype of the exoskeleton with the selected active and passive degrees of freedom from the conclusion of the work in chapter 4 and chapter 5 has been designed and manufactured at the University of Leeds. The purpose of this prototype is to build and set up an accurate virtual 3 dimensional model of the exoskeleton robot by accurate geometric collection of reflective markers data for purposes of dynamic simulations, parametric design of active and passive actuation systems of the exoskeleton while assisting the user inside to 100% assistant during the activity of gait cycle.

The exoskeleton prototype consists of rigid links connecting to each other by 14 hinge joints with each degree of freedom active solely at the joint of the exoskeleton. The segment links do share similarities in geometric properties (i.e. length and axis of rotation) with the exoskeleton being anthropomorphic to the user specific lower limb body parts. The joints share similar kinematics with the healthy human at selected degrees of freedom, by closely fitting the exoskeleton prototype and the user inside by aligning the human and the exoskeleton axes of rotations.

The principle of inertia in rigid body is commonly defined by Newton's first law of motion which describes the motion of a matter in the space throughout the time and how the forces can affect that. The gravity is always acting during the simulation work counting the weight of each segment specifically by adding the weight of the human user and weight of the exoskeleton (including the hardware and actuation system estimated weight).

The simulation solid works model is fixed at the front of the stance foot, allowing the common assumption to have a fixed point with the ground to avoid complex modelling of contacts between the exoskeleton and the ground.

The gait cycle simulation of the robot starts just after toe off and finishes just before the heel strike, all the forces exerted to the ground and the reaction forces exerted to the robot from the ground to be at equilibrium at all point during the simulation by fixing the front of the stance foot to the defined virtual ground (no other contact point with ground), thus the reaction forces are in equilibrium.

6.2 Simulation setup and assumptions

The solid works motion analysis in this work has the following mechanism setups in order to apply Euler's equations of the motion and Newton's Raphson's iteration methods to work accordingly.

6.2.1 Rigid body

The segments and joints of the exoskeleton have been set to rigid bodies this means there is no internal deflection within a part and there is no deformation during the simulation of the motions.

6.2.2 Fixed part

The chosen fixed part is set at the front of the stance foot, this indicates the fixed part has zero degrees of freedom and a reference frame for the rest of the moving rigid bodies.

6.2.3 Moving parts & joints

Moving parts in solid works automatically have six degrees of freedom unless constraints are applied at their connection points (joints) to restrict their degrees of freedom. The exoskeleton design have seven moving parts in each leg (front of the foot at the stance leg is fixed).

The exoskeleton model consists of:

- Tight link
- Shank link
- Hip rotation
- Hip inversion/eversion and back
- Ankle link
- Ankle inversion/eversion
- Front of the foot
- Back of the foot

All the moving parts are anthropomorphic to the human joints as close as possible.

The joints used are active only in one plane at a time, the joints along with their active degree of freedom are;

- Hip flexion/extensions
- Hip abductor/adductor
- Hip internal/external rotation
- Knee flexion/extension
- Ankle flexion/extension
- Ankle inversion/eversion
- Foot flexion/extension

6.2.4 Motion motors in dynamic simulation

Motors have been defined for controlling the movement of the bodies of the exoskeleton in the model.

The motion analysis simulation consists of two parts, inverse kinematics and inverse dynamics. During the inverse kinematics linear position motors have been added at the specific experimentally captured points on the exoskeleton. The inputs for these linear motors are the measured positions of the reflective markers (x, y and z) on the exoskeleton prototype (the prototype and the Solid works simulation model share the exact same mechanical characteristics. This step is purely for the purpose of the model building, the outputs of this simulation are the linear and angular velocities and acceleration of the parts and the joints.

The inverse dynamic simulation uses rotary motors at the joints of the exoskeleton which have inputs from the angular velocities at those joints, the inverse dynamic simulation will provide kinetic characteristics of the system such as torque, forces and power acting at the output joints of the exoskeleton system.

6.2.5 Gravity and external forces

The mass of the system is a great variable specially in deriving the kinetics of the system. The direction and magnitude of the gravitational vector has been set in the opposite direction of the rotational plane of the exoskeleton, with value of $(0, -1, 0)$ and the magnitude has been set $\approx 9.81 \frac{m}{s^2}$.

No other external forces are assumed to be acting on the frame apart from the gravity for purposes of this simulation.

6.3 Theory ADAMS solver

The package used to perform the kinematic and dynamic simulations (inverse dynamics and inverse kinematics on the exoskeleton model is solid works motion. The solid works motion uses the ADAMS solver to perform the robot dynamic and kinematic simulations.

An introduction to the Newton Raphson method and the Newton like method for the solution of non-linear system is presented in Appendix B Virtually all analysis modes in ADAMS use this algorithm. In this introduction the focus is on equation formulation and solution. The concept of generalized coordinates, as well as equations that govern the most representative types of analyses that can be performed by the ADAMS/Solver; i.e., Initial Condition Analysis, Kinematic Analysis, Dynamics Analysis, and equation of motions have been explained.

The solver uses the modified Newton Raphson iteration method in each time step, the solver predicts the position of parts based on initial conditions or the previous time step, the time step used is (0.0001) which results in more iterations and a more critical solution for solving the simulation.

To integrate the differential equations in such a way that algebraic constraint equations are satisfied at every time step, the GSTIFF integration method,

which is a variable order, variable step size integration method to define equation of motions, was used. This method is a fast and accurate way of computing equation of motion and displacement for motion analysis.

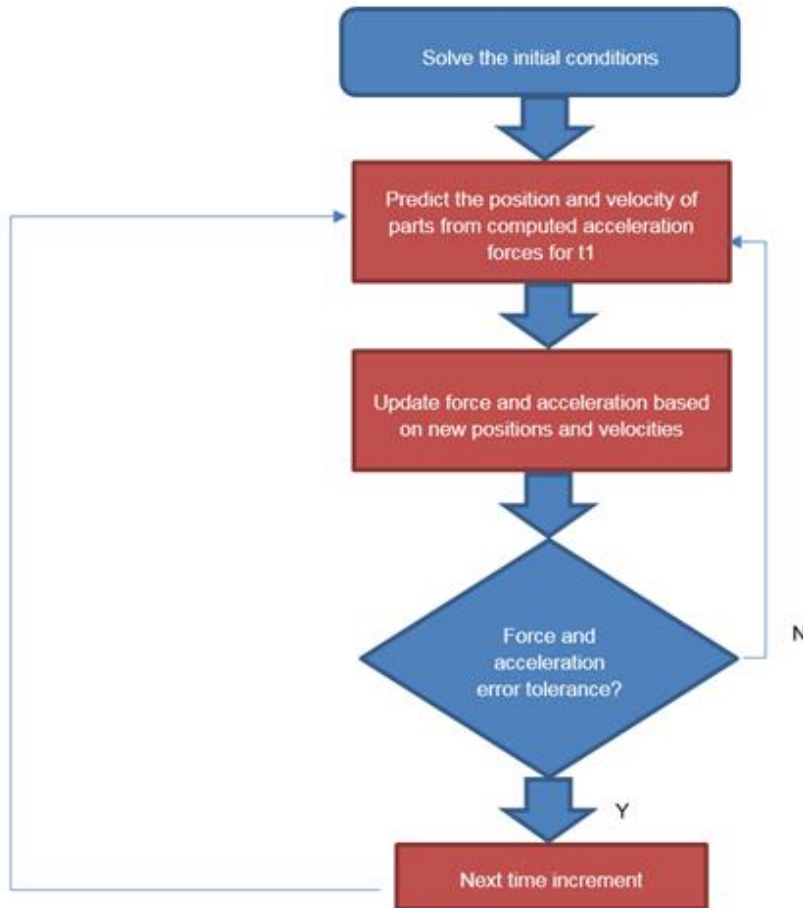


Figure 6.1 ADAMS motor solver iteration method

Note: t1 is the time recorded initial time

The solution must satisfy the velocity of parts, mates connecting parts, forces and accelerations. The answer is iterated until certain accuracy is reached for that time step and satisfy the force and acceleration error tolerances before moving to the next time increment.

6.4 Simulation of inverse kinematics of the exoskeleton carrying human

6.4.1 Exoskeleton experiment for the purpose of 3D model building

The initial prototype of the assistive exoskeleton with 14 degrees of freedom was built at the University of Leeds, by the help of a master's student on the assistive exoskeleton project (Hip and Knee), and the author of this thesis (Ankle and Foot). The prototype is size adjustable to accommodate user's height of 175 ± 15 cm. The size can be even further adjustable with small modification to the frame if needed.

The prototype was adjusted to the appropriate size of the user with the most efficient gait. The most efficient gait was investigated and determined as explained in Chapter 4.

The joint of the user and the exoskeleton were aligned as close as possible, specifically at the sagittal plane joints such as knee flexion/extension, hip flexion/extension and ankle flexion/extension.

In order to investigate the kinetics and kinematics of the exoskeleton it was desired to create a 3 dimensional CAD model of the exoskeleton in solid works package.

The initial positions of the exoskeleton has to be collected and measured experimentally by defining an origin in the laboratory reference. The position of the reflective marker's on the exoskeleton frame from the set markers by using the Qualisys package and motion capture technique has been identified.

6.4.2 Experimental procedure

The experiment consisted of using the exoskeleton frame while having the frame accurately fitted to the user's rotational axes of the joints by direct measurement and alignment at the laboratory of sport science in the University of Leeds.

The reflective markers were placed directly on the shaft of each joint of the exoskeleton, other group of reflective markers were placed on the body of the frame. Reflective markers were also placed on the body of the user for tracking the kinematic interaction between the exoskeleton and the user.

The exoskeleton foot consists of one degree of freedom about the mid-section of the foot to give the user the flexibility to achieve toe off and heel strike. This is essential as mentioned previously the front of the foot during the stance phase is fixed to the ground during the dynamic simulation for purposes of avoiding modelling contact which can have a high complexity but not a great contribution to the active and passive actuation design specifications.

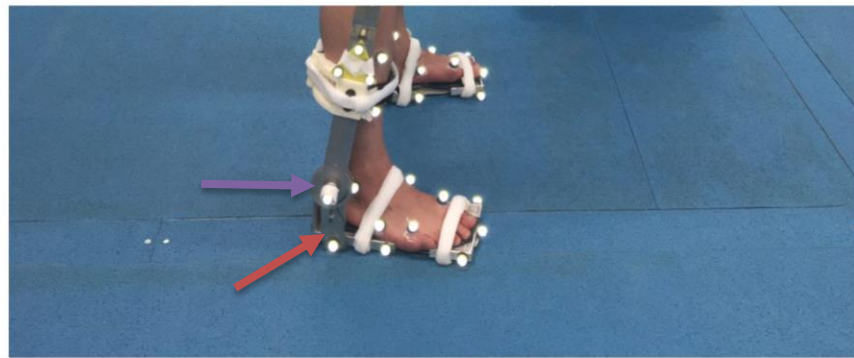
The front of the exoskeleton foot is defined by placing three reflective markers at two end points of the exo foot and in the middle distance between them, as shown in Figure 6.2.



Figure 6.2 Exoskeleton shoe, ankle and knee motion capture experimental setup front view

The initial positions and their positions during the motion from the set laboratory origin is found by placing two markers at the back of the exoskeleton foot in the superior and inferior (top and bottom) positions, along with two markers on each lateral and medial sides to recognise the position of the hinge placed at the foot of the exoskeleton.

The ankle joint of the exo has two degrees of freedom (flexion/extension, inversion/eversion), which is aiming to mimic the motion of the natural human ankle as close as possible.



**Figure 6.3 Exo shoe and ankle motion capture experimental setup side view. Red arrow: position of the inversion/eversion ankle marker
Purple arrow: position of the flexion/extension ankle marker**

The inversion/eversion position is recognised by tracking the marker placed at the appropriate inversion/eversion hinge joint as shown by the red arrow in Figure 6.3. The flexion/extension movement of the exoskeleton is identified from placing a marker on the shaft of the rotary joint of the exoskeleton ankle shaft as shown by the purple arrow in Figure 6.3.

The knee joint of the exo has one degree of freedom in the sagittal plane and its movement is recognised from placing a reflective marker on the hinge of the joint's shaft. The hip of the exoskeleton has three degrees of freedom (flexion/extension, abduction/adduction and internal/external rotation), the reflective markers are all placed at the end of each joint's shaft as shown in Figure 6.4.

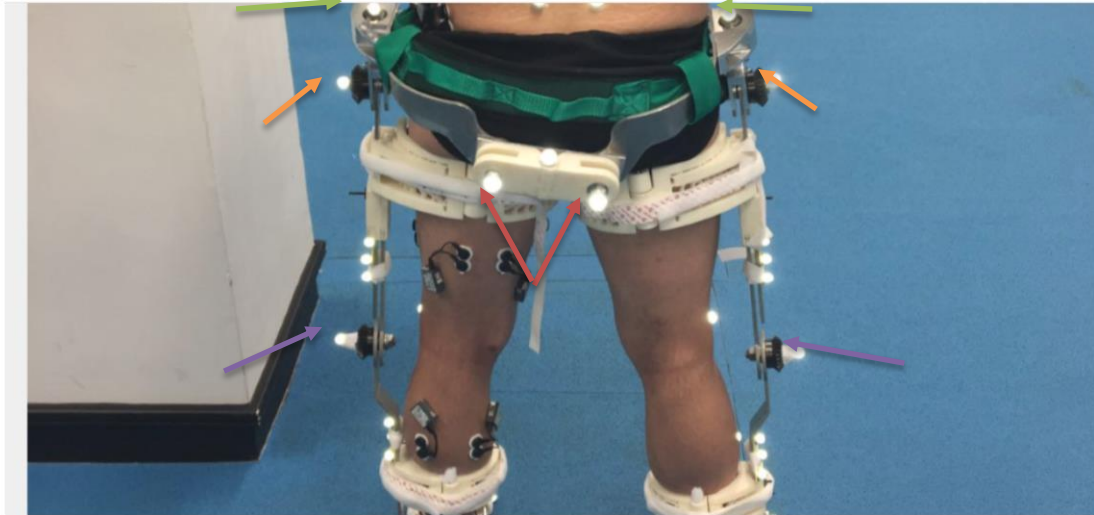


**Figure 6.4 Exoskeleton knee and hip motion capture experiment back view. Red arrow: position of the inversion/eversion hip marker
green arrow: position of the internal/external rotation hip marker
Orange arrow: position of the flexion/extension hip marker
Purple arrow: position of the flexion/extension knee marker**

The user is a healthy subject which uses its own effort to power the unactuated joints of the exoskeleton for the purpose of computer model building and reading the positions of the placed reflective markers during the static and dynamic (gait over the force platforms) trials.

6.5 Linear velocity motion motors for solving the inverse kinematics of the exoskeleton model

The aim of this research is to be able to power and move the exoskeleton joints as close as the healthy human joints in the most efficient way in terms of power consumed. It has been recognized that the exo is expected to be anthropomorphic with the aim of aligning the axes of rotations between the user and the exoskeleton as close as possible. It is also recognized they have major differences, such as rigidity geometry and different inertia between the exoskeleton and human segments. Such differences would cause kinematic and kinetic differences between human and the exoskeleton, which lead to differences in dynamics, thus using the CGA data as a direct or estimated design requirement is not reliable for parametric designs as mentioned before (Chu, 2005). In other similar work done by (Walsh et al., 2006a, Wang et al., 2011), the designed springs and actuation system have used the CGA data of human for active and passive actuation design. The work of some researchers (Walsh et al., 2006a, Wang et al., 2011) uses human joint stiffness to select and design the springs for the exoskeleton, from the mentioned differences between the dynamics of the human and the exoskeleton this can risk the accuracy of the design specifications of the motors and spring system which have led to an inefficient system in similar cases.

This chapter is focusing on building the 3D computational model of the exoskeleton. The purpose of the model is to be used as a platform for full dynamic and parametric design of the exoskeleton.

This method is aiming to increase the metabolic efficiency of the robot by having the closest motion to the human natural and efficient walking to minimise any external forces created between the human and robot.

To build the computational model the initial positions of the exo joint with respect to each other and the ground in X, Y and Z planes had to be collected with a set global reference in the motion capture laboratory. The prototype had 14 degrees of freedom as a lower limb exoskeleton which had been designed

with the aim of following the human joint's axes of rotations as close as possible.

The motion capture experiment was used to capture and collect the positions of the exo's reflective markers in the Qualisys package, the linear positions were inputted to the exoskeletons CAD model in the solid works motion (ADAMS solver) where the linear positions were inputted as linear motors at the end effectors (positions of the joints markers). The simulation used the reflective markers position data collected from the exoskeleton frame and joints as a source to build the virtual model to solve the model's inverse kinematics.

The simulation then can accurately progress to the inverse dynamic part (2nd simulation), where the angular velocities can be the driving forces of the exoskeleton.

The linear velocity motors solving the exoskeleton simulation are shown in Figure 6.5.

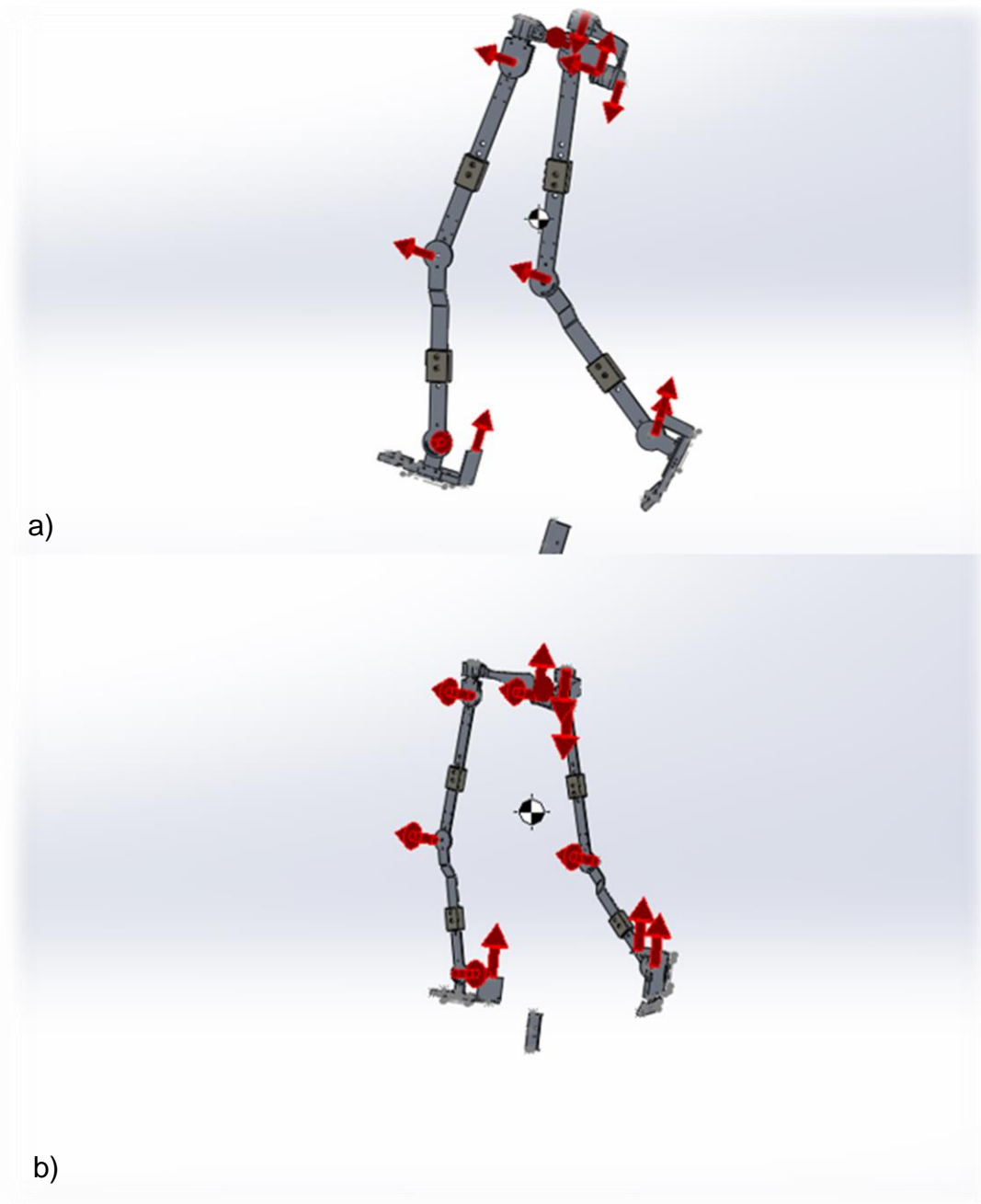


Figure 6.5 Linear position motion motors, inputted from captured experimental positions in all planes for solving inverse kinematic simulation of the exoskeleton gait a) Isometric view b) Side view

6.6 Rotary velocity motors for solving the inverse dynamics of the exoskeleton model

As mentioned in the previous section linear velocities were collected and inputted to the exo model from the motion capture experiment while the healthy user powers the exoskeleton, this computes output as angular displacement at the exo joints.

In the 2nd part of the simulation the model is ready to be inputted by angular velocities at the joints, which is using integral techniques to find the acceleration of the joints which can be used to calculate the torques at the joint by following the newton's second law of motion stating acceleration is produced when a force acts on a mass, this is done by using the inverse dynamic simulation. The simulation then provides the full kinetics of the exoskeleton as the output.

The weight of the human body segments have been taken into account for each segment (limb) by finding the weight of the limb from Table 6.1 as a ratio of the limb's weight to the total weight of the user, extracted from the literature collected in a study by (de Leva, 1996) which used young athletic Caucasian males and females as subjects.

Table 6.1 Percentage weight of human body segments (Leva, 1996)

Segment	Average (%)
Head & neck	6.81
Trunk	43.02
Upper arm	2.63
Fore arm	1.5
Thigh	14.47
Shank	4.57
foot	1.33

The weight of the exo also consists of the weight of the frame, joints, preliminary designed actuation system, bearings, shafts and the control system used in the preliminary design.

The specification of the actuation and control system used in the preliminary design is adopted from (ChiaLin Yeoh 2015).

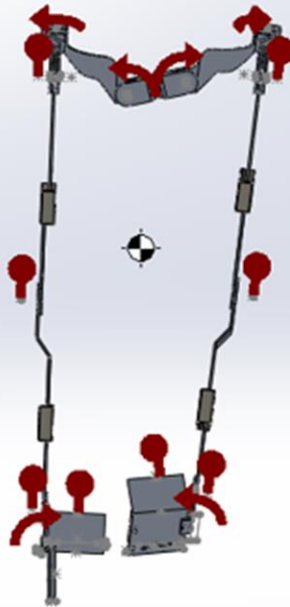
Once the inverse dynamics is performed, the model can then be used as a design platform which can be inputted by the angular displacement data from the real human joint (Visual3D human model).

The input for the rotary motors to solve the first inverse dynamics of the model used the calculated angular velocities from the output of the inverse kinematic simulation explained in section 6.4

The input of the simulation (angular velocities at the exo joints) then substituted by the angular velocities calculated from the human model (visual3D model) as an input explained in Chapter 5.

The exoskeleton is powered by 14 motion motors that activate joints at the foot, ankle, knee and hip as shown in Figure 6.6.

a)



b)

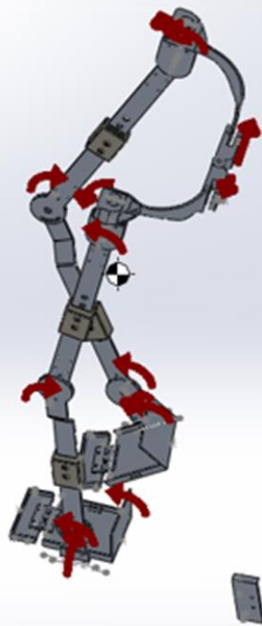


Figure 6.6 Rotary angular velocity motion motors to solve inverse dynamics input from forward kinematic results a) Back view b) Side view

The purpose is to take advantage of the shared characteristics of an anthropomorphic design (axes of the rotations) for finding the design specifications of the robot. This has the advantage of the healthy human motions to be the driving force thus there will be minimal interaction between

the human and the robot and vice versa which lowers the metabolic effort from the user inside.

6.7 Summary

This chapter explained the numerical method along with equation of motions used to perform inverse kinematic and inverse dynamic simulations on the exoskeleton model as covered in section 6.3

The laboratory measured initial positions of the exoskeleton's joints and links of the first prototype was used as inputs of the mentioned simulations.

The simulation was performed by using an exact CAD model of the 14 degrees of freedom prototype in SolidWorks, which uses ADAMS solver.

The inverse kinematics used linear position motors to find the required angular displacement and velocity at the joints of the frame.

The computed angular velocity results from the linear motor simulation, were inputted as the rotational velocity at the joints of the exoskeleton for the inverse dynamic simulation, while the skeleton carries the weight of the initially estimated hardware (gear, electrical actuators, ball bearings, encoders, brackets and housing) along with the weight of the frame and the human user inside.

The purpose of this chapter was to successfully build a size adaptable exoskeleton model which can perform inverse dynamic simulation from any inputted angular or linear kinematic motion data, while using the exoskeleton's own geometry and mass and inertia characteristics.

Chapter 7

Exoskeleton active actuation parametric design

7.1 Introduction

This chapter is providing the active actuation system parametric design and specification for the robot at the powered degrees of freedom. The robot is considered to be carrying the human user inside, while providing 100% assistant to the user to match the ability of the healthy human gait.

The work in this chapter also investigates the kinematics of the robot skeleton frame compared to the healthy human gait under no restrictions to satisfy that the robot will not imply any external forces to the user inside under operation in order to minimise the user's metabolic effort.

The exoskeleton dynamic gait simulation was used to find how the various kinematic from the various collected human walking CGA affects the efficiency of the robot's actuation system, by comparing the power consumptions of the actuation system.

The most efficient healthy human motion was identified in Chapter 5 (gait speed at 0.6 m/s) found to have the most efficient kinematic and kinetic outputs compared to other subjects.

The simulation model solves for one complete gait combining the stance and swing phase.

Ankle inversion/eversion and foot flexion/extension power values are found to be very close to zero due to lack of displacement at these degrees of freedoms, thus the future work recommends to use springs and elastic materials (steel spring or leaf spring designs) to withstands the torques applied at these degrees of freedoms while provides the required flexibility and passive actuation the user requires, other joints needs to be supported by activate actuations.

7.2 Most efficient exoskeleton mechanical power consumption

The average angular joint velocity from trials of all five subjects involved in the clinical gait analysis experiment, have been extracted using the Visual3D simulations of their human models. The dimension of the exoskeleton model built in Chapter 6 has been resized to align with different user's lengths and appropriate dimensions. The extracted angular velocities from the visual3D simulations were inputted to the motion simulation of the exoskeleton (ADAMS solver), the kinetic requirements of the exoskeleton was compared between all the five subjects by inputting the angular velocities to the joints of the exoskeleton and performing an inverse dynamic simulations, using the exoskeleton model built in Chapter 6.

Figure 7.1 shows the mechanical power consumption simulated for the exoskeleton according to the subjects, angular velocities at the sagittal plane joints of ankle, knee, and hip, which are the most power consuming joints as shown in this figure.



Figure 7.1 The power consumption simulated for the exoskeleton according to the subjects angular velocities at the sagittal plane joints of ankle, knee, and hip.

Subject 1 inputted kinematics proved to consume the lowest power consumptions outputs from the exoskeleton model, subject 1 was the heaviest

subject across the users but has the lowest speed and most evenly distributed joint mechanical power, in comparison to other four participants.

In Chapter 5 from the human model inverse dynamic simulations, subject 1 was found to have the most efficient gait kinematic and kinetic, this also follows in simulation of the exoskeleton joints power consumption by implying exoskeleton geometry and inertias while carrying the user inside on 100% assistance.

Subject 1 was therefore chosen input for parametric design of the active and passive actuation systems as he had the most efficient gait.

The purpose of the developed model as discussed in Chapter 6 is to be used as a platform adaptable to any kinematics for providing an accurate parametric design of the active actuation system and any necessary design specifications.

7.3 Comparison of exoskeleton and healthy human kinematics

The exoskeleton simulation model uses angular velocity at the joints of the human as motion inputs to carry the joint of the exoskeleton.

This set to be as a design requirement and a safety concern as insures to avoid any unwanted forces acting on the user as well as minimising the metabolic effort of the user inside, by having the robot following the most natural kinematics of the human.

This section represents the angular displacements at the joint of the exoskeleton which were extracted from the dynamic simulation in Solidworks2016 motion analysis (ADAMS solver). The data shown in the red graphs in the follow on section are the angular displacements captured and calculated in the visual3D software representing the kinematic characteristics of the human model. The exoskeleton frame and the human user do not share the exact same geometry, but the exoskeleton was fit anthropomorphically so the users joint axes of rotation are aligned with that joints on the exoskeleton, thus the angular displacement at the joints are similar but not exactly the same at all times. Due to difference in human compared to robot joint alignment,

offsets and different geometrical properties variations can be seen in the results section below, especially in the non-sagittal joints where more significant offsets and differences can be seen.

7.3.1 Ankle angular displacement-human vs robot

7.3.1.1 Flexion/extension

Figure 7.2 presents the angular displacement of the human ankle joint in red and the exoskeleton's ankle joint in blue, the ankle is the most efficient joint during the human gait as found out from the metabolic measurement in Chapter 4, thus it is essential for the exoskeleton ankle joint to follow the natural user's ranges of movements. As shown in Figure 7.2 the exo has close pattern and angular displacement values as the human ranges of movements. Both human and exoskeleton joints are going through an extension at the initial stance of about -8° , followed from the foot flat to pre swing stage. Both human model and exoskeleton joints also go through the biggest flexion of up to $\approx +10^\circ$ for human and $\approx +4^\circ$ for the exoskeleton. From the stance to swing phase until about 80% of the gait (mid swing) stage the ankle joint goes through its biggest extension phase which has a peak value around $\approx -16^\circ$. From the mid swing till the final heel strike the ankle is flexing to around $\approx -5^\circ$ in both human and the exoskeleton, as shown in the figure.

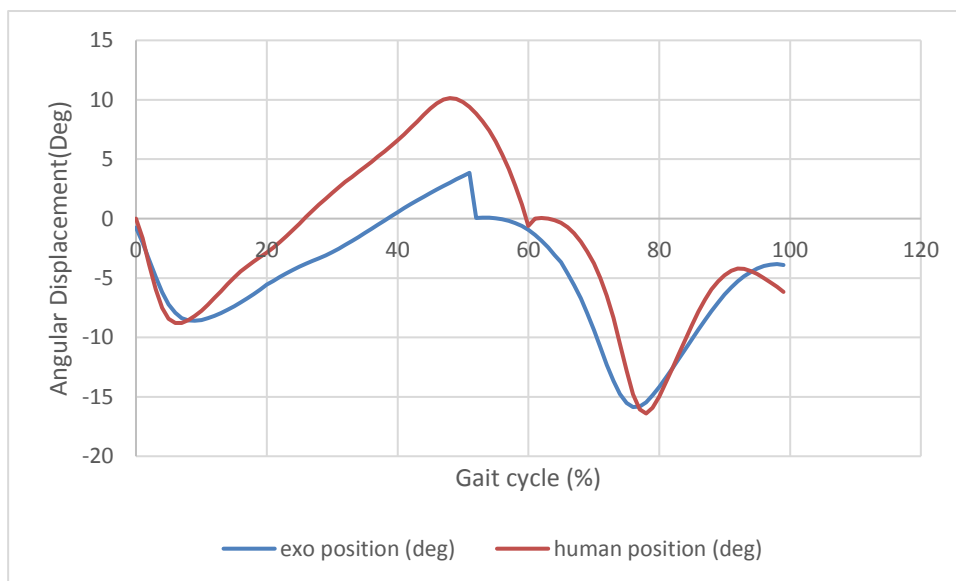


Figure 7.2 Ankle flexion/extension angular displacement from exo and human CGA data

7.3.1.2 Inversion/eversion

Figure 7.3 represents the non-sagittal degree of freedom in the ankle joint of the proposed exoskeleton design. The human data have almost similar patterns as the exoskeleton kinematics but the exoskeleton has slightly larger ranges of movements from pre swing to terminal swing phase but following the same pattern as the natural human movement. The maximum difference in the values are around 2 *degree* which occurred from the initial swing to mid swing phase (20 to 80% of the gait cycle), while the ankle is in the adduction mode. This range of deflection is allowed as it has been tested to be within the subject natural range of movement.

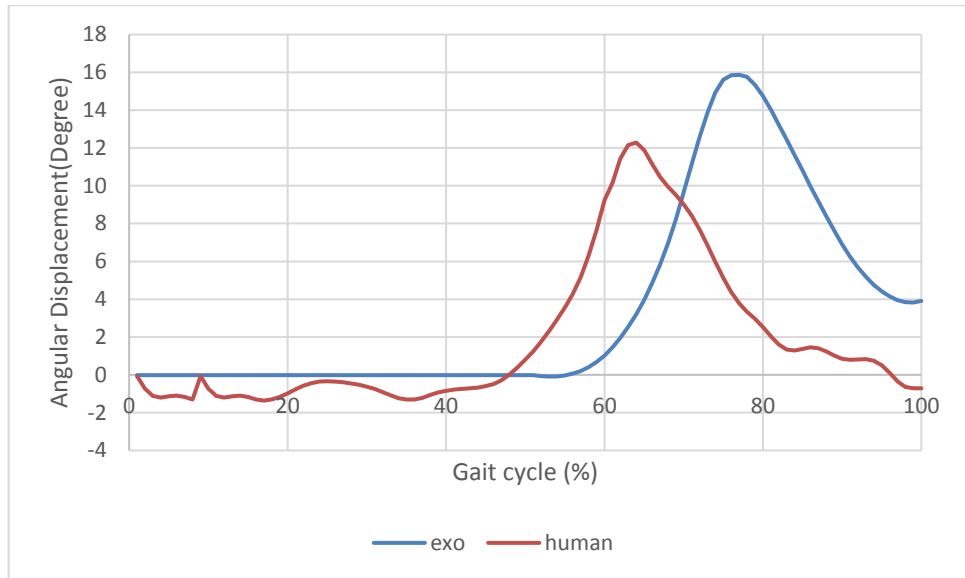


Figure 7.3 Ankle inversion eversion angular displacement from exo and human CGA data

7.3.2 Knee angular displacement human vs robot

7.3.2.1 Flexion/extension

Figure 7.4 shows the range of movement at the knee flexion/extension of the robot in blue and the human CGA measured in red, the two have very similar motions as expected due to the exo knee joint has more accurate anthropomorphic fit with the user's joint, thus is one of the joints with more accurate axis alignment.

From the initial contact, the knee joint in both the exo and the human are going through a small extension of up to $+10^\circ$ right until the next initial contact at the other leg about 50% in the gait cycle, when the knee direction of motion changes as the joint is going through its largest range of movement of up to -60° . This finishes at the end of the initial swing which the knee goes through an extension to move the swing leg forward. At the tibia contact which is about 87% of the gait cycle the knee has a small flexion before finishing with another extension.

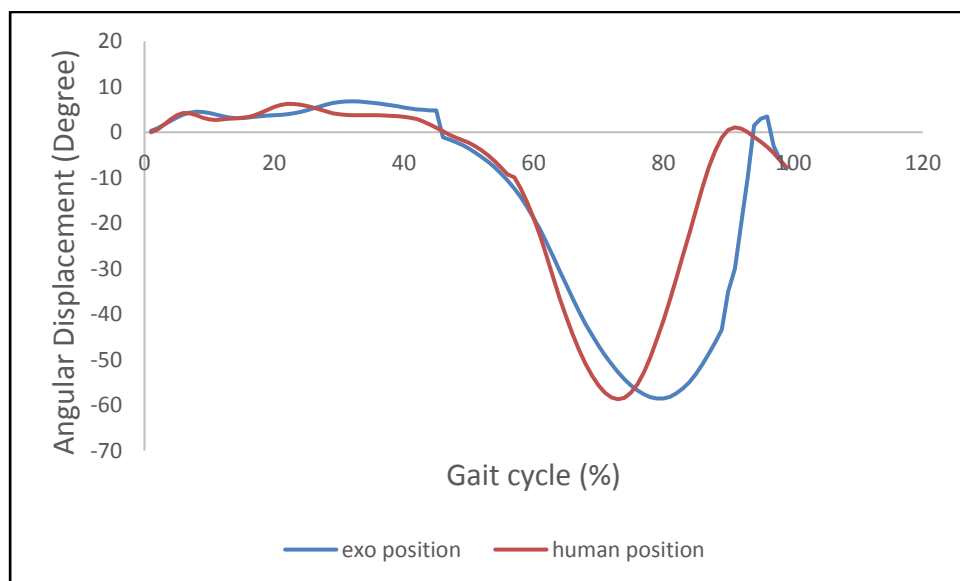


Figure 7.4 Knee flexion extension angular displacement from exo and human CGA data

7.3.3 Hip angular displacement-human vs robot

7.3.3.1 Flexion/extension

The hip flexion occurs during the stance phase of the gait cycle, from the initial contact and it carries on until the toe off about 60% of the gait cycle. The maximum value of the human hip measured is $\approx -33^\circ$ and the exo had a smaller peak value of $\approx -25^\circ$. The exoskeleton and the human hip movement in the sagittal plane then goes through an extension in the swing phase to achieve forward motion of the bodies, the peak values in both human and the robot reached $\approx +10^\circ$ as shown in Figure 7.5.

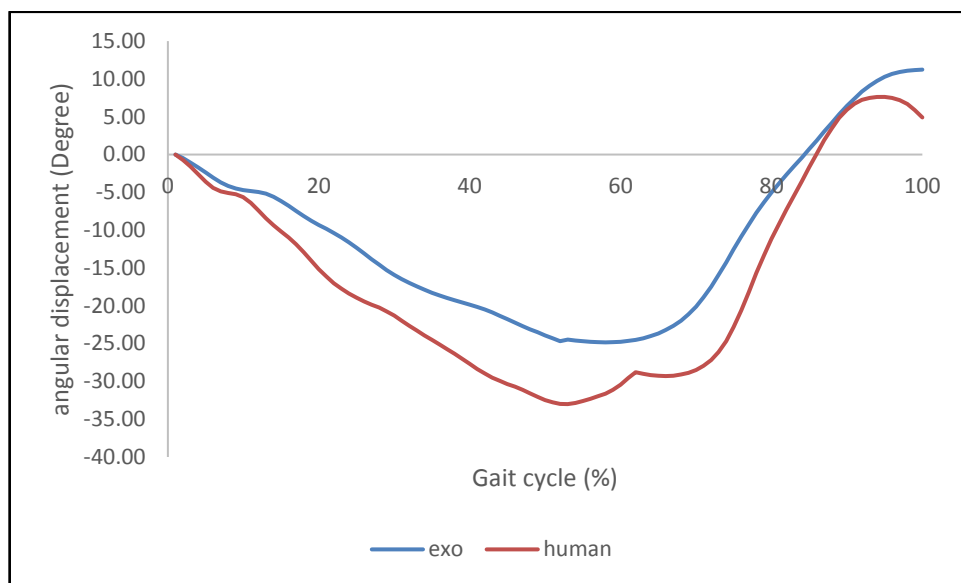


Figure 7.5 Hip flexion/extension angular displacement from exo and human CGA data

7.3.3.2 Abduction/adduction

The human and exoskeleton hip goes through an adduction from the first initial contact until the second initial contact (at the other leg) about 50% of the gait cycle, the value reaches up to a maximum of $\approx +10^\circ$. Figure 7.6 shows the hip goes through and abduction from the second initial contact until end of the initial swing about 70% of the gait cycle, until the hip goes back to its neutral position in the coronal plane. The final adduction occurs from the initial swing until the end of the mid swing about 87% through the gait cycle before a small abduction to returning into neutral hip position.

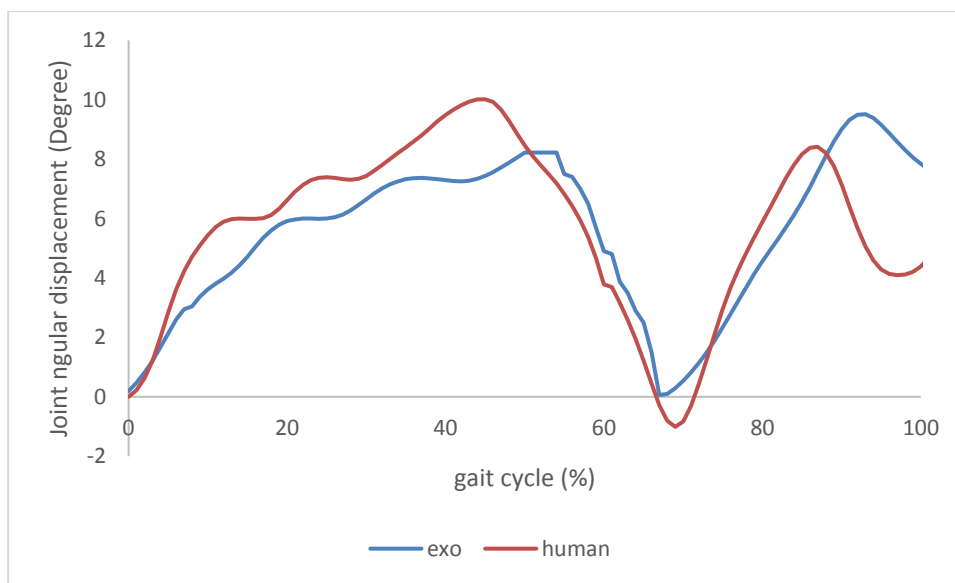


Figure 7.6 Hip abduction/adduction angular displacement from exo and human CGA

7.3.3.3 Internal/external rotation

The both models (human and robot) have similar patterns but it can be improved by placing the rotation of the exo more anthropomorphic to the human hip rotation axis as a future work. The rotation at both models follow a harmonic motion throughout the gait with the maximum internal rotations during the distance phase about 10-20% of the gait cycle, and the mid swing from 73-87% of the gait cycle to peak values ≈ 5 to 10° . The maximum external rotations occurs during terminal stance phase 30-50% gait cycle, and terminal swing phase of 87-100% of the gait cycle, reaching peak values of ≈ -5 to -10° , as shown in Figure 7.7.

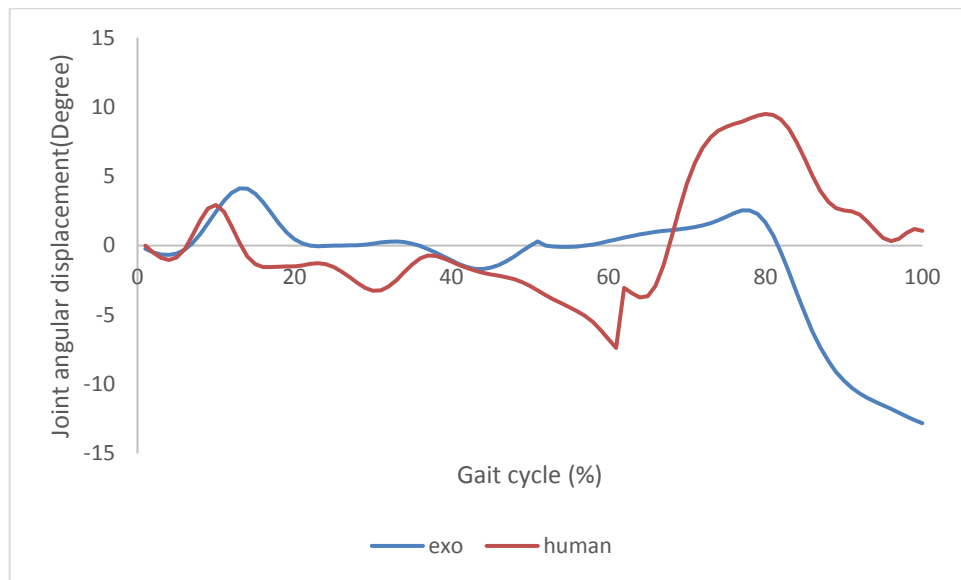


Figure 7.7 Hip rotation angular displacement from exo and human CGA

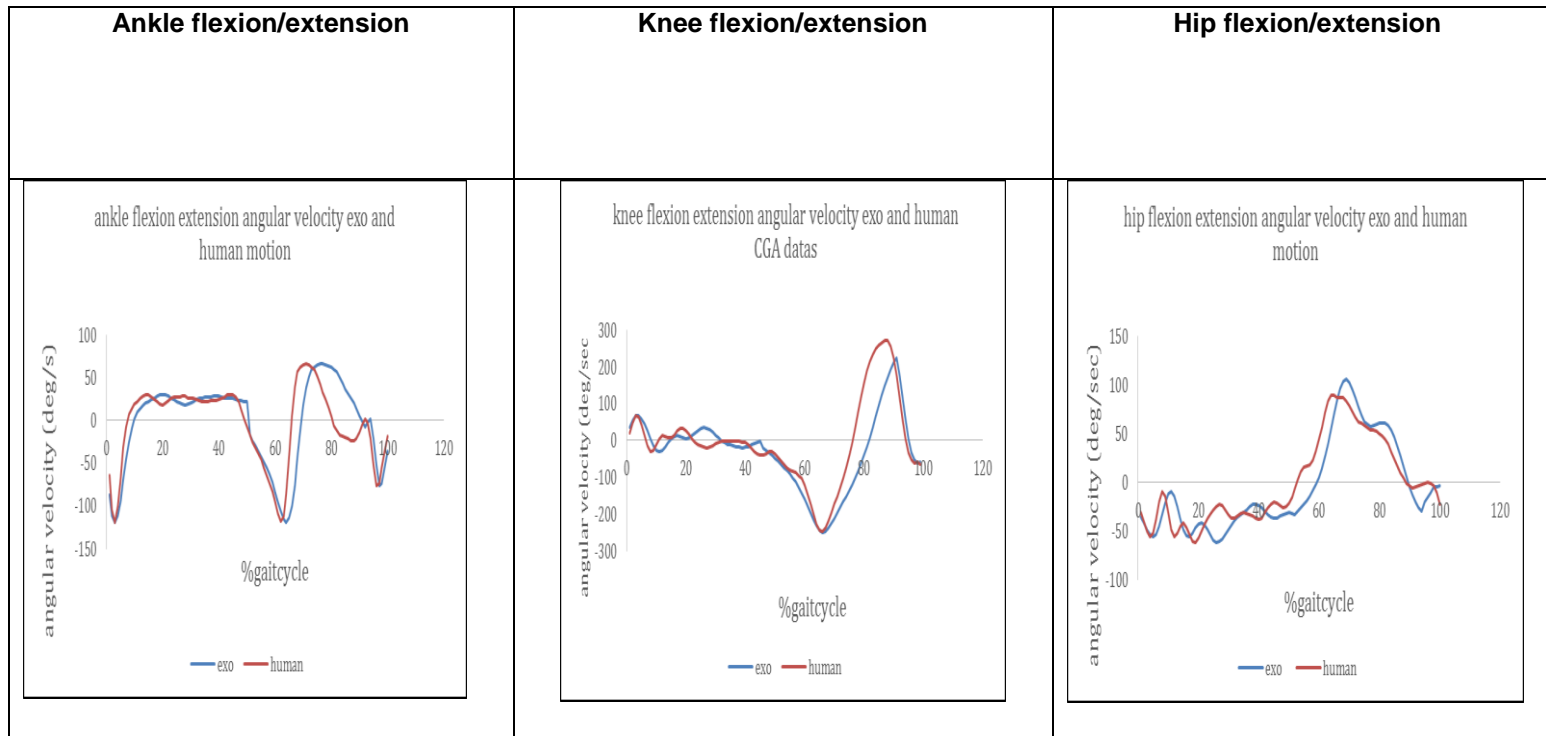
7.4 Velocity results

Table 7.1 shows the angular velocities in the sagittal plane joints for the purpose of further verification of the kinematic outputs by comparing the two solvers together, the visual 3D solver results were verified in the Analysis of human locomotion and exoskeleton frame requirements with the measured data in the literature (Cavagna and Margaria, 1966).

The red curves represented in Table 7.1 are the angular velocity values of CGA data of healthy human joints.

The data in blue graphs are the velocity at the joints of the exoskeleton for one full gait cycle. The human kinematics were used to calculate the kinetic specification of the robot while following the human at its most efficient captured motion. The small difference between the red and blue data is negligible as it was expected due to the two models (human and exoskeleton) having different geometrical properties and more rigidity to be expected in the exoskeleton.

Table 7.1 Human Vs Exo angular velocities in the sagittal plane



7.5 Robot's joint power requirements

7.5.1 Ankle joint power

The highest power at the entire system occurs at the ankle joint during the stance phase. During the double support the actuation system require to generate the positive peak value around $\approx +40 \text{ watts}$ while the ankle is flexing as shown in Figure 7.8. The ankle then goes through an extension which requires the actuation system to absorb the power (negative work) reaching peak value $\approx -67 \text{ watts}$ at pre swing (55% of the gait cycle). The power graph shows majority of the work is expended for power absorbing by the system, but still keeps close to a harmonic shape, the average value is $\approx -22 \text{ watts}$.

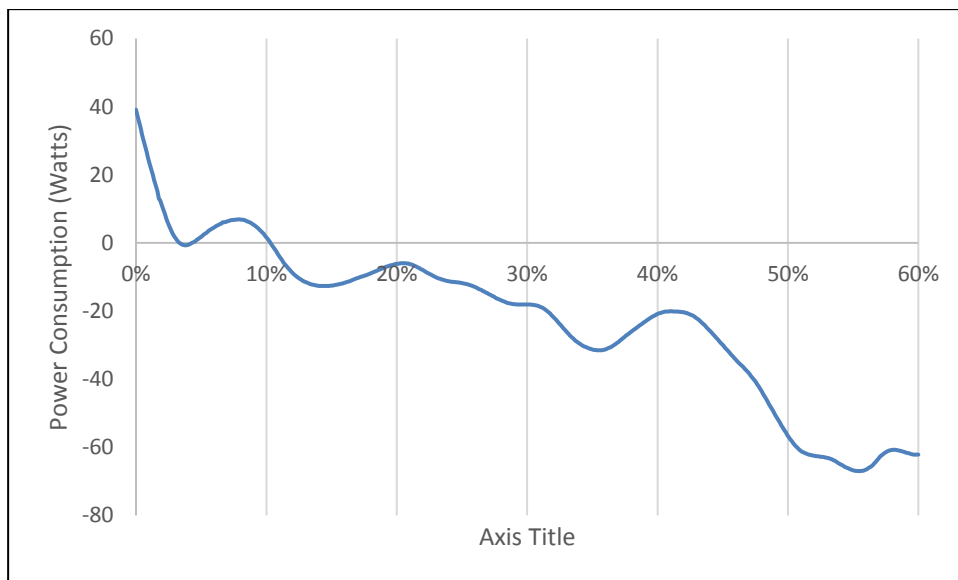


Figure 7.8 Exoskeleton stance ankle flexion/extension power consumption

During the swing phase, as shown in Figure 7.9, the ankle goes through a harmonic flexion followed by an extension which has a peak value of $+1.5 \text{ watts}$ of power required to be generated and the system absorbed required power is at a peak value of -2.7 watts around toe off (60% of the gait cycle).

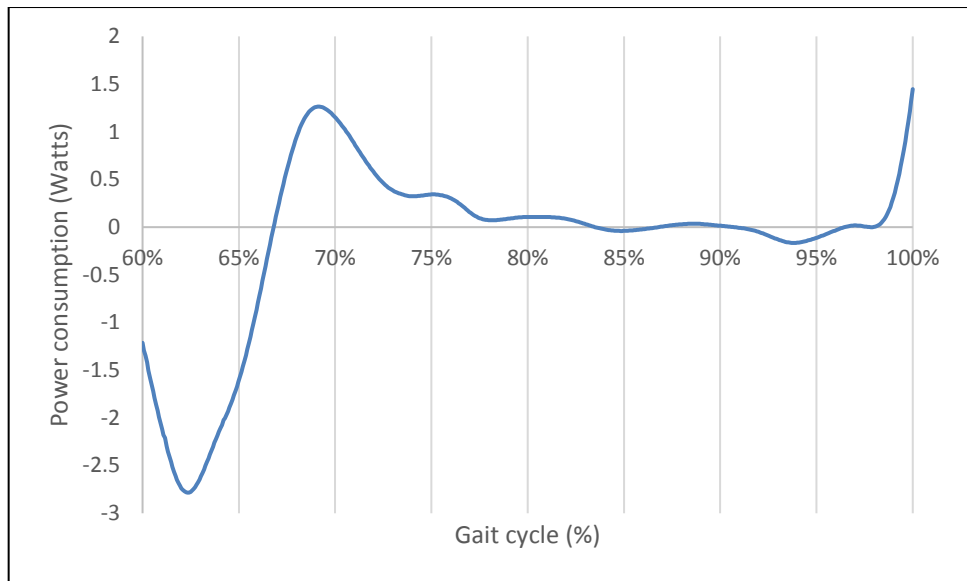


Figure 7.9 Exoskeleton swing ankle flexion/extension power consumption

7.5.2 Knee joint power

The stance knee has the third highest power generated requirements with a peak value of $\approx +55$ watts and power absorption occurring at flexion of the knee during the initial stance at ≈ -5.5 watts, with an average positive power consumption of $\approx +8$ watts during the loading response before going through the pre swing, as shown in Figure 7.10.

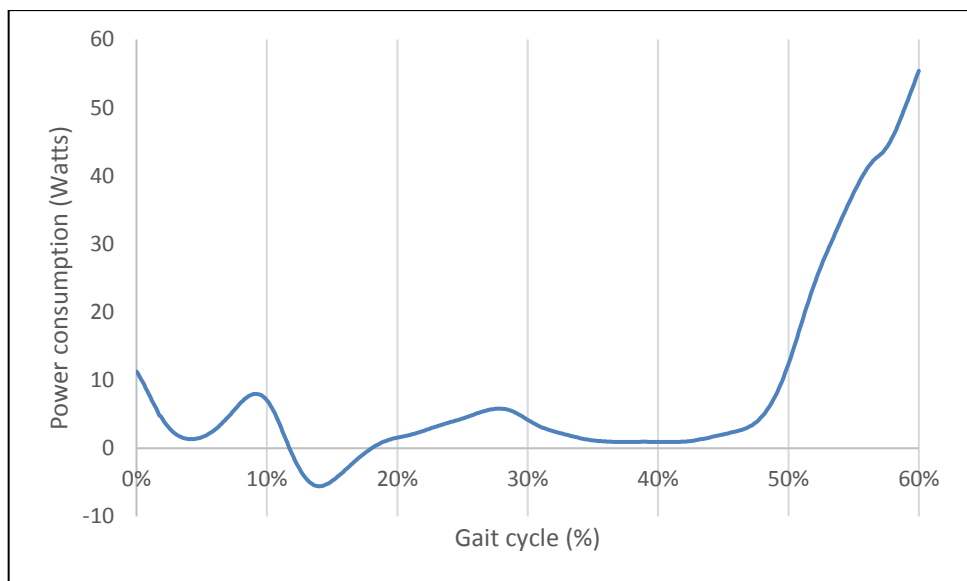


Figure 7.10 Exoskeleton stance knee flexion/extension power consumption

The knee swing flexion reaches its power absorbed peak value ≈ -11 watts, during the mid-swing and terminal swing stage. The extension of the knee during the swing mode requires for the exo active actuation system to generate power at peak value $\approx +53.5$ watts, with an average value of $\approx +16$ watts during the pre swing and the initial swing stages, as shown in Figure 7.11.

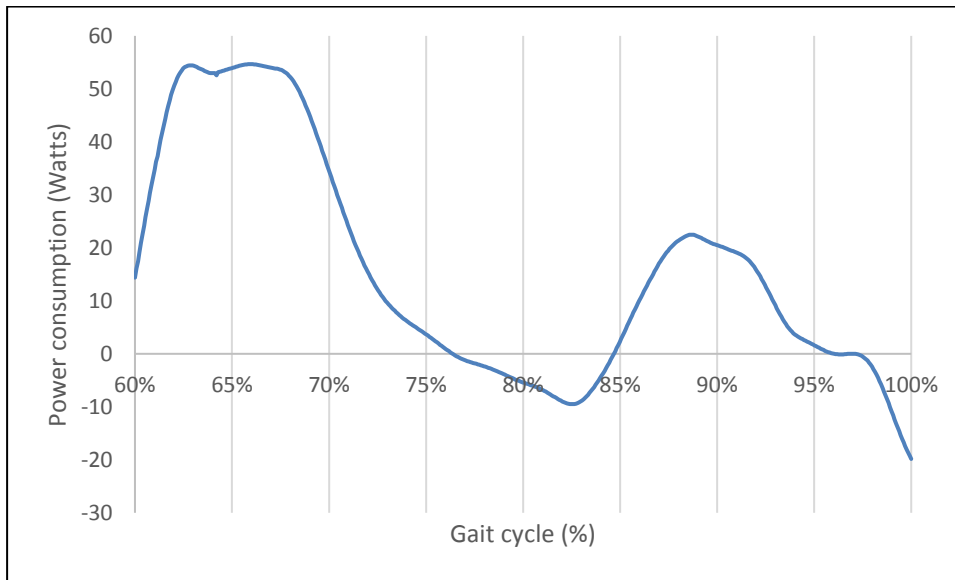


Figure 7.11 Exoskeleton swing knee flexion/extension power consumption

7.5.3 Hip joint power

In the sagittal plane during the stance phase the hip goes through an extension at the end of the loading response, mid stance and beginning of the pre swing phases, with an average value of $\approx +24$ watts, and a peak value reaching $\approx +35$ watts as shown in Figure 7.12.

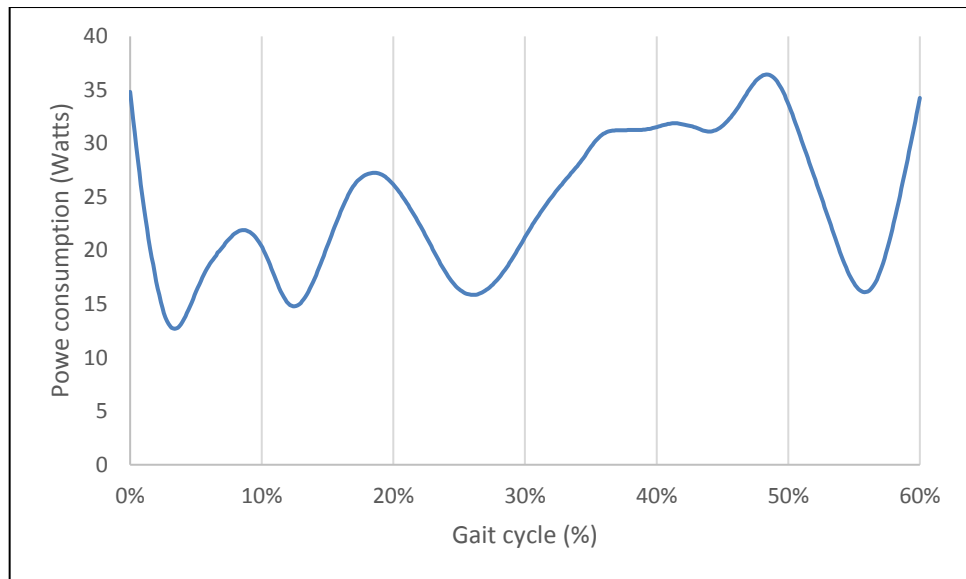


Figure 7.12 Exoskeleton stance hip flexion/extension power consumption

During the swing mode at the initial contact the hip goes through a big power expenditure, with a peak power generated occurring at extension of the hip in the mid swing phase reaching values at $\approx +92 \text{ watts}$ with an average value of $\approx +22 \text{ watts}$. The negative peak value occurs while the hip is flexing in the sagittal plane at the initial stages of the terminal swing reaching negative power of $\approx -68 \text{ watts}$ as shown in Figure 7.13.

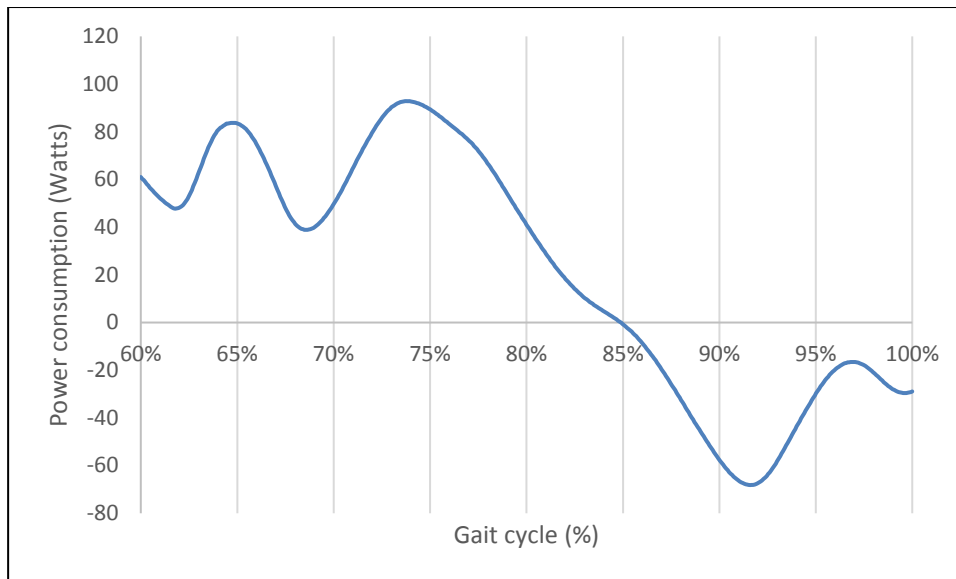


Figure 7.13 Exoskeleton swing hip flexion/extension power consumption

The maximum hip adduction at the stance phase occurs during the initial contact and at the end of the mid stance and pre swing reaching a value of $\approx +8$ watts. The majority of the forces are in the opposite direction (power absorbed) thus the average power consumption is ≈ -5 watts with a peak value of abduction occurring during the loading response, midstance and pre swing phases, reaching its peak value at ≈ -23 watts as shown in Figure 7.14.

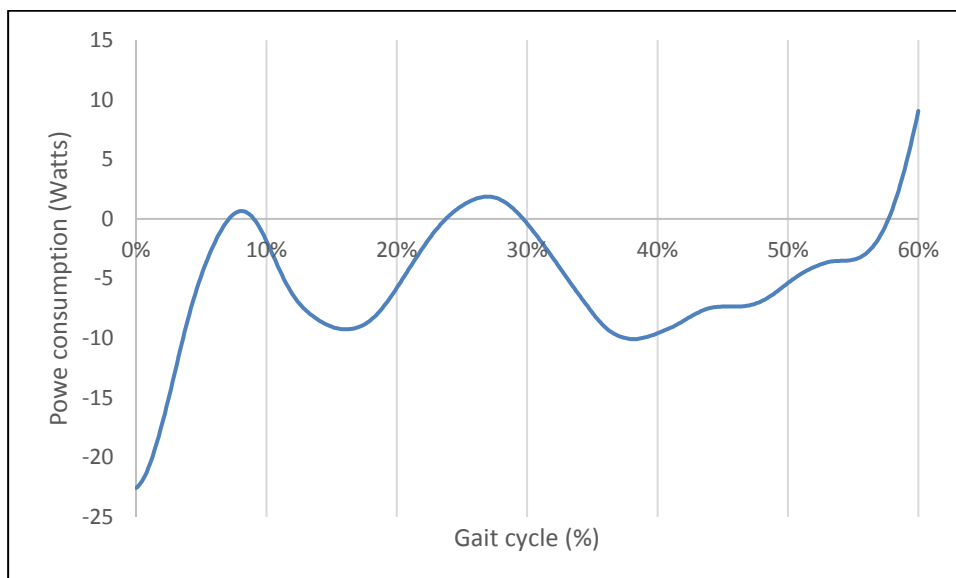


Figure 7.14 Exoskeleton stance hip abduction/adduction power consumption

During the swing phase shown in Figure 7.15, most of the power are absorbed by the ssystem which requires the actuation system to act in opposite direction with an average value of ≈ -1.5 *watts* during the initial and mid swing phases. The peak absorbed power was calculated at ≈ -24 *watts*, the power generated at the end of the terminal swing stage is reaching its peak value of $\approx +7$ *watts*.

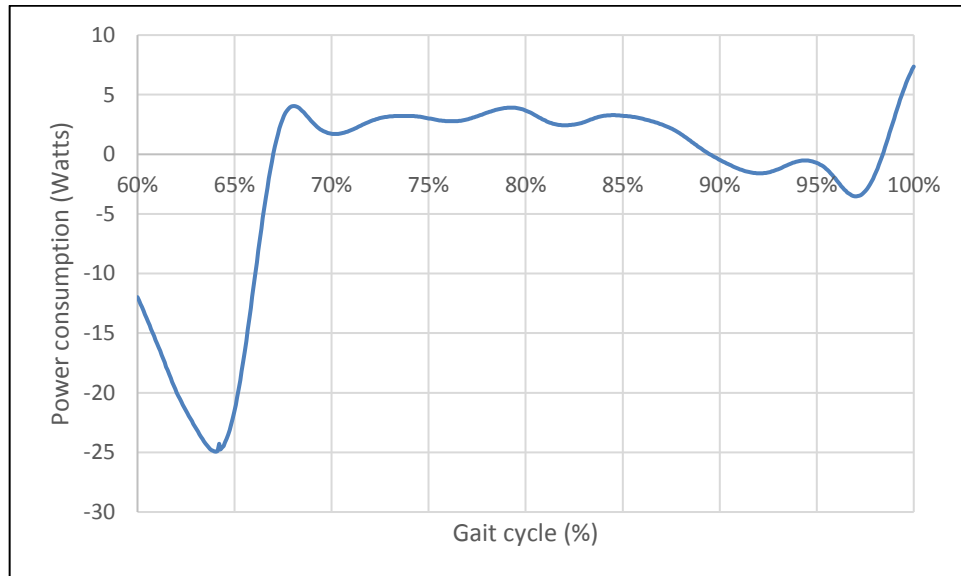


Figure 7.15 Exoskeleton swing hip abduction/adduction power consumption

Figure 7.16 shows the external rotation occurring at the pre swing phase reaching its peak value of ≈ -15 *watts* before the hip joint goes through an internal rotation at the loading response (foot flat) phase, and prior to reaching a peak value at the initial contact of $\approx +52$ *watts*.

The hip rotation during the stance phase has close to zero line power consumption values with a small average of $\approx +2.5$ *watts* from midstance to pre-swing phases.

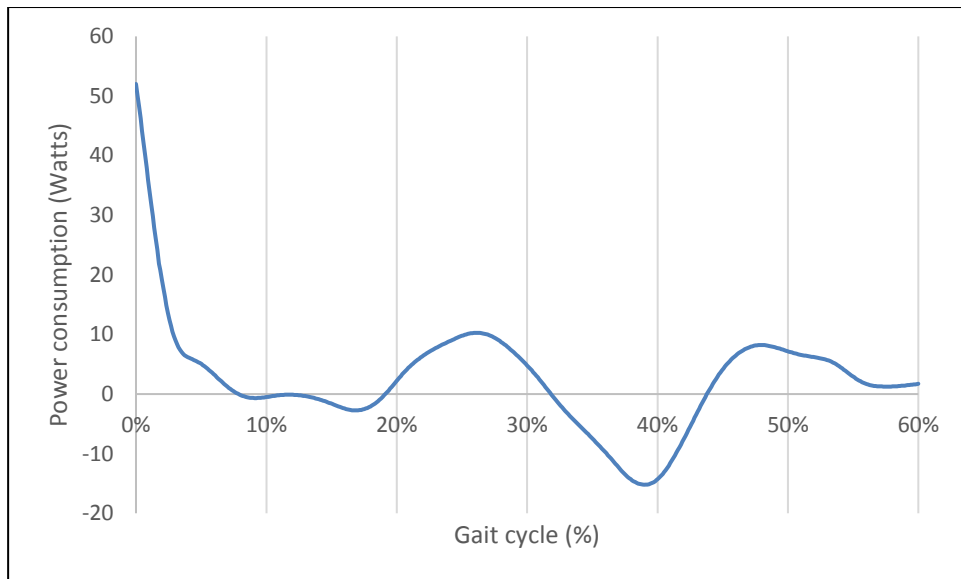


Figure 7.16 Exoskeleton stance hip rotation power consumption

During the swing phase majority of the power is expended for the internal rotation occurring at the end of the pre-swing phase reaching a peak value of $\approx +13\text{watts}$. During the terminal swing, hip goes through its largest external rotation in the swing phase reaching a peak value around $\approx -14\text{ watts}$ as shown in Figure 7.17. The average hip rotation power consumption in the swing phase is close to the zero line and the average value after the mid swing is as small as $\approx -0.2\text{ watts}$.

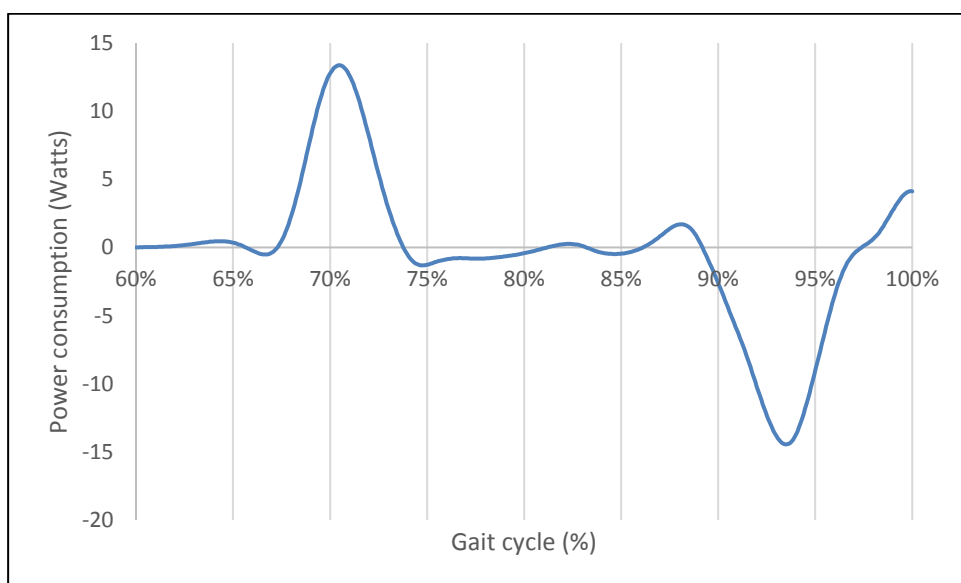


Figure 7.17 Exoskeleton swing hip rotation power consumption

7.6 Comparison of healthy human and exo joints power consumption

The kinematic data from healthy human gait cycle was compared to the gait of the robot in this chapter, in sections 7.3 and 7.4 .

This section compares the power consumption of the robot and how it differs at specific joints of the exoskeleton, the difference in patterns and values between the healthy human and simulated exoskeleton joint powers helps to support the theory of not using CGA data to set the actuation system or other exoskeleton designs specifications.

From equation of motion shown in Appendix B, the mass, geometry and moment of inertias are different between the exoskeleton and the human, which resulted in different patterns of power curves as shown in this section. Joints such as the ankle inversion/eversion and foot flexion/extension both in the human and robot were found to have very low power consumption. This is due to very small torque acting around these degrees of freedom which are chosen to be passively activated by elastic materials such as leaf springs for the purposes of flexibility as future works.

Other active degrees of freedom have been compared in this section.

The human model results are all shown in blue curves and the exoskeleton model results shown in red curves in this section.

The comparison between the results below shows the assumption of using CGA data directly to design exoskeletons specifically in the non-sagittal joints is not accurate, and the exoskeleton's mass, geometry and mechanical properties needs to be used.

7.6.1 Ankle Joint

During the swing phase, the human and the robot do not consume a lot of mechanical power and the power consumption value is close to zero. The exo ankle joint has a peak value of +65 Watts, the human ankle of the same user has a peak value of +83 *Watts*, but the exoskeleton ankle as shown in Figure 7.18 consumes more energy as it covers a larger area under its power consumption curve. This is expected as mentioned before and it is due to differences in mass and inertias between the robot and the human. The results

also seem to be following a similar range of power consumption values, which means the exoskeleton is not implying unnatural forces to the user inside.

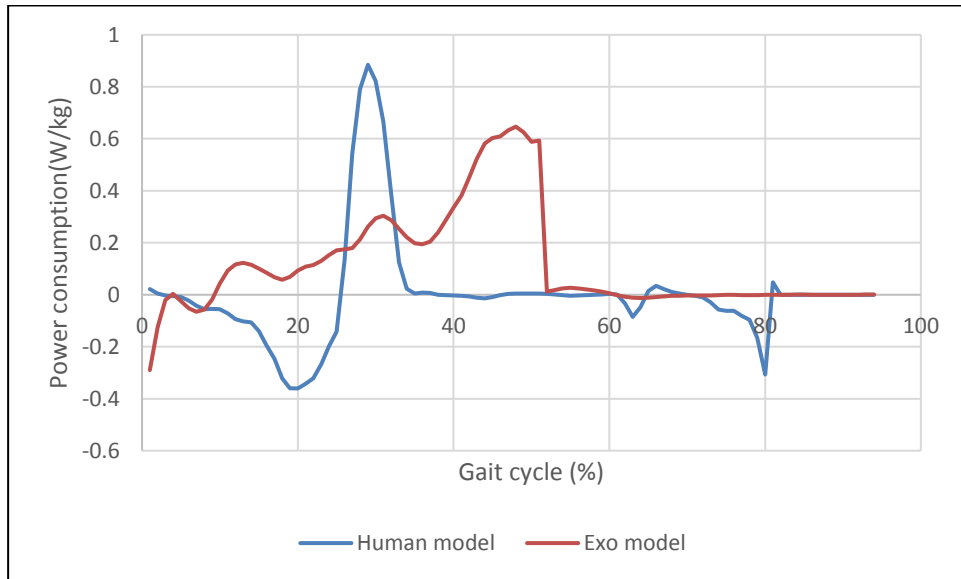


Figure 7.18 Ankle flexion/extension power consumption comparison healthy human vs robot during one gait cycle

7.6.2 Knee Joint

The knee joint of the exoskeleton is within similar power consumption values similar to the measured and simulated healthy human joint but with less fluctuation in direction, due to the exo knee being more rigid. The peak powers are close with exo knee where active actuation would peak at +0.54 watts compared to the human +0.40 Watts, and -0.8 Watts and -0.26 Watts, as shown in Figure 7.19.

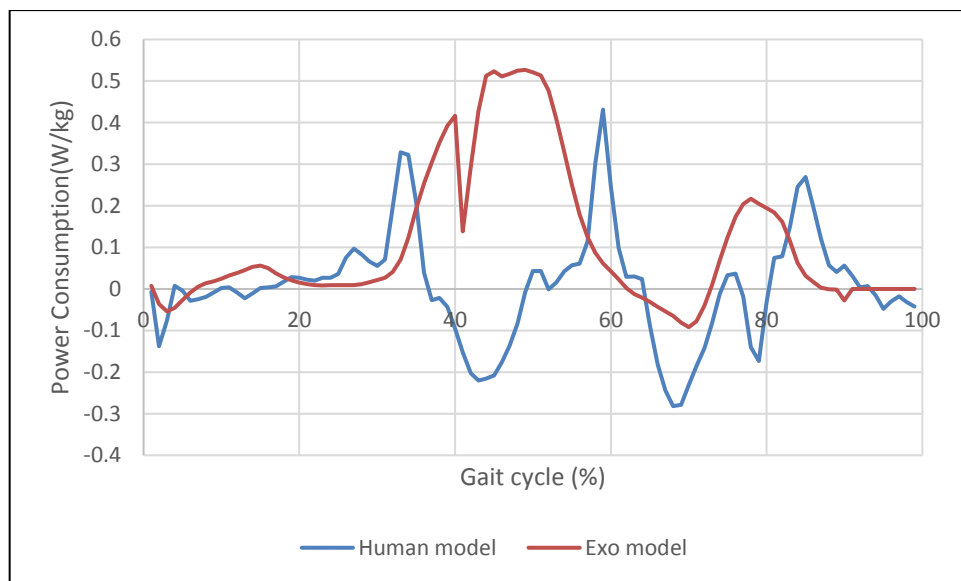


Figure 7.19 Knee flexion/extension power consumption comparison healthy human vs robot during one gait cycle

7.6.3 Hip Joint

The sagittal degree of freedom of the exoskeleton hip was found to be consuming more power than the hip flexion/extension joint in the human. The power consumption values are within similar ranges as shown in Figure 7.20. The main power consumption occurs during the swing phase.

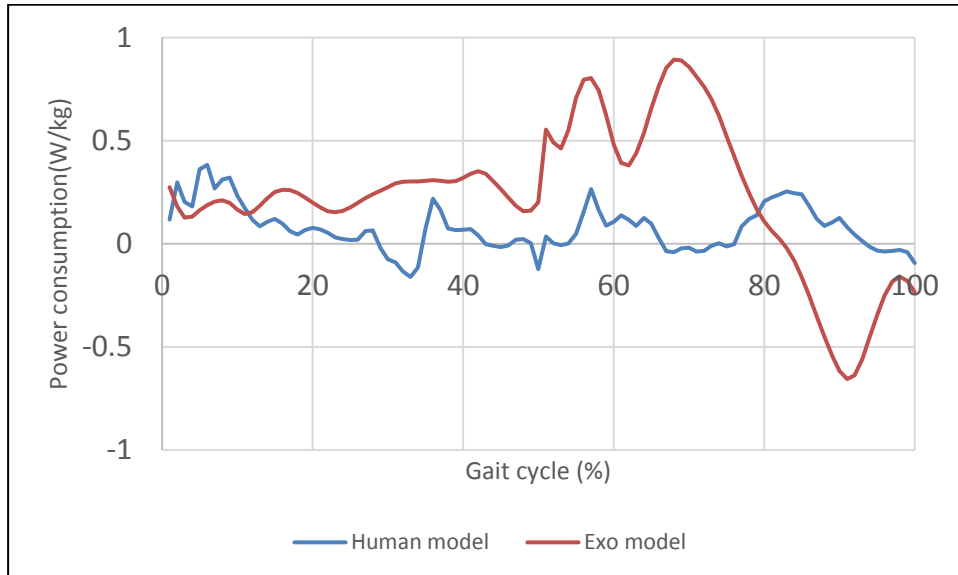


Figure 7.20 Hip flexion extension power consumption comparison healthy human vs robot during one gait cycle

The hip abduction/adduction in the exoskeleton was found to be consuming more power compared to the human model's simulated power consumption as shown in Figure 7.21. As found in section 7.3.3 there is a significant difference in the angular displacements, which can cause this power consumption difference along with the mass properties of the exoskeleton to be at a larger scale compared to that of the human model.

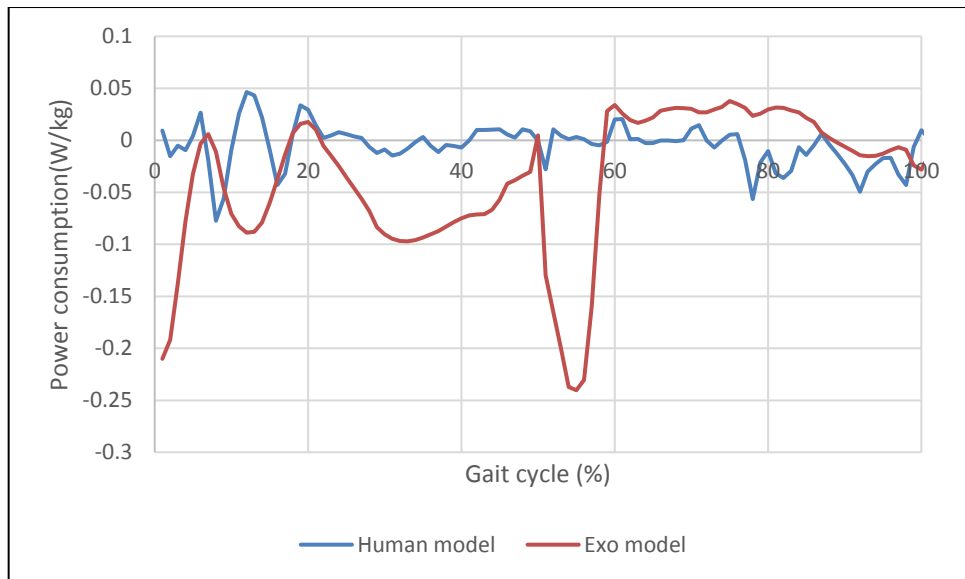


Figure 7.21 Hip abduction/adduction power consumption comparison healthy human vs robot during one gait cycle

The hip rotation found to consume less power at the exo joint compared to the healthy human power required as shown in Figure 7.22. This benefits lowering the metabolic effort of the user by reducing the mechanical power produced while following the same displacements as in the healthy human

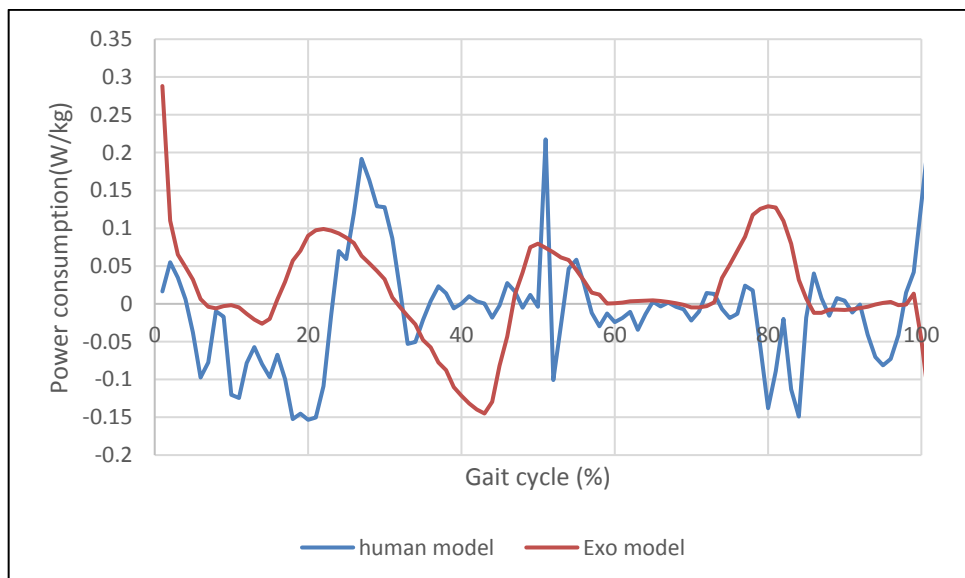


Figure 7.22 Hip rotation power consumption comparison healthy human vs robot during one gait cycle

7.7 Parametric design of the active actuation and gear system

The exoskeleton's gait simulation results determine the specification that the power system is required to achieve.

The active actuation design requirement and technical specifications are shown in Table 7.2.

Table 7.2 Active system design requirements output at the joints of the exoskeleton

Joint ID	Max Required output torque at the joint (N.m)	Max Required speed at the joint (rpm)	Max required Power at the joint (W)	RMS required torque at the joint (N.m)	RMS required speed at the joint (rpm)	Max continues power required at the joint (W)
Stance Ankle F/E	211.70	2.54	56.30	61.67	2.13	13.6
Stance Knee F/E	175.81	3.41	67.73	77.14	1.6	12.9
Stance Hip F/E	177.6	5.12	95.3	89.31	3.19	29.83
Stance Hip A/A	188.21	2.17	25.6	52.24	0.8	4.38
Stance Hip Rotation	100.65	5.21	54.90	53.50	1.66	9.3

Note: F/E : Flexion/Extension, A/A : Abduction/Adduction

As shown, the maximum power output is at the hip flexion/extension with value of 95.3 Watts, and continues power value of 29.83 Watts. This is mainly due to the high angular speed at the joint as well as high torque demand. Respectively, the ankle and the knee flexion/extension degrees of freedoms are among the second and third highest power consuming degree of freedoms.

The chosen motor has to be able to accommodate the maximum and continues power required at the output shaft acting on the joint as shown in Table 7.2. The chosen active electric motor system (Servo Motor SMH60-

series) can produce up to 200 watts of power as shown in Table 7.3, which accommodates the required 95.3 Watts (hip flexion/extension) of maximum power found in the simulation. As shown in Figure 7.25 the chosen motor can satisfy all the active power required at all the active joints with the same model of the motor and gearing system.

Table 7.3 Active system design requirements-motor

Motor Model ID	Rated Power (W)	Rated Torque (N.m)	Rated Speed (rpm)	Maximum Torque (N.m)	Rotor Moment of Inertia (kgcm ²)	Rated Current (A)	Maximum Current (A)	Weight (Kg)
Servo Motor SMH60-203026	200	0.64	3000	1.92	0.375	1.6	4.8	1.3

The technical specifications and details of the actuation system is shown in Table 7.3. The selected motor is to accommodate for all designed active degrees of freedom.

In order for the power system to achieve the specified torques, speeds and powers, the planetary gear system is recommended to be used in line with the electric motor to reduce the torque requirements by increasing the rotational speed of the motor shaft. Details of the gearing system is shown in Table 7.4. The planetary gear head can continuously transmit up to 100 watts of power which is within the requirement limit and it has the desired reduction ratios of up to 156:1.

Table 7.4 Active system design specifications-gear

Gear ID	Max transmittable power continuous (W)	Max Continues Torque (N.m)	Max Continues input speed (rpm)	Max Intermittent power continuous (W)	Max Intermittent Torque (N.m)	Max Intermittent input speed (rpm)	Max Efficiency (%)	Gear Ratios available (X:1)	Weight (Kg)	Number of stages
Maxon planetary gear head GPX4 2	100	15	8000	125	22.5	10000	72	113,126,156	0.46	3

Figure 7.23 represent the performance curve of the active electric actuation system by plotting the torque vs angular speed capabilities of the motor.

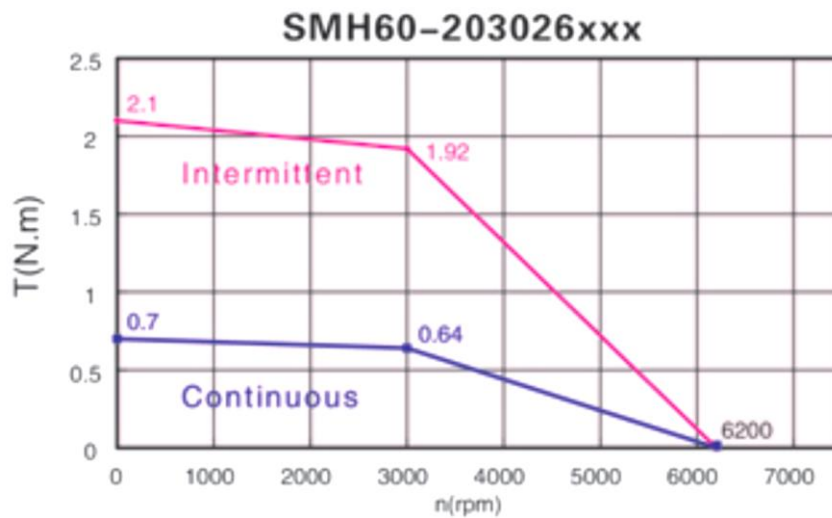


Figure 7.23 Performance curve of the selected servo motor SMH60 series (Kinavo)

The motor under the continuous operation at 0 speed can generate up to 0.7 Nm of force and also can work at 3000 rpm and still generate up to 0.64 Nm of continuous force.

The intermittent performance at no speed is 2.1 Nm, while it can perform up to 1.92 Nm at 3000 rpm which is within the required specifications.

The chosen gear system needs to have a high reduction rate due to the high torque low RPM ratio. The chosen planetary design gear can withstand high torques and minimises any backlash in the system. As shown in Table 7.4 the Maxon GPX42 model reaches the appropriate gear ratios of 126 and 156 by 3 stage design and can run up to 100W of continuous power as can be seen in Figure 7.24 (Kinavo).

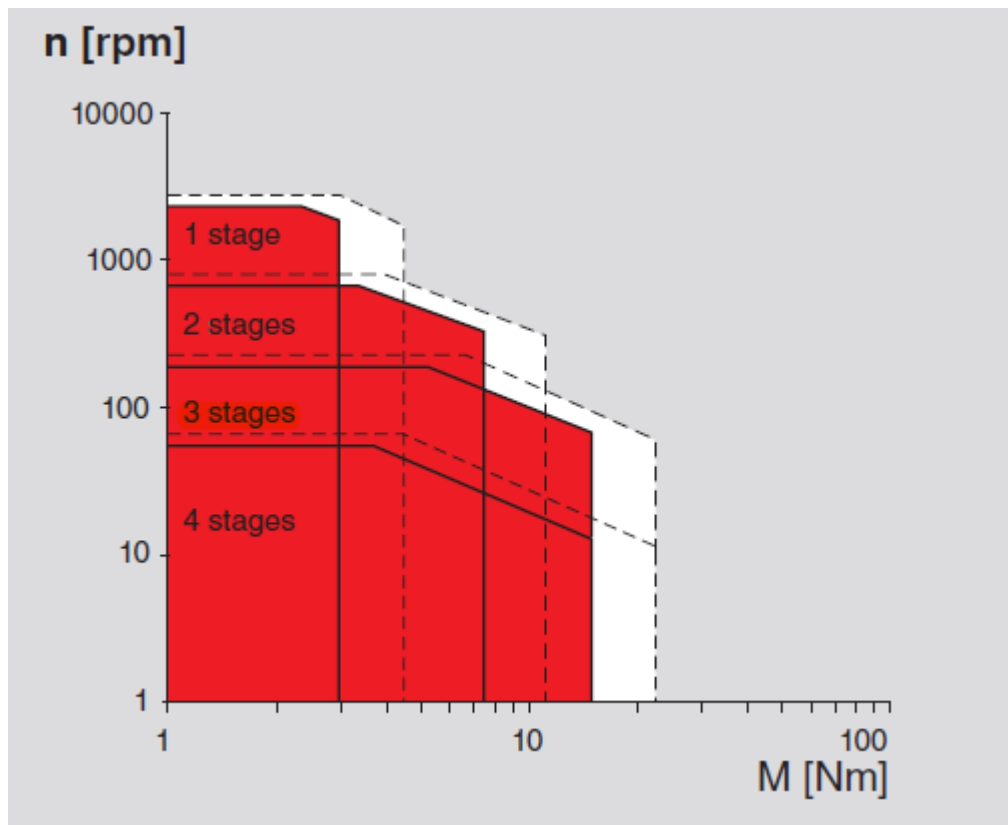


Figure 7.24 Maxon-GPX45 Performance Curve

Figure 7.25 shows that the designed active system is capable of handling the required speeds and torques in order for the exoskeleton to walk itself and the human user inside.

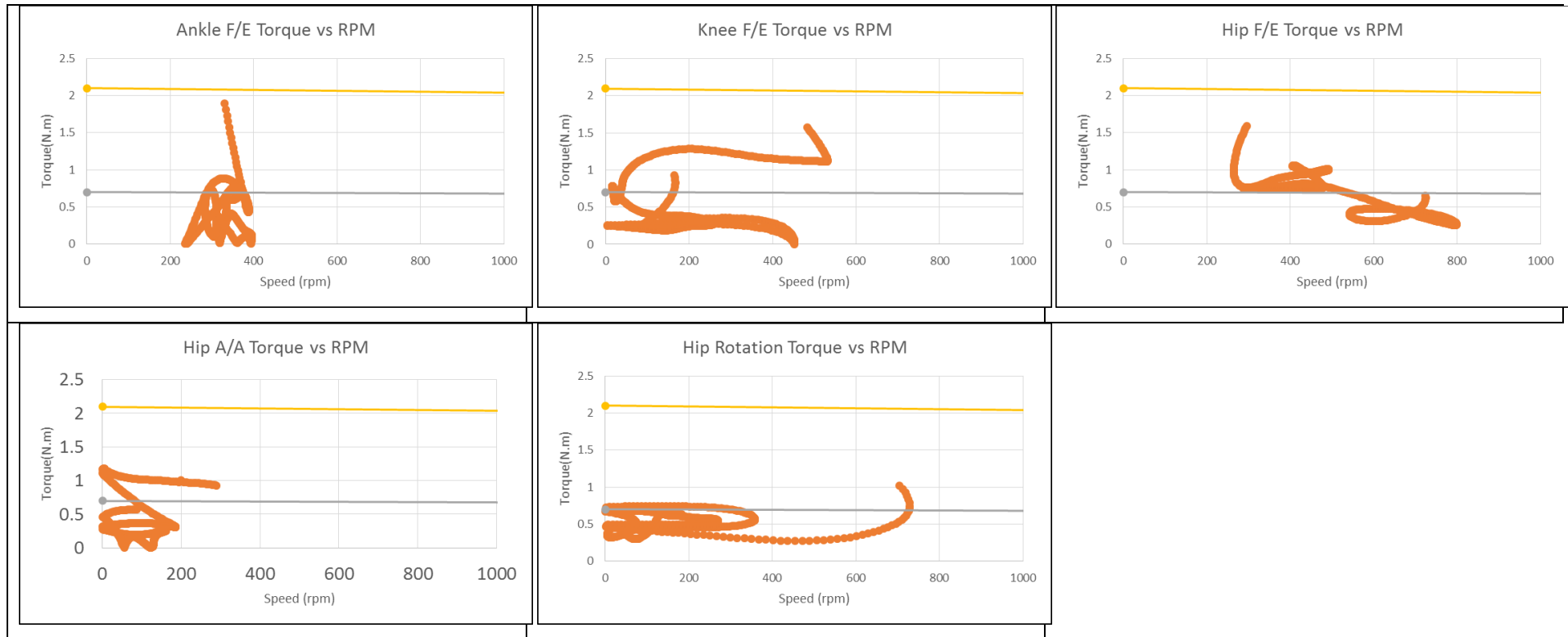


Figure 7.25 Specified and motor performance (torque vs speed) curves

The yellow line represents the motor torque output under intermittent performance.

The grey line represents the motor torque output under continues operation.

The orange curves represents the torque output required to be actuated at the required speed.

The yellow lines shown in Figure 7.25 indicate the intermittent threshold of the chosen servo motor, and the grey lines indicate the continuous threshold performance of the actuation system. The kinematic and kinetic output is shown with orange dots.

The detailed drawing and technical specifications of the electric motor system along with the planetary gear head are shown in Appendix C.

7.8 Summary

This chapter investigated the collected CGA kinematics of various healthy human angular displacements as inputs for inverse dynamic analysis of the robot joints. The results in section 7.2 showed that CGA gait with the lowest velocity and smallest angular displacement to have the lowest power consumption and least effort for the robot to perform a healthy humanoid gait.

Section 7.3 showed the displacements of the robot joints and also compared them with the inputted healthy human angular displacement data were found to be following a closer pattern specifically with the sagittal joints where the joints are aligned closer to the human. The non-sagittal joints results were found to be following similar patterns, but future potential research can focus on better fitting of the non-sagittal robot joint closer to the human user joints.

In section 7.4 the angular velocity curves showed a close mapping of curves between the human and robot joints angular velocities.

The active system degrees of freedom and their power requirements curves extracted from the inverse dynamic analysis of the robot model were shown in section 7.5. The power consumption of the robot joints were compared with the healthy human joints power consumptions for the purposes of a better insight to the frame design as well as verifying the robot simulation to be following similar patterns as the healthy human with some differences due to differences in mass, geometry and inertia properties between the exoskeleton and the healthy human. This section was aiming to systematically assess the statements raised by the assistive exoskeleton designers to avoid using the human kinetics as a base for the design of their active and passive actuation, frame and control systems. The work also concludes the importance of the

non-sagittal joints (specifically in the hip joint) that need to be actively actuated and the designers need to design their exoskeletons for non-sagittal joints as well, instead of just sagittal alone, in order to lower the metabolic effort of the users.

Chapter 8

Exoskeleton passive system parametric design (energy storage and release)

8.1 Introduction

The aim here is to develop a 3D dynamic model of the exoskeleton which is adaptable to various designs and specifications, the model is capable of simulating dynamic forces during the humanoid gait of the exoskeleton for the active and passive system requirements and specifications while the robot is carrying the human inside.

By using the 3D model (with the experimentally measured initial position data), it is possible to simulate and analysis the dynamic properties of the exoskeleton in all three planes in seven degrees of freedom for each leg (stance and swing).

The exoskeleton model in the SolidWorks motion analysis is capable of placing and simulating springs (linear and torsional) and damping (linear and torsional) dynamics of the following passive actuation systems.

The purpose of this chapter is to lower the peak torque and power requirements found for the active actuators where possible by the use of passive elements.

Effective exoskeleton active actuation parametric design will result in a lighter exoskeleton system by using smaller motors and gear boxes.

The energy storage and release mechanisms can make the robot kinetics to perform more metabolically efficient by lowering the generated powers around the human user's joints inside. The design is optimised to be fitted with torsional spring and damper at the joints, by evaluating the elastic characteristics of each degree of freedom during the set motion of the humanoid gait cycle.

The exoskeleton joints stiffness and damping coefficients have been calculated from the SolidWorks model by the least square mean method

explained in section 8.2 the joints suitable for the passive system were selected, the selection was assessed by the effects on the joints instantaneous power consumption before and after the implication of the passive system. The selected passive joints all contributed in two ways: the reduction of the peak powers and reduction in the average mechanical power consumption (making the power vs time curve closer to zero line).

8.2 Torsional spring design

A torsional spring represents the displacement dependent force acting between two parts over a distance and along a particular direction, for design simplification linear springs were looked at, but the model is capable of adapting to nonlinear springs too.

The location of the spring is defined on two distal and proximal parts of the revolute joints where they share the same joint axis. Torsional spring was used as it can be placed directly on the centre of the joint where the human user is sharing the axis of rotation closest with the exoskeleton frame, but the model is adoptable to linear springs and other spring designs too.

SolidWorks motion model calculates the spring force based on the relative displacement between the two parts, the stiffness of the spring and the fabrication of the free length. When the spring force is negative, the spring is in stretched position relative to the free length. The magnitude of the spring force is based on the stiffness and initial force acting on the spring. Equation (8-1) shows the spring relationship (van Dijk et al., 2011).

(8-1)

$$F = -K(X - X_0)^n + F_0$$

Where X is the distance between the two set point of the defined spring, K is the spring stiffness coefficient ($K > 0$), F_0 is the preload of the spring, n is the exponent value and X_0 is the length of the spring at pre load ($X_0 > 0$).

The positive force of the spring means the two parts (end points of the spring) are repelling as the negative force indicates the two parts are compressing towards each other.

8.2.1 Joint stiffness

The rotary motion motors in the simulation (angular velocity inputs) at the joints of the exoskeleton cause the rotational motion at the axes of the joints of the exoskeleton in SolidWorks motion model. The joints are aligned with the axes of the user's joints specifically at the sagittal joints. To find the spring stiffness of the exoskeleton, the relationship between the rotational kinetic (torque at the joint) and the rotational kinematic (angular displacement) has been graphed by using equation (8-2 provides the spring characteristic (stiffness of the joint).

(8-2)

$$K = \frac{dT}{d\theta_j}$$

Where T is the joint torque and θ_j is the joint angular displacement.

The design is using the linear parallel springs, linear springs are less complicated in terms of design and control. From a study considering the design of parallel and series springs by (Wang et al., 2011) which compared the SEA (series elastic actuation) and PEA (parallel elastic actuation) in terms of efficiency in design it was found that the PEA has lowered both the torque and power demand as the SEA can only reduce the peak motor powers by decoupling motor mass from the load and improve the performance of force control. Thus in this work the PEA has been considered and optimised.

During the modelling work for passive systems the following assumptions were considered:

- Any friction in the active (motion motors) and passive (torsional springs) and any gearing system is neglected as the joints of the exoskeleton will have bearings to minimise the friction to as low as possible. in the modelling work this was shown by using mates between the joints, which the joints assumed to be bushing (friction assumed to be zero, roller bearings have been used in the prototype joints).
- The spring used can be engaged and disengaged when needed by a clutch system (time pins and cam mechanisms).

- The power output value has counted in for the inertias of the motor and gearing system (the revised weight of the designed power system found in chapter 7 was included in the mass of the segments of the exo model).

8.3 Joint damping

8.3.1 Translational damper

The translational dampers are used as a resistive element to smoothen out oscillations encountered through forces caused by the active motor systems and passive spring systems. The force created by the damper is dependent on the instantaneous velocity vectors between the two distal and proximal parts on the joint (end points of the damper) with the shared axis of rotation between the parts (joint axis).

The force equation for translational damper element in the model is given in equation (8-3).

(8-3)

$$F = c \times v^n$$

Where c is the damping coefficient, v is the relative velocity between the two end point, and n is the exponent. The exponent can be defined from the best fit line to the torque vs velocity curve, used to achieve the best RMS value to closest to 1. The gradient of the best fit line of the torque vs angular velocity curve is the translational damping coefficient of that joint.

8.4 Optimization method used for parallel elastic actuator

To be able to adapt the spring system for energy storage and release purposes (linear parallel spring), an optimization method was used for fitting the best gradient to the torque against the angular displacement graph of individual joints of the exoskeleton. The method used is the least square method, which find the minimum positive stiffness at the joint, the direction of the spring is decided from the line which covers the majority of the graph (bigger K value).

The following optimization formula was written and evaluated in Mat lab for individual joints as shown in equation (8-4).

(8-4)

$$f(K_p) = \sum_{i=1}^N [T_i - K_p(\theta_{j,i} - \theta_E)]^2$$
$$\min_{K_p \in (0, +\infty)} f(K_p)$$

The least mean square method mentioned above in equation (8-4) is aiming to find the spring which distribute the torque most evenly through the torque angle curves as represented in section 8.6

The least mean square optimization code was also run for finding the best fit in the Torque vs Angular speed graphs for finding the damping coefficient of the joints. The optimization solution is presented in section 8.6

8.5 Passive (spring and dampers) and active (motors) system simulation model

The torsional springs along with torsional dampers were used to lower the size of the motors by lowering torque requirements of the motors through storing the energy and releasing in time. This is only efficient if the springs used have the right stiffness. The stiffness of the exoskeleton joints were determined by the method explained in section 8.2.1 of this chapter.

The joints using springs where it is feasible (energy storing tenancy), are shown in Figure 8.1; the ankle flexion/extension during the stance phase, the hip rotation active at all gait cycle (stance+swing), and the hip abduction/adduction passive mechanism to be active during stance and swing phases. The grey rotational arrows shown in Figure 8.1 represent the torsional spring acting around the selected joints, while the red rotational arrows represent the active actuators acting around the joint both simultaneously during one step gait of the exoskeleton, while the green arrow represents the acting gravity force on the model.

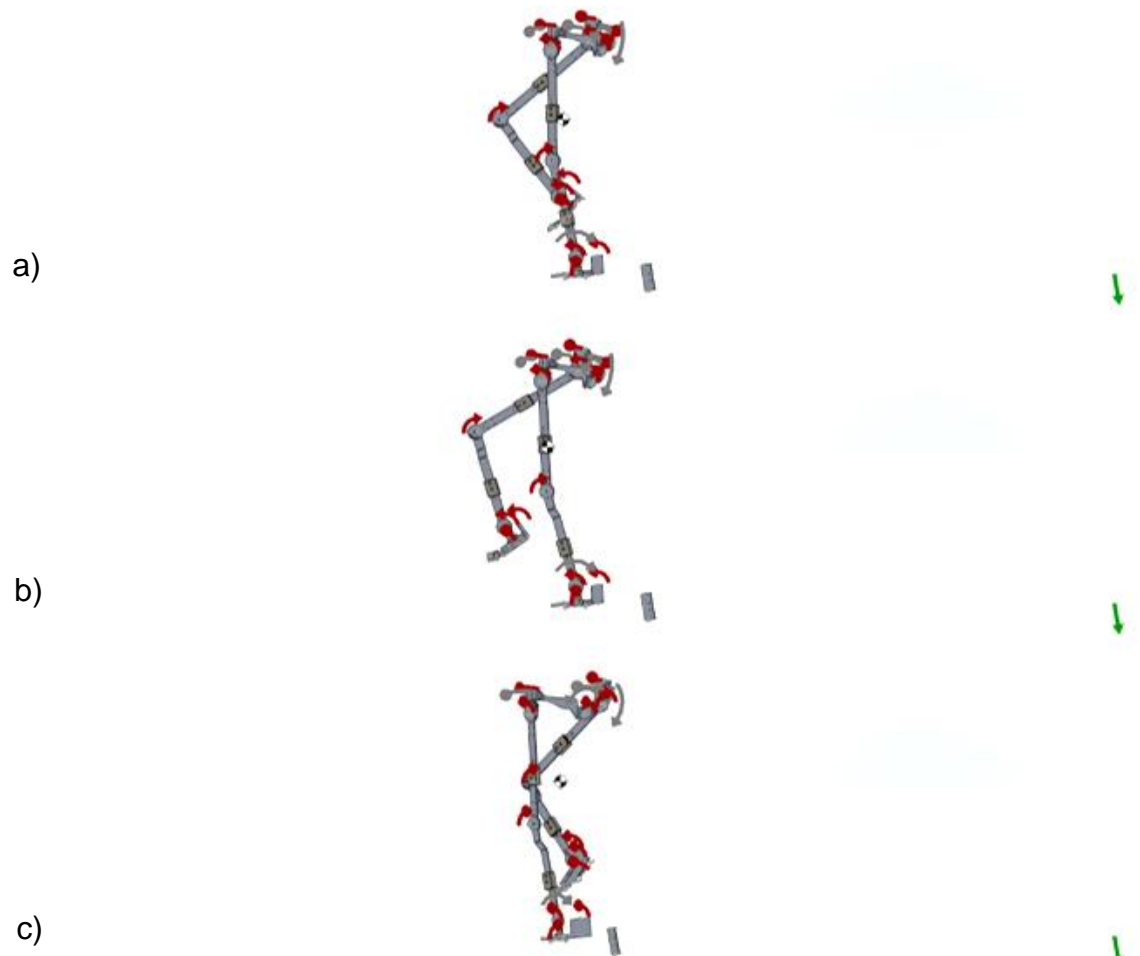


Figure 8.1 Passive system inverse dynamic simulation to find new actuation system requirements a) Initial swing inverse dynamics with spring and actuation system b) Mid swing inverse dynamics with spring and actuation system c) Terminal stance inverse dynamic with spring and actuation system

The inverse dynamic simulation used the passive system to calculate the new motor requirements.

8.6 Results

8.6.1 Ankle flexion/extension

The stance phase consists of the initial 60% of the gait cycle and is where the biggest torques and forces are exerted into the exoskeleton joints by the active power system. The ankle joint starts from $\approx +2 \text{ deg}$ and goes through a big flexion until it reaches its maximum flexion at $\approx -9 \text{ deg}$ as shown in Figure 8.2. This occurs at the initial contact during the heel strike phase of the gait cycle, at this stage the spring system absorbs the negative energy as a braking aid to the active motoring system. The spring is under compression during this phase. After the initial heel off stage the ankle joint is going through an extension. The passive system is using the flexion of the ankle to store most of the negative energy inserted by the system and to release enhancing where the positive power acting (power generated to the exoskeleton) until the remaining of the swing phase. Thus it helps the efficiency of the active actuation system by a small increase in the maximum peak power requirements but a massive decrease in the peak power requirement in the negative direction.

From -9 to $+4 \text{ deg}$ the ankle torque is going through a harmonic pattern where the power changes with peak values ranging from $\approx +156 \text{ Nm}$ to -197 Nm , the passive system is using this change in direction of power to lower the power expenditure of the active system by storing the negative powers and release to the power to the system. The exoskeleton's ankle joint stiffness at the stance phase was calculated to be $\approx 14.1 \text{ Nm/deg}$.

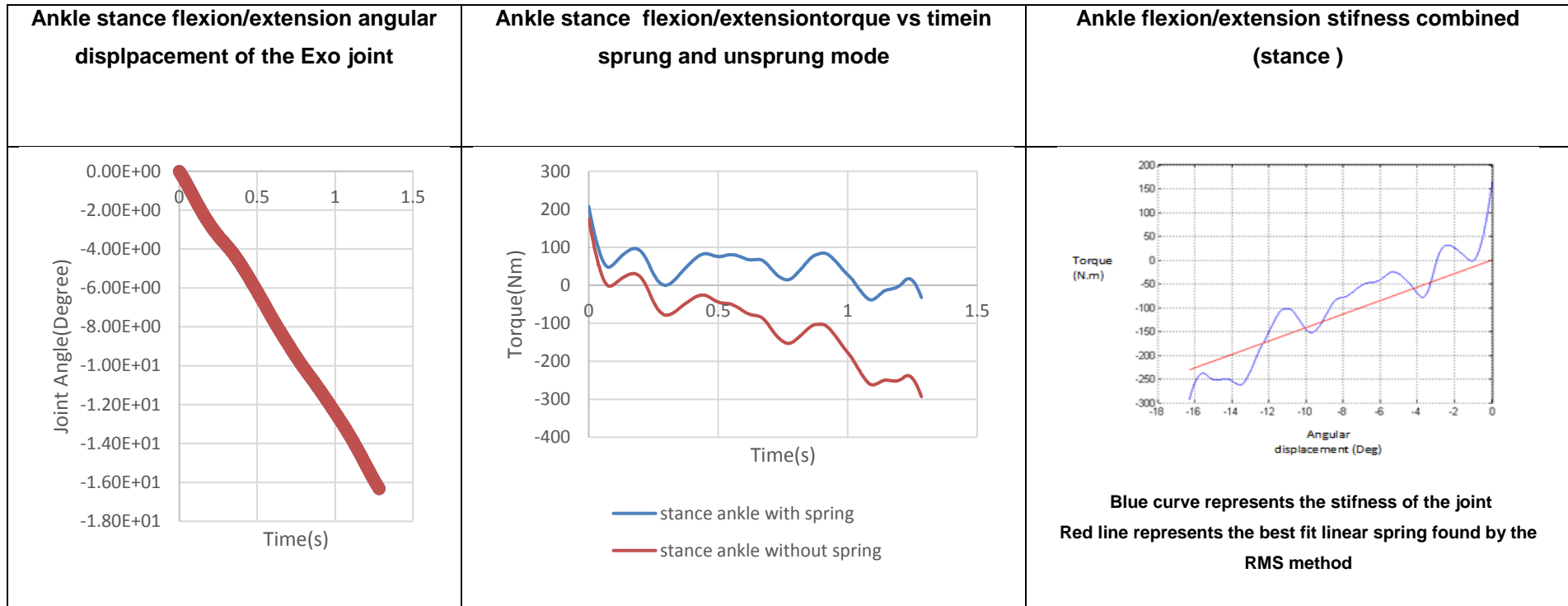


Figure 8.2 Exoskeleton ankle flexion/extension stance phase displacement springs, Exo ankle flexion/extension stance phase power consumption with and without passive system, Exo ankle flexion/extension stance phase Torque vs angular displacement (joint stiffness)

The stiffness along with torque requirement and angular displacement changes have been investigated in three phases i.e. the swing, the stance and the combined (swing+stance). During the swing as shown in Figure 8.3, the joint has a higher stiffness which means the average of the torque distribution along the angles of the joint are at the highest $\approx 62 \text{ Nm/deg}$

The torque vs time graph of the total activity of the gait cycle stance and the swing phase is shown in Figure 8.3. The majority of the troques required to be inserted by the active actuation system are occuring at the stance phase and during the motor's peak power consumption in both directions are $\approx +1$ and -3 watts compared to the stance phase peak powers of $\approx +44$ and -67 watts . The angular displacements during the swing phase is larger than the stance phase as shown in Figure 8.3. The ankle joint dynamic analysis (of kinetic and kinematic) shows the ankle flexion/extension has high torque and relativley small angular displacement during the stance phase which has an stifness value $\approx 14.1 \text{ Nm/deg}$, as the swing phase has very small torques and a larger angular displacement which results in a small stifness value $\approx 0.046 \text{ Nm/deg}$. Thus the design of the ankle passive system is focusing on activating the spring during the stance phase (tension and compression), and disengaing by a mechanical stop or time pin (a clutch sysytem) during the swing phase with an engagement angle $\approx 0.8 \text{ deg}$ in the same direction with the motor at the ankle stance phase (opposite direction to motion of the body in the sagittal plane). Simillar clutch system was designed and tested in research work by (Sawicki and Ferris, 2009).

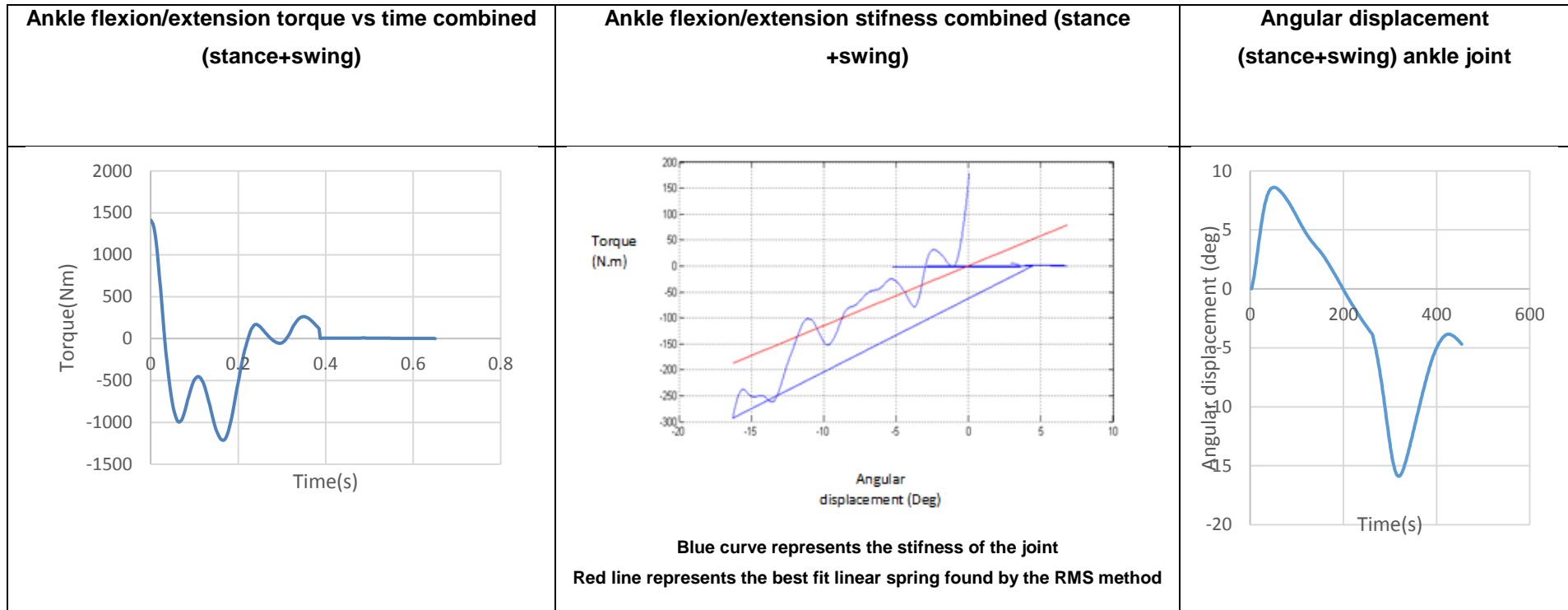


Figure 8.3 Exoskeleton ankle flexion/extension stance swing phase displacement springs, Exo ankle flexion/extension stance swing phase Torque vs time without passive system, Exo ankle flexion/extension stance swing phase Torque vs angular displacement (joint stiffness).

The second spring design consists of a spring with smaller stiffness which is active during the entire gait cycle (stance+swing). This spring stiffness was found by having the torque vs angular displacement graph of the ankle joint during the stance and the swing phase. Using the optimisation method i.e. the best fit line through the least mean square values of torque vs angular

Displacement as shown in Figure 8.3, the k value was found to be $\approx 36.102 \text{ Nm/deg}$. This design is considered to be inefficient due to lack of energy storage compared to the energy required by the motor to work with a spring.

Due to the ankle spring system only being active in the stance phase and being disengaged through the swing phase, it will not make the use of dampers at the ankle joint efficient unless the system is engaging and disengaging with the rest of the passive system. In that case using a damper sufficient for the stance phase will have a damping coefficient value of 0.465 Nms/deg .

The designed dampers would work with the springs as part of the passive mechanism, thus the dampers at the ankle joint can save only a small power expenditure but they increase the peak power output requirement of the active actuation system. The power generation of the motor system in negative direction is also negligible. To avoid complexity, in the design using dampers in the ankle joint is avoided.

8.7 Hip rotation

The swing hip rotation starts from $\approx 0 \text{ deg}$ at the initial heel off stage at the hip rotation is loading by going through internal rotation of $\approx +1 \text{ deg}$ during the heel off phase, the joint motion goes through an external extension until it reaches $\approx -4 \text{ deg}$. The majority of the displacements and torques exerted to the stance hip rotation joint of the exoskeleton is occurring during this time, from heel off to beginning of the mid stance. The motor torque during this time with no passive system are ranging between peak values of $\approx -27 \text{ to } +63 \text{ Nm}$. The motion is harmonic which is ideal for the spring system to use the force in the opposite direction to the motion of the exoskeleton to store and release energy in different time steps to achieve lower peak values for the active actuation system. By including the passive system into the inverse dynamic simulation of the robot, the peak values have changed to $\approx -20 \text{ to } +64 \text{ Nm}$, as shown in Figure 8.4. From the mid stance to the pre-swing phase the swing hip rotation joint's displacement and torque expenditure is closer to zero. The angular displacement peak values ranging from $\approx -0.26 \text{ to } +1.7 \text{ deg}$, the mechanical power peak values also ranging from $\approx -12 \text{ to } +13 \text{ watts}$. The passive system is keeping the same value with an increase in the positive values as releasing the stored energy from the earlier stage mentioned above, the decrease in peak power value to $\approx -11 \text{ to } +4 \text{ watts}$ as shown in Figure 8.4. The calculated stiffness value found to be at $K \approx 0.88 \text{ Nm/deg}$.

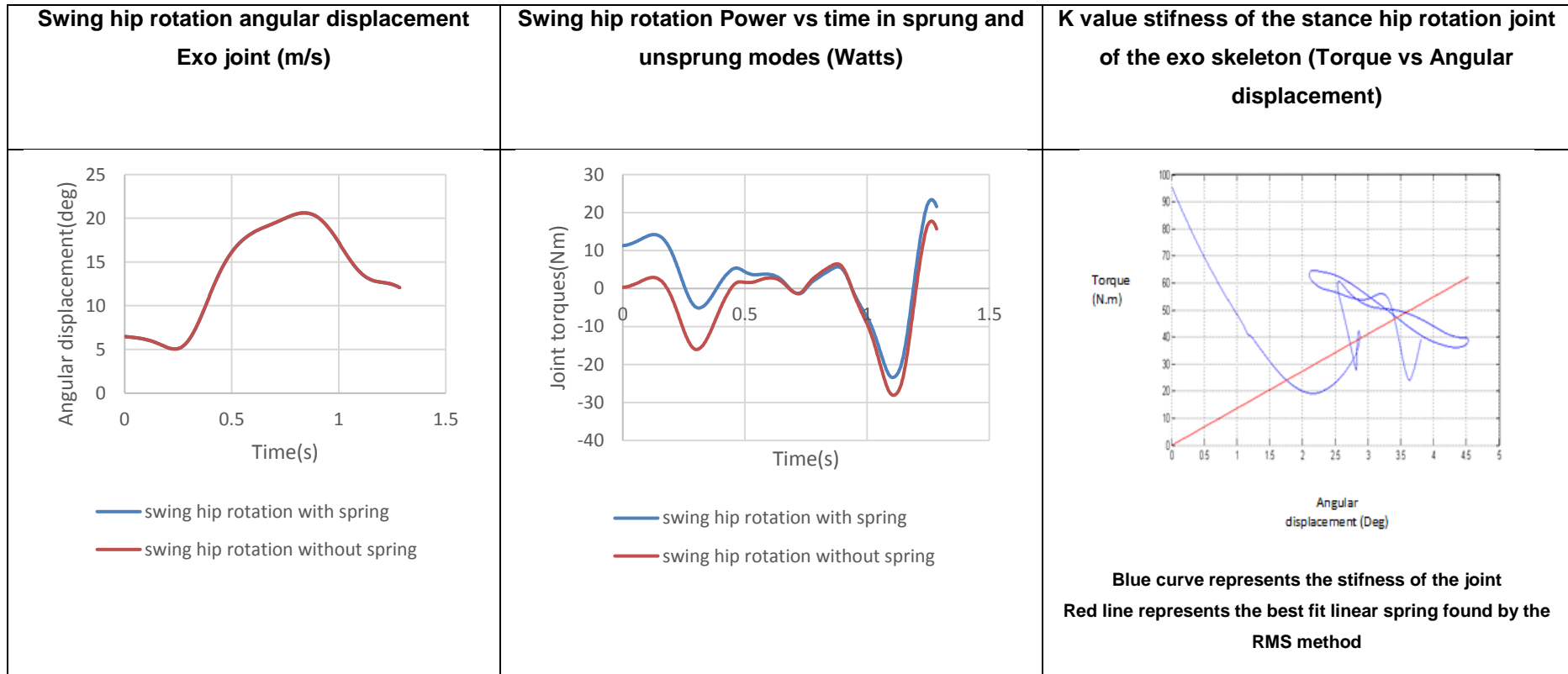


Figure 8.4 Exoskeleton hip rotation swing phase displacement springs, Exo hip rotation swing phase power consumption with and without passive system, Exo hip rotation swing phase Torque vs angular displacement (joint stiffness)

The stance hip rotation goes through a larger amount of torque and significantly smaller angular displacement during the stance phase compared to the torques and angular displacement during the swing phase, as shown in Figure 8.4. The peak torque value during the swing phase is $\approx +23 Nm$ compared to the peak torque value of $\approx +95 Nm$ occurring during the stance phase. The angular displacement is covering half the peak angles during the stance phase in comparison with the swing phase. Thus the stiffness between the stance and swing phase of the hip rotation is large. This makes the passive system a lot more efficient if it was designed for the stance phase alone, where most of the energy generation and absorption is occurring. The active motor system will provide the hip rotation required energy with the passive system being disengaged during the swing phase.

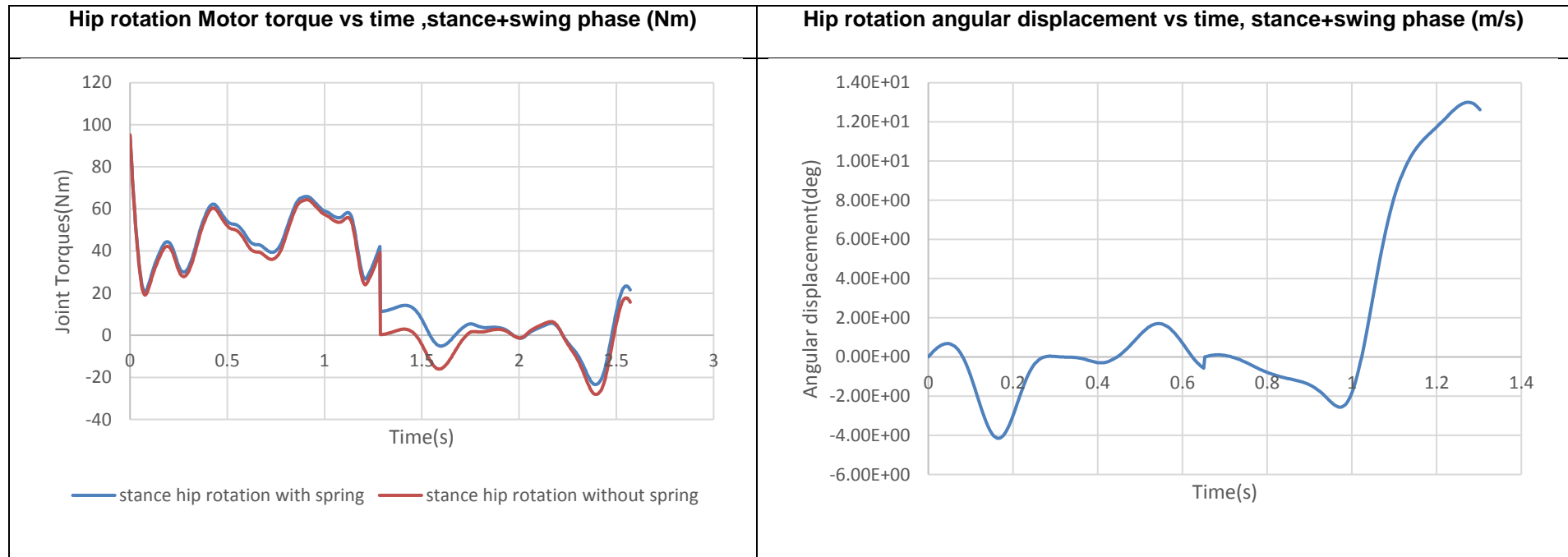


Figure 8.5 Exoskeleton hip rotation motor torque vs time, stance+swing with and without springs, exo hip rotation angular displacement vs time, stance+swing phase

8.7.1 Hip Abduction/adduction

The stance and swing phases of hip joint abduction/adduction have similar torque peak and RMS values and similar ranges of movements as shown in Figure 8.5, thus the spring can be active in both stance and the swing phase. The found k value is $\approx 15.6192 \text{ Nm/deg}$, with the free angle acting at $\approx 0.95 \text{ deg}$, so the spring in both stance and swing phases does not rely on the active system to perform extra work to support the passive system.

The spring is a uni-directional torsional spring as during the stance phase it stores energy and compresses during the adduction phase and releases the stored energy during the abduction phase. The positive torque peak values in the stance phase have been decreased from $\approx +79 \text{ Nm}$ to $\approx +20 \text{ Nm}$, while the torque peak values absorbed have fallen from $\approx -109 \text{ Nm}$ to $\approx -134 \text{ Nm}$.

The spring releases torque and helps the active actuation system during the abduction of the hip joint and compresses during the hip abduction in the swing phase. Positive torque peak values in the swing phase have been fallen from $\approx +40 \text{ Nm}$ to $\approx +27 \text{ Nm}$, while the torque peak values absorbed rise from $\approx -12 \text{ Nm}$ to $\approx -49 \text{ Nm}$ as shown in Figure 8.6.

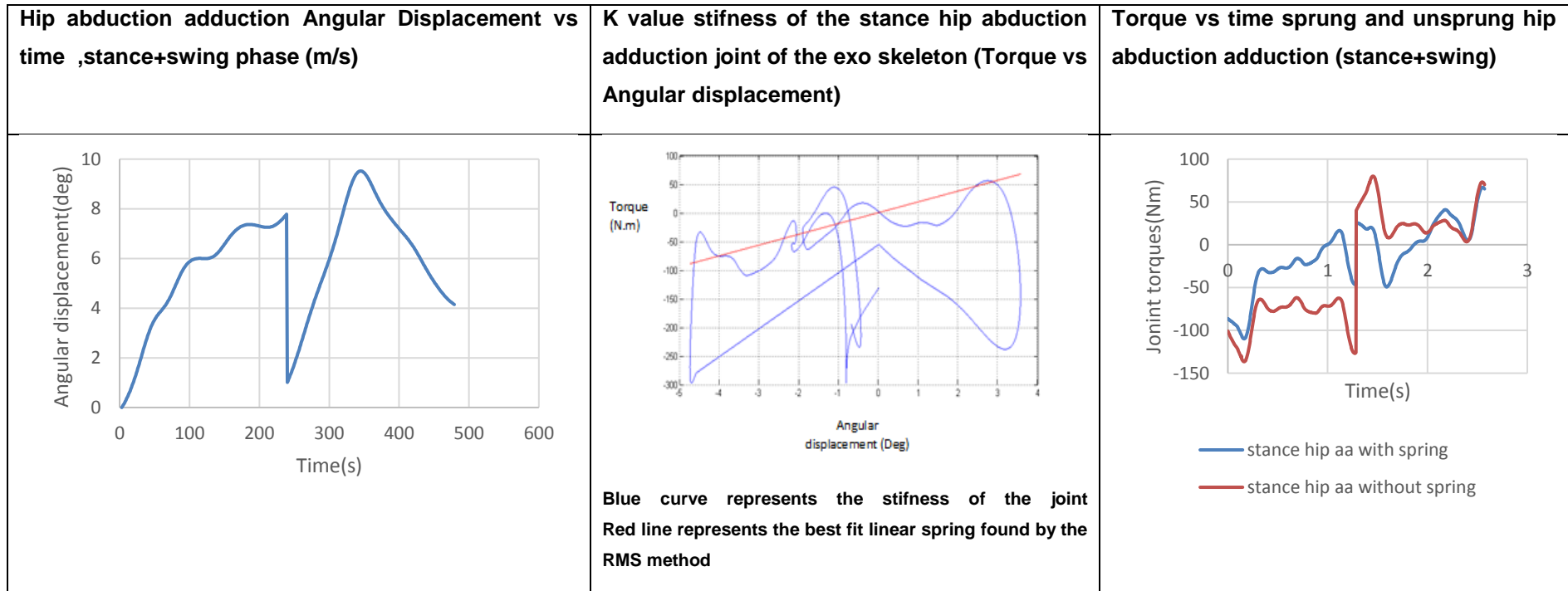


Figure 8.6 Exoskeleton hip abduction/adduction angular displacement vs time ,stance swing phase (m/s) spring, exo hip abduction/adduction stance+ swing phase power torque vs time with and without passive system, exo hip abduction/adduction stance+ swing phase torque vs angular displacement.

8.8 Spring parametric design

The found stiffness of the joints presented in section 8.6 the three most dynamic suitable joints to be passively activated were found to be ankle flexion/extension, hip rotation and hip abduction/adduction. The hip rotation is found to be the spring with smallest stiffness of $0.88 \frac{Nm}{deg}$ compared to the ankle flexion/extension of $14.1 \frac{Nm}{deg}$ and hip abduction/adduction with stiffness of $15.6 \frac{Nm}{deg}$. A local specialist torsional spring makers JB springs ltd have been consulted to provide a manufactural design of the springs. Figure 8.7, shows the spring's drawing of the torsional springs provided by JB Springs Ltd. The spring is capable of handling the highest spring constant of $15.6 \frac{Nm}{deg}$.

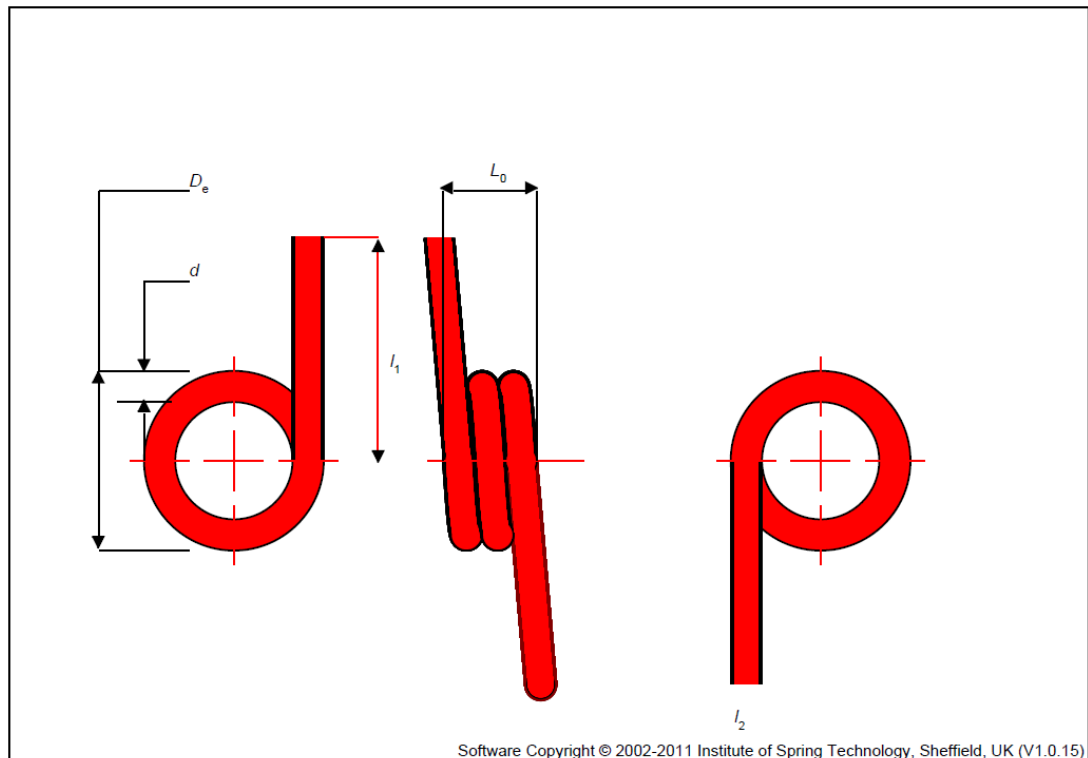


Figure 8.7 Spring drawing of the torsional springs provided by JB Springs Ltd.

The detailed design specification of the springs are presented in Table 8.1, for all selected three joints.

Table 8.1 Detailed design specifications of the torsional springs for all selected passive joints

	Symbol	Unit	Ankle FE	HIP AA	Hip Rotation
Wire Diameter	D	mm	14.00	14.00	3.50
Outside diameter	D_e	mm	80.50	70.50	40.00
Total Coils	n_t	-	2	2	2
Spring Rate	R_s	Nmm/Deg	14100.00	15600.00	880.00
Torsional Moment	M	Nmm	151109.00	177854.00	1613.00
Deflection	d	deg	10.00	10.00	15.00
Body length	L_0	mm	42.00	42.00	38.75
Length Leg 1	l_1	mm	100.00	100.00	100.00
Length Leg2	l_2	mm	100.00	100.00	100.00
Weight		Kg	0.58	0.58	0.02

Note: F/e : Flexion/Extension, A/A : Abduction/Adduction

8.8.1 Results with active system and spring weight included

The dynamic behaviour of the springs was simulated by using the spring elements with specified spring stiffness and the appropriate torsional spring in SolidWorks motion tools by using the ADAMS inverse dynamic solver. The simulations showed improved efficiency when including the new design weight factor of the springs as well as investigating the dynamic effects of the springs on the system.

Under an assumption of not including the weight of any housing and connectors between the passive system and the frame. The simulation is adaptable to any new calculated weights.

The results prove the spring simulations with the added weight characteristics are significantly more efficient to be used at the selected joints as shown below.

8.8.2 Ankle

The weight of the designed torsional spring is 0.58 kg and has its greatest effect on the total power consumption of the ankle joint during the stance phase due to higher range of movement compared to the swing phase of the ankle joint, as shown in Figure 8.8.

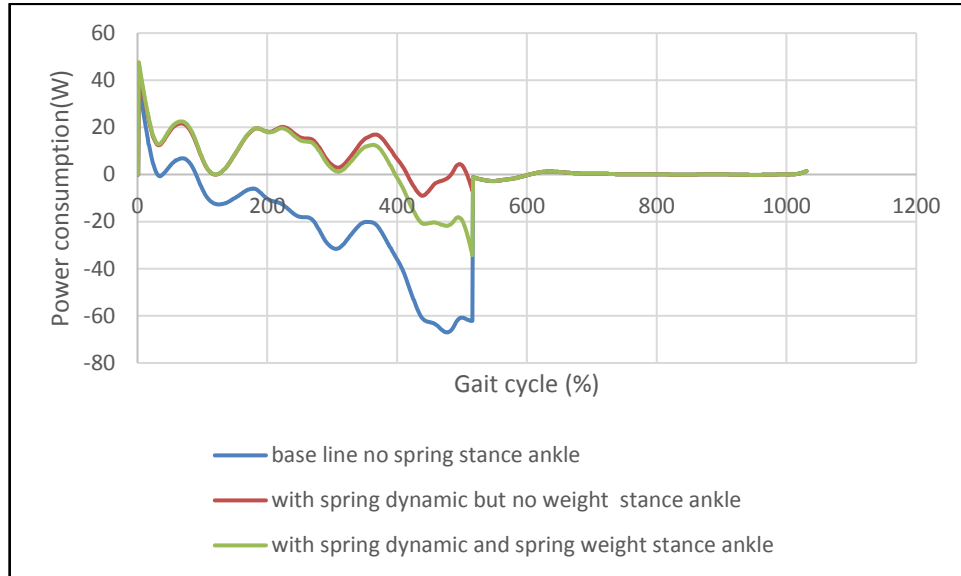


Figure 8.8 Ankle power consumption with weight of the springs included

8.8.3 Hip rotation

The hip rotation has the smallest spring stiffness value in comparison with the other two passive system with stiffness of 0.88 Nm/Deg . It has the lightest spring design with a weight of 0.02 kg , As such it will not affect the power consumption compared with no weight factor, as shown in Figure 8.9.

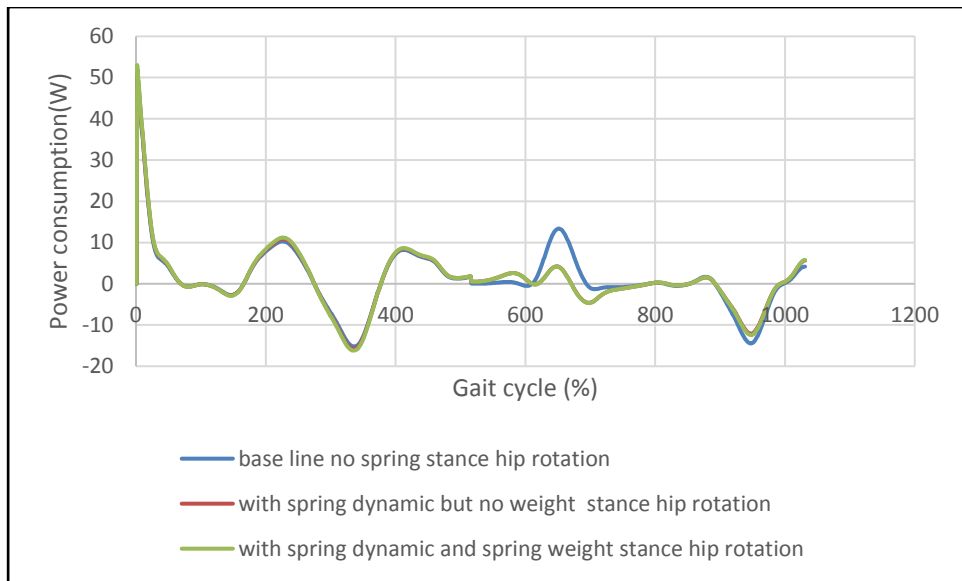


Figure 8.9 Hip rotation power consumption with weight of the springs included

8.8.4 Hip abduction/adduction

The torsional spring used in hip abduction/adduction has a weight of $0.58kg$ and has its most effect on the raise of its power consumption due to the high weigh at the initial swing phase where the biggest range of motion occurs at the hip abduction/adduction joint, as shown in Figure 8.10.

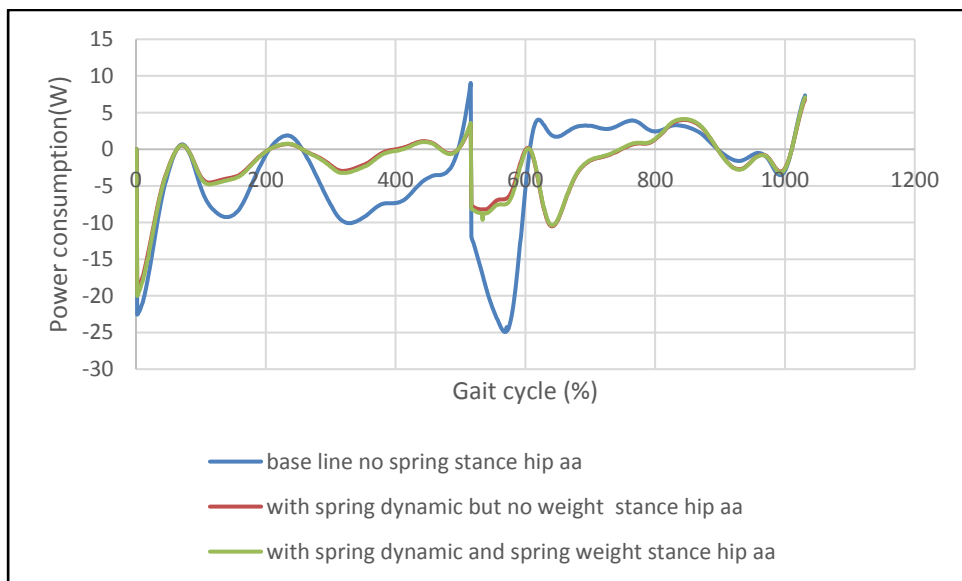


Figure 8.10 Hip aa (abduction/adduction) power consumption with weight of the springs included

8.9 Discussion

8.9.1 Ankle flexion/extension

The stance ankle consumes the largest power from the motors as shown previously in section 8.6 the required maximum power generated occurs during the stance phase. This is due to the high torques required to change the state of exoskeleton from the static position into a dynamic motion. The extension of the ankle costs the motors to generate up to $\approx +39\text{Watts}$, while the flexion of the ankle costs the motor to generate up to $\approx -66\text{Watts}$. Thus the passive system chosen to be active in the stance phase. The energy inserted at the initial contact during the extension of the ankle joint was used to wind (compress) the spring, thus the motor peak values with the passive system remains pretty much the same with a small increase to $+46\text{watts}$ from $+39\text{watts}$ of power consumption without any passive system. During the release phase of the passive system which occurs immediately after the initial contact as shown in Figure 8.11, it results in a significant reduction of the required power generation of the active actuation system and peak values during the flexion phase, decreasing the power output in the negative direction to $\approx -9\text{watts}$ and reducing the power consumption which is discussed in illustrated in Figure 8.11. The energy reduction is due to the spring working with active actuation system by releasing their stored energy into the system. The pattern of storing energy during the extension phase and releasing in the flexion of the ankle joint can be seen in remaining of the stance phase as shown in Figure 8.11.

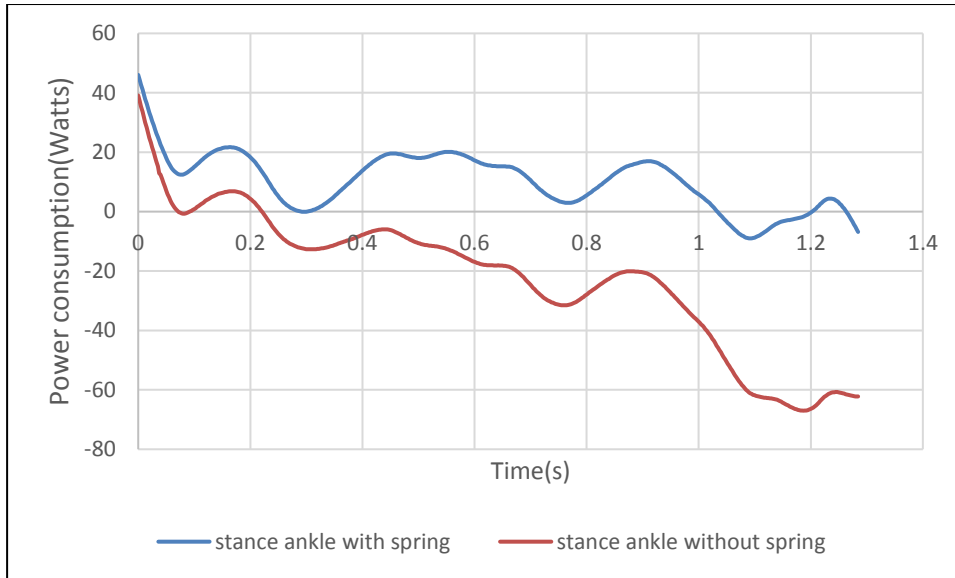


Figure 8.11 Exoskeleton stance ankle power consumption vs time with and without passive system

The passive system at the ankle joint alone is saving around 46% of power consumption of the joint's total power consumption, this is about 6982watts of power consumed for one gait.

8.9.2 Hip Joint

8.9.2.1 Hip abduction/adduction

The hip abduction/adduction spring characteristic is a unidirectional spring, as the direction of the spring needs to be changed with the change from stance to swing phase, to achieve the most efficient power consumption of the system.

Due to the similarity in kinetics and kinematics of the exo hip abduction and adduction, the same spring can be used and it does not require a gearing or clutch system to deactivate the spring at any point. The free angle of the spring found to be 0.95 degrees. This is the angle at which the spring activates and can be achieved by mechanical pins on the joint or frame depending on the detailed design.

During the stance phase the spring is activated in the same direction with the actuation system. At the initial contact the spring system is increasing power requirement as the spring is working in opposite direction and the energy is expended for unwinding the spring. The peak powers have increased from

around 30watts to about 42watts. At the loading response immediately after the initial contact the passive system decreases the power requirement of the actuation system by storing the energy by winding (compression state), and have reduced the peak powers from around -116 watts to around -87 watts. The power consumed during the stance phase by using the spring with stiffness of 15.62 Nm/deg has made the actuated power consumed 23% more efficient compared to the active system with no spring. The stance phase has mechanical power consumption of around 1200 watts, the value saved in half of the gait which is the stance phase alone.

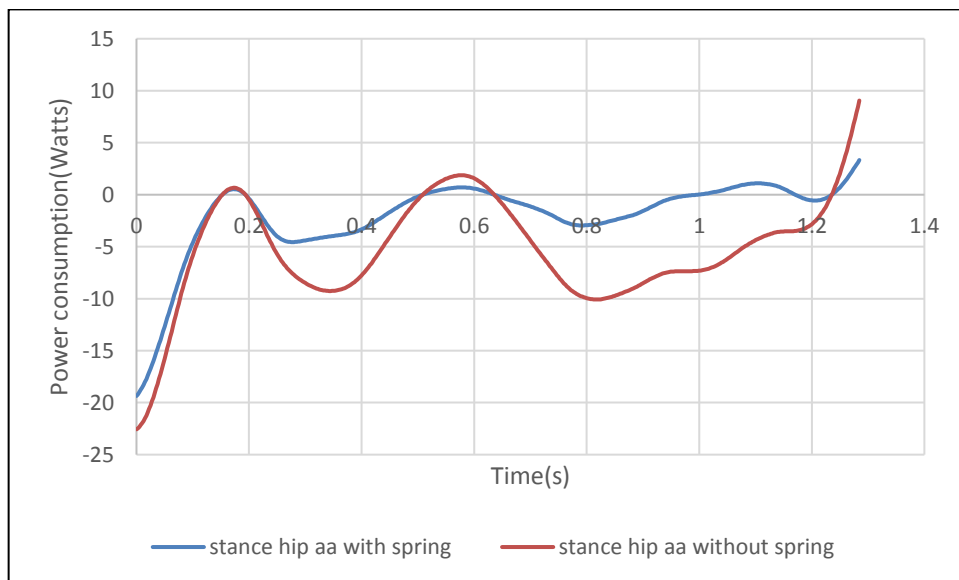


Figure 8.12 Exoskeleton stance hip abduction/adduction power consumption vs time with and without passive system

The spring during the swing phase changes its direction and works against the direction of motor's rotation (uni directional spring). At the swing phase the spring is storing the energy during the adduction of the hip joint, and releases the energy at the abduction movement as shown in Figure 8.13.

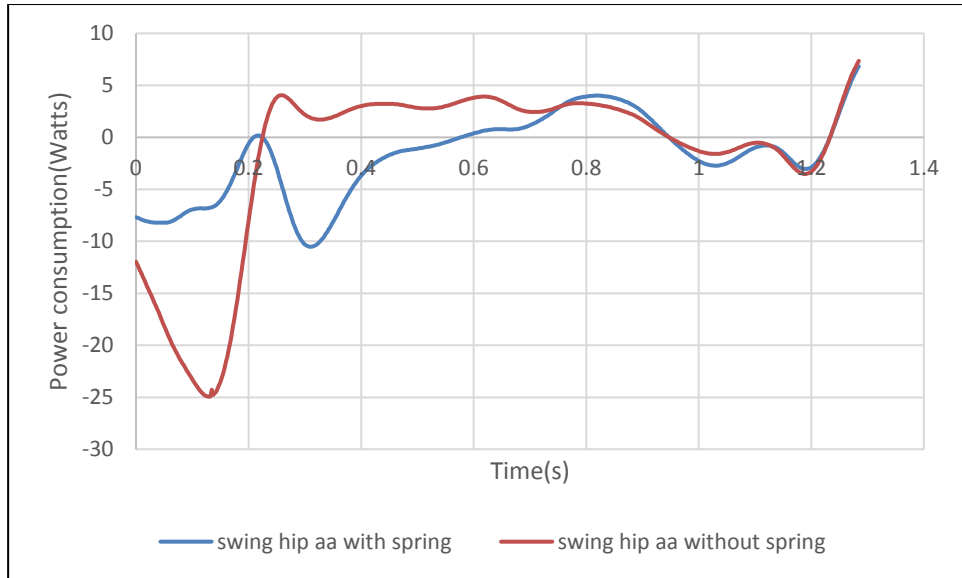


Figure 8.13 Exoskeleton swing hip abduction/adduction power consumption vs time with and without passive system

8.9.2.2 Hip Rotation

During the hip rotation at the stance phase, the system is not engaged and as shown in Figure 8.14, there is no difference in the change of power consumption between the active and passive modes.

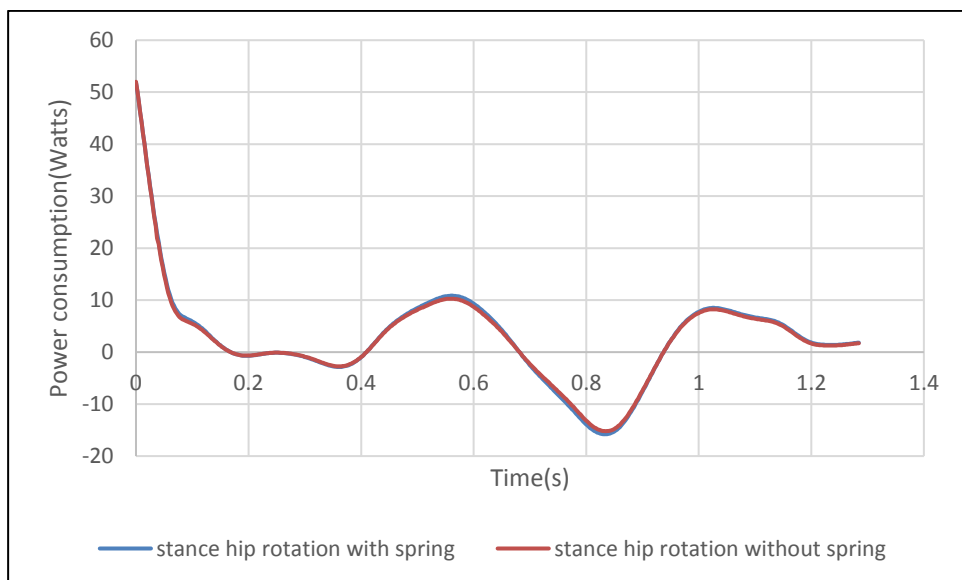


Figure 8.14 Exoskeleton stance hip rotation power consumption vs time with and without passive system

The passive torsional spring activates during the swing phase of hip rotation. At the initial swing, the hip rotation spring increases the work of the motor by

using the motor power to wind the torsional spring. At the mid-swing phase the torsional spring unwinds and helps releasing stored energy in the same direction as the active system. This results in a decrease of the usage of the active system during the preswing by minimising the peak power consumption of the motor with and without passive system from $+13\text{ W}$ to $+4\text{ W}$. The active system goes through a final winding of the spring at the end of the mid-swing phase, and results in the power consumption increase of the active system from -0.87 W to -4.6 W . The winded spring then releases its stored energy during the terminal swing phase where the biggest negative power expenditure of the active system is, reducing the power requirement of the active system from -14.3 W to -12 W as shown in Figure 8.15.

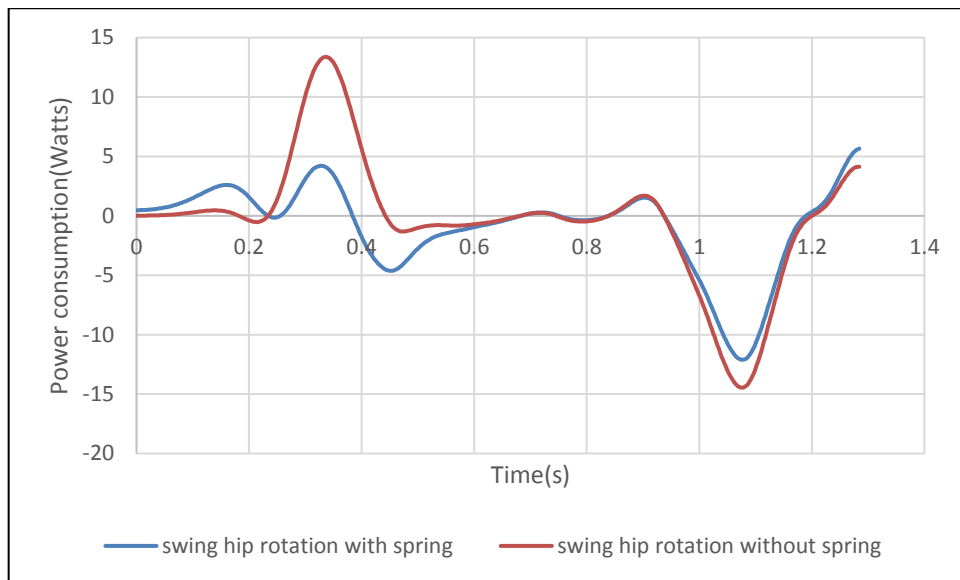


Figure 8.15 Exoskeleton swing hip rotation power consumption vs time with and without passive system

8.9.3 Passive system energy saving contribution

The passive system at the ankle stance phase has the highest contribution in comparison with the total power saved at other passive joints with around 4.5% of total power system reduction as shown in Table 8.2. This is due to high elastic behaviour in the ankle stance phase and matching linear spring characteristics. The second most energy saved power system is at the hip abduction/adduction during the stance and the swing phase which is found to save up to 1% of the total power consumption of the entire system. The passive system was found to save up to 5.6% of the total instantaneous power consumption of the entire system.

The passive system increases the efficiency of the system in more than just decreasing the instantaneous power expenditure by lowering the peak torques and powers that the motors need to provide, which results in smaller and lighter actuation systems. In all the selected passive joints the peak power outputs have decreased by more than 50% as shown in the figure presentation in section 8.8 .

Table 8.2 Efficiency of the passive system from kinetic data simulated

Joint and DOF	Phase of gait cycle	Spring stiffness $\left(\frac{Nm}{deg}\right)$	Damping coefficient $t\left(\frac{Nm}{s}\right)$	Instantaneous power saved (Watts)	%tile efficiency contribution at the joint power consumption	%tile efficiency of the total power consumption of the system
Ankle (flexion/extension)	Stance	14.10	0.46	6982.64	12.99617	4.45
Hip (abduction/adduction)	Stance	15.70	N/A	1770.09	21.82	0.65
Hip (abduction/adduction)	Swing	15.70	N/A	955.2198	5.137728	0.24
Hip (rotation)	Swing	0.90	1.10	318.68	20	0.21

8.10 Summary

From using both the simulation and optimisation techniques the stiffness of all 14 degrees of freedom of the robot have been investigated.

This section successfully identifies which joints have the elastic behaviour in the activity of the robot during the one step gait. This is done by the ability of the joint to store the inserted force from the active actuation system into a torsional spring and release in a time which supports the performance of the active actuation systems. The appropriate joints are the ankle flexion/extension, hip internal/external rotation and hip abduction/adduction.

As shown in the discussion section the ankle flexion/extension is capable of saving the most energy and contribute toward the power consumption saving more than any other joint, the next biggest savers are the torsional springs used at the hip abduction/adduction followed by the hip rotation. In total introducing this passive spring system reduces the total power consumption of the system by 5.55%.

Chapter 9

Summary, conclusions and future work

9.1 Summary and assessment of the research objectives

The research aim of this project is to improve on the design of the assistive lower limb exoskeletons by improving the accuracy of mechanical design specifications. The robotic exoskeleton is expected to follow the human motions as close as possible for providing an efficient gait with the aim of minimizing the energy expenditure of the user.

Chapter 1 defines the aims and objective of the project in greater details. In this chapter the main objectives of this project have been set to investigation on metabolic efficiency of individual degrees of freedom to be used as a physiological insight in selecting the robot frame requirements, other objective was a systematic approach and study into identifying an efficient human kinematics (motion and velocity) for the robot to follow, in order to minimise any external forces acting from the robot to the user. Another objective of this work is to create a platform and establish a methodology which designers could use to accurately extract the needed design specifications (frame, active actuation, passive actuation and control).

This chapter introduces the novelty of the work to be the unique design approach in finding the parametric design and specifications of the passive and active actuation systems and frame design and selecting the most efficient active and passive degrees of freedom by considering the mechanics and energetic of the human and the robot in walking activity.

The other novelty of the project is using the efficient healthy human kinematics as motions of the robot dynamics during the activity of the human walking as a method to minimise the human and robot unwanted interactions, in order to minimise the energy expenditure of the user inside.

Other novelty of this project comes in investigating the motion of the robot in all planes and an insight to the elastic behaviour of some joints and segments and their motion which resulted in introducing passive systems that helped to

reduce the actuation systems peak torques and power expenditure by means of elastically storing and saving energy and releasing it at the appropriate time to make the motion of the robot gait more efficient by generating less power from the active system.

Due to lack of literature data available on the non-sagittal plane healthy human joints kinematics and kinetics, an independent CGA study of human gait was done at the University of Leeds as explained in chapter 3. The research objective was to find the most suitable human kinematics as the input of the robot motions along with finding the dependency of variables such as speed, joints and limbs displacement on the mechanical work.

The physiological measurement of human VO₂ consumption was used to verify various non-sagittal joints efficiencies as a design approach in selecting the exoskeleton necessary degrees of freedom as presented in chapter 4. This is done by applying similar mechanical restriction as an exoskeleton will have on the selected joints, and comparing the outcomes with to the base line of the healthy human with no restrictions.

In order to investigate and verify further the CGA data of the most efficient gait, an inverse dynamic on the human models simulation was computed to find the joints and total mechanical work of five healthy subjects, along with experimentally collected reaction forces at various speeds in a series of trials as discussed in details in chapter 5.

To fulfil the objective of using the exact geometry and mass and inertia properties of the exoskeleton robot, a prototype of an anthropomorphic robot with 14 degrees of freedom was designed and manufactured at the University of Leeds. For the purpose of accurate simulation model building and dynamic studies the prototype was worn and powered by a human user and the initial positions were collected by using motion capture technology. The inverse kinematic and inverse dynamic simulation with robot initial position was performed as described in chapter 6. The result is a simulation model which is adaptable in design and various motions and can be used as a platform for various assistive robot design and studies.

The works from chapter 5 and 6 were combined and used to input the most efficient motion of the human into robot kinematic which results in providing

the requirements of the actuation systems and forces on the frame, presented in chapter 7, along with the parametric design of the active actuation systems. The human and the robot motions were also compared for the purpose of verifications and claims of designing a robot with minimal internal and external interactions with the user inside for fulfilling an efficient energetic gait with 100% assistance from the robotic exoskeleton.

Chapter 8 concentrates on finding the elasticity and damping characteristics in all 14 degrees of freedom and designing and simulating the passive and active systems to improve the efficiency of the robotic system during the gait. A full parametric design of the torsional spring system has also been provided, along with simulation results verifying the efficiency and power saving abilities from using the designed passive system.

9.2 Conclusions

The reviewed designs of robotic exoskeletons vary by their chosen degrees of freedom and which degrees are activated by using an actuation system. Other issues such as kinematic inaccuracy between the robot and the human and the effect of that on inaccurate estimation of the designed active and passive system used in the robot design have been considered by researchers. Existing designs such as BLEEX and MIT have used clinical gait analysis of the human walking for determining their design specifications for their actuation system and frame design prior to building of the final device. The designers have also mentioned working on the assumption of the exoskeleton to have the same kinematics as the user inside. The same assumption has also been made in designing the passive systems (springs and dampers) in the existing exoskeleton systems. The used CGA data of the human joints are not good kinematics or kinetics indications for designing the passive system of the robot which has caused inefficiency in the system design and also inefficiency in metabolic consumption of the user inside as proved in previous works.

As current reviews identify, there is a lack of biomechanical and physiological consideration in the existing designs, researchers also point to the lack of information on assessing the performance of such robots by means of biomechanical and physiological measurements to identify if the device is metabolic and energy efficient in lowering the effort of the user for performing the desired tasks with help of the robot.

This conclusion aims to point out the necessity of working with experimental and simulation tools to accurately use the robots kinematics and kinetics in sizing and designing the active and passive actuation systems and establishing other system requirements, instead of just using human walking data as an estimate. Thus this research work aimed to extract the exact kinematic and kinetic behaviour of the robot itself by using experimental and simulation work.

During a clinical gait analysis, data of healthy human users were collected from five healthy participants at the University of Leeds, this is done for the purposes of adopting an efficient healthy human motions into the robot

kinematics to minimise any unwanted external and internal forces between the exoskeleton and the user. All the healthy human kinematics and kinetics have been verified by clinical gait analysis data from the literature, for purposes of model verifications. These kinetic results (joint mechanical power consumption) were used to find the most efficient power distribution throughout the joints of the human, the velocities from the participant with the most efficient mechanical power consumptions were then used as inputs into the exoskeleton dynamic model of walking.

Many prototypes which enhance the user's physical performances have been designed from the previous research but not many information has been available on what effect the selected designs have on the metabolic cost rate of their users. Also there is not any information on how the active and passive number of degrees of freedom for the exoskeleton have been selected. The gap in research field of exoskeletons as mentioned, is the need of research into the human robot physiological interactions, by taking human biomechanics into consideration at the design stage.

One of the major challenges with designing the assistive exoskeletons is the limitation on activating as many joint as possible, this issue is related to the high concentration of the mass at each mechanical joint due to the active and passive actuations systems, force transportation mechanisms, electrical hardware, and power supply system weights. The joint restriction method shown in Chapter 4 can be used as guidance for the design of the assistive exoskeletons to identify the most affective joints with the highest effect on the entire power consumption of the users.

The results from Chapter 4 found the power consumption of the following degrees of freedoms have raised the base line consumption; ankle inversion/eversion, hip abduction/adduction and hip rotation. The restriction on the upper body joints was found to help with stabilizing the user but does not have significant effect on elevating the metabolic power consumption of the human.

Human body can be looked at as a mechanical system, having bones as the frame and the joints as the degrees of freedom which transfers the forces to other limbs, in this system the muscles are the active actuators and ligaments

work as the springs and dampers in this mechanical system. The human level ground walking is majorly affecting the lower body than the upper body as it is a lower body activity.

A study done in this work found an efficient speed of walking which consumes less metabolic power. The speed that the exoskeleton is desired to be walking is considered to be 0.6 m/s which is within the walking speed for population with lower muscle abilities.

The main activity of the upper body during the human walking on a treadmill is the swing of the arm, shoulder and torso, the intensity of the swing is directly related to the speed that the human is walking at. There are two hypothesis on the upper body swing mechanism. The first hypothesis, indicates that the main limbs responsible for the force generation in the swing is the movements in the legs and pelvis, as the transferred force will result in movements in the shoulder and elbow joint. The second hypothesis, indicates that the main force caused this swing is generated at the shoulder joint.

The results from the study in this work supports the first hypothesis mentioned above and indicated that the arm swing does not have a great effect on the metabolic cost of the subject during walking at low speeds. The restriction on some of the upper body joints (shoulder flexion/extension, elbow flexion/extension) has shown to have a diverse effect on the efficiency of walking.

The results on the lower limbs indicate the significant effect of the non-sagittal plane joints, it is obvious the human walking is mainly a sagittal plane activity thus it is not possible to restrict any sagittal plane joints of the lower limb joints, but restricting the tested 3 lower limb joints in this study (ankle inversion/eversion, hip rotation and hip abduction/adduction) do still have a significant effect on lowering the metabolic cost efficiency during the human walking.

These results can lead to a whole new concept in design and use of exoskeleton devices by designing more activated joints for the lower limbs consisting of two degrees of freedom joint at the ankle, one DOF at the knee, and three DOF at the hip joint of each leg. A passive supportive structure for the upper body joints could be considered as it may not have a direct effect

on lowering the metabolic cost rate but it can reduce the vertical excursion of the centre of mass and other effects such as increasing the mechanical stability, and reduction in vertical ground reaction moments.

This work also concludes from comparing the kinematics, kinetics and energetics of walking trials using five healthy subjects and verifies the most efficient gait to be the subject with the lowest speed, lowest displacement to be having the lowest torques at the joints, lowest muscle activity and reaction forces, and also lowest mechanical power consumption. To verify these, the kinematics of the human (angular velocity at the joints) was used as the input of the exoskeleton dynamic simulation, all the averages from the five participants were inputted to their specific size adjusted exoskeleton and rerun the simulations. Thus the most efficient gait and input to the design of the exoskeleton was chosen to be the subject with the lowest power consumption and the lowest speed.

The laboratory measured initial positions of the exoskeleton's joints and frame of the first prototype was used for the purpose of gaining the most accurate results from the inverse kinematic and inverse dynamic simulations of both robots.

During these simulations the skeleton carries the weight of the initially estimated hardware (gear, electrical actuators, ball bearings, encoders, brackets and housing) along with the weight of the frame and the human user inside.

The purpose of developing a computer model was to successfully build a size adaptable exoskeleton model which can perform inverse dynamic simulation from any inputted angular or linear kinematic motions, while using the exoskeleton's own geometry and mass and inertia characteristics to produce parametric designs of active actuation system and other design requirements.

The power consumption of the robot joints were compared with the healthy human joints power consumptions for the purposes of a better insight to the frame design as well as verifying the robot simulation to be following similar patterns as the healthy human, with some differences due to the differences in mass and inertia properties between the exoskeleton and the healthy human. This was aimed to support the statements raised by the assistive

exoskeleton designers to avoid using the human kinetics to design the actuation, frame and control systems. The work also concludes the importance of the non-sagittal joints (specifically in the hip joint) to be actively actuated and that the designers need to consider non-sagittal joints into their design, in order to lower the metabolic effort of the users.

The passive system designs at the ankle stance phase has the highest contribution for increasing the mechanical efficiency of the active system with around 4.5% of total power system reduction, this is due to high elastic behaviour in the ankle stance phase and matching linear spring characteristics. The second most energy saved power system is the hip abduction/adduction during the stance and the swing phase which is found to save up to 1% of the total power consumption of the entire system. The passive system was found to save up to 5.6% of the total instantaneous power consumption of the entire system.

The passive system increases the efficiency of the system in more than just decreasing the instantaneous power expenditure, this is done by lowering the peak torques and powers that the motors need to provide, which results in smaller and lighter actuation systems and exoskeleton. In all the selected passive joints the peak power outputs have been decrease by more than 50%.

9.3 Future work

For the future of this work, it is recommended to build a new and improved prototype frame with new actuation systems (motors and springs) along with design of the clutch system for 3 selected passive joints.

The controller for this assistive exoskeleton is being developed in the robotics group at the university of Leeds, the future project is recommended to use the controller with the new specification found in this work and take real measurements such as muscle activation, metabolic consumption, torque and displacement experimentally to verify the performance of the robot and its effects on the user.

The work on the elasticity of the joints can also be optimised for nonlinear spring mechanisms and be compared with the torsional springs suggested for purposes of increasing the efficiency of the robot system.

A more detailed research on the positioning of the non-sagittal joints anthropomorphically is also recommended for a smoother and more efficient operation of the robot, in order to follow the human kinematics closer.

List of References

- ALEXANDER, R. M. & BENNETCLARK, H. C. 1977. Storage of Elastic Strain-Energy in Muscle and Other Tissues. *Nature*, 265, 114-117.
- BANALA, S. K., AGRAWAL, S. K. & SCHOLZ, J. P. 2007. Active Leg Exoskeleton (ALEX) for gait rehabilitation of motor-impaired patients. *2007 IEEE 10th International Conference on Rehabilitation Robotics, Vols 1 and 2*, 401-+.
- BASTIEN, G. J., WILLEMS, P. A., SCHEPENS, B. & HEGGLUND, N. C. 2005. Effect of load and speed on the energetic cost of human walking. *European Journal of Applied Physiology*, 94, 76-83.
- BEYL, P., VAN DAMME, M., VAN HAM, R. & LEFEBER, D. 2008. Design and control concepts of an exoskeleton for gait rehabilitation. *2008 2nd IEEE Ras & Embs International Conference on Biomedical Robotics and Biomechatronics (Biorob 2008), Vols 1 and 2*, 103-108.
- BIGLANDRITCHIE, B. & WOODS, J. J. 1976. Integrated Electromyogram and Oxygen-Uptake during Positive and Negative Work. *Journal of Physiology-London*, 260, 267-277.
- BIOMECHANICS, C. M. 2016. *Standard Anatomical Conventions* [Online].
- BIONICS, A. 2017. *EKSO exoskeleton* [Online].
- BOHANNON, R. W. 1997. Comfortable and maximum walking speed of adults aged 20-79 years: Reference values and determinants. *Age and Ageing*, 26, 15-19.
- BOILLEE, S., VANDE VELDE, C. & CLEVELAND, D. W. 2006. ALS: a disease of motor neurons and their nonneuronal neighbors. *Neuron*, 52, 39-59.
- BRAMBLE, D. M. & LIEBERMAN, D. E. 2004. Endurance running and the evolution of Homo. *Nature*, 432, 345-52.
- CAVAGNA, G. A. & MARGARIA, R. 1966. Mechanics of Walking. *Journal of Applied Physiology*, 21, 271-&.
- CAVAGNA, G. A., MARGARIA, R. & SAIBENE, F. P. 1963. External Work in Walking. *Journal of Applied Physics*, 18, 1-+.
- CENCIARINI, M. & DOLLAR, A. M. 2011. Biomechanical considerations in the design of lower limb exoskeletons. *IEEE Int Conf Rehabil Robot*, 2011, 5975366.

- CHIALIN YEOH , E. T., LIAM TURNER , PAL-EMIL ROMANO , THOMAS HALL. 2015. *Design of an assistive exoskeleton*. Master's of engineering, University of Leeds.
- CHU, A. 2005. *Design of the Berkeley Lower Extremity Exoskeleton (BLEEX)*. Doctor of Philosophy, UNIVERSITY OF CALIFORNIA, BERKELEY.
- COLLINS, S. H., WIGGIN, M. B. & SAWICKI, G. S. 2015. Reducing the energy cost of human walking using an unpowered exoskeleton. *Nature*, 522, 212-+.
- COLOMBO, G., JOERG, M., SCHREIER, R. & DIETZ, V. 2000. Treadmill training of paraplegic patients using a robotic orthosis. *Journal of Rehabilitation Research and Development*, 37, 693-700.
- CORREA, T. A., CROSSLEY, K. M., KIM, H. J. & PANDY, M. G. 2010. Contributions of individual muscles to hip joint contact force in normal walking. *J Biomech*, 43, 1618-22.
- CYBERDYNE. *WHAT'S HAL* [Online]. Available: <https://www.cyberdyne.jp/english/products/HAL/>.
- CYBERDYNE, I. 2017. *CYBERDYNE* [Online].
- DE LEVA, P. 1996. Adjustments to Zatsiorsky-Seluyanov's segment inertia parameters. *J Biomech*, 29, 1223-30.
- DOKE, J., DONELAN, J. M. & KUO, A. D. 2005. Mechanics and energetics of swinging the human leg. *Journal of Experimental Biology*, 208, 439-445.
- DOKE, J., DONELAN, J. M. & KUO, A. D. 2007. Mechanics and energetics of swinging the human leg (vol 208, pg 439, 2005). *Journal of Experimental Biology*, 210, 2399-2399.
- DOLLAR, A. M. & HERR, H. 2008. Lower extremity exoskeletons and active orthoses: Challenges and state-of-the-art. *Ieee Transactions on Robotics*, 24, 144-158.
- DONELAN, J. M., KRAM, R. & KUO, A. D. 2002. Mechanical work for step-to-step transitions is a major determinant of the metabolic cost of human walking. *Journal of Experimental Biology*, 205, 3717-3727.
- ELFTMAN, H. 1939. Forces and energy changes in the leg during walking. *American Journal of Physiology*, 125, 339-356.

- ESQUENAZI, A., TALATY, M., PACKEL, A. & SAULINO, M. 2012. The ReWalk Powered Exoskeleton to Restore Ambulatory Function to Individuals with Thoracic-Level Motor-Complete Spinal Cord Injury. *American Journal of Physical Medicine & Rehabilitation*, 91, 911-921.
- FARRIS, D. J., ROBERTSON, B. D. & SAWICKI, G. S. 2013. Elastic ankle exoskeletons reduce soleus muscle force but not work in human hopping. *J Appl Physiol (1985)*, 115, 579-85.
- FARRIS, R. J., QUINTERO, H. A. & GOLDFARB, M. 2012. Performance Evaluation of a Lower Limb Exoskeleton for Stair Ascent and Descent with Paraplegia. *2012 Annual International Conference of the IEEE Engineering in Medicine and Biology Society (Embc)*, 1908-1911.
- FERRIS, D. P., SAWICKI, G. S. & DALEY, M. A. 2007. A physiologist's perspective on robotic exoskeletons for human locomotion. *International Journal of Humanoid Robotics*, 4, 507-528.
- GAMS, A., PETRIC, T., DEBEVEC, T. & BABIC, J. 2013. Effects of Robotic Knee Exoskeleton on Human Energy Expenditure. *Ieee Transactions on Biomedical Engineering*, 60, 1636-1644.
- GERARD J. TORTORA, B. H. D. 2006. *Principles of Anatomy and Physiology*.
- GOTTSCHALL, J. S. & KRAM, R. 2003. Energy cost and muscular activity required for propulsion during walking. *Journal of Applied Physiology*, 94, 1766-1772.
- GRABOWSKI, A., FARLEY, C. T. & KRAM, R. 2005. Independent metabolic costs of supporting body weight and accelerating body mass during walking. *Journal of Applied Physiology*, 98, 579-583.
- GRIFFIN, T. M., ROBERTS, T. J. & KRAM, R. 2003. Metabolic cost of generating muscular force in human walking: insights from load-carrying and speed experiments. *Journal of Applied Physiology*, 95, 172-183.
- GUIZZO, E. & GOLDSTEIN, H. 2005. The rise of the body bots. *Ieee Spectrum*, 42, 50-56.
- HAXTON, H. A. 1944. Absolute muscle force in the ankle flexors of man. *Journal of Physiology-London*, 103, 267-273.
- HOPKER, J. G., JOBSON, S. A., GREGSON, H. C., COLEMAN, D. & PASSFIELD, L. 2012. Reliability of Cycling Gross Efficiency Using the

- Douglas Bag Method. *Medicine and Science in Sports and Exercise*, 44, 290-296.
- ISHIKAWA, M., KOMI, P. V., GREY, M. J., LEPOLA, V. & BRUGGEMANN, G. P. 2005. Muscle-tendon interaction and elastic energy usage in human walking. *Journal of Applied Physiology*, 99, 603-608.
- KAWAMOTO, H., KANBE, S. & SANKAI, Y. 2003. Power assist method for HAL-3 estimating operator's intention based on motion information. *Ro-Man 2003: 12th IEEE International Workshop on Robot and Human Interactive Communication, Proceedings*, 67-72.
- KAZEROONI, H. 2006. The Berkeley Lower Extremity Exoskeleton project - That which does not stabilize will only make us stronger. *Experimental Robotics IX*, 21, 291-301.
- KAZEROONI, H., RACINE, J. L., HUANG, L. H. & STEGER, R. 2005. On the control of the Berkeley Lower Extremity Exoskeleton (BLEEX). *2005 IEEE International Conference on Robotics and Automation (ICRA), Vols 1-4*, 4353-4360.
- KAZEROONI, H. & STEGER, R. 2006. The Berkeley Lower Extremity Exoskeleton. *Journal of Dynamic Systems Measurement and Control-Transactions of the Asme*, 128, 14-25.
- KIM, W., LEE, S., KANG, M., HAN, J. & HAN, C. 2010. Energy-efficient Gait Pattern Generation of the Powered Robotic Exoskeleton using DME. *IEEE/Rsj 2010 International Conference on Intelligent Robots and Systems (Iros 2010)*, 2475-2480.
- www.kinavo.com/en/index.as
- LEE, S. & SANKAI, Y. 2005. Virtual impedance adjustment in unconstrained motion for an exoskeletal robot assisting the lower limb. *Advanced Robotics*, 19, 773-795.
- LENZI, T., ZANOTTO, D., STEGALL, P., CARROZZA, M. C. & AGRAWAL, S. K. 2012. Reducing Muscle Effort in Walking through Powered Exoskeletons. *2012 Annual International Conference of the IEEE Engineering in Medicine and Biology Society (Embc)*, 3926-3929.
- LI, Y., WANG, W. J., CROMPTON, R. H. & GUNTHER, M. M. 2001. Free vertical moments and transverse forces in human walking and their role in relation to arm-swing. *Journal of Experimental Biology*, 204, 47-58.

- LOW, K. H., LIU, X. P. & YU, H. Y. 2005. Development of NTU wearable exoskeleton system for assistive technologies. *2005 IEEE International Conference on Mechatronics and Automations, Vols 1-4, Conference Proceedings*, 1099-1106.
- LU, T. W. & O'CONNOR, J. J. 1999. Bone position estimation from skin marker co-ordinates using global optimisation with joint constraints. *J Biomech*, 32, 129-34.
- MARGARETA NORDIN , V. H. F. 2001. *Basic Biomechanics of the Musculoskeletal System*.
- MOCHON, S. & MCMAHON, T. A. 1980. Ballistic Walking - an Improved Model. *Mathematical Biosciences*, 52, 241-260.
- MOESLUND, T. B., MADSEN, C. B. & GRANUM, E. 2005. Modelling the 3D pose of a human arm and the shoulder complex utilising only two parameters. *Integrated Computer-Aided Engineering*, 12, 159-175.
- NEPTUNE, R. R., ZAJAC, F. E. & KAUTZ, S. A. 2004. Muscle mechanical work requirements during normal walking: the energetic cost of raising the body's center-of-mass is significant. *Journal of Biomechanics*, 37, 817-825.
- ONEN, U., BOTSALI, F. M., KALYONCU, M., TINKIR, M., YILMAZ, N. & SAHIN, Y. 2014. Design and Actuator Selection of a Lower Extremity Exoskeleton. *IEEE-Asme Transactions on Mechatronics*, 19, 623-632.
- ORTEGA, J. D., FEHLMAN, L. A. & FARLEY, C. T. 2008. Effects of aging and arm swing on the metabolic cost of stability in human walking. *Journal of Biomechanics*, 41, 3303-3308.
- PANDOLF, K. B., HAISMAN, M. F. & GOLDMAN, R. F. 1976. Metabolic Energy-Expenditure and Terrain Coefficients for Walking on Snow. *Ergonomics*, 19, 683-690.
- PANDY, M. G. & ANDRIACCHI, T. P. 2010. Muscle and joint function in human locomotion. *Annu Rev Biomed Eng*, 12, 401-33.
- PERKINS, K. A., EPSTEIN, L. H., MARKS, B. L., STILLER, R. L. & JACOB, R. G. 1989. The effect of nicotine on energy expenditure during light physical activity. *N Engl J Med*, 320, 898-903.
- PERRY J , B. J. M. 2010. *Gait Analysis , Normal and Pathological Function*.

- PONTZER, H., HOLLOWAY, J. H., RAICHLIN, D. A. & LIEBERMAN, D. E. 2009. Control and function of arm swing in human walking and running (vol 212, pg 523, 2009). *Journal of Experimental Biology*, 212, 894-894.
- RAADE, J. W., AMUNDSON, K. R. & KAZEROONI, H. 2005. Development of hydraulic-electric power units for mobile robots. *Proceedings of the Asme Fluid Power Systems and Technology Division - 2005*, 12, 27-34.
- RALL, J. A. 1985. Energetic aspects of skeletal muscle contraction: implications of fiber types. *Exerc Sport Sci Rev*, 13, 33-74.
- ROBERTSON, D. G. E. & WINTER, D. A. 1980. Mechanical Energy Generation, Absorption and Transfer Amongst Segments during Walking. *Journal of Biomechanics*, 13, 845-854.
- SANDRA J. SHULTZ , P. A. H., DAVID H. PERRIN 2005. *Examination of muscles injuries*
- SAWICKI, G. S. & FERRIS, D. P. 2009. Powered ankle exoskeletons reveal the metabolic cost of plantar flexor mechanical work during walking with longer steps at constant step frequency. *J Exp Biol*, 212, 21-31.
- SHAMAEI, K., SAWICKI, G. S. & DOLLAR, A. M. 2013. Estimation of Quasi-Stiffness and Propulsive Work of the Human Ankle in the Stance Phase of Walking. *Plos One*, 8.
- SOULE, R. G. & GOLDMAN, R. F. 1969. Energy Cost of Loads Carried on Head, Hands, or Feet. *Journal of Applied Physiology*, 27, 687-&.
- SPOOR, C. W. & VELDPAUS, F. E. 1980. Rigid Body Motion Calculated from Spatial Coordinates of Markers. *Journal of Biomechanics*, 13, 391-393.
- SWIFT, J. K. L. A. M. 2008. *The Clinical Orthopedic Assessment Guide*, 2nd edition
- THURSTON, A. P. 1919. *Metal Construction of Aircraft*.
- UMBERGER, B. R. 2008. Effects of suppressing arm swing on kinematics, kinetics, and energetics of human walking. *Journal of Biomechanics*, 41, 2575-2580.
- VAN DEN BOGERT, A. J. & SU, A. 2008. A weighted least squares method for inverse dynamic analysis. *Computer Methods in Biomechanics and Biomedical Engineering*, 11, 3-9.

- VAN DIJK, W., VAN DER KOOIJ, H., VAN DER KOOIJ, H. & HEKMAN, E. 2011. A Passive Exoskeleton with Artificial Tendons Design and experimental evaluation. *2011 IEEE International Conference on Rehabilitation Robotics (Icrr)*.
- VAN HEDEL, H. J. & GROUPE, E. S. 2009. Gait speed in relation to categories of functional ambulation after spinal cord injury. *Neurorehabil Neural Repair*, 23, 343-50.
- VENEMAN, J. F., KRUIDHOF, R., HEKMAN, E. E. G., EKKELENKAMP, R., VAN ASSELDONK, E. H. F. & VAN DER KOOIJ, H. 2007. Design and evaluation of the LOPES exoskeleton robot for interactive gait rehabilitation. *IEEE Transactions on Neural Systems and Rehabilitation Engineering*, 15, 379-386.
- WALKING, R. M. T. 2013.
- WALLING, A. D. 1999. Amyotrophic lateral sclerosis: Lou Gehrig's disease. *Am Fam Physician*, 59, 1489-96.
- WALSH, C. J., ENDO, K. & HERR, H. 2007. A quasi-passive leg exoskeleton for load-carrying augmentation. *International Journal of Humanoid Robotics*, 4, 487-506.
- WALSH, C. J., PALUSKA, D., PASCH, K., GRAND, W., VALIENTE, A. & HERR, H. 2006a. Development of a lightweight, underactuated exoskeleton for load-carrying augmentation. *2006 IEEE International Conference on Robotics and Automation (Icra), Vols 1-10*, 3485-3491.
- WALSH, C. J., PALUSKA, D., PASCH, K., GRAND, W., VALIENTE, A. & HERR, H. 2006b. Development of a lightweight, underactuated exoskeleton for load-carrying augmentation. *2006 IEEE International Conference on Robotics and Automation (Icra), Vols 1-10*, 3485-+.
- WALSH, C. J., PASCH, K. & HERR, H. 2006c. An autonomous, underactuated exoskeleton for load-carrying augmentation. *2006 IEEE/Rsj International Conference on Intelligent Robots and Systems, Vols 1-12*, 1410-1415.
- WANG, S., VAN DIJK, W. & VAN DER KOOIJ, H. 2011. Spring uses in exoskeleton actuation design. *IEEE Int Conf Rehabil Robot*, 2011, 5975471.

- WATERS, R. L. & MULROY, S. 1999. The energy expenditure of normal and pathologic gait. *Gait & Posture*, 9, 207-231.
- WINTER, D. A. 2009. *Bio mechanics of human walking*
- YAN, T. F., CEMPINI, M., ODDO, C. M. & VITIELLO, N. 2015. Review of assistive strategies in powered lower-limb orthoses and exoskeletons. *Robotics and Autonomous Systems*, 64, 120-136.
- YEO WEI HONG, Y.-J. K., WEI-HONG YEO, CHEN-HUNT TING, YEA-DAT CHUAH, JER-VUI LEE AND & CHOK, E.-T. 2013. Lower Extremity Exoskeleton: Review and Challenges Surrounding the Technology and its Role in Rehabilitation of Lower Limbs *Australian Journal of Basic and Applied Sciences*, 7(7): 520-524, 2013
- ISSN 1991-8178
- ZOSS, A. B., KAZEROONI, H. & CHU, A. 2006. Biomechanical design of the Berkeley lower extremity exoskeleton (BLEEX). *Ieee-Asme Transactions on Mechatronics*, 11, 128-138.

APPENDICES

A. Visula3D Solver and methodology

B. ADAMS solver and methodology

C. Active actuation system design and specification

Appendix A

A.1 Visual 3D solver

To obtain a measurement of sectional segments a local coordinates system (LCS) was defined in the laboratory of Leeds University as a reference point for collection of the body position and full motion. In visual 3D to obtain the coordinate and configuration of the point \bar{A} , representing the coordinate vector for the location of the segment coordinate system (SCS), to the reference or local coordinate system (LCS) point \bar{P} is defined the coordinate by multiplying the rotation matrix T by the measured segment coordinate vector, the configuration of the point is defined by the translation vector \bar{O} between the SCS and LCS, as shown in equation A-A-1.

$$\bar{P} = T\bar{A} + \bar{O}$$

A-1

The least square method was used to compute the position and orientation of the point on SCS in the reference to the set laboratory reference LCS. The location of the point \bar{A} is measured and the location of the \bar{P} is set and measured, as the body goes through the motion the solver determines orientation matrix and the translational vector by minimizing the sum square error of the expression A-1, where m is the number of measured markers on the segment which has to be more than two to be able to define a segment this solution is adopted from (Spoor and Veldpaus, 1980).

$$\sum_{i=1}^m ((\bar{P}_i - T\bar{A}_i) - \bar{O})^2$$

A-2

With constraint of

$$T^t T = I$$

A-3

The research from the (Lu and O'Connor, 1999) shows some inaccuracy during this measurements can be due to movement of the measured targets due to soft tissue artefacts can be minimised by using global optimization technique or inverse kinematic. The visual 3D solver is based on the technique presented by (Lu and O'Connor, 1999). The global optimisation method uses the orientation matrix and the translation vectors as the function of the set coordinates, thus equation A-A-2 reformulates to A-A-4.

$$\bar{P} = T_{(q)} \bar{A} + \bar{O}_{(q)}$$

A-4

The work on the least square optimization to find the functions of the new orientation matrix and translation vector is mentioned by (van den Bogert and Su, 2008) optimises for the new orientation and configuration of the body according to the set coordinates as shown in equation A-A-5.

$$\sum_{i=1}^{mt} ((\bar{P}_i - T_{(q)} \bar{A}_i) - \bar{O}_{(q)})$$

A-5

A.1.1 Inverse dynamics used in visual 3D

Inverse dynamics calculation is used to investigate the kinetical behaviour between the segments of the joints. The forces during the CGA are typically consist of external forces (i.e. Ground reaction forces or forces acting from adjacent links), and the moments created at the segments from muscle and ligament from performing work. Visual 3D uses the following techniques to estimates a local coordinate system along with algorithm with equations of motions to quantify the moments and forces exerting at the segments.

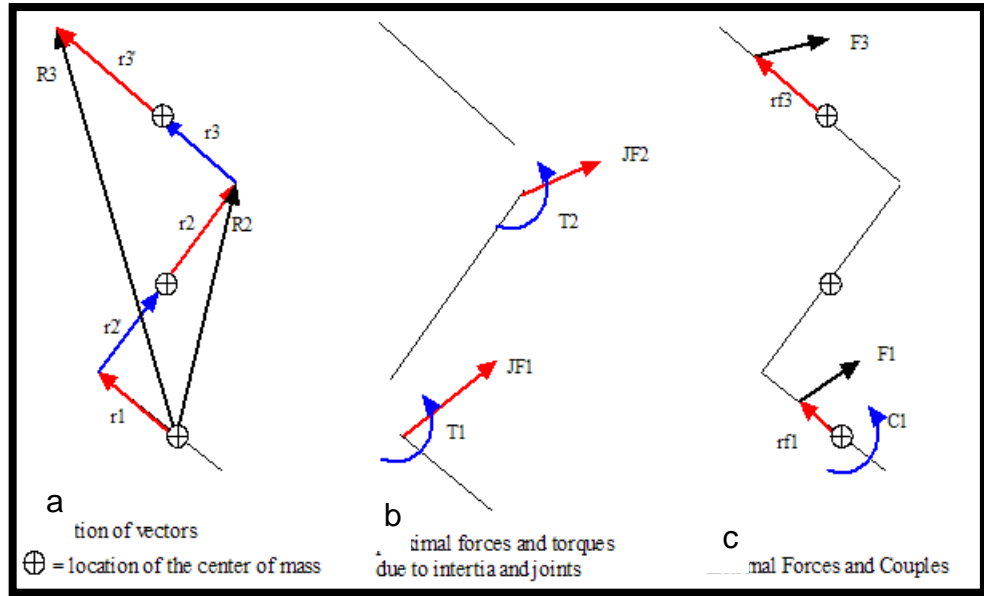


Figure A-1 local coordinate system (biomechanics, 2016).

- a) Defines location of centre of mass**
- b) proximal forces and torques due to inertia and joints**
- c) External forces and couples**

To calculate the kinematics of the CGA motions such as joint angles, joint velocities, and joint accelerations. Visual 3D counts in the rate of kinematic change between the reference coordinate system and the resolution coordinate system between the distal and proximal segments.

A.1.2 König theorem kinetics.

The König theorem is a mathematical method used to calculate the kinetic energy within the body and system of particles. The calculated kinetic energy is using the velocities of particle in compared to centre of mass of the whole body

The total energy of the body is calculated by summation of the potential energy and kinetic energy of each body segment relative to the surroundings, as shown by equation A-A-6.

$$E_{tot,wb} = \sum_{i=1}^n (m_i g h_i + \frac{1}{2} m_i V_i^2 + \frac{1}{2} m_i K_i^2 \omega_i^2)$$

For the i_{th} segment of centre of mass relative to the surroundings, the height is defined as the h_i and the linear velocity is defined as v_i . The angular velocity and the radius of gyration are shown by ω_i and K_i around its centre of mass of the particular segment. The term g is the acceleration due to the gravity.

The summation of all the segment potential energy compared to the surrounding's present the total potential energy of the system as shown in equation A-A-7.

$$MHg = \sum_{i=1}^n m_i h_i g$$

A-7

The linear velocity of each segment of the body relative to the surrounding is the velocity of centre of the mass of the whole body in compare to the surroundings added by the linear velocity of the i_{th} segment in relation to the centre of the mass of the whole body, equation A-A-8 represents this relationship.

$$V_i = V_{cg} + V_{r,i}$$

A-8

Where V_{cg} the velocity of the centre of mass of the whole is body relative to the surroundings, and $V_{r,i}$ is the linear velocity of the i_{th} segment to the whole body.

The solver's assumes the equal and opposite vertical displacement of the body segments cancel which results in sum of the linear moments of the segments relative to the centre of mass of the whole body to be zero. The kinetic energy calculated can be expressed in the König theorem shown in equation A-A-9.

$$\frac{1}{2} \sum_{i=1}^n m_i V_i^2 = \frac{1}{2} M V_{cg}^2 + \frac{1}{2} \sum_{i=1}^n m_i V_{r,i}^2$$

A-9

The total energy of the system is calculated by combining equations A-7 and A-6, as expressed in equation A-A-10.

$$E_{total\ wb} = Mgh + \frac{1}{2}MV_{cg}^2 + \sum_{i=1}^n \left(\frac{1}{2}m_iV_{r,i}^2 + \frac{1}{2}m_iK_i^2\omega_i^2 \right)$$

A-10

The first two terms $Mgh + \frac{1}{2}MV_{cg}^2$ computes the external energy captured by the force platforms used in the motion capture experiment. The internal energy of the segments is summed and computed from the second part of section $\sum_{i=1}^n \left(\frac{1}{2}m_iV_{r,i}^2 + \frac{1}{2}m_iK_i^2\omega_i^2 \right)$ in equation A-A-10.

A.1.3 Measurement of external work

The external work is a resultant of the external force acting on the centre of the mass of the whole body by the amount of displacement of the centre of the mass of the whole body done compared to the global coordinate system as shown in equation A-A-11.

$$W_{external} = F D \cos\phi = F_f D_f + F_v D_v + F_l D_l$$

A-11

The resultant force and displacement vector for the centre of the mass of the whole body acts in frontal, vertical, and lateral direction. according to (Cavagna et al., 1963) the work in the lateral direction is small enough to be neglected and only consider the work in the frontal and vertical plane. The work in the frontal plane is calculated by displacement of the mass in the frontal plane and the rate of change in the velocity in the frontal direction (acceleration in the frontal direction). The vertical work is summation of the gravitational and vertical acceleration of the centre of the mass of the whole body by the mass of the whole body and displacement in the vertical direction as shown in equation A-A-12.

$$W_{external} = M a_f D_f + M(g + a_v) D_v$$

A-12

A.1.4 Computation of internal work

During the static trial measurements a local coordinate was allocated to each segment by taking the proximal segment as the reference segment. The local coordinate segment is a Cartesian coordinate system.

The segment local coordinate system uses equation of motion shown in A-A-13 to find the proximal segment's joint moment at the local coordinate system of segment;

$$C'_i = I_i \alpha'_i + \omega'_i \times (I_i \omega'_i)$$

A-13

Where:

C'_i = the moment computed at the proximal end of the local segment.

I_i = the moment of inertia of the segment i

α'_i = the angular acceleration of the segment i

ω'_i = the angular velocity of the segment i

The proximal joint force consist of summation of the force created by the motion of the segment using newton's second law of motion , added to any applied external forces to the segment, the following equation of motion A-A-14 was used.

$$F_{proximal} = \sum_{i=1}^n m_i (a_i + g) + \sum_{j=1}^q F_q$$

A-14

Where:

$F_{proximal}$ =proximal joint force

a_i = acceleration of the segment i

n = number of distal segments connected in chain

q =number of external forces

F_q = applied external forces

The calculated internal moment from visual 3D represent a summation of the inertial forces and exerted moments, any other external forces acting at the local segment, combination of equation A-A-13 and equation A-A-14 for the total moment resultant from all the forces at the local segment is derived from the following equation A-A-15:

$$M_{proximal} = \sum_{i=1}^n (C_i + R_i \times A_i) + \sum_{j=1}^q (P_j \times F_q) + \sum_{k=1}^p \tau_k$$

A-15

Where:

p =number of external moments

P_j = vector from the external force to the proximal joint

R_i =distance between the local centre of gravity of the segment and the proximal joint

$A_i = m_i(a_i + g)$

A.1.5 Solving nonlinear equations. (The Newton Raphson Method)

The newton Raphson method used by solid work's simulation solver adopted from MCS ADAMS solver in order to find the root \dot{x} of a non linear equation taking the count of one dimension as shown in equation A-A-16.

A-16

$$f(x) = 0$$

Equation A-15 takes the assumption of the function $f: \mathbb{R} \rightarrow \mathbb{R}$ is differentiable.

To calculate the new configuration $x^{(1)}$ of the root, the Newton Raphson's method uses an initial input with approximate of the root $x^{(0)}$ by taking a derivative of the function with respect with the variables as shown in equation A-A-17.

A-17

$$x^1 = x^0 - \frac{f(x^{(0)})}{f'(x^{(0)})}$$

The solver updates the value of x by linearizing function f at the point $x^{(0)}$ as shown in equation which defines equation A-18.

$$f(x) \approx f(x^{(0)}) + f'(x^{(0)})(x - x^0) \Rightarrow x^{(1)} = x^{(0)} - \frac{f(x^{(0)})}{f'(x^{(0)})}$$

A.1.5.1 Newton like method

The down side with the newton Raphson's method is the new update of the position will require a new computation process for finding the derivative of both function and the derivative of the function which can be expensive for the solver. The newton like method does not update the derivative of the root in every step and after several iteration updating the new derivative root value (which is also referred to as Jacobian).

The solver uses a n dimensional vector $q \in \mathbb{R}^n$ as the root x , as shown in equation A-A-19.

A-19

$$f(q) = \begin{bmatrix} f_1(q) \\ f_2(q) \\ \dots \\ f_{n-1}(q) \\ f_n(q) \end{bmatrix} = 0$$

The solver uses a linear configuration shown in equation A-19 for finding the new position $q^{(1)}$.

A-19

$$q^{(1)} = q^{(0)} - [F(q^{(0)})]^{-1} f(q^{(0)})$$

The Jacobian $F(q^{(0)})$ value used in equation A-A-19 to find the new position value in root linearization to find the new coordinates by taking partial derivative of the following functions as shown in equation A-20.

A-20

$$F(q^{(0)}) = \left[\frac{\partial f_i}{\partial q_j} \right]_{q=q_0}$$

Appendix B

B.1 Generalised coordinates used in ADAMS

In order for the motion solver to be able to define the configuration of each part of the system at the selected time instance, a generalised coordinate system has to be defined, the solver uses Cartesian coordinates to define the position of the rigid body p , as shown in equation B-1.

B-1

$$p = \begin{bmatrix} x \\ y \\ z \end{bmatrix}$$

To define the orientation of the rigid body the solver uses the Euler's angles shown in matrix ε in 3-1-3 sequence rotation, as shown in equation B-2.

$$\varepsilon = \begin{bmatrix} \psi \\ \phi \\ \theta \end{bmatrix}$$

To calculate the body's longitudinal velocity u the derivative of the position is performed by following equation B-B-2.

B-2

$$u = \dot{p}$$

To find the angular velocity ϖ a derivative of the Euler's angles multiplied by the translation matrix B is done as shown in equation B-3.

$$\varpi = B\dot{\varepsilon}$$

Where the translation matrix B is:

B-3

$$B = \begin{bmatrix} \sin\phi\sin\theta & 0 & \cos\phi \\ \cos\phi\sin\theta & 0 & -\sin\phi \\ \cos\theta & 1 & 0 \end{bmatrix}$$

To define the acceleration \dot{A} of the body the time derivative of the angular velocity and the orientation matrix A is shown in equation B-4.

B-4

$$\dot{A} = A\omega$$

Where the orientation matrix of the body is defined by the 3-1-3 Euler's rotation sequence of the angles as shown in the matrix in equation B-4.

$$A = \begin{bmatrix} \cos\psi\cos\phi - \sin\psi\cos\theta\sin\phi & -\cos\psi\sin\phi - \sin\psi\cos\theta\cos\phi & \sin\psi\sin\theta \\ \sin\psi\cos\phi + \cos\psi\sin\phi & -\sin\psi\sin\phi + \cos\psi\cos\theta\cos\phi & -\cos\psi\sin\theta \\ \sin\theta\sin\phi & \sin\theta\cos\phi & \cos\theta \end{bmatrix}$$

The matrix A is used to determine the derivative of the rotating bodies in 3D space.

B.2 Joints in ADAMS

For the solver to define the vector for the entire mechanical system with n amount of bodies in any given time and the position, equation B-5 is used.

B-5

$$q = [q_1^T \ q_2^T \ \dots \ q_{nb}^T]^T = [q_1 \ q_2 \ \dots \ q_n]^T$$

In this model the coordinates will have constraint acting in between them which allocates how much freedom of the movement is between the coordinates, these constraints are recognised as joints. The constraints algebraic assumption is shown in equation B-6.

$$\phi(q) = 0$$

The sum of all the constraints from all the joints in the entire model is shown in equation B-6.

B-6

$$\phi(q) = [\phi_1^T(q)\phi_2^T(q) \dots \phi_{n_j}^T(q)]^T = [\phi_1(q)\phi_2(q) \dots \phi_m(q)]^T$$

Where n_j is the number of joints in the entire system and m is the total number of constraints caused by the joints in the entire system, the value of the total number of general coordinates at the joints should be greater than the number of constrained acting by those joints for the system to be fully defined and solvable.

The velocity kinematic constraint is a resultant of the first derivative of the position constraint as shown in equation B-7.

B-7

$$\phi_q(\dot{q}) = 0$$

The acceleration kinematic constraint is the result of second derivative of equation B-7, and is shown below in equation B-8.

B-8

$$\phi_q \ddot{q} = -(\phi_q \dot{q})_q \dot{q} \equiv \tau$$

Once the kinematic constraint position, velocity and acceleration are satisfied it can verify the model and the joints are working accordingly and obeying during the time.

B.2.1 Motions in ADMAS

The motion is defined by the generalised coordinate of the system depending on time, also a first derivative and second derivative of the coordinate system will solve for the velocity and acceleration of the segment respectively to time, as shown in equation B-9 respectively shows the motion equations used to solve for position, velocity, and acceleration of the coordinates.

B-9

$$\begin{aligned}\phi(q, t) &= 0 \\ \phi_q(q, t) \cdot \dot{q} &= -\phi_t(q, t) \\ \phi_q(q, t) \cdot \ddot{q} &= -(\phi_q \dot{q})_q \dot{q} - 2\phi_{qt} \dot{q} - \phi_{tt}(q, t)\end{aligned}$$

B.2.2 Initial condition analysis

The IC (initial condition) analysis is aiming to compute a consistent configuration of the mechanical system at the initial stage of the simulation, by taking the count of the constraints and configuration of the position of all segments at time zero.

B.2.2.1 IC analysis position

The solver is using optimization method in finding the best fit from the inputted positions by minimizing the cost function as well as satisfying the constraints at the joints

The optimization method presented for $q \in R^n$, minimize;

B-10

$$f(q) = \frac{1}{2}(q - q^0)^T W(q - q^0)$$

The optimization of the function of the coordinate in equation B-11 is subject to the constraint acting on the joint shown in equation B-11.

B-11

$$\phi(q, t) = 0$$

Where W is the diagonal matrix of the weights.

The optimization method then linearized from the nonlinear constraints in the vicinity of q^0 , as shown in the new form by B-12 is:

B-12

$$\phi(q, t) = \phi(q^0, t_0) + \phi_q(q^0, t_0)(q - q^0)$$

The solver's chosen optimization method uses Lagrange method in finding the normal of the intersected coordinates were constraint level curves have the minima value to the level curve (coordinates) of the function, the order of the linearization to find the appropriate coordinate is shown below.

The optimization assumes $d \equiv q - q^0$, as the function to minimise in equation 14 changes to its new form in equation B-13.

$$f(d) = \frac{1}{2} d^T W d$$

As mentioned above the optimization is done by taking all the constraints at the joints of the, as shown in equation B-13.

B-13

$$\phi(q^0, t) + \phi_0(q^0, t_0)d = 0$$

The Lagrange method to solve this convex optimization problem in two condition takes partial time dependent derivative of the $d = q - q^0$ value and another partial derivitaive of the Lagrange number. Equation is shown below:

B-14

$$F(d, \lambda) = F(d) + \lambda^T (\phi(q^0) + \phi_q(q^0)d)$$

The linearization form after taking the partial derivative of d and λ values of equation B-14, is shown in equation B-15.

B-15

$$\begin{bmatrix} W & \phi_0^T(q^0) \\ \phi_0 & 0 \end{bmatrix} \begin{bmatrix} d \\ \lambda \end{bmatrix} = \begin{bmatrix} 0 \\ -\phi(q^0) \end{bmatrix}$$

The new configuration is determined from the given q^0 value and the computed d value from, by adding the values together as shown in equation B-16.

B-16

$$q = q^0 + d$$

The new coordinate configuration calculated has to satisfy the initial imposed constraint defined from equation above if this does not correspond the solver assumes the new configuration as the new q^0 value and re computes the new configuration with the new initial condition value.

B.2.2.2 IC analysis velocity

The solver uses the same algorithm as mentioned in the IC analysis position but the variables have taken the first derivative, the form of the cost function. The first derivate to define the IC velocity is shown in equation B-17.

B-17

$$f(\dot{q}_1, \dots, \dot{q}_n) = \frac{1}{2} (\dot{q} - \dot{q}_0)^T W (\dot{q} - \dot{q}_0)$$

The optimization is subject to the first derivative of the constraints at the joint as shown in equation B-18.

B-18

$$\phi_q(q, t_0) \cdot \dot{q} + \phi_t(q, t_0) = 0$$

B.2.2.3 IC analysis acceleration and force

The force and acceleration is using the constraint acceleration mentioned in equation B-19, and equation of the motion of the system in a linearized format as shown in equation B-19.

B-19

$$\begin{bmatrix} M & \phi_q^T(q^0) \\ \phi_q(q^0) & 0 \end{bmatrix} \begin{bmatrix} \ddot{q} \\ \lambda \end{bmatrix} = \begin{bmatrix} F \\ \tau \end{bmatrix}$$

The first row of the matrix is linearized for of equation of the motion used, and the second row is to find the acceleration at the initial condition of the system, and M is the general mass matrix of the system.

The Lagrange value calculated from equation B-19 used to determine the force and torques caused by the constraints to find the reaction forces acting from the joints by using equationsB-20 and B-21.

B-20

$$F^C = - \frac{\partial \phi^{(j)}}{v_i} \lambda^{(j)}$$

B-21

$$T^{(C)} = - \left\{ \frac{\partial \phi^{(j)}}{\omega_i} \right\} \lambda^{(j)}$$

Where C indicates the Cartesian coordinate quantities, and values obtained by taking partial derivative of the constraint vectors with respect to their velocities v_i is the Cartesian velocity of the body and ω_i is the global angular velocity by the Lagrange multiplier value found from equation B-21.

B.3 Kinematic analysis position, velocity and acceleration

The kinematic analysis uses constraint imposed to be equal to the generalised coordinates in the model, some constraints are defined as motions.

The constraint equation are nonlinear , the solver uses Taylor-expansion based linearization method to extract the linearized equation of the constraint in order to find the new coordinates q_1 at time t_1 as shown in equation B-22. The Taylor expansion uses partial derivative of the function evaluated at different each coordinate.

B-22

$$\phi(q_1, t_1) = \phi(q_0, t_1) + \phi_q(q_0, t_1)(q_1 - q_0)$$

The kinematic velocity constraint equations are linearized and the first order derivative of the positions in equation B-22 would evaluate the next step's velocity.

Acceleration computed by linearizing the acceleration function mention in equation B-11 , which is same as the first line of the matrix in equation B-19. The generalised acceleration is solved by using the second derivative of equation B-22 and then the value of \ddot{q} is inputted to compute the Lagrange multiplier value from the following linear system shown in equation B-23.

B-23

$$\phi_q^T \lambda = F - M\ddot{q}$$

B.3.1 Dynamic analysis using motion solver

To define equation of motion the kinetic energy and how it is defined in the solver is separated in to translational and rotational velocity and weight factors. The Cartesian velocity u and mass matrix M used to find the linear (Cartesian) velocity. The angular velocity ω and inertia matrix about the local reference frame J is used to compute the rotational kinetic energy, the total kinetic energy is defined from equation B-24.

$$K = \frac{1}{2} u^T M u + \frac{1}{2} \overline{\omega^T J \omega}$$

The general forces is consist of applied force and torques on the body shown as Q in equation B-24.

B-24

$$Q = \begin{bmatrix} (\Pi^P)^T f \\ (\Pi^R)^T \bar{n} \end{bmatrix}$$

Where the projection operator of the point of application (Π^P) is a partial delivaritive of the velocity of the application of the external force with aspect of the linear velocity. And the projection operator of the applied torque (Π^R) is the partial derivative of the angular displacement of the joint with aspect of the derivative of Euler's angle at each coordinate.

B.3.2 Equations of motions

Equation of motion defined in the solver uses the Lagrange method in finding intersection coordinate where the constraint and coordinates intersect, the used second order differential equation used to find the general forces in the system as shown in equation B-25.

B-25

$$\frac{d}{dt} \left[\left\{ \frac{\partial K}{\partial \dot{q}} \right\}^T \right] - \left\{ \frac{\partial K}{\partial q} \right\}^T + \phi_q^T \lambda = Q$$

From general coordinates point of view equation B-25 can be expanded to Cartesian coordinate (linear velocity, linear acceleration) and Euler coordinates (angular velocity, angular acceleration), equation B-25 is reformulated as equation B-26.

B-26

$$\frac{d}{dt} \begin{bmatrix} \left(\frac{\partial K}{\partial u} \right)^T \\ \left(\frac{\partial K}{\partial \zeta} \right)^T \end{bmatrix} - \begin{bmatrix} \left(\frac{\partial K}{\partial p} \right)^T \\ \left(\frac{\partial K}{\partial \varepsilon} \right)^T \end{bmatrix} + \begin{bmatrix} \phi_p^T \lambda \\ \phi_\varepsilon^T \lambda \end{bmatrix} = \begin{bmatrix} (\Pi^p)^T f \\ (\Pi^R)^T \bar{n} \end{bmatrix}$$

Where:

Linear (Cartesian coordinate) acceleration is represented by B-27 and the angular (Euler coordinate) acceleration is represented by B-28.

B-27

$$\frac{d}{dt} \left(\frac{\partial K}{\partial u} \right)^T = M \dot{u}$$

B-28

$$\left(\frac{\partial K}{\partial p} \right)^T = 0$$

To compute the configuration of the part by using the conversion matrix B and vector of the moment of inertia of the part and the Euler's angle as shown below.

$$\Gamma \equiv \frac{\partial K}{\partial \zeta} = B^T \overline{J} B \zeta$$

The solver solves for the two general forces, translational force and momentum on the joint by the following two equations which are extracted and reformulated from equation B-28, as equations of motions used to solve the inverse dynamic problem of the gait of the robot.

Equations of motions used are shown in B-29 run in all 3 coordinates for every joint of the system and then the solver stacks together all equations of the motions together for the entire system

B-29

$$M\dot{u} + \phi_p^T \lambda = (\Pi^p)^T f$$

$$\dot{\Gamma} - \frac{\partial K}{\partial \varepsilon} + \phi_\varepsilon^T \lambda = (\Pi^R)^T \bar{n}$$

$$\Gamma - B^T \overline{J} B \zeta = 0$$

$$\dot{p} - u = 0$$

$$\dot{\varepsilon} - \zeta = 0$$

Appendix C

C.1 Electric motor system design and specification.

Kinavo
SMH Product Manual

6

SMH60 Technical Information

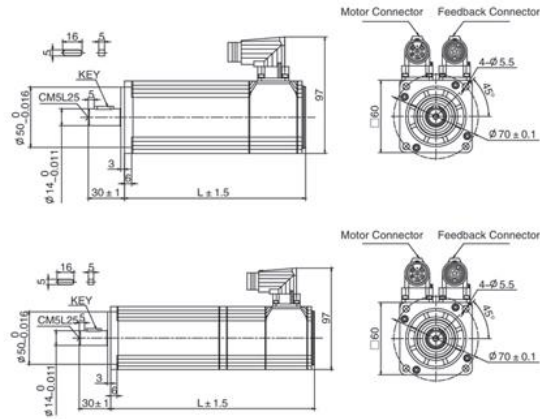
6.1 Technical Data

Motor Type	SMH60—203026xxL SMH60—203026xxC SMH60-203026XXXM	SMH60—403026xxL SMH60—403026xxC SMH60-403026XXXM
Rated power P _n (W)	200	400
Rated torque T _n (Nm)	0.64	1.27
Rated speed \bar{n} (rpm)	3000	3000
Rated current I _n (A)	1.6	3.1
DC Link Voltage U _{DC} (V)	300	300
Maximum torque T _m (Nm)	1.92	3.81
Maximum current I _m (A)	4.8	9.3
Standstill torque T _s (Nm)	0.7	1.4
Standstill current I _s (A)	1.8	3.41
Voltage constant K _e (V/krpm)	29	29
Torque constant K _t (Nm/A)	0.48	0.48
Resistance line-line R _L (Ω)	8.02	3.52
Inductance line-line L _L (m H)	16.3	7.8
Electrical time constant T _e (ms)	2.03	2.22
Mechanical time constant T _m (ms)	2.26	1.35
Rotor moment of inertia J _m (kgcm ²)	0.375	0.51
Pole number	6	6
Max. voltage rising du/dt (kV/μs)	8	8
Insulation class	F	F
Max. radial force F _r (N)	180	180
Max. axial force F _a (N)	90	90
Weight (Kg)	1.3	1.8
Feedback device	2500p/rev incremental encoder or Resolver (sin--cos)	
Temperature sensor	KTY84-130(If Fitted)	
Cooling method	Totally enclosed non-ventilated	
Protection level	IP65,shaft sealing IP54	
Environmental conditions	Temperature	-20℃~40℃
	Humidity	Below 90%RH (No dewing)
	Environment	Far away active gas, combustible gas, oil drop, ash.
	Installation altitude	Up to 1000m: rated power Above 1000m: 1.5% power Decreasing per 100m,max.4000m
Rating conditions	Mounting	Black Aluminum flange 255x255x6mm
	Temperature	60K housing temperature rising at 40℃ ambient

SMH60 Technical Information

6.2 Product Dimension Drawing

6.2.1 SMH60 C series dimension (unit: mm)



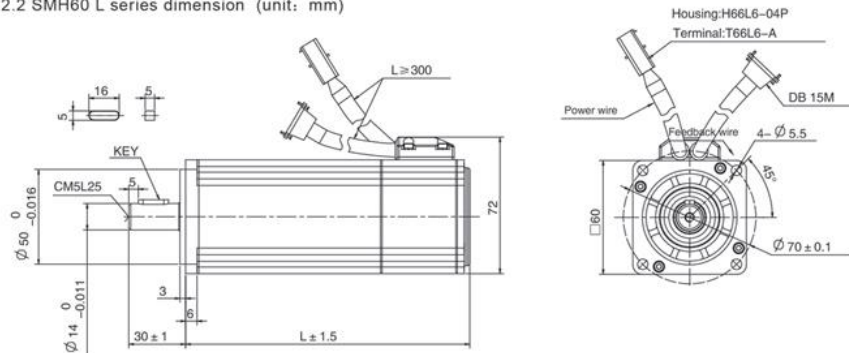
SMH60 C series Length Without Brake (Unit: mm)

Power (W)	L
200	120
400	150

SMH60 C series Length With Brake (Unit: mm)

Power (W)	L
200	164
400	194

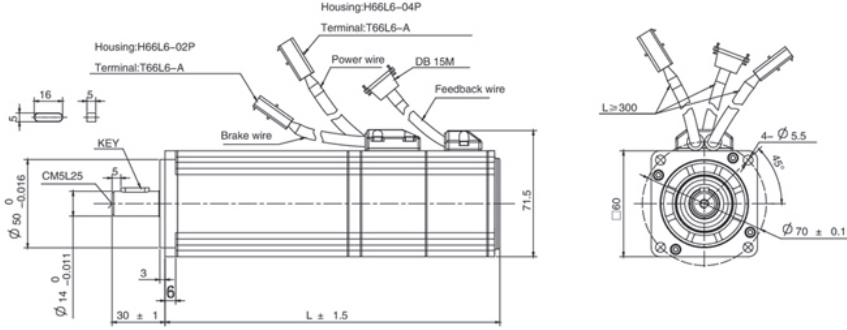
6.2.2 SMH60 L series dimension (unit: mm)



SMH60 L series Length Without Brake (Unit: mm)

Power (W)	L	
	Fit Encoder	Fit Resolver
200	120	115
400	150	145

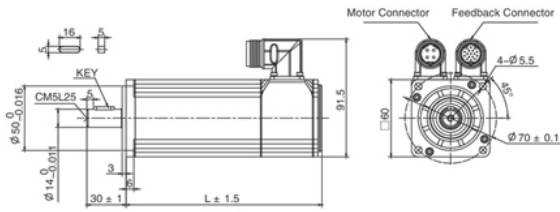
SMH60 Technical Information



SMH60 L series Length With Brake (Unit: mm)

Power (W)	L	
	Fit Encoder	Fit Resolver
200	159	154
400	189	184

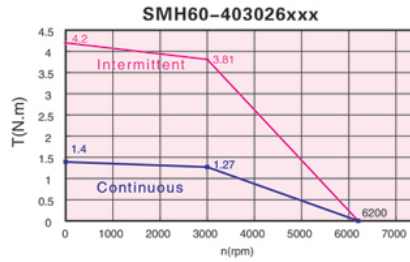
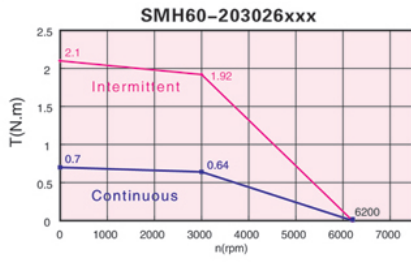
6.2.3 SMH60 M series dimension (unit: mm)



SMH60 M series Length Without Brake (Unit: mm)

Power(W)	L
200	120
400	150

6.3 SMH60 Series Performance Curve



C.2 Planetary gear system design and specification

Configure and order your drive online.
xdrives.maxonmotor.com

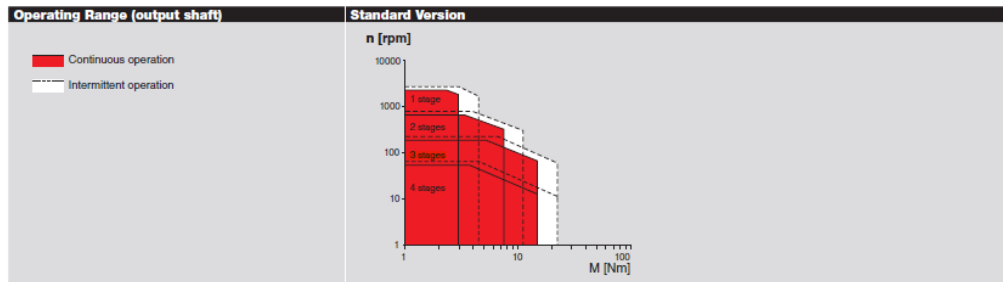
GPX 42 Planetary Gearhead Ø42 mm

Configurable



maxon X drives

Key Data	Standard Version
Max. transmittable power	W 590
Max. continuous torque	Nm 15.0
Max. continuous input speed	rpm 9000
Ambient temperature	°C -40 ... +100
Bearing at output	Ball bearing



Specifications	Standard Version			
	1	2	3	4
Number of stages				
Max. transmittable power (continuous)	W 590	240	100	20
Max. transmittable power (intermittent)	W 725	300	125	25
Max. continuous torque	Nm 3.0	7.5	15.0	15.0
Max. intermittent torque	Nm 4.5	11.3	22.5	22.5
Max. continuous input speed	rpm 8000	8000	8000	8000
Max. intermittent input speed	rpm 10000	10000	10000	10000
Max. efficiency	% 90	81	72	64
Average backlash no load	° 0.6	0.8	1.0	1.0
Max. axial load (dynamic)	N 150	150	150	150
Max. radial load, 12 mm from flange	N 120	240	360	360
Gearhead length L1	mm 37.4	51.9	66.4	80.9
Weight	g 260	360	460	560

Configuration	Standard Version			
Number of stages	1	2	3	4
Reduction	X:1 3.5, 4.3	12, 15, 19, 21, 26	43, 53, 66, 74, 81, 113, 126, 156	150, 186, 230, 257, 285, 319, 353, 394, 441, 488, 546, 676, 756, 936
Version	Standard			
Flange	Standard flange/configurable flange			
Shaft	Length/feather key			

maxon Modular System	Page	Dimensions Standard Version	M 1:2
maxon DC motor			
DCX 35 L	75		

